

Rijeka — Croatia — 25-29 September, 2023

International Conference on Highly Flexible Slender Structures

Book of Extended Abstracts



UNIRI



iacm



THREAD
EUROPEAN TRAINING NETWORK



HFSS 2023

International Conference on Highly Flexible Slender Structures

Organised by



University of Rijeka



Faculty of Civil Engineering

Book of Extended Abstracts

Editors:

Martin Arnold

Gordan Jelenić

Edita Papa Dukić

Rijeka, Croatia, 25-29 September, 2023.



This project has received funding from the European Union's Horizon 2020 research and innovation programme under the Marie Skłodowska-Curie grant agreement No 860124



Published by

University of Rijeka, Faculty of Civil Engineering
Radmile Matejčić 3, 51000 Rijeka, Croatia

Printed by:

Tiskara GRAFIKA HELVETICA d.o.o.

Issues: 115 copies

ISBN 978-953-6953-61-5

Copyright © University of Rijeka, Faculty of Civil Engineering, Rijeka, Croatia, 2023.

Scientific Committee

Martin ARNOLD, Martin Luther University Halle-Wittenberg
Rudolf BEHA, Leitner Ropeways
Oliver BRÜLS, University of Liège
Elena CELLEDONI, National Technical University of Norway Trondheim
José ESCALONA, University of Seville
Heike FAßBENDER, Technische Universität Braunschweig
Johannes GERSTMAYR, University of Innsbruck
Gordan JELENIĆ, University of Rijeka
Sigrid LEYENDECKER, Friedrich Alexander University Erlangen-Nürnberg
Joachim LINN, Fraunhofer ITWM Kaiserslautern
Sina OBER-BLÖBAUM, University of Paderborn
Edita PAPA DUKIĆ, University of Rijeka

Local Organising Committee

Nina ČEH, University of Rijeka
Sara GRBČIĆ ERDELJ, University of Rijeka
Gordan JELENIĆ, University of Rijeka
Teo MUDRIĆ, University of Rijeka
Edita PAPA DUKIĆ, University of Rijeka
Jan TOMEČ, University of Rijeka
Laura GRBAC, University of Rijeka

The results presented in this publication reflect only the authors' views and the European Research Executive Agency is not responsible for any use that may be made of the information it contains.

Preface

The structural systems or their parts which are both highly flexible and slender may be found in exceedingly diverse applications in various engineering fields including aeronautical, automotive, biomedical, civil, mechanical and textile engineering continually opening new and exciting industrial challenges for scientific advancement in experimental methods, theory, numerical procedures and software development.

The applications may include multi-filament cables, multi-wired harnesses, taut stranded wires or composite beams in which main challenges arise in constitutive modelling on the stress resultant-strain measure level due to cross-sectional material heterogeneity, which is one important area of research to which the conference will be devoted. Another research area is geometrically consistent spatial discretisation schemes as well as modelling interactions of slender structures in self-contact and with their environment in operating conditions including frictional contact effects. System-level simulation methods and geometric time-integration algorithms able to deal with dynamic interactions between many flexible slender elements and their environment in large-scale models while respecting and preserving non-linear mathematical structure of a problem, involving also those defined on Lie groups, make yet another research area of particular importance for the conference.

The conference is organised in mini-symposia devoted to constitutive modelling, contact mechanics, geometric integration, coupling of beams and solids, textile and fibrous materials and layered structures, as well as a general programme to include wider applications of highly flexible slender structures. The importance of modernising graduate-level curricula in modelling slender structures will also be discussed during a conference mini-symposium, while another one is devoted to the role Prof. Miran Saje had in promotion of computational mechanics in this geographic area, particularly in establishment or development of competent research teams at the Civil Engineering faculties in Ljubljana and Rijeka.

This Book of Extended abstracts collects all the contributions contained within the general programme and the mini-symposia as well as those provided by eight world-renowned scientists of all generations coming from the most prestigious research centres in Europe and America: These eminent researchers have provided cutting-edge scientific contributions in numerical modelling of highly flexible slender structures throughout their career and in recognition of their achievements they have been invited to the conference as key-note speakers.

In addition, special conference sessions are devoted to the future of the young researchers nearing the completion of their early-stage development, in which two dedicated professionals will help them prepare both for the continuation of their career in academia as well as industry. The sessions will be designed to provide specific horizontal skills related to preparation of future job applications and writing research-grant proposals. In the year in which the University of Rijeka celebrates its 50th anniversary we are proud to welcome you at HFSS 2023 and wish you a successful professional event that will strengthen existing and help create new collaborations as well as spur new research ideas and initiate fruitful scientific debate. In addition, we hope that you will enjoy your stay in Rijeka, return from the conference with a number of memorable experiences and a desire to visit it again.

On behalf of HFSS 2023 Scientific Committee
Gordan Jelenić

Dear participants of the HFSS 2023 conference,

The Marie Skłodowska-Curie Actions (MSCA) are the European Union's reference programme for doctoral education and postdoctoral training. In October 2019, we started the MSCA Innovative Training Network THREAD - Numerical Modelling of Highly Flexible Structures for Industrial Applications that has received funding from the European Union's Horizon 2020 research and innovation programme (<https://thread-etn.eu/>). THREAD is a network of ten universities, one research institute and one small industrial enterprise from Austria, Belgium, Croatia, France, Germany, Norway, Slovenia and Spain who cooperate with twelve industrial partners from most of these countries as well as Finland, Italy and Sweden. After four years of joint work, we will complete THREAD's network-wide training programme at this International Conference on Highly Flexible Slender Structures (HFSS 2023).

The THREAD network with its 14 projects for early-stage researchers (ESRs) brought young mechanical engineers together with mathematicians to develop mechanical models and numerical methods for designing highly flexible slender structures, and to support the development of future virtual prototyping tools. At HFSS 2023, the currently active early-stage researchers of the THREAD project as well as all THREAD early-stage researchers who have already completed successfully their 36-month ESR projects plan to report on recent research results. Most of them are now on the way to the final phase of their PhD projects. The list of topics being addressed in the extended abstracts of their contributions to HFSS 2023 is impressive, focussing on the three THREAD research work packages on constitutive modelling, on contact and friction in mechanics of flexible slender structures and on geometric integration methods for non-linear structural dynamics.

We are very grateful to the European Community on Computational Methods in Applied Sciences (ECCOMAS) for awarding the HFSS 2023 conference the status of an ECCOMAS Thematic conference and to the International Association for Computational Mechanics (IACM) for supporting HFSS 2023 as an IACM Special interest conference. The PhD students of the THREAD network will strongly benefit from the opportunity to present their close-to-final scientific achievements in the inspiring atmosphere of such an international audience. To support these young scientists who are at an early stage of their scientific career, we offer at HFSS 2023 two workshops on preparing job applications and future grant proposals.

The International Conference on Highly Flexible Slender Structures would not have been possible without the enthusiasm and extraordinary amount of work put in by the local organisers at the Faculty of Civil Engineering of the University of Rijeka. We are very grateful to all of them and look forward to five days of interesting presentations and lively discussions on this timely topic of research.

Martin Arnold
Coordinator of THREAD

Table of Contents

Invited Lectures	1
Configurational Forces in Variable-Length Beams for Flexible Multibody Dynamics <i>Olivier A. Bauchau, Shilei Han</i>	3
Simulating fibre assemblies: from Hollywood illusions to physical predictions <i>Florence Bertails-Descoubes</i>	5
Inverse Dynamics of Geometrically Exact Strings and Beams <i>Peter Betsch, Timo Ströhle</i>	9
Experiments and Constitutive Models for Cable Structures in the Automotive Industry <i>Vanessa Dörlich</i>	11
How Relaxation of Compatibility in Time can Simplify the Floating Frame of Reference Formulation in Flexible Multibody Dynamics <i>Michel Géradin</i>	15
Group-Equivariant and Cochain Projection Based Variational Discretizations of Lagrangian PDEs <i>Melvin Leok</i>	17
Generalized Interaction Potentials in the Geometrically Exact Beam Theory <i>Christoph Meier, Maximilian J. Grill, Wolfgang A. Wall</i>	23
Using the Special Euclidean Group to Model Flexible Multibody Systems <i>Valentin Sonneville</i>	25
General programme	27
Thermo- and Chemoelastic 3D Beam Modelling and Simulation with Isogeometric Collocation Methods <i>J.C. Alzate Cobo, O. Weeger</i>	29
Physical Validation for the Simulation of Flexible Slender Structures <i>B. Bauer, A. Bosten, M. Roller, M. Hawwash, O. Brüls, J. Linn</i>	31
Towards realistic modelling of nanotrusses: coupling MD, ML and FEM <i>M. Čanađija, V. Košmerl, M. Zlatić</i>	33
An efficient isogeometric analysis formulation for geometrically exact beam structures with complex shape and topology <i>D. Ignesti, G. Ferri, E. Marino</i>	35
Elastic Ribbons: the missing link between rods <i>S. Neukirch, B. Audoly, F. Bertails-Descoubes, R. Charrondiere, V. Romero</i>	37
Indirect shape adaptation of compliant arches using active supports <i>P. Varkonyi, A.Á. Sipos</i>	39

MS-1: Constitutive modelling for flexible slender structures.....	41
An Energy Stable Discontinuous Galerkin Approach for the Geometrically Exact Intrinsic Beam Model <i>C. Bleffert, L. Dreyer, M. Röhrig-Zöllner.....</i>	43
Modelling the Mechanical Behaviour of Unshielded Twisted Pair Cables Including Frictional Contact <i>M. Hawwash, V. Dörlich, J. Linn.....</i>	45
Nonlinear computation of cable structures with anisotropic plasticity using high-order elements <i>A. Hildebrandt-Raj, P. Sharma, S. Diebels, A. Düster.....</i>	47
Static and dynamic analysis of geometrically and materially nonlinear spatial frame like structures <i>S. Kusuma Chandrashekhara, D. Zupan.....</i>	49
Inelastic Constitutive Behaviour and Hysteresis Operators – Modelling and Simulations for 2D Cosserat Rods <i>D. Manfredi, V. Dörlich, J. Linn, M. Arnold.....</i>	51
Constrained optimization for part-through crack computation <i>S.J. Michel, A. Á. Sipos.....</i>	53
Finite element beams based on non-linear micropolar theory <i>L. Obrezkov, M. Matikainen, R. Kouhia.....</i>	55
Vibrations of an inclined cable with a lumped mass <i>M. Patreider, M. Wenin, T. Furtmüller, C. Adam.....</i>	57
On the bending of spiral strands <i>M.A. Saadat, D. Durville.....</i>	59
On the number of congruent hinges of masonry arches at failure <i>A. Á. Sipos.....</i>	61
Homogenised stiffness coefficients of unloaded endoscope shafts <i>M. Stavole, R.T. Sato Martin de Almagro, V. Dörlich, S. Leyendecker.....</i>	63
Experimentally validated conservative nonlinear modes of highly flexible structures by phase resonance testing and effect of damping <i>O. Thomas, M. Debeurre, C. Giraud-Audine, A. Grolet, S. Benacchio.....</i>	65
Investigation of the influence of the inner structure on the stiffness of a cable under pure torsion <i>C. Tsegouog, P. Sharma, V. Dörlich, J. Linn, S. Diebels.....</i>	67
Simulation and Parametrization of Nonlinear Elastic Behaviour of Cables <i>T. Zhao, F. Schneider-Jung, J. Linn, R. Müller.....</i>	69
MS-2: Contact and friction in mechanics of flexible slender structures.....	71
Geometrically exact beam-to-beam contact interactions embedded in a finite volume-based discretisation framework <i>S. Bali, Ž. Turković, P. Cardiff, A. Ivanković, V. Pakrashi.....</i>	73

On the Evaluation of the Tangential Slip Increment in Quasi-static Beam-to-Beam Contact Problems <i>O. Brüls, A. Bosten</i>	75
An arbitrary Lagrangian-Eulerian geometrically exact beam formulation applied to reeving systems <i>O. Devigne, O. Brüls</i>	77
Numerical analysis of the rope-sheave contact interaction using the Arbitrary Lagrangian-Eulerian approach <i>J.L. Escalona</i>	79
A total Lagrangian Petrov-Galerkin SE(3) Cosserat rod finite element formulation <i>S.R. Eugster, J. Harsch, S. Sailer</i>	81
Efficient simulation of ropeway systems with multibody systems <i>J. Gerstmayr, K. Ntarladima</i>	83
An Invariant Bézier FE-formulation for the Analysis of Slender Beams <i>L. Greco, M. Cuomo, D. Castello</i>	85
Rotation parametrization and interpolation strategies for Petrov-Galerkin rod finite elements – a family of Cosserat rod formulations <i>J. Harsch, S. R. Eugster</i>	87
Accurate contact detection and response in fibre assemblies with friction <i>E. Hohnadel, O. Crespel, T. Métivet, F. Bertails-Descoubes</i>	89
A numerical bending study of sandwiched beams with a mortar line-to-line contact formulation <i>A.V. Kulkarni, A. Bosten, V. Dörlich, O. Brüls, J. Linn</i>	91
Investigating the compaction of open ring stacks through real and numerical experiment <i>T. Métivet, E. Hohnadel, T.G. Sano, T. Kawata, F. Bertails-Descoubes</i>	93
Real-time co-simulation of wire-rope systems <i>N. Mohammadi, A. Rouvinen, P. Korkealaakso, J.L. Escalona</i>	95
Optimal Control for locomotion of contractile slender bodies on frictional bodies <i>J. Munoz, A. Bijalwan</i>	97
Coupling of bending and axial motion in highly flexible axially moving beams modelled with ALE <i>K. Ntarladima, J. Gerstmayr</i>	99
Towards a complete Riemannian metric on the space of elastic rods <i>P. Reiter, E. Döhrer, H. Schumacher</i>	101
Untangling the physics of self-locking in tight knots <i>A. Teixeira da Silva, T. Métivet, V. Gramegna, M. Skouras, F. Bertails-Descoubes</i>	103
Unbiased line-to-line contact method for static frictionless beam-to-beam contact <i>J. Tomec, G. Jelenić</i>	105
Sliding flexible rods: non-material finite elements and configurational forces <i>Y. Vetyukov, A. Humer</i>	107

MS-3: Geometric integration methods for non-linear structural dynamics.....	109
Test equations for Lie group time integration	
<i>M. Arnold</i>	111
Lie group integrators for mechanical systems and their stability	
<i>E. Çokaj, M. Arnold, E. Celledoni, A. Leone, D. Murarui, B. Owren, D. Tumiotto</i>	113
Computing normal forms of quadratic differential algebraic equations	
<i>A. Grolet, A. Vizzaccaro, M. Debeurre, O. Thomas</i>	115
Higher order fractional variational integrators	
<i>K. Hariz-Belgacem, F. Jiménez, S. Ober-Blöbaum</i>	117
Machine learning applications for mechanical systems	
<i>A. Leone, E. Celledoni, D. Murari, B. Owren</i>	119
2D Euler elastica in constrained environments	
<i>M. Stavole, R.T. Sato Martin de Almagro, S. Leyendecker</i>	121
Emergy-momentum conserving time integrator for geometrically exact beam dynamics	
<i>J. Tomec, G. Jelenić</i>	123
Implementation and Stability Issues of Lie Group Integrators for Cosserat Rod Models with Constraints	
<i>D. Tumiotto, M. Arnold</i>	125
MS-4: Teaching the science of modelling and simulation of slender flexible structures for application in industry: A curriculum for early stage researchers.....	127
THREAD—Numerical modelling of highly flexible structures for industrial applications. Design of a training programme	
<i>E. Celledoni, S. Leyendecker, B. Owren</i>	129
Teaching small and large deformation flexible multibody dynamics	
<i>J.L. Escalona</i>	131
Preparing students for a PhD position in application-oriented research on flexible slender structures	
<i>J. Linn, V. Dörlich</i>	133
MS-5: Advanced models and numerical formulations for the interaction of beams and the coupling of beams with solids.....	135
A note on modelling potential-based interactions between plane beams	
<i>A. Borković, M.H. Gfrerer, B. Marussig, R.A. Sauer</i>	137
An isogeometric three-field mixed finite element formulation of nonlinear beam structures with extensible directors	
<i>M.J. Choi, R.A. Sauer, S. Klinkel</i>	139

Nonlinear Dynamics of Complex 3D Rod Assemblies <i>R.E. Dickinson, A. Palmeri, T.I. Marjoribanks</i>	141
Transitioning from solids to first-order shear deformable beams <i>S. Klarmann, J. Wackerfuß, S. Klinkel</i>	143
Coupling 1D beam elements with 3D solid elements for the modelling of fibre-reinforced composites <i>V. Poussard, C. Gandiolle, D. Durville</i>	145
A finite strain isogeometric solid beam element with assumed natural strain method <i>A. Shafqat, O. Weeger, B.X. Xu</i>	147
A mixed-dimensional beam-to-solid interaction framework: From embedded fibers to contact <i>I. Steinbrecher, C. Meier, A. Popp</i>	149
MS-6: Slender beam-like structures with scientific passion – mini-symposium in honour of prof. Miran Saje	151
A review of beam formulations with consistent equilibrium in a cross-section <i>P. Češarek</i>	153
Kinematically exact beam with embedded discontinuity <i>P. Češarek, M. Saje</i>	155
Nonlinear dynamics of highly flexible beam structures: frequency domain-based finite element computation of the nonlinear modes <i>M. Deburre, A. Grolet, O. Thomas</i>	157
On the convergence of nonconforming finite element solutions to the unique solution of Reissner's Elastica <i>R. Flajs, M. Saje</i>	159
Interdependence of helicoidal and fixed-pole interpolation in linear elasticity with linked interpolation, and application in FE modelling of Cosserats' continuum <i>L. Grbac, G. Jelenić</i>	161
Enhanced finite-element performance in high-curvature micropolar pure-bending <i>S. Grbčić Erdelj, G. Jelenić, A. Ibrahimbegović</i>	163
Rough and sharp estimates of extensional and transverse shear strains for equilibrium configurations of elastic Cosserat rods <i>J. Linn, F. Schneider-Jung, M. Roller, T. Hermansson</i>	165
Overview of numerical models for mechanical analysis of beam elements in fire developed by Chair of mechanics at UL FGG <i>A. Ogrin, R. Pečenko, S. Bratina, T. Hozjan</i>	167
Buckling of slender layered composite columns with incomplete interaction between the layers <i>S. Schnabl, M. Saje, I. Planinc, G. Turk, G. Jelenić</i>	169
Low-order analytical solution for vibration of tensioned cables <i>A. de M. Wahrhaftig, E. M. de O. Lopes, G. R. do Amaral, J. M. Balthazar, K.M.M. Ribeiro</i>	171

On solving the kinematical equations of Cosserat beams <i>D. Zupan, E. Zupan, A. Ogrin</i>	173
Challenges in dynamics of non-linear beams <i>D. Zupan, P. Češarek, E. Zupan, M. Gams</i>	175
MS-7: Modelling and simulation of textile and fibrous materials	177
Finite element analysis of textile cords in rubber-cord composites under compressive loadings: a filament scale approach <i>G. Auteri, M. Chassagne, D. Durville, J. Neggers</i>	179
Modelling the friction between yarns within a laid-strand synthetic ropes by hyperelastoplasticity in finite deformation <i>G. Bles, L. Civier, N. Hamila, P. Dava, Y. Marco</i>	181
Characterizing a yarn's mechanical behaviour on microscale level using a high-fidelity geometrical fiber model <i>A. Bral, L. Daelemans, J. Degroote</i>	183
Technological and modelling aspects of the fiber level modelling of textile yarns <i>Y. Kyosev, A.M. Schmidt</i>	185
Study of Frictional Contact Interactions within Jacquard Harness in Weaving Process for 3D Interlock Fabrics <i>S. E. Mermouli, D. Durville, P. del Sorbo, B. Tranquart, D. Coupé</i>	187
Modelling a braiding process as a constrained multibody system with frictional contacts <i>I.K. Patil, A. Cosimo, O. Brüls</i>	189
MS-8: Modelling beam-like layered structures with compliant interfaces	191
An inverse approach treating large rotations to simulate composite single-layer peeling-based disassembly <i>M. Becker, M. Imbert, M. May</i>	193
Finite Element Model for Simulation of Complex Delamination in Three-Dimensional Composite Beams <i>D. Lolić, M. Brojan, D. Zupan</i>	195
Experimental validation of a novel numerical model for rate-dependent mode-I failure of adhesive joints <i>L. Škec, G. Alfano</i>	197
Author Index	201

Invited Lectures

Configurational Forces in Variable-Length Beams for Flexible Multibody Dynamics

Olivier A. Bauchau¹, Shilei Han²,

¹ University of Maryland, Department of Aerospace Engineering, obauchau@umd.edu

² School of Aerospace Engineering, Beijing Institute of Technology, shilei1.han@gmail.com

Keywords: Configurational forces, Finite Elements, ALE Formulation

1. Introduction

Sliding beams and cables are used in many engineering applications such as cranes, elevators, or deployable space structures; furthermore, they can approximate the behavior of biological systems such as human muscles. In other applications, sliding appendages such as joints, concentrated loads, or rigid bodies move along beams or cables. For simplicity of the exposition, the term “sliding beams” will be used to refer to both problems: sliding beams and beams with sliding appendages.

The dynamic behavior of these structures, often treated as geometrically nonlinear beams or cables, has attracted the attention of numerous researchers in recent years. For simplicity, the axial motion of the beams is often prescribed a priori. In reality, this axial motion results from the dynamic behavior of the system and hence, must be determined as part of the solution process. The present paper focuses on this problem.

Hamilton’s variational principle is used to derive the weak and strong forms of the equations of motion for sliding beams. Due to the presence of sliding motion, the action integral is now defined over a time-varying material domain and the process of taking variations of this action integral must be handled carefully. The variation of functionals defined over time-varying domains appears in many engineering applications and numerous researchers have tackled this problem. For instance, variation of the cost functional in free-endpoint optimal control problems leads to the transversality condition at the free end time, variation of the potential energy functional of a beam contacting a rigid obstacle yields an additional boundary conditions determining the contact region, and first- and second-order variations of functionals defined over time-varying material domains are central to shape optimization.

Theoretically, action integrals defined over time-varying material domains can be transformed into action integrals over time-invariant reference domains through proper coordinate transformations. The variation process then becomes straightforward and the results can be transformed back to time-varying material domains. Reynolds’ transport theorem expresses this procedure mathematically: it relates the time derivative of an integral over a given control volume to the time derivative of the integrand and boundary fluxes. Clearly, Reynolds’ transport theorem still holds when replacing the time derivative with a variation.

In general, structural dynamics problems are investigated using the Lagrangian formulation; typically, for beam problems, the “material” or “Lagrangian coordinate” is selected as the arc-length coordinate of a material particle of the beam’s axial line in its undeformed configuration. This coordinate is used to track down the beam’s motion as it deforms in space. For sliding beams, this collection of material coordinates is time varying: for instance, an elevator cable comprises a time-varying collection of material particles as portions of the cable are reeled in or out of the capstan.

In finite element implementations, it is convenient to mesh the structure with a constant number of elements to avoid the costly re-meshing of the entire problem at each time step. The implementation of this approach requires the introduction of a “mesh coordinate.” For instance, it is expeditious to model an elevator cable with a fixed number of elements although its length varies in time. Mesh coordinate $\xi \in [\xi_0, \xi_f]$ is introduced, where coordinates ξ_0 and ξ_f identify the root and end points of the variable-length cable and if the cable is modeled with N elements of equal length, the length of each element is $(\xi_f - \xi_0)/N$. Mesh coordinate ξ varies along the length of the cable but no longer identifies a specific material particle of the cable. Of course, a one-to-one map relates the material and mesh coordinates.

This approach, known as the Arbitrary Lagrangian-Eulerian (ALE) formulation, has been developed by numer-

ous authors for geometrically nonlinear sliding beams [1, 2, 3]. As will be shown in this paper, configurational forces arise at the sliding boundaries of the structure, affecting the boundary conditions at these points. Failure to identify these configurational forces properly can result prescribing erroneous boundary conditions.

Configurational forces were first introduced by Eshelby [4] to describe the driving forces acting on defects or singularities in solids; these forces arise from variations of the material configuration. A number of authors have investigated configurational forces in beams and cables both theoretically and experientially. Recently, a novel ALE formulation for dynamics problems of geometrically exact sliding beams was developed by the first author based on dual quaternion kinematics. Material motions of the rigid-sections are decomposed into mesh motions (with mesh coordinates held fixed) and convective terms that take into account the relative motion of the material and mesh coordinates. Integration by parts then yields both strong and weak forms of the mechanical and configurational momentum equations together with the natural boundary conditions for mechanical and configurational forces at the endpoints. Although the aforementioned process is clear, integration by parts for terms involving time and spatial derivatives is complex and error prone.

This paper addresses the problem of sliding beams with special emphasis on situations where the axial motion of the beam is not prescribed a priori. Hamilton's variational principle is used to derive the weak and strong forms of governing equations for sliding beams. Because the action integral is defined on a non-material domain, Reynolds' transport theorem is applied to transform the variation of the action integral into the integral of the variation of the integrand and boundary flux terms then appear.

Consequently, the variation of the integrand yields the strong form of the mechanical and configurational momentum equations and the boundary flux terms yield the natural boundary conditions for the mechanical and configurational forces. The configurational momentum equations are shown to be a linear combination of their mechanical counterparts and hence, are redundant.

A weak form of the same equations is also developed by performing spatial integration by parts. In this weak form, the configurational and mechanical momentum equations become independent because they combine in an integral sense the strong mechanical and configurational momentum equations with their respective natural boundary conditions.

The configurational boundary conditions are scrutinized closely and shown to involve discontinuities in the axial force and strain energy density. While the first discontinuity was identified by numerous researchers, the second appears to have been ignored by most, although both are shown to be of the same order of magnitude.

In view of these observations, two formulations are proposed: (1) the *domain-based formulation* that combines the weak forms of mechanical and configurational momentum equations and (2) the *boundary-based formulation* that combines the weak form of mechanical momentum equations with the natural boundary conditions for the configurational forces.

Numerical examples have been presented to validate and compare the two proposed formulations. The predictions of both formulations are found to be in good agreement with those obtained from an ABAQUS model using contact pairs. The domain-based formulation has a convergence rate of three or four for three- or four-node beam elements, respectively, while that of boundary-based formulation is one order lower. Clearly, the proper treatment of the configurational forces at the boundaries impacts the accuracy of the model significantly.

References

- [1] L. Vu-Quoc and S. Li. Dynamics of sliding geometrically-exact beams: large angle maneuver and parametric resonance. *Computer Methods Applied Mechanics and Engineering*, 120:65–118, 1995.
- [2] K. Behdinan, M. C. Stylianou, and B. Tabarrok. Dynamics of flexible sliding beams-non-linear analysis part I: Formulation. *Journal of Sound and Vibration*, 208(4):517–539, 1997.
- [3] K. Behdinan and B. Tabarrok. Dynamics of flexible sliding beams - Nonlinear analysis Part II: Transient response. *Journal of Sound and Vibration*, 208(4):541–565, 1997.
- [4] J. D. Eshelby. The force on an elastic singularity. *Philosophical Transactions of the Royal Society of London. Series A, Mathematical and Physical Sciences*, 244:87–112, 1951.

Simulating fibre assemblies: from Hollywood illusions to physical predictions

Florence Bertails-Descoubes¹

¹ Univ. Grenoble Alpes, CNRS, Inria, Grenoble INP, LJK, Grenoble, France, Florence.Descoubes@inria.fr

Keywords: Numerical simulation, thin elastic structures, frictional contact, virtual prototyping, validation

What is the common feature between *Final Fantasy: the Spirits Within* (2001), *Moana* (2016), and *Avatar, the Way of Water* (2022)? These three computer-animated movies, though made at different periods of time over the three last decades, have all requested huge efforts and energy to capture, as realistically as possible, the motion of one of the most familiar fibrous object: human hair. Should it be long, braided, wavy, or fuzzy, hair is one of the most visible and fascinating features of a human character; as such it greatly contributes to the visual asset of a movie, and enriches its storytelling. More broadly, since the advent of modern computers in the 1960's, Computer Graphics has always striven to develop powerful simulation tools for capturing fascinating phenomena of our everyday life, such as cloth folding, granular flowing, or plant fluttering in the wind. Animating hair virtually and giving the illusion that it is real has become an endless quest since the 2000's.



Figure 1: Simulating the combing of a curly hair wisp with frictional contact ©ELAN team at Inria, 2023.

From very distinct fields... Computer scientists were not the first to draw their attention to fibre systems. Many physicists and mathematicians aimed for centuries at understanding the principles governing those complex mechanical phenomena, providing a number of continuous models for thin elastic rods [1] and frictional contact [2]. In the XXth century, industrial applications such as process automatisation and new ways of transportation boosted the field of Mechanical Engineering, and in particular the finite-element modelling of elastic fibres – called 'beams' in that community. There however, not much room for fantasy nor entertainment: material strength, reliability of mechanisms, and safety, stood for the main priorities. Assimilated to failure cases, large displacements of structures, buckling, tearing, entanglement, and even dynamics, were at that time considered as undesirable behaviors, thus restraining the search for corresponding numerical models. In contrast, Computer Graphics, from its very beginning, was eager to capture such peculiar phenomena, with the sole aim to produce spectacular images and create astonishing stories.

... to recent convergences Nowadays however, although the image production still remains the core activity of the Computer Graphics community, more and more research studies are directed in this community towards the virtual and real prototyping of mechanical systems, notably driven by a myriad of new applications in the virtual try-on and fashion industries, e.g., hairstyling or personalised textile manufacturing. Furthermore, the advent of additive fabrication is currently boosting research in the free design of new mechanisms for various applications, from architecture design [3] to the fabrication of metamaterials [4]. Computer scientists are hence faced with new challenges including methodology and skills for quantitative validation and predictive simulation.

In parallel, the Mechanical Engineering industry has recently shown some growing interest into the modelling of dynamic phenomena prone to large displacements, buckling, contact and friction. For instance, vehicle and aircraft manufacturers encounter large-scale problems involving buckling or entanglement of thin structures such as nylon or carbon fibers [5]; they clearly need predictive, but also robust and efficient numerical tools for simulating and optimising their new fabrication processes, which shares many common features with the large-scale simulation scenarii traditionally studied in Computer Graphics applications.

Furthermore, since a few decades, a new generation of physicists became interested again in the understanding of visually fascinating phenomena, and started investigating the tight links between geometry and elasticity [6].

Common fibrous objects such as twined plants, knitted cloth, bird nests or human hair, have thus regained some popularity among the community in Nonlinear Physics [7, 8, 9]. The term 'extreme mechanics' [10] has been coined precisely to designate all kinds of phenomena involving large displacements, nonlinear deformations, buckling instabilities, or dynamics with dry frictional contact – thus falling outside the standard, well-studied regimes. A major breakthrough was to show that instabilities emerging from such nonlinear (and even nonsmooth) regimes, previously considered as the first route toward failure in engineering structures, could in turn be harnessed to activate matter and program new materials with specific functions: the field of functional materials was born [11], together with a myriad of applications ranging from deployable structures and new metamaterials to soft locomotion [12, 13, 14]. Beyond offering a formidable tool for complementing experimental investigations when laboratory experiments are too cumbersome or costly to perform, numerical exploration rapidly started being perceived by physicists as a valuable tool for getting insights into the early search for analytic solutions, thus fully participating in the modelling stage and physical understanding. Here again, the simulation of fibrous materials turns out to become crucially requested for improving the understanding of physical phenomena unexplored so far, and for designing new materials with controlled properties.

Overall, it turns out that over the last decades, Computer Graphics, Mechanical Engineering, and Nonlinear Physics have finally ended up sharing a strong common interest for simulating extreme mechanical phenomena – and in particular fibrous systems – in a predictive way, while possessing very complementary skills. Unfortunately, in spite of all these observed convergences, Computer Graphics and Computational Mechanics/Physics remain today desperately compartmentalised.

Predictive simulation of fibre assemblies In this talk I will show that although building a simulator that is both predictive and scalable remains an open challenge when dealing with extreme mechanics, advances towards this goal can be made possible thanks to a pluridisciplinary modelling approach combining skills across Physics, Mechanics, and Computer Graphics. In particular, I will present the numerical models that we have been building in the ELAN group at Inria for the last ten years in order to achieve reliable dynamic simulations of fibre packings subject to large displacements, should it be for special effects, virtual prototyping, or physical exploration [15, 16, 17, 18, 19]. Our methodology draws inspiration from Nonlinear Physics for the simplicity and elegance of the reduced rod models, the scaling laws, and the controlled experiments developed there; Mechanical Engineering for the convergence properties of discrete element formulations and the robustness of frictional contact methods, especially within the context of nonsmooth mechanics; and Computer Graphics, for the efficiency and agility of the algorithms and free softwares deployed for optimisation solvers, contact detection, and code benchmarking.

References

- [1] E. Cosserat and F. Cosserat. *Théorie des corps déformables*. Hermann, 1909.
- [2] C.-A. Coulomb. *Théorie des machines simples: en ayant égard au frottement de leurs parties et à la roideur des cordages*. Chapitre.com (new edition), 1781.
- [3] J. Panetta, M. Konaković-Luković, F. Isvoranu, E. Bouleau, and M. Pauly. X-shells: A new class of deployable beam structures. *ACM Transactions on Graphics*, 38(4), July 2019.
- [4] C. Schumacher, S. Marschner, M. Gross, and B. Thomaszewski. Mechanical characterization of structured sheet materials. *ACM Transactions on Graphics*, 37(4), July 2018.
- [5] D. Durville. Numerical simulation of entangled materials mechanical properties. *Journal of Materials Science*, 40:5941—5948, 2005.
- [6] B. Audoly and Y. Pomeau. *Elasticity and Geometry: from hair curls to the nonlinear response of shells*. Oxford University Press, 2010.
- [7] A. Goriely and S. Neukirch. Mechanics of climbing and attachment in twining plants. *Physical Review Letters*, 97:184302, Nov 2006.
- [8] R. Goldstein, P. Warren, and R. Ball. Shape of a ponytail and the statistical physics of hair fiber bundles. *Physical Review Letters*, 108:078101, Feb 2012.

- [9] N. Weiner, Y. Bhosale, M. Gazzola, and H. King. Mechanics of randomly packed filaments — the “bird nest” as meta-material. *Journal of Applied Physics*, 127(5):050902, 2020.
- [10] K. Krieger. Extreme mechanics: buckling down. *Nature*, 488(7410):146–147, August 2012.
- [11] Pedro M. Reis. A Perspective on the Revival of Structural (In)Stability With Novel Opportunities for Function: From Buckliphobia to Buckliphilia. *Journal of Applied Mechanics*, 82(11), 09 2015. 111001.
- [12] B. Lefevre, C. Douthe, and O. Baverel. Buckling of elastic gridshells. *Journal of the International Association for Shell and Spatial Structures*, 56(185), 2015.
- [13] F. Connolly, C. Walsh, and K. Bertoldi. Automatic design of fiber-reinforced soft actuators for trajectory matching. *Proceedings of the National Academy of Sciences*, 114(1):51–56, 2017.
- [14] C. Baek, A. Sageman-Furnas, M. Jawed, and P. Reis. Form finding in elastic gridshells. *Proceedings of the National Academy of Sciences*, 115(1):75–80, 2018.
- [15] G. Daviet, F. Bertails-Descoubes, and L. Boissieux. A hybrid iterative solver for robustly capturing coulomb friction in hair dynamics. *ACM Transactions on Graphics*, 30(6):1–12, dec 2011.
- [16] V. Romero, M. Ly, A.-H. Rasheed, R. Charrondière, A. Lazarus, S. Neukirch, and F. Bertails-Descoubes. Physical validation of simulators in Computer Graphics: A new framework dedicated to slender elastic structures and frictional contact. *ACM Transactions on Graphics*, 40(4):Article 66: 1–19, August 2021.
- [17] E. Hohnadel, J. Marthelot, I. Andrade-Silva, T. Métivet, O. Pouliquen, and F. Bertails-Descoubes. Frictional three-point bending test: disentangling the role of friction through real and numerical experiments. In *European Solid Mechanics Conference ESMC 2022*, Galway, Ireland, July 2022.
- [18] E. Hohnadel, O. Crespel, T. Métivet, and F. Bertails-Descoubes. Accurate contact detection and response in fibre assemblies with friction. In *ECCOMAS Thematic Conference and IACM Special Interest Conference*, Rijeka, Croatia, September 2023.
- [19] T. Sano, E. Hohnadel, T. Kawata, T. Métivet, and F. Bertails-Descoubes. Randomly stacked open cylindrical shells as functional mechanical energy absorber. *Communications Materials*, 4(59), August 2023.

Inverse Dynamics of Geometrically Exact Strings and Beams

Peter Betsch, Timo Ströhle

Institute of Mechanics, Karlsruhe Institute of Technology, Germany, peter.betsch@kit.edu

Keywords: Flexible Multibody Dynamics, Feedforward Control, Servo Constraints, Space-Time Finite Elements, Differentially Flat Systems

1. Introduction

In the standard forward dynamics problem of mechanical systems the forces acting on the system are assumed to be given and the goal is to determine the motion of the system. In contrast to that, in the inverse dynamics problem the motion of the system is partially prescribed and the goal is to determine the actuating forces along with the motion of the whole system. The talk will focus on the inverse dynamics of flexible multibody systems including geometrically exact elastic strings and beams. While numerical methods for the forward dynamics problem are well-established, the inverse dynamics problem is particularly challenging and reliable numerical methods still have to be developed.

Numerical methods for the solution of the forward dynamics problem commonly rely on the semi-discretization approach (also called ‘method of lines’). In the semi-discretization approach the underlying system of partial differential equations governing the motion of geometrically exact structural models is first discretized in space, typically by applying finite elements, and subsequently discretized in time by applying some time-stepping scheme. In the talk we will point out that the semi-discretization approach is not particularly suitable for the inverse dynamics problem.

2. The Inverse Dynamics Problem

An example of the type of inverse dynamics problem under consideration is shown in Fig. 1. The planar flexible manipulator consists of two rigid links ($\mathcal{B}_1, \mathcal{B}_2$) and an elastic link \mathcal{B}_3 , which is modeled by applying the geometrically exact (or Simo-Reissner) beam formulation. In the inverse dynamics problem the trajectory of the end-effector $(\boldsymbol{\gamma}, \Theta) \in \mathbb{R}^2 \times \mathbb{S}^1$ is prescribed over time. Here, $\boldsymbol{\gamma}$ refers to the translational motion of the right boundary of the beam, while Θ characterizes the orientation of the cross-sectional area at the right boundary of the beam. The goal is to determine the three joint-torques m_A, m_B and m_C actuating the system such that the prescribed motion of the end-effector is realized. In the wake of determining the three actuating joint-torques, the motion of the whole system needs to be determined as well.

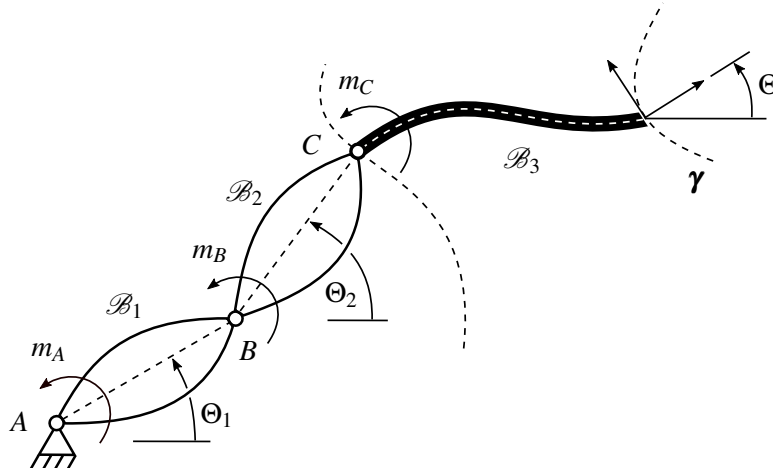


Figure 1: Planar flexible manipulator consisting of two rigid links ($\mathcal{B}_1, \mathcal{B}_2$) and an elastic link \mathcal{B}_3 .

3. Simultaneous Discretization in Space and Time

To prescribe the motion of the end-effector, the notion of ‘servo-constraints’ [1] can be applied. In the context of finite-dimensional mechanical systems the application of servo-constraints leads to differential-algebraic equations (DAEs) governing the inverse dynamics problem. In comparison to standard holonomic constraints, servo-constraints often lead to an increase of the index of the DAEs. The increased index of the DAEs is typically related to the notion of ‘differential flatness’ [2]. In fact, the differential flatness of the system is an important property which ascertains the controllability of the system. Applying the semi-discretization approach to flexible bodies such as elastic strings or beams converts the infinite-dimensional mechanical system into a finite-dimensional one. Appending servo-constraints to the semi-discrete equations of motion again yields DAEs describing the inverse dynamics problem. However, this approach can lead to (i) an excessively high index of the resulting DAEs and, (ii) may affect the differential flatness of the resulting discrete system.

To solve the inverse dynamics problem of infinite-dimensional mechanical systems we propose a simultaneous discretization approach in space and time [3, 4]. In particular, we propose a space-time finite element method in which (i) both test and trial functions are continuous and, (ii) servo-constraints are enforced weakly. Numerical examples demonstrate that the newly devised method is capable to accurately solve the inverse dynamics problem under consideration.

References

- [1] W. Blajer, K. Kołodziejczyk. *Control of Underactuated Mechanical Systems with Servo-Constraints*, Non-linear Dynamics, 50 (2007) 781-791.
- [2] R. Altmann, P. Betsch, Y. Yang. *Index Reduction by Minimal Extension for the Inverse Dynamics Simulation of Cranes*, Multibody System Dynamics, 36 (2016) 295-321.
- [3] T. Ströhle, P. Betsch. *A Simultaneous Space-Time Discretization Approach to the Inverse Dynamics of Geometrically Exact Strings*, Int. J. Numer. Meth. Engng, 123 (2022) 2573-2609.
- [4] T. Ströhle, P. Betsch. *Inverse Dynamics of Geometrically Exact Beams*, Proceedings of the ECCOMAS Congress 2022 – 8th European Congress on Computational Methods in Applied Sciences and Engineering, Oslo, Norway, 5-9 June 2022.

Experiments and Constitutive Models for Cable Structures in the Automotive Industry

Vanessa Dörlich

Mathematics for the Digital Factory
Fraunhofer Institute for Industrial Mathematics (ITWM)
Fraunhofer-Platz 1, 67663 Kaiserslautern, Germany
vanessa.doerlich@itwm.fraunhofer.de

Keywords: Cable Structures, Enhanced Constitutive Models, Experiments, Model Parameterization

1. Introduction

Highly flexible slender structures and their mechanical behavior are relevant in various industries ranging from aerospace engineering to medical applications. In automotive industry, the relevance of flexible slender structures grows steadily as new drive systems, assistance systems and on-board electronics require new cable types. This leads to a total length of up to 9 kilometers of cables and hoses used in a modern car. The mechanical characteristics of single cables and cable structures need to be considered in computer-aided engineering. Simulations are for example used in design space analysis, assembly planning and analysis of typical load cases which occur when cable structures are (repeatedly) deformed during their lifetime.



Figure 1: Examples of single cables (left) and cable bundles with different taping patterns (right).

Cables are compound structures, since they typically consist of at least two different materials (metallic wires and polymeric coating) with spiral wire strands as inner core. The complexity of the flexible structure increases further, as cables are usually assembled in bundles using tape, tubes or wrappings in automotive applications, see Figure 1, right. Thus, interactions between single cables and between cables and the casing occur and affect the resulting deformations of the structure leading to complex constitutive behavior. Furthermore, cables show anisotropic behavior due to their structure, e.g. their elastic stiffness parameters for bending, torsion and tension cannot be converted into each other. Thus, separate bending, torsion and tension experiments are necessary to characterize the deformation behavior of a cable, assuming their load cases are not coupled.

Cables and cable structures can be modeled using Cosserat rod models [1], where the constitutive laws are formulated in the sectional quantities of the rod. In continuum mechanics, constitutive laws yield the possibility to model different kinds of experimentally observed phenomena. Their model parameters connect the model to reality and can be determined using suitable experiments.

In section 2., the state of the art of experimental methods for cable structures will be explained. Recent developments in research on non-standard constitutive behavior of cable structures, constitutive models and their data-based parameterization will be outlined in section 3.

2. Experimental mechanics for cable structures

The experimentally observed deformation behavior of a structure and the specific application load case determine the choice of a suitable constitutive law. The experimenter will need to decide if the load case requires taking into account rate-dependent or hysteresis effects. Furthermore, the range of expected deformations is relevant, i.e. if the deformations will remain small or reach large values. Different load sequences will reveal different phenomena.

Experiments for highly flexible slender structures are inspired by experimental mechanics for elastic beams,

e.g. three-point bending, standard torsion or uniaxial tension [2]. In bending, however, large deformations can occur, such that experiments like standard three-point bending for small deflections are not sufficient to investigate the full range of practically relevant bending curvatures. To that end, bending load cases such as pure bending [2] or the geometrically non-linear bending load case presented in [3, 4] are better suited to investigate the bending behavior of flexible slender structures and parameterize suitable constitutive models, see Figure 2.

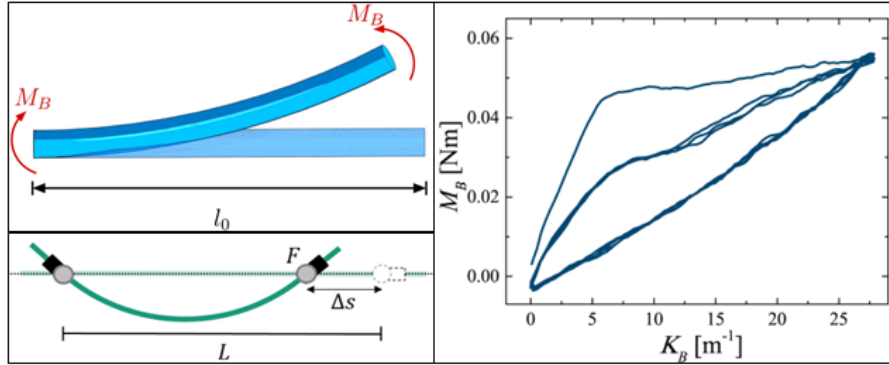


Figure 2: Left: Relevant bending load cases for cable structures: Pure bending (top) and geometrically non-linear bending (bottom). Right: Results of a cyclic pure bending experiment on a single cable.

Due to their complex multi-component structure, inelastic behavior has to be expected when cable structures exceed the range of small deformations. In order to investigate such effects properly, cyclic experiments have to be performed. Even for single cables, static hysteresis curves can be observed for a quasi-static experimental procedure, i.e. at sufficiently small deformation rates, see Figure 2 [5]. In dynamic load cases where rate-dependent behavior is relevant, experimental procedures need to be amended further. A practical approach to determine a suitable set of dynamic parameters in order to consider damping effects in dynamic cable simulations is given in [6].

3. Constitutive behavior of cable structures: Characteristics and parameterization

Despite the fact that experimental results show inelastic behavior when cable structures are deformed, it is state of the art in technical applications, e.g. in the software package IPS Cable Simulation [7], to consider only linear elastic behavior in quasi-static simulations. While this may seem like a drastic simplification, the linear elastic model will yield sufficiently accurate results for most applications, especially concerning the shape of the flexible slender structure [8]. The parameterization of linear elastic models for cable simulations using standard measurements is well established. However, the measurement of effective linear elastic model parameters for cable bundles is a time-consuming and tedious task, considering that in one car up to a hundred cable types are bundled together in several hundred different cable bundles. Thus, the estimation of effective cable bundle stiffnesses is desirable and was executed in [9]. Here, a data-based approach using Gaussian process regression was used to train models for the estimation of effective cable bundle stiffnesses based on easily available input such as single cable parameters and the used taping pattern. The data base used for training consisted of around 500 bundle data sets containing information about the bundle composition, the measured bundle stiffnesses and the measured parameters of the single cables in a bundle. The authors showed that this approach can be used to quickly estimate model parameters for cable bundles with sufficient accuracy, but without the necessity for further measurements once the model is trained. Interactions between single cables and cables and the casing are implicitly taken into account in this approach, as they influence the training data base.

In certain application cases, enhanced constitutive models are necessary, for example if more exact results for resulting forces or moments are required. Zhao et al. [3] propose a method to consider non-linear elastic behavior in a Cosserat rod model. They present a procedure to determine a state-dependent stiffness characteristic from experimental measurements using an inverse method. An iterative method is used to implement the non-linear characteristic in a two-dimensional Cosserat rod model, making it available for numerical simulations.

Model complexity will be increased even further, when cyclic loading and remaining (plastic) deformations

are relevant. Then, inelastic behavior typically needs to be considered. Due to their complex structure, (pseudo)damage and plasticity can occur. Inelastic constitutive laws for geometrically exact rods have been formulated based on the sectional quantities in [5] and [10]. In the former, pure bending experiments on a cable were the foundation for the parameter determination. Latest research activities consider a more flexible data-based modeling approach of inelastic effects utilizing hysteresis operators [11], which emulate inelastic effects in a generic, phenomenological manner without the need of a priori assumptions on the material behavior.

4. Conclusions

The present contribution gives an overview over experimental methods for cable structures as basis for constitutive modeling. Depending on the specific application, the relevant load case and observed effects, an appropriate constitutive model has to be chosen to connect simulations to reality. Furthermore, model parameters have to be accessible in experiments.

References

- [1] S.S. Antman. *Nonlinear Problems of Elasticity*, Springer, 2005.
- [2] V. Dörlich, J. Linn, S. Diebels. *Flexible beam-like structures – experimental investigation and modeling of cables*, Advances in Mechanics of Materials and Structural Analysis: In Honor of Reinhold Kienzler (2018) 27 – 46
- [3] T. Zhao, F. Schneider-Jung, J. Linn, R. Müller. *Simulating Nonlinear Elastic Behaviour of Cables Using an Iterative Method*, 8th European Congress on Computational Methods in Applied Sciences and Engineering, 2022.
- [4] MeSOMICS[®], www.mesomics.eu
- [5] V. Dörlich, P. Cesarek, J. Linn, S. Diebels. *Experimental investigation and numerical modeling of resultant-based bending plasticity in cables*, Proceedings of 8th ECCOMAS Thematic Conference on Multibody Dynamics, 2017.
- [6] D. Jungkenn, F. Schneider-Jung, F. Andersson, J. Linn. *Realistic parameters for dynamic simulation of composite cables using a damped Cosserat rod model*, ECCOMAS Thematic Conference on Multibody Dynamics, 2021.
- [7] IPS Cable Simulation, <https://flexstructures.com/products/ips-cable-simulation/>
- [8] V. Dörlich, J. Linn, T. Scheffer, S. Diebels. *Towards viscoplastic constitutive models for cosserat rods*, Archive of Mechanical Engineering, 63 (2016) 215–230
- [9] L. Burger, V. Dörlich, M. Burger, J. Linn, F. Schneider. *Estimation of Cable Bundle Stiffness Based on Gaussian Process Regression*, In: Ehrhardt, M., Günther, M. (eds) Progress in Industrial Mathematics at ECMI 2021, Springer, Mathematics in Industry, 39 (2021)
- [10] O. Weeger, D. Schillinger, R. Müller. *Mixed isogeometric collocation for geometrically exact 3D beams with elasto-visco-plastic material behavior and softening effects*, Computer Methods in Applied Mechanics and Engineering, 399 (2022)
- [11] D. Manfredo, V. Dörlich, J. Linn, M. Arnold. *Data based constitutive modelling of rate independent inelastic effects in composite cables using Preisach hysteresis operators*, Multibody System Dynamics (2023)

How relaxation of compatibility in time can simplify the floating frame of reference formulation in flexible multibody dynamics

Michel Géradin¹

¹ University of Liège, Belgium and Institute for Advanced Study, Technical University of Munich, Germany

Keywords: flexible multibody dynamics, two-field formulation, substructuring, rotating systems.

1. Introduction

Most formulations of flexible multibody dynamics are based on the assumption that the elastic velocity is the partial time derivative of the kinematic field. As a result, the set of equilibrium equations governing the dynamics of the system is a set of second-order equations in time in the form

$$\mathbf{f}(\mathbf{q}, \dot{\mathbf{q}}, \ddot{\mathbf{q}}) + \mathbf{B}^T \boldsymbol{\lambda} = \mathbf{p}(t) \quad (1)$$

which is classically solved using a time integration scheme adapted to second-order system. Complexity of their explicit expression arises from the convection terms resulting from the large rotations in the system. Such complexity can be reduced by relaxing compatibility in time, thus recasting the second-order equation system (1) in the two-field form

$$\mathbf{f}(\mathbf{q}, \dot{\mathbf{q}}, \mathbf{v}, \dot{\mathbf{v}}) + \mathbf{B}^T \boldsymbol{\lambda} = \mathbf{p}(t) \quad (2)$$

$$\mathbf{v} = \mathbf{h}(\mathbf{q}, \dot{\mathbf{q}}) \quad (3)$$

where the discretized kinematic and velocity fields \mathbf{q} and \mathbf{v} are treated as independent, and with $\mathbf{h}(\mathbf{q}, \dot{\mathbf{q}})$ being an appropriate expression of generalized velocity which arises naturally from the development of the time derivative of the kinematic field.

2. Floating frame of reference formulation of an elastic body undergoing uniform rotation

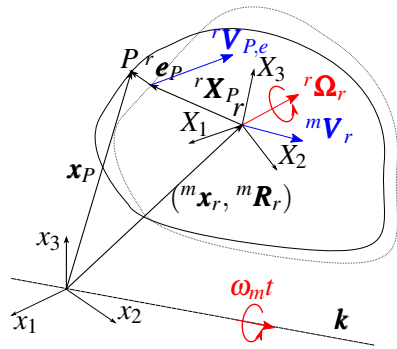


Figure 1: Kinematic description of a deformable body in a rotating frame.

The general motion \mathbf{x}_P of a flexible body undergoing rotation with uniform angular velocity ω_m about a rotation axis \mathbf{k} will be decomposed into 3 successive frame transformations: rotation motion $\mathbf{R}(\omega_m t)$ at constant angular velocity, rigid motion $({}^m \mathbf{x}_r, {}^m \mathbf{R}_r)$ of a body frame r relative to the rotating frame, and elastic motion ${}^r \mathbf{e}_P$ relative to the body frame:

$$\mathbf{x}_P = \mathbf{R}_m(\mathbf{k}\omega_m t)({}^m \mathbf{x}_r + {}^m \mathbf{R}_r({}^r \mathbf{X}_P + {}^r \mathbf{e}_P)) \quad (4)$$

and the associated velocity field can be split in the form

	Velocity	Motion field derivative
Frame translation	${}^m \mathbf{V}_r$	${}^m \dot{\mathbf{x}}_r + \tilde{\omega}_m {}^m \mathbf{x}_r$
Frame rotation	${}^r \tilde{\boldsymbol{\Omega}}_r$	${}^m \mathbf{R}_r^T ({}^m \dot{\mathbf{R}}_r + {}^r \tilde{\omega}_m {}^m \mathbf{R}_r)$
Elastic motion	${}^r \mathbf{V}_{P,e}$	${}^r \dot{\mathbf{e}}_P + ({}^m \mathbf{R}_r^T ({}^m \dot{\mathbf{R}}_r + {}^r \tilde{\omega}_m {}^m \mathbf{R}_r)) {}^r \mathbf{e}_P$

It can be shown that the dual form of kinetic energy can be obtained in the fully uncoupled form [1]

$$\mathcal{K}^*({}^m \mathbf{V}_r, {}^r \boldsymbol{\Omega}_r, {}^r \mathbf{V}_{P,e}) = \frac{1}{2} m_B {}^m \mathbf{V}_r^T {}^m \mathbf{V}_r + \frac{1}{2} {}^r \boldsymbol{\Omega}_r^T \mathbf{J} {}^r \boldsymbol{\Omega}_r + \frac{1}{2} \int_V {}^r \mathbf{V}_{P,e}^T {}^r \mathbf{V}_{P,e} \rho dV \quad (5)$$

provided that the essential condition of orthogonality $\int_V {}^r \mathbf{V}_{P,e}^T \mathbf{U} \rho dV = \mathbf{0}$ between velocity and rigid body motions fields is fulfilled, and with m_B and \mathbf{J} being the mass and tensor of inertia of the body about its center of mass.

The two-field formulation results then from a Legendre transformation [2] by which the kinetic energy is expressed in the mixed form

$$\begin{aligned} \mathcal{H}^{\star\star}({}^m\mathbf{x}_r, {}^m\mathbf{R}_r, {}^r\mathbf{e}_P, {}^m\mathbf{V}_r, {}^r\mathbf{\Omega}_r, {}^r\mathbf{V}_{P,e}) &= \frac{1}{2}m_B {}^m\mathbf{V}_r^T ({}^m\dot{\mathbf{x}}_r + \tilde{\boldsymbol{\omega}}_m {}^m\mathbf{x}_r) + \frac{1}{2}{}^r\mathbf{\Omega}_r^T \mathbf{J} ({}^r\boldsymbol{\omega}_m + {}^r\mathbf{W}_r) \\ &+ \frac{1}{2} \int_V {}^r\mathbf{V}_{P,e}^T ({}^r\mathbf{e}_P + ({}^r\tilde{\boldsymbol{\omega}}_m + {}^r\tilde{\mathbf{W}}_r) {}^r\mathbf{e}_P) \rho dV - \mathcal{H}^{\star}({}^m\mathbf{V}_r, {}^r\mathbf{\Omega}_r, {}^r\mathbf{V}_{P,e}) \end{aligned} \quad (6)$$

with, for sake of conciseness, the angular velocity notations ${}^r\boldsymbol{\omega}_m = {}^m\mathbf{R}_r^T \boldsymbol{\omega}_m$ and ${}^r\tilde{\mathbf{W}}_r = {}^m\mathbf{R}_r^T {}^m\dot{\mathbf{R}}_r$.

3. Finite element discretization

Finite discretization is achieved using a $3 \times n$ set $\mathbf{N} = \text{diag}(\mathbf{N}_1, \mathbf{N}_2, \mathbf{N}_3)$ of shape functions to discretize the elastic motion and velocity fields

$${}^r\mathbf{e}_P = \mathbf{N}\mathbf{q} \quad \text{and} \quad {}^r\mathbf{V}_{P,e} = \mathbf{N}\mathbf{v} \quad (7)$$

The discretized equations of motion are then described in terms of the mass and stiffness matrices \mathbf{K} and \mathbf{M} and the matrices of gyroscopic origin $\mathbf{G}({}^r\boldsymbol{\omega}_m + {}^r\mathbf{W}_r)$, $\mathbf{A}({}^r\boldsymbol{\omega}_m + {}^r\mathbf{W}_r)$, $\mathbf{S}(\mathbf{q})$ and $\mathbf{S}(\mathbf{v})$. We get the contributions

	time compatibility	equilibrium
CM translation	${}^m\mathbf{V}_r = {}^m\dot{\mathbf{x}}_r + \tilde{\boldsymbol{\omega}}_m {}^m\mathbf{x}_r$	$-m_B ({}^m\dot{\mathbf{V}}_r + \tilde{\boldsymbol{\omega}}_m {}^m\mathbf{V}_r) - m_B \tilde{\boldsymbol{\omega}}_m {}^m\mathbf{V}_r$
CM rotation	${}^r\mathbf{\Omega}_r = {}^r\boldsymbol{\omega}_m + {}^r\mathbf{W}_r$	$-{}^r\mathbf{J}\dot{\mathbf{\Omega}}_r - ({}^r\tilde{\mathbf{W}}_r + {}^r\tilde{\boldsymbol{\omega}}_m)({}^r\mathbf{J}\mathbf{\Omega}_r + \mathbf{S}(\mathbf{q})\mathbf{v}) - \mathbf{S}(\mathbf{q})\dot{\mathbf{v}} + \mathbf{S}(\mathbf{v})\dot{\mathbf{q}}$
elastic kernel	$\mathbf{v} = \dot{\mathbf{q}} + \mathbf{A}({}^r\boldsymbol{\omega}_m + {}^r\mathbf{W}_r)\mathbf{q}$	$-\mathbf{K}\mathbf{q} - \mathbf{M}\dot{\mathbf{v}} - \mathbf{G}({}^r\boldsymbol{\omega}_m + {}^r\mathbf{W}_r)\mathbf{v} = \mathbf{0}$

The expression of the gyroscopic matrices \mathbf{G} , \mathbf{A} and \mathbf{S} becomes quite simple in the case when the choice of shape functions is isotropic: $\mathbf{N}_i = \mathbf{N}^*$, $i = 1, 2, 3$, as it is the case for 3-D solid modeling. They can then be written in terms of the one-dimensional mass kernel

$$\mathbf{M}^* = \int_V \mathbf{N}^{\star T} \mathbf{N}^* \rho dV \quad \text{and the associated } \mathbf{S}_i \text{ matrices} \quad \mathbf{S}_i = \varepsilon_{ijk} \mathbf{L}_j^T \mathbf{M}^* \mathbf{L}_k \quad i = 1, 2, 3 \quad (8)$$

where \mathbf{L}_j are Boolean matrices allowing component-wise splitting of \mathbf{q} and \mathbf{v} . We get then, with $\boldsymbol{\alpha} = {}^r\boldsymbol{\omega}_m + {}^r\mathbf{W}_r$,

$$\mathbf{A}(\boldsymbol{\alpha}) = \text{diag}(\tilde{\boldsymbol{\alpha}}), \quad \mathbf{S}(\mathbf{q})\mathbf{v} = [\mathbf{q}^T \mathbf{S}_i \mathbf{v}] = -\mathbf{S}(\mathbf{v})\mathbf{q}, \quad \mathbf{G}(\boldsymbol{\alpha}) = -\sum_i \alpha_i \mathbf{S}_i \quad (9)$$

4. Conclusion

Relaxing compatibility in time allows simplifying the floating frame of reference formulation of an elastic body. It can be shown [1] that the resulting motion equations can easily be reduced to superelement form using Herting's modal synthesis method [3]. In the oral presentation, the example of a flexible system rotating at high speed will be presented to demonstrate the efficiency of the proposed methodology.

Acknowledgments

The author acknowledges support from the Technical University of Munich—Institute for Advanced Study.

References

- [1] Michel Géradin and Valentin Sonneville. A two-field approach to multibody dynamics of rotating flexible bodies. *Multibody System Dynamics*, pages 1–41, 2023.
- [2] R Courant and Hilbert D. *Methods of mathematical physics*, volume 2. Interscience Publishers, New York, 1962.
- [3] DN Herting. A general purpose, multi-stage, component modal synthesis method. *Finite elements in analysis and design*, 1(2):153–164, 1985.

Group-Equivariant and Cochain Projection Based Variational Discretizations of Lagrangian PDEs

Melvin Leok¹

¹ University of California, San Diego, mleok@ucsd.edu

Keywords: Variational Integrators, Compatible Discretization, Geometric Integration, Field Theories, Structure-Preservation

1. Introduction

Compatible discretizations, such as finite element exterior calculus, provide a discretization framework that respect the cohomological structure of the de Rham complex, which can be used to systematically construct stable mixed finite element methods. Multisymplectic variational integrators are a class of geometric numerical integrators for Lagrangian and Hamiltonian field theories, and they yield methods that preserve the multisymplectic structure and momentum-conservation properties of the continuous system. We investigate the synthesis of these two approaches, by constructing discretization of the variational principle for Lagrangian field theories utilizing structure-preserving finite element projections. In our investigation, compatible discretization by cochain projections plays a pivotal role in the preservation of the variational structure at the discrete level, allowing the discrete variational structure to essentially be the restriction of the continuum variational structure to a finite-dimensional subspace. The preservation of the variational structure at the discrete level will allow us to construct a discrete Cartan form, which encodes the variational structure of the discrete theory, and subsequently, we utilize the discrete Cartan form to naturally state discrete analogues of Noether’s theorem and multisymplecticity, which generalize those introduced in the discrete Lagrangian variational framework by Marsden et al. [1]. We will study both covariant spacetime discretization and canonical spatial semi-discretization, and subsequently relate the two in the case of spacetime tensor product finite element spaces.

2. Multisymplectic Formulation of Classical Field Theories

The variational principle for Lagrangian PDEs involve a multisymplectic formulation [1, 2]. The base space X consists of independent variables, denoted by $(x^0, \dots, x^n) \equiv (t, x)$, where $x^0 \equiv t$ is time, and $(x^1, \dots, x^n) \equiv x$ are space variables. The dependent field variables, $(y^1, \dots, y^m) \equiv y$, form a fiber over each spacetime basepoint. The independent and field variables form the configuration bundle, $\pi : Y \rightarrow X$. The configuration of the system is specified by a section of Y over X , which is a continuous map $\phi : X \rightarrow Y$, such that $\pi \circ \phi = 1_X$. This means that for every $(t, x) \in X$, $\phi((t, x))$ is in the fiber $\pi^{-1}((t, x))$ over (t, x) .

For ODEs, the Lagrangian depends on position and its time derivative, which is an element of the tangent bundle TQ , and the action is obtained by integrating the Lagrangian in time. In the multisymplectic case, the Lagrangian density is dependent on the field variables and the partial derivatives of the field variables with respect to the spacetime variables, and the action integral is obtained by integrating the Lagrangian density over a region of spacetime. The multisymplectic analogue of the tangent bundle is the first jet bundle J^1Y , consisting of the configuration bundle Y , and the first partial derivatives of the field variables with respect to the independent variables. In coordinates, we have $\phi(x^0, \dots, x^n) = (x^0, \dots, x^n, y^1, \dots, y^m)$, which allows us to denote the partial derivatives by $v_{\mu}^a = y^a_{,\mu} = \partial y^a / \partial x^{\mu}$. We can think of J^1Y as a fiber bundle over X . Given a section $\phi : X \rightarrow Y$, we obtain its first jet extension, $j^1\phi : X \rightarrow J^1Y$, that is given by

$$j^1\phi(x^0, \dots, x^n) = (x^0, \dots, x^n, y^1, \dots, y^m, y^1_{,0}, \dots, y^m_{,n}),$$

which is a section of the fiber bundle J^1Y over X . We refer to sections of J^1Y of the form $j^1\phi$, where ϕ is a section of Y , as holonomic. The configuration space is the space of sections of Y and the velocity phase space is the space of holonomic sections of J^1Y . The Lagrangian density is a bundle map $\mathcal{L} : J^1Y \rightarrow \wedge^{n+1}(T^*X)$ and hence, induces a map on the space of sections $\mathcal{L} : \Gamma(J^1Y) \rightarrow \Omega^{n+1}(X)$. Thus, we can define the action functional $S : \Gamma(Y) \rightarrow \mathbb{R}$ by $S[\phi] = \int_X \mathcal{L}(j^1\phi)$. Hamilton’s principle states that $\delta S = 0$, subject to compactly supported variations. As we will see, this is the basis of Lagrangian multisymplectic variational integrators [1].

The variational structure of a Lagrangian field theory is given by the Cartan form, which in coordinates has the expression

$$\Theta_{\mathcal{L}} = \frac{\partial L}{\partial v_{\mu}^a} dy^a \wedge d^n x_{\mu} + \left(L - \frac{\partial L}{\partial v_{\mu}^a} v_{\mu}^a \right) d^{n+1}x. \quad (1)$$

This can be defined intrinsically as the pullback of the canonical $(n+1)$ -form on the dual jet bundle by the covariant Legendre transform $\mathbb{F}\mathcal{L} : J^1Y \rightarrow J^1Y^*$. Then, the action can be expressed as $S[\phi] = \int_X \mathcal{L}(j^1\phi) = \int_X (j^1\phi)^* \Theta_{\mathcal{L}}$. The variation of the action is then expressed as

$$dS[\phi] \cdot V = - \int_X (j^1\phi)^* (j^1V \lrcorner \Omega_{\mathcal{L}}) + \int_{\partial X} (j^1\phi)^* (j^1V \lrcorner \Theta_{\mathcal{L}}),$$

where $\Omega_{\mathcal{L}} = -d\Theta_{\mathcal{L}}$ defines the multisymplectic form and j^1V denotes the jet prolongation of the vector field V (for details, see [3]). Hence, the variation of the action is completely specified by the Cartan form; we will show that a finite element discretization of the variational principle gives rise to a discrete form and subsequently we will express variational properties of the discrete system in terms of the discrete Cartan form.

3. Finite Element Exterior Calculus

The notion of compatible discretization is a research area that has garnered significant interest and activity in the finite element community, motivated by the seminal work of Arnold et al. [4] on finite element exterior calculus that provides a broad generalization of Hiptmair's work on mixed finite elements for electromagnetism [5]. This arises from the fundamental role that the de Rham complex of exterior differential forms plays in mixed formulations of elliptic partial differential equations, and the realization that many of the most successful mixed finite element spaces, such as Raviart–Thomas and Nédélec elements, can be viewed as finite element subspaces of the de Rham complex that satisfy a bounded cochain projection property, so that the set of mixed finite elements form a subcomplex that provides stable approximations of the original problem.

4. Group-equivariant interpolation

The study of group-equivariant approximation spaces [6] for functions taking values on manifolds is motivated by the applications to geometric structure-preserving discretization of Lagrangian and Hamiltonian PDEs with symmetries. In particular, when the Lagrangian density for a Lagrangian PDE with symmetry is discretized using a Lagrangian multisymplectic variational integrator constructed from an approximation space that is equivariant with respect to the symmetry group, the resulting numerical method automatically preserves the momentum map associated with the symmetry of the PDE. In essence, such variational discretizations exhibit a discrete analogue of Noether's theorem, which connects symmetries of the Lagrangian with momentum conservation laws.

Many intrinsic geometric flows such as the Ricci flow and the Einstein equations involves computing the evolution of a Riemannian or pseudo-Riemannian metric on spacetime. Additionally, these intrinsic geometric flows can often be formulated variationally, so it is natural to consider group-equivariant approximation spaces taking values on Riemannian or pseudo-Riemannian metrics with a view towards constructing variational discretizations that preserve the associated momentum maps.

A now standard approach to constructing an approximation space for functions taking values on a Riemannian manifold that is equivariant with respect to Riemannian isometries is the method of geodesic finite elements introduced independently by Sander [7] and Grohs [8]. Given a Riemannian manifold (M, g) , the geodesic finite element $\varphi : \Delta^n \rightarrow M$ associated with a set of linear space finite elements $\{v_i : \Delta^n \rightarrow \mathbb{R}\}_{i=0}^n$ is given by the Fréchet (or Karcher) mean,

$$\varphi(x) = \arg \min_{p \in M} \sum_{i=0}^n v_i(x) (\text{dist}(p, m_i))^2,$$

where the optimization problem involved can be solved using optimization algorithms developed for matrix manifolds (see Absil et al. [9], and references therein). The spatial derivatives of the geodesic finite element can be computed in terms of an associated optimization problem. The advantage of the geodesic finite element approach is that it inherits the approximation properties of the underlying linear space finite element, but it can be expensive to compute, since it entails solving an optimization problem on a manifold.

An alternative approach to group-equivariant interpolation for functions taking values on symmetric spaces was introduced in Gawlik and Leok [6], which, in particular, is applicable to the interpolation of Riemannian and pseudo-Riemannian metrics. It uses the generalized polar decomposition [10] to construct a local diffeomorphism between a symmetric space and a Lie triple system, and thereby lift a scalar-valued interpolant to a symmetric space-valued interpolant.

5. Lagrangian Variational Integrators

Variational integrators (see [11], and references therein) are a class of geometric structure-preserving numerical integrators that are based on a discretization of Hamilton's principle. They are particularly appropriate for the simulation of Lagrangian and Hamiltonian ODEs and PDEs, as they automatically preserve many geometric invariants, including the symplectic structure, momentum maps associated with symmetries of the system, and exhibit bounded energy errors for exponentially long times.

In the case of Lagrangian ODEs, variational integrators are based on constructing computable approximations $L_d : Q \times Q \rightarrow \mathbb{R}$ of the exact discrete Lagrangian,

$$L_d^E(q_0, q_1, h) = \text{ext}_{\substack{q \in C^2([0, h], Q) \\ q(0) = q_0, q(h) = q_1}} \int_0^h L(q(t), \dot{q}(t)) dt,$$

which can be viewed as Jacobi's solution of the Hamilton–Jacobi equation. Given a discrete Lagrangian L_d , one introduces the discrete action sum $\mathbb{S}_d = \sum_{k=0}^{n-1} L_d(q_k, q_{k+1})$, and then the discrete Hamilton's principle states that $\delta \mathbb{S}_d = 0$, for fixed boundary conditions q_0 and q_n . This leads to the discrete Euler–Lagrange equations,

$$D_2 L_d(q_{k-1}, q_k) + D_1 L_d(q_k, q_{k+1}) = 0,$$

where D_i denotes the partial derivative with respect to the i -th argument. This implicitly defines the discrete Lagrangian map $F_{L_d} : (q_{k-1}, q_k) \mapsto (q_k, q_{k+1})$ for initial conditions (q_{k-1}, q_k) that are sufficiently close to the diagonal of $Q \times Q$. It is also equivalent to the implicit discrete Euler–Lagrange equations,

$$p_k = -D_1 L_d(q_k, q_{k+1}), \quad p_{k+1} = D_2 L_d(q_k, q_{k+1}),$$

which implicitly defines the discrete Hamiltonian map $\tilde{F}_{L_d} : (q_k, p_k) \mapsto (q_{k+1}, p_{k+1})$, which is automatically symplectic. This clearly follows from the fact that these equations are precisely the characterization of a symplectic map in terms of a Type I generating function. The two equations in the implicit discrete Euler–Lagrange equations can be used to define the discrete Legendre transforms, $\mathbb{F}^\pm L_d : Q \times Q \rightarrow T^*Q$:

$$\begin{aligned} \mathbb{F}^+ L_d : (q_0, q_1) &\rightarrow (q_1, p_1) = (q_1, D_2 L_d(q_0, q_1)), \\ \mathbb{F}^- L_d : (q_0, q_1) &\rightarrow (q_0, p_0) = (q_0, -D_1 L_d(q_0, q_1)). \end{aligned}$$

The following commutative diagram illustrates the relationship between the discrete Hamiltonian flow map, discrete Lagrangian flow map, and the discrete Legendre transforms,

$$\begin{array}{ccccc} & & (q_k, p_k) & \xrightarrow{\tilde{F}_{L_d}} & (q_{k+1}, p_{k+1}) & & \\ & \nearrow \mathbb{F}^+ L_d & & & & \nwarrow \mathbb{F}^- L_d & \\ & & & & & & \\ (q_{k-1}, q_k) & \xrightarrow{F_{L_d}} & (q_k, q_{k+1}) & \xrightarrow{F_{L_d}} & (q_{k+1}, q_{k+2}) & & \\ & \nwarrow \mathbb{F}^- L_d & & & \nearrow \mathbb{F}^+ L_d & & \end{array}$$

If the discrete Lagrangian is invariant under the diagonal action of a Lie group G , i.e., $L_d(q_0, q_1) = L_d(gq_0, gq_1)$, for all $g \in G$, then the discrete Noether's theorem states that there is a discrete momentum map that is automatically preserved by the variational integrator. The bounded energy error of variational integrators can be understood by performing backward error analysis [12, 13], which then shows that the discrete flow map is approximated with exponential accuracy by the exact flow map of the Hamiltonian vector field of a modified Hamiltonian. Similarly, backward error analysis for Lagrangian variational integrators is considered in [14].

6. Multisymplectic Hamiltonian Variational Integrators.

For Hamiltonian PDEs (see, for example, Marsden and Shkoller [15]) the action is a functional on the field and multimomenta values (more precisely, sections of the restricted dual jet bundle),

$$S[\phi, p] = \int [p^\mu \partial_\mu \phi - H(\phi, p)] d^{n+1}x,$$

where the integration is over some $(n+1)$ -dimensional region of spacetime. The variational principle gives the De Donder–Weyl equations $\partial_\mu p^\mu = -\partial H/\partial \phi$, $\partial_\mu \phi = \partial H/\partial p^\mu$. Defining $z = (\phi, p^0, \dots, p^n)$ and K^μ as the $(n+2) \times (n+2)$ skew-symmetric matrix with value -1 in the $(0, \mu+1)$ entry, 1 in the $(\mu+1, 0)$ entry, and 0 in every other entry (with indexing from 0 to $n+1$), the De Donder–Weyl equations can be written in the form

$$K^0 \partial_0 z + \dots + K^n \partial_n z = \nabla_z H.$$

This formulation of Hamiltonian PDEs was studied in Bridges [16]; in particular, it was shown that such a system admits a multisymplectic conservation law of the form $\partial_\mu \omega^\mu(V, W) = 0$, where the ω^μ are two-forms corresponding to K^μ and the conservation law holds when evaluated on first variations V, W . For discretizing such equations, multisymplectic integrators have been developed which admit a discrete analogue of this multisymplectic conservation law (see, for example, Bridges and Reich [17]). Such multisymplectic integrators have traditionally not been approached from a variational perspective.

However, in Tran and Leok [18], we developed a systematic method for constructing variational integrators for multisymplectic Hamiltonian PDEs which automatically admit a discrete multisymplectic conservation law and a discrete Noether’s theorem by virtue of the discrete variational principle. The construction is based on a discrete approximation of the boundary Hamiltonian that was introduced in Vankerschaver et al. [19],

$$H_{\partial U}(\varphi_A, \pi_B) = \text{ext} \left[\int_B p^\mu \phi d^n x_\mu - \int_U (p^\mu \partial_\mu \phi - H(\phi, p)) d^{n+1}x \right],$$

where $\partial U = A \sqcup B$, boundary conditions are placed on the field value ϕ on A and normal momenta value on B , and one extremizes over the sections (ϕ, p) over U satisfying the specified boundary conditions. The boundary Hamiltonian is a generating functional in the sense that the Type II variational principle generates the normal momenta value along A and the field value along B ,

$$\frac{\delta H_{\partial U}}{\delta \varphi_A} = -p^n|_A, \quad \frac{\delta H_{\partial U}}{\delta \pi_B} = \phi|_B.$$

A variational integrator is then constructed by first approximating the boundary Hamiltonian using a finite-dimensional function space and quadrature, and subsequently enforcing the Type II variational principle. For example, with particular choices of function spaces and quadrature, Tran and Leok [18] recover the class of multisymplectic partitioned Runge–Kutta methods.

We take a different approach in several regards. First, we focus on Lagrangian field theories as opposed to Hamiltonian field theories. For Hamiltonian field theories, the momenta are related to the field and its derivative by the Legendre transform; this falls out from the variational principle so one does not need to enforce it beforehand. Thus, in this sense, the momenta and field values can be considered as independent before enforcing the variational principle. On the other hand, for Lagrangian field theories, the Lagrangian depends on both the field value and its first derivative, so one cannot naively treat the two as independent; that is, the Lagrangian depends on holonomic sections of the jet bundle. As we will see, this will mean that we need to pay particular attention to the holonomic condition when discretizing via a finite element projection. Furthermore, as opposed to constructing variational integrators from a generating functional (the analogue in the Lagrangian framework would be the boundary Lagrangian, see Vankerschaver et al. [19]), we instead investigate directly discretizing the variational principle $\delta S = 0$ utilizing projections into finite-dimensional subspaces. Finally, for simplicity, we do not utilize any quadrature approximations of the various integrals which we encounter; for strong nonlinearities in the Lagrangian, one generally has to utilize quadrature to construct an efficient discretization. We will assume exact integration in order to keep the exposition simple, but the theory that we outline is also applicable to the case of quadrature approximation by first applying the quadrature approximation of the action before enforcing the variational principle, so that the resulting discretization is still variational.

7. Main Contributions

We study the variational finite element discretization of Lagrangian field theories from two perspectives; we begin by investigating directly discretizing the full variational principle over the full spacetime domain, which we refer to as the “covariant” approach, and subsequently study semi-discretization of the instantaneous variational principle on a globally hyperbolic spacetime, which we refer to as the “canonical” approach. This can be considered a discrete analogue to the program initiated in Gotay et al. [3, 20], which lays the foundation for relating the covariant and canonical formulations of Lagrangian field theories through their (multi)symplectic structures and momentum maps. One of the goals of understanding the relation between these two different formulations is to systematically relate the covariant gauge symmetries of a gauge field theory to its initial value constraints. This is seen, for example, in general relativity, where the diffeomorphism gauge invariance gives rise to the Einstein constraint equations over the initial data hypersurface (see, for example,ourgoulhon [21]). When one semi-discretizes such gauge field theories, the discrete initial data must satisfy an associated discrete constraint. We aim to make sense of the discrete geometric structures in the covariant and canonical discretization approaches as a foundation for understanding the discretization of gauge field theories.

Acknowledgments

This project was supported by NSF under grants DMS-1411792, DMS-1345013, DMS-1813635, DMS-2307801, by AFOSR under grants FA9550-18-1-0288, FA9550-23-1-0279, and by the DoD under grant 13106725 (Newton Award for Transformative Ideas during the COVID-19 Pandemic).

References

- [1] J. E. Marsden, G. W. Patrick, and S. Shkoller. Multisymplectic geometry, variational integrators, and nonlinear PDEs. *Commun. Math. Phys.*, 199(2):351–395, 1998.
- [2] J. E. Marsden, S. Pekarsky, S. Shkoller, and M. West. Variational methods, multisymplectic geometry and continuum mechanics. *J. Geom. Phys.*, 38(3-4):253–284, 2001.
- [3] M. J. Gotay, J. Isenberg, J. E. Marsden, and R. Montgomery. Momentum maps and classical relativistic fields. Part I: Covariant field theory. (preprint, [arXiv:physics/9801019 \[math-ph\]](https://arxiv.org/abs/physics/9801019)), 1998.
- [4] D. N. Arnold, R. S. Falk, and R. Winther. Finite element exterior calculus, homological techniques, and applications. *Acta Numer.*, 15:1–155, 2006.
- [5] R. Hiptmair. Finite elements in computational electromagnetism. *Acta Numerica*, 11:237–339, 2002.
- [6] E. S. Gawlik and M. Leok. Interpolation on symmetric spaces via the generalized polar decomposition. *Found. Comput. Math.*, 18(3):757–788, 2018.
- [7] O. Sander. Geodesic finite elements on simplicial grids. *Int. J. Numer. Meth. Eng.*, 92(12):999–1025, 2012.
- [8] P. Grohs. Quasi-interpolation in Riemannian manifolds. *IMA J. Numer. Anal.*, 33(3):849–874, 2013.
- [9] P.-A. Absil, R. Mahony, and R. Sepulchre. *Optimization Algorithms on Matrix Manifolds*. Princeton University Press, Princeton, NJ, 2008.
- [10] H. Z. Munthe-Kaas, G. R. W. Quispel, and A. Zanna. Generalized polar decompositions on Lie groups with involutive automorphisms. *Found. Comput. Math.*, 1(3):297–324, 2001.
- [11] J. E. Marsden and M. West. Discrete mechanics and variational integrators. *Acta Numer.*, 10:317–514, 2001.
- [12] E. Hairer. Backward analysis of numerical integrators and symplectic methods. *Ann. Numer. Math.*, 1:107–132, 1994.
- [13] G. Benettin and A. Giorgilli. On the Hamiltonian interpolation of near to the identity symplectic mappings with application to symplectic integration algorithms. *J. Stat. Phys.*, 74:1117–1143, 1994.
- [14] Mats Vermeeren. Modified equations for variational integrators. *Numer. Math.*, 137:1001 – 1037, 2017.
- [15] J. E. Marsden and S. Shkoller. Multisymplectic geometry, covariant Hamiltonians, and water waves. *Mathematical Proceedings of the Cambridge Philosophical Society*, 125(3):553–575, 1999.

- [16] T. J. Bridges. Multi-symplectic structures and wave propagation. *Math. Proc. Cambridge Philos. Soc.*, 121(1):147–190, 1997.
- [17] T. J. Bridges and S. Reich. Numerical methods for Hamiltonian PDEs. *Journal of Physics A: Mathematical and General*, 39(19):5287–5320, apr 2006.
- [18] B. Tran and M. Leok. Multisymplectic Hamiltonian variational integrators. *International Journal of Computer Mathematics (Special Issue on Geometric Numerical Integration, Twenty-Five Years Later)*, 99(1):113–157, 2022.
- [19] J. Vankerschaver, C. Liao, and M. Leok. Generating functionals and Lagrangian partial differential equations. *J. Math. Phys.*, 54(8):082901 (22 pages), 2013.
- [20] M. J. Gotay, J. Isenberg, J. E. Marsden, and R. Montgomery. Momentum maps and classical relativistic fields. Part II: Canonical analysis of field theories. (preprint, [arXiv:physics/0411032\[math-ph\]](https://arxiv.org/abs/physics/0411032)), 2004.
- [21] E.ourgoulhon. 3+1 formalism in general relativity. *Lecture Notes in Physics*, 846, 2012.

Generalized Interaction Potentials in the Geometrically Exact Beam Theory

Christoph Meier¹, Maximilian J. Grill¹, Wolfgang A. Wall¹

¹ Institute for Computational Mechanics, Technical University of Munich
christoph.anton.meier@tum.de / maximilian.grill@tum.de / wolfgang.a.wall@tum.de

Keywords: Geometrically Exact Beam Theory, Generalized Interaction Potentials, Inter-Molecular Forces

The talk presents a universal framework to formulate generalized section-section interaction potentials (SSIP) within the geometrically exact beam theory [1]. By exploiting the fundamental kinematic assumption of undeformable cross-sections, an objective (i.e., frame-invariant) description of SSIPs via a minimal set of six (translational and rotational) relative coordinates, either in spatial or in material form, is proposed. Based on work-pairing, work-conjugated section-section interaction forces and moments, either in spatial or in material form, are identified that can be consistently derived from a variational principle. Interestingly, it is shown that hyperelastic stored-energy functions relating the deformation measures and stress-resultants of the well-known geometrically exact Simo-Reissner beam theory can also be identified as SSIPs when considering the asymptotic limit of small relative distances and rotations between the interacting cross-sections. Moreover, the proposed variational problem formulation is demonstrated to be of a very general nature, thus allowing for the formulation of translational and rotational constraints between arbitrarily oriented cross-sections based on either a penalty or a Lagrange multiplier potential. Applications include fiber-based structures and materials in technical and biological systems, where the proposed approach allows to model short- or long-ranged intermolecular (e.g., electrostatic, van der Waals or repulsive steric) interactions between fibers in geometrically complex arrangements (see Figure 1(b)) and to formulate translational and rotational coupling constraints between different fibers (e.g., cross-linked polymer chains) or between fibers and a matrix phase (see Figure 1(a)).

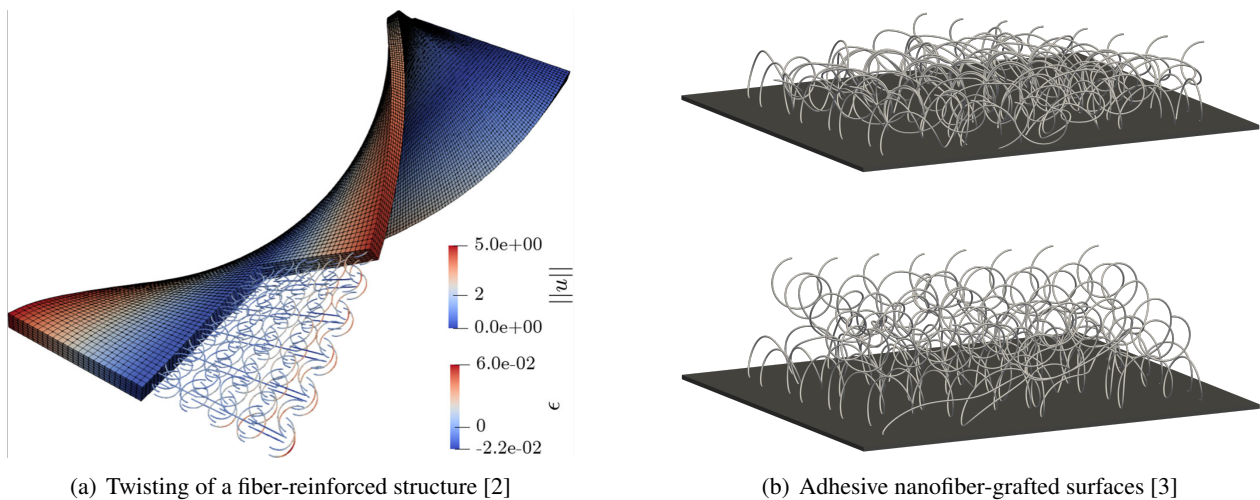


Figure 1: Potential application scenarios for generalized section-section interaction potentials

References

- [1] C. Meier, M.J. Grill, W.A. Wall. *Generalized section–section interaction potentials in the geometrically exact beam theory: Modeling of intermolecular forces, asymptotic limit as strain-energy function, and formulation of rotational constraints*, International Journal of Solids and Structures 276 (2023) 112255
- [2] I. Steinbrecher, A. Popp, C. Meier. *Consistent coupling of positions and rotations for embedding 1D Cosserat beams into 3D solid volumes*, Computational Mechanics 69 (2022) 701-732
- [3] M.J. Grill, W.A. Wall, C. Meier. *Asymptotically consistent and computationally efficient modeling of short-ranged molecular interactions between curved slender fibers undergoing large 3D deformations*, submitted for publication, arXiv preprint arXiv:2208.03149

Using the special Euclidean group to model flexible multibody systems

Valentin Sonneville

Chair of Applied Mechanics, Technical University of Munich,
Boltzmannstr. 15, 85748 Garching, Germany
valentin.sonneville@tum.de

Keywords: Modeling, Local Frames, Numerical methods, Lie group

This presentation gives an overview and outlook on a comprehensive finite-element approach developed for the efficient design and accurate analysis of flexible multibody systems of arbitrary topology, featuring kinematic joints and highly flexible slender components ([1, 2, 3, 4] and references therein). The framework uses mathematical models and numerical solution methods constructed using tools from group theory and differential geometry, particularly Lie groups.

One of the fundamental challenges in modeling articulated systems is the presence of large amplitude motions of and within the system, leading to strong kinematic (geometric) non-linearity. A central concept to address this challenge is that of frames and frame transformations, which belong to a specific Lie group namely the special Euclidean group. This mathematical structure inherently couples rotation and translation and can be represented through various means such as homogeneous transformation matrices and dual quaternions. Because it provides a rigorous treatment of rigid-body transformations, the framework enables the consistent definition of frame-invariant relative motions in kinematic joints and deformation measures in flexible components.

The framework adopts a local frame approach, employing the frames attached to material points on bodies to resolve locally derivatives such as velocity and strain, as well as finite relative motions occurring within joints. This approach naturally filters out geometric non-linearities and yields equilibrium equations referred to as *intrinsic* due to their dependence solely on local quantities. These equations take the form of differential-algebraic equations on a Lie group, whose powerful mathematical apparatus can be exploited to streamline the development of efficient geometrically-consistent methods. For instance, it facilitates the implementation of beam finite elements that circumvent shear locking issues and enables the derivation of time integration methods that avoid global parameterization and, consequently, singularities. Additionally, the reduced non-linearities afforded by the formalism bring significant computational advantages. Notably, the iteration matrix utilized in implicit integration schemes is insensitive to overall large amplitude motions, instead influenced solely by local relative transformations, such as deformations in flexible elements and relative motions in kinematic joints. The efficient management of the computation and factorization of the iteration matrix significantly improves solver efficiency.

The presentation will be structured as follows. The fundamental mechanical concepts that drive the reliance of the formalism on frames and frame transformations will be recapitulated and emphasis will be placed on their manipulation as elements of the special Euclidean group, discussing coupled rotation-translation and practical aspects of representation and parameterization. The presentation will then explore some of the mathematical complexities inherent in this framework and aim at demonstrating the practical benefits through illustrative examples. Additionally, a small python package that illustrates the computer implementation of the framework will be made available.

References

- [1] O. A. Bauchau and V. Sonneville. The motion formalism for flexible multibody systems. *Journal of Computational and Nonlinear Dynamics*, 17(3), 2022. 030801.
- [2] V. Sonneville, O. Brüls, and O. A. Bauchau. Interpolation schemes for geometrically exact beams: a motion approach. *International Journal of Numerical Methods in Engineering*, 112(9):1129–1153, 2017.
- [3] V. Sonneville and O. Brüls. A formulation on the special Euclidean group for dynamic analysis of multibody systems. *Journal of Computational and Nonlinear Dynamics*, 9(4), 2014.
- [4] V. Sonneville, A. Cardona, and O. Brüls. Geometrically exact beam finite element formulated on the special euclidean group. *Computer Methods in Applied Mechanics and Engineering*, 268:451–474, 2014.

General Programme

Thermo- and Chemoelastic 3D Beam Modeling and Simulation with Isogeometric Collocation Methods

J.C. Alzate Cobo ¹, O. Weeger ¹

¹ Technical University of Darmstadt, alzate@cps.tu-darmstadt.de

Keywords: Cosserat Rods, Isogeometric Analysis, Collocation Methods, Thermoelasticity, Volumetric Strain

1. Introduction

The shift towards more sustainable energy sources allows for lattice structures to play a role in the design of future generations of Li-ion batteries. In particular, three-dimensional electrode architectures have the potential to provide shorter ion-diffusion paths due to greater surface-to-volume ratios of the active electrode material [1]. Thus, the power density of batteries can be improved, which leads to shorter charging times [1]. However, the modeling and simulation of lattice structures (let alone their optimization) with commonly used methods, such as full continuum finite elements, is computationally expensive. A way to mitigate this adversity is the use of beam theories for the modeling of slender microstructures. However, an efficient numerical scheme for the solution of 3D beams that allows for large volumetric strain, induced primarily by Li-ion diffusion, has not been found in the literature. This contribution aims to provide essential steps in this direction.

For the Cosserat rod model, a mixed isogeometric collocation method that alleviates shear locking phenomena has already been developed and validated for a linear elastic material model with small elastic strains [2]. This method has been recently extended as to capture inelastic material behaviours, i.e., to include elasto-viscoplastic material behavior with softening effects [3]. In this contribution, the model is further enhanced by the mechanical effects of volumetric strains resulting from a temperature or a concentration field, i.e., one-dimensional diffusion processes are incorporated. Consequently, the presented model represents the starting point for the coupling between thermodynamics, chemo-mechanics, beam theory, and isogeometric analysis.

2. Thermo- or chemoelastic Cosserat rod formulation

The steady state balance of linear and angular momenta, together with the sourceless, steady state diffusion equation for the one-dimensional temperature or chemical concentration field are described as follows:

$$\mathbf{f}_n(s) = \mathbf{n}'(s) = 0 \quad \text{with} \quad \mathbf{n}(s) = \mathbf{R} \mathbf{C} \boldsymbol{\varepsilon} \quad \text{and} \quad \boldsymbol{\varepsilon}(s) = \mathbf{R}^\top \mathbf{r}' - \mathbf{e}_3 - \alpha(c_0 - c) \mathbf{e}_3, \quad (1)$$

$$\mathbf{f}_m(s) = \mathbf{m}'(s) + \mathbf{r}'(s) \times \mathbf{n}(s) = 0 \quad \text{with} \quad \mathbf{m}(s) = \mathbf{R} \mathbf{D} \boldsymbol{\kappa} \quad \text{and} \quad \boldsymbol{\kappa}(s) = \text{axl}(\mathbf{R}^\top \mathbf{R}), \quad (2)$$

$$f_c(s) = q'(s) = 0 \quad \text{with} \quad q(s) = -\lambda A c'. \quad (3)$$

Here, the unknown, primary variables of the beam of length L are the current position of the centerline $\mathbf{r}(s) : [0, L] \rightarrow \mathbb{R}^3$, the orientation of the cross-section $\mathbf{R}(s) : [0, L] \rightarrow SO(3)$, as well as the axial concentration field $c(s) : [0, L] \rightarrow \mathbb{R}$. From these, the translational strains $\boldsymbol{\varepsilon}(s) \in \mathbb{R}^3$ and rotational strains $\boldsymbol{\kappa}(s) \in \mathbb{R}^3$ are computed, with $(\bullet)'$ denoting the derivative w.r.t. the arc-length parameter s of the initial configuration. The terms $\mathbf{n}(s) \in \mathbb{R}^3$ and $\mathbf{m}(s) \in \mathbb{R}^3$ represent the internal forces and moments in the current configuration, and $q(s) \in \mathbb{R}$ the thermal or chemical flux. The coupling of mechanical and diffusion effects is achieved through the term $\alpha(c_0 - c(s))\mathbf{e}_3$ in Eq. (1), where $\alpha(s)$ is a (potentially concentration dependent) expansion coefficient, $c_0 \in \mathbb{R}$ the initial concentration, and $\mathbf{e}_3 \in \mathbb{R}^3$ is a unit vector that allocates the thermal/chemical strain to the axial component within the translational strain vector. The matrices $\mathbf{C}(s) \in \mathbb{R}^{3 \times 3}$ in Eq. (1) and $\mathbf{D}(s) \in \mathbb{R}^{3 \times 3}$ in Eq. (2) represent the (potentially concentration dependent) constitutive matrices of the model. Furthermore, the area of the cross-section is represented by $A(s)$ and the thermal/chemical conductivity of the material by $\lambda(s)$.

3. Isogeometric collocation method

The nonlinear, coupled problem expressed by Eqs. (1) to (3) is numerically solved with isogeometric analysis. In order to do so, the centerline curve $\mathbf{r}(s)$, a quaternion field $\mathbf{q}(s)$ used for the parameterization of $\mathbf{R}(s)$, and the concentrations $c(s)$ are discretized as B-spline curves $\mathbf{r}(s) \approx \mathbf{r}_h(s) = \sum_{i=1}^n N_i(s) \mathbf{r}_i$, $\mathbf{q}(s) \approx \mathbf{q}_h(s) = \sum_{i=1}^n N_i(s) \mathbf{q}_i$,

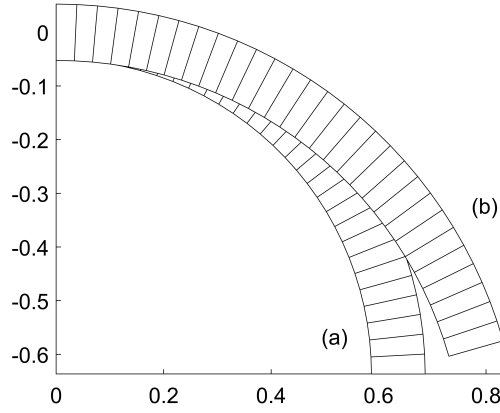


Figure 1: Elastic (a) and thermo/chemoelastic (b) response of cantilever beams subject to the same bending moment.

and $c(s) \approx c_h(s) = \sum_{i=1}^n N_i(s) c_i$. Here, $\mathbf{r}_i, \mathbf{q}_i$ and c_i are the control points and $N_i(s) : [0, L] \rightarrow \mathbb{R}$ the n B-spline basis functions. To determine the unknown control points, the approximate solutions $\mathbf{r}_h, \mathbf{q}_h$ and c_h are then introduced into the strong form of Eqs. (1) to (3) and into suitable boundary conditions [2]. Subsequently, the equations are collocated at a set of n points $\tau_i \in [0, L]$. The resulting system of nonlinear coupled equations of size $8n \times 8n$, is solved with Newton's method. Therefore, the linearization of Eqs. (1) to (3) is required. Consequently, the tangent stiffness matrix $\mathbf{K}(\mathbf{r}_i, \mathbf{q}_i, c_i) \in \mathbb{R}^{8n \times 8n}$ is computed by calculating the derivatives of $\mathbf{f}_n, \mathbf{f}_m, \mathbf{f}_q$ and \mathbf{f}_c w.r.t. the control points $\mathbf{r}_i, \mathbf{q}_i$ and c_i .

4. Results

The coupling of the volumetric thermal/chemical strain with the mechanical part of the formulation is demonstrated in Fig. 1, where the swelling of the cross-section visibly increases the bending stiffness of the structure. Figure 1 (a) shows the pure bending response of an originally straight cantilever beam and see (b) the thermo/chemo-mechanical response of the same beam when it is additionally subject to a volumetric thermal/chemical strain of 5%.

5. Conclusions and outlook

The presented formulation presents a direct extension to the already validated method presented by Weeger et al. [2] and provides an additional steps towards conformal merging of CAD systems with beam theories capable of reproducing multiphysical, inelastic behaviour. The formulation presented in this contribution reaches its limits when simulating beams with large volumetric strains. However, this problem will be treated in subsequent work, together with the inclusion of radial diffusion phenomena.

Acknowledgments

The authors acknowledge financial support of the Deutsche Forschungsgemeinschaft (DFG, German Research Foundation) – grant no. 460684687.

References

- [1] J. W. Long, B. Dunn, D. R. Rolison, and H. S. White. *Three-dimensional battery architectures*, Chemical Reviews, 104 (2004) 4463-4492.
- [2] O. Weeger, S.-K. Yeung, M. Dunn. *Isogeometric collocation methods for Cosserat rods and rod structures*, Comput. Methods Appl. Mech. Eng., 316 (2017) 100-122.
- [3] O. Weeger, D. Schillinger, R. Müller. *Mixed isogeometric collocation for geometrically exact 3D beams with elasto-visco-plastic material behavior and softening effects*, Comput. Methods Appl. Mech. Eng., 399 (2022) 115456

Physical Validation for the Simulation of Flexible Slender Structures

Benjamin Bauer ¹, Armin Bosten ^{1,2}, Michael Roller ¹, Muhannad Hawwash ¹, Olivier Bruls ², Joachim Linn ¹

¹ Fraunhofer ITWM, Kaiserslautern, Germany,
 [benjamin.bauer, michael.roller, muhannad.hawwash, joachim.linn]@itwm.fraunhofer.de
² University of Liège, Liège, Belgium, [a.bosten, o.bruls]@uliege.be

Keywords: Slender elastic structures, cable simulation, code validation, computing methodologies

1. Introduction

This contribution considers physical validation of simulation software with commercial or research background. Romero et. al [1] proposed a framework within computer graphics consisting of four benchmark tests for physical validation of simulation tools for flexible slender structures as examined by the THREAD project.

We apply the rod and shell models implemented in the commercial software Industrial Paths Solutions [2, 3], and the research code ODIN [4] to three benchmark tests illustrated by equilibrium states in Fig. 1. The models are tailored to efficient simulation and thus share the motivational aspects prevailing in computer graphics. In the process of simulation, we not only study the models behind the software employed, but also the numerical behavior of the benchmark tests. We observe that the simulation results match the master curves from [1] for parameter ranges relevant to the application field even for comparably coarse meshes.

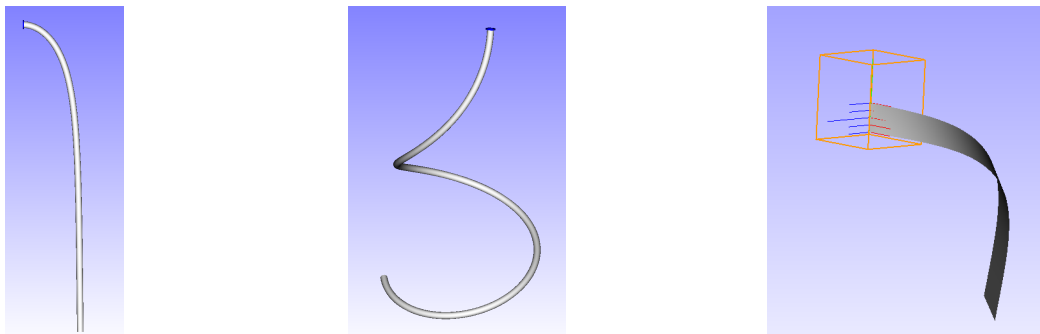
2. Cantilever Bending

The first benchmark may deploy a shell or a rod, this means structures that are thin in one or two directions, respectively. We clamp the specimen of interest at one end (for the shell such that the direction of gravity stands normal on the center surface) and free the other end. Under the influence of gravity, the object bends downwards as displayed for the rod in Fig. 1a. In this course, the coordinate ratios $\frac{\Delta y}{\Delta x}$ measured between the end points depends on the dimensionless gravito-bending parameter

$$\Gamma_{rod} = \frac{\rho A_{\circ} g L^3}{EI} \quad \Gamma_{shell} = \frac{\rho A_{\square} g L^3}{Dw}$$

with geometrical parameters length L , shell width w , cross-section areas A , and second moment of area I , and mechanical parameters density ρ , Young’s modulus E , flexural rigidity D , and gravity g .

Figure 2 displays the semi-analytic master curve and the simulation results for the IPS beam and shell on a logarithmic scale. For rather coarse discretizations (e.g. 15 elements in the length dimension for the shell) and high values $\Gamma > 5e3$ the simulations deviate from the master curve, but compute the physically correct solutions for lower values or finer discretizations. Notably, the range of meaningful magnitudes of Γ for simulation of circular and flat cables is $[10^0, 10^2]$ and $[10^0, 10^3]$, respectively.



(a) Cantilever bending (rod)

(b) Bend-twist bifurcation

(c) Lateral buckling

Figure 1: Exemplary equilibrium states for the three benchmark examples inspected in this contribution.

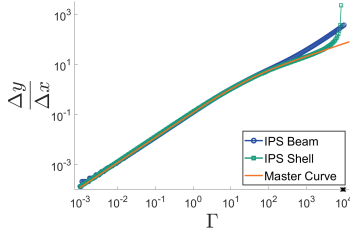


Figure 2: Cantilever benchmark computed for the IPS cable segment (rod, blue) and the IPS flat cable (shell, green). The markers match the orange master curve.

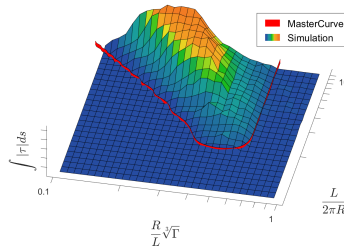


Figure 3: Integrated Frenet torsion of the equilibria in the Bend-Twist benchmark in IPS. Ground truth determined by the master curve displayed as red wall.

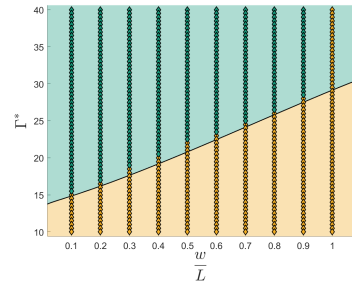


Figure 4: Overview of Lateral Buckling benchmark in IPS. Three-dimensional configurations in green and stable two-dimensional states in orange.

3. Bend-Twist Bifurcation

The coupling of bending and twist induces phenomena which are demanding to capture by rod or beam simulation. We fixate a naturally circular rod vertically at one end such that the initial tangent and the direction of gravity coincide. The fraction $\frac{L}{R}$ of length L and natural bending radius R , and the gravito-bending parameter Γ as dimensionless parameters decide whether the planar equilibrium state is stable or slight perturbations lead to buckling to a three-dimensional state such as in Fig. [1b](#).

We observe a numerically very challenging behavior of the Bend-Twist benchmark manifesting in choice of perturbation and subsequent decision for plane or spatial state. In particular, we need to approximate the Frenet torsion from discrete points and then integrate its absolute value numerically, as globally vanishing Frenet torsion characterizes plane states. Figure [3](#) displays the integrated absolute torsion in a height map for different test samples varying in bending radius and gravity which quantitatively well fits together with the master curve.

4. Lateral Buckling

When clamping a ribbon such that its width dimension equals the direction of gravity, the gravito-bending parameter Γ and the aspect ratio of width to length $\frac{w}{L}$ decide whether the planar state is a stable equilibrium or a lateral buckling occurs at the slightest perturbation as depicted in Fig. [1c](#).

Figure [4](#) shows that the shell model can compute the bifurcation point quantitatively well even for rather coarse discretizations as long as $w < L$. Naturally, distinct choices of geometry and material parameters lead to different conditioning in the numerics and thus to significant variations of the shell behavior.

Acknowledgments

The author's want to thank Florence Bertails-Descoubes and Sébastien Neukirch for insightful discussions and advice on the benchmarks presented in this work.

References

- [1] V. Romero, M. Ly, A.-H. Rasheed, R. Charrondière, A. Lazarus, S. Neukirch, F. Bertails-Descoubes. Physical validation of simulators in Computer Graphics: A new framework dedicated to slender elastic structures and frictional contact. *ACM Transactions on Graphics*, 2021, 40 (4), pp. 1-19 .
- [2] J. Linn, T. Stephan. Fast Simulation of Quasistatic Cable Deformations using Discrete Rod Models. In C.L. Bottasso, P. Masari, L. Trainelli: *Multibody Dynamics 2007*. Milano 2007
- [3] A. Ibrahimbegovic, F. Frey. Stress resultant geometrically non-linear shell theory with drilling rotations. *Computer Methods in Applied Mechanics and Engineering*, 1994, 118 (3-4), pp. 265–284
- [4] Odin: research code for the simulation of nonsmooth flexible multibody systems. University of Liège, Department of Aerospace and Mechanical Engineering. Released as open source under the Apache v2 license.

Towards realistic modelling of nanotrusses: coupling MD, ML and FEM

Marko Čanadija¹, Valentina Košmerl², Martin Zlatić³

¹ Faculty of Engineering, University of Rijeka, Vukovarska 58, 51000 Rijeka, Croatia,
marko.canadija@riteh.hr

² Faculty of Engineering, University of Rijeka, Vukovarska 58, 51000 Rijeka, Croatia,
valentina.kosmerl@riteh.hr

³ Faculty of Engineering, University of Rijeka, Vukovarska 58, 51000 Rijeka, Croatia, martin.zlatic@riteh.hr

Keywords: nanotrusses, molecular dynamics, machine learning, finite element method

1. Introduction

Although nanotechnological progress has been very rapid in recent decades, the mechanical description of the realistic behavior of nanostructures is still in its infancy. The usual approach is to apply macroscopic methods directly. This can lead to some success, but the main problem is that some effects occur at the nanoscale that are not present at the macroscale. This gives rise to the so-called size or nonlocal effects. In the context of rods and beams, this subject has been studied extensively, and a variety of solutions exist. These include finite elements suitable for such tasks. Unfortunately, all of these solutions rely on a material parameter known as the nonlocal parameter. The exact values of this parameter for different materials are still unknown, although some attempts to determine it can be found in the literature.

For this purpose, we use another possibility in the present study. The focus is on single-walled carbon nanotubes (SWCNTs). SWCNTs with a larger length-to-diameter ratio are slender and flexible structures, and in the present case we focus on the axial behavior of $L/D=5$ SWCNTs that are not so slender. First, a comprehensive set of molecular dynamics simulations of uniaxial tension and compression tests are performed. These constitute a dataset that is used for machine learning. The trained neural network is then coupled to FEM to provide the stress-strain behavior and tangent operators, enabling mechanical analyzes of nanotruss structures.

2. Molecular dynamics

It is well known that the stress-strain response of a carbon nanotube depends on the chirality parameters n and m . Since the SWCNT diameter is a function of chirality, this also means that the stress-strain curve is size dependent, i.e., it is affected by the diameter. This topic has been extensively studied in the literature, see a recent contribution in [1]. Since the goal of the present study is to create a model that is as general as possible, a wide range of single-walled carbon nanotubes has been studied, including all possible configurations up to a diameter of 4 nm.

Although finite element models exist that are based primarily on the harmonic potential, these models are difficult to reconcile with molecular dynamics simulations. Molecular dynamics simulations are usually considered as an option that is closest to reality. This is a starting point for this research. The widely used LAMMPS code was chosen as the simulation tool. 818 different SWCNT configurations were prepared and tested in tension and compression at room temperature until failure. To alleviate issues due to stochastic vibrations of SWCNT induced by temperature, all simulations were performed three times. Three tensile and three compressive sets were averaged and used as the dataset for the machine learning algorithm. The potential used was AIREBO, modified to better account for behavior close to the fracture. The remaining modeling details are omitted and can be found in [1, 2].

The obtained results clearly show differences in the extreme values of stress and strain. In the compression test, all SWCNTs fail by shell-like buckling, Fig. 1. In addition, the SWCNTs with the smallest diameter can withstand much larger stresses in compression than those with the largest.

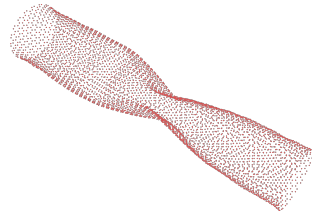


Figure 1: Failure by buckling of (20,20) SWCNT during compression.

3. Machine learning and finite element framework

The dataset obtained through the MD simulations is then used to train the neural network in TensorFlow/Keras. Particular attention is paid to enforcing convexity of the model so that it can be used in nonlinear FEM simulations. The architecture is based on [3] and has been extended to include the ability to integrate and differentiate the network. The trained neural network is then coupled to the Abaqus FE code via the UMAT subroutine.

4. Example

The proposed framework has been tested on a large number of examples, and only a brief insight is given here. The uniaxial compression and tension of a (20,20) SWCNT is considered. The stress-strain curves obtained from MD and ML based FEM are shown in Fig. 2. It is clear that both approaches give the same quality of results, but the FEM approach has a much lower computational cost.

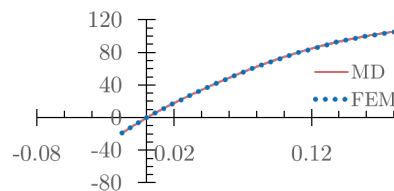


Figure 2: True stress (GPa) - true strain (-) curves of (20,20) SWCNT as obtained by MD and ML based FEM.

5. Conclusions

The proposed framework is based on the development of a neural network to represent the uniaxial behavior of SWCNTs derived from molecular dynamics simulations. The trained network is then coupled with a finite element code and can be used to simulate large nanotrusses that cannot be analyzed within a realistic time frame using classical molecular dynamics.

Acknowledgments

This work has been supported in by Croatian Science Foundation under the project IP-2019-04-4703, and under the project Young Researchers' Career Development Project – Training New Doctoral Students. This support is gratefully acknowledged.

References

- [1] M. Čanađija. *Deep learning framework for carbon nanotubes: Mechanical properties and modeling strategies*, Carbon, 184 (2021) 891–901
- [2] V. Košmerl, I. Štajduhar, M. Čanađija. *Predicting stress–strain behavior of carbon nanotubes using neural networks*, Neural Computing and Applications, 34 (2022) 17821–17836
- [3] B. Amos, L. Xu, J. Z. Kolter. *Input convex neural networks*, 34th International Conference on Machine Learning, D. Precup, Y. W. Teh, 146–155, 2017.

An efficient isogeometric analysis formulation for geometrically exact beam structures with complex shape and topology

Diego Ignesti¹, Giulio Ferri², Enzo Marino³

¹ Department of Civil and Environmental Engineering, University of Florence, diego.ignesti@unifi.it

² Department of Civil and Environmental Engineering, University of Florence, giulio.ferri@unifi.it

³ Department of Civil and Environmental Engineering, University of Florence, enzo.marino@unifi.it

Keywords: Isogeometric Collocation; Spatial curved beams; Bishop frame; Finite rotations; SO(3).

1. Introduction

We present a robust and efficient multi-patch formulation, based on the Isogeometric Collocation (IGA-C) method, for the solution of shear-deformable spatial beam structures with arbitrary initial curvature and complex topology. In this contribution we extend to the geometrically nonlinear (exact) regime the recent results obtained in [1].

IGA-C methods have already been employed for the simulation of three-dimensional shear-deformable curved beams, for the geometrically linear [2],[3] and nonlinear [4] cases by adopting the classical Serret-Frenet (SF) local frame. However, this choice prevents the generalization of the formulation since the SF frame is not defined at points with vanishing curvature. To circumvent this limitation, the proposed approach is based on the combination of a rotation-minimizing frame (Bishop frame) with the exponential map for $SO(3)$ (Rodrigues formula) to compute the beam curvature and its derivative. Figure 1 shows an example where the local Bishop frame (Figure 1c) is well defined compared to the SF case (Figure 1b) for a demanding spatial beam geometry, referred to as Spivak curve.

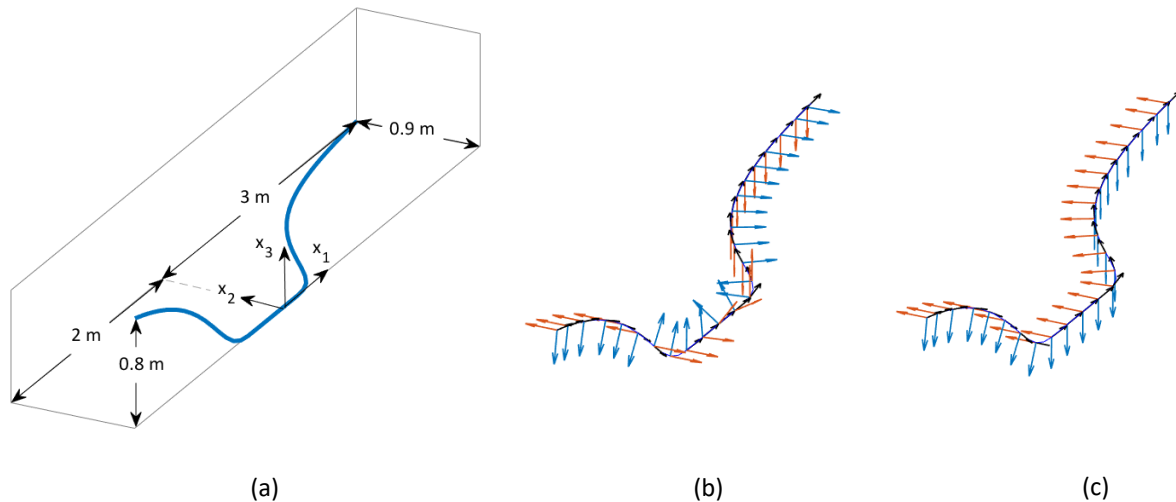


Figure 1. The Spivak curve (whose equation can be found, e.g., in [1]) defined on the interval $I = [-2,3]$ (a), local Serret-Frenet frame (b) and the adopted rotation-minimizing frame (Bishop frame) (c).

We will show how our formulation based on the Bishop frame not only permits bypassing the known issues related to the SF frame, but also does not require the Darboux vector and its derivative, which are both affected by the critical aspects of the SF frame. Moreover, the adopted Bishop frame does not suffer the instabilities related to possible ill-defined torsion (zero-curvature points), since it is set through an approximation technique. For further details, also regarding the computation of the rotation operator and the beam curvature, the reader may refer to [1].

2. Solution of the governing equations and numerical results

The well-known equations governing the geometrically exact beam problems, once transformed in a displacement-based form by adopting a linear elastic material, are solved in the strong form. To do that, first an $SO(3)$ -consistent linearization is performed, then the equations are discretized through B-spline basis

functions and finally collocated at the Greville points. Finite rotations are updated by using the (material) incremental rotation vector [5].

The resulting computational strategy is high order accurate in space, thanks to the smoothness of the basis function, and extremely efficient due to: i) no elements integration; ii) minimal parameterization of finite rotations; iii) easy multi-patch coupling thanks to global reference frame. An example of the capabilities of the proposed formulation to simulate beam structures with highly complex shape and topology is shown in Figure 2.

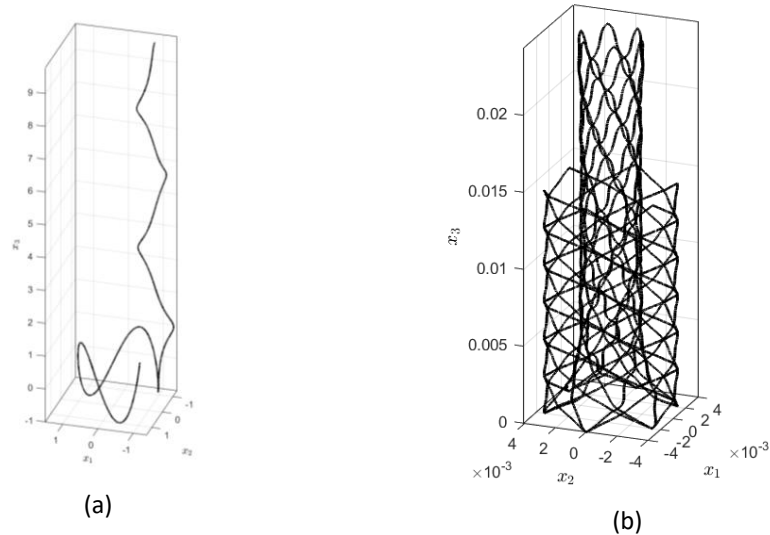


Figure 2. Comparison between the deformed and undeformed configuration of a curved (Lissajous) beam (a) and a cardiovascular stent (b). Both structures are clamped at one end and pulled in the x_3 direction.

3. Conclusions

The present contribution is focused on a geometrically exact beam formulation suitable for structures with complex shape and topology. The main novelty lies in the combination of an efficient SO(3)-consistent isogeometric collocation scheme for the solution of geometrically exact beams with a robust technique for the reconstruction of complex geometries. We believe that this work has the potential to impact all the engineering fields for which high efficiency is fundamental, e.g., the design of programmable and architected materials.

References

- [1] D. Ignesti, G. Ferri, F. Auricchio, A. Reali, and E. Marino, *An improved isogeometric collocation formulation for spatial multi-patch shear-deformable beams with arbitrary initial curvature*, *Comput Methods Appl Mech Eng*, 403 (2023), p. 115722.
- [2] F. Auricchio, L. Beirão da Veiga, J. Kiendl, C. Lovadina, and A. Reali, *Locking-free isogeometric collocation methods for spatial Timoshenko rods*, *Comput Methods Appl Mech Eng*, 263 (2013), 113–126.
- [3] E. Marino, S. F. Hosseini, A. Hashemian, and A. Reali, *Effects of parameterization and knot placement techniques on primal and mixed isogeometric collocation formulations of spatial shear-deformable beams with varying curvature and torsion*, *Computers and Mathematics with Applications*, 80, no. 11 (2020), 2563–2585.
- [4] E. Marino, *Locking-free isogeometric collocation formulation for three-dimensional geometrically exact shear-deformable beams with arbitrary initial curvature*, *Comput Methods Appl Mech Eng*, vol. 324 (2017), 546–572.
- [5] E. Marino, J. Kiendl, and L. De Lorenzis, *Isogeometric collocation for implicit dynamics of three-dimensional beams undergoing finite motions*, *Comput Methods Appl Mech Eng*, 356 (2019), 548–570.

Elastic Ribbons: the missing link between rods and plates

S. Neukirch¹, B. Audoly², F. Bertails-Descoubes³, R. Charrondière³, V. Romero³

¹ Sorbonne University & CNRS, UMR 7190 d'Alembert Institute for Mechanics, Paris, France

² Lab. Mechanics of Solids, CNRS, Inst. Polytechnique de Paris, 91120 Palaiseau, France

³ Univ. Grenoble Alpes, INRIA, CNRS, Grenoble INP, LJK, France

Keywords: bifurcation, dimensional reduction, plates, numerical path-following, curvature-based discretisation.

1. Introduction

We model elastic deformations of long and flat structures, which we call ribbons. These ribbons may be naturally flat or with intrinsic curvature. Modeling eventually leads to a set of ordinary differential equations for the statics of the structure, which we solve with different numerical approaches. Depending on the aspect ratio of the cross-section different models are used, from Kirchhoff to Sadowsky equations.

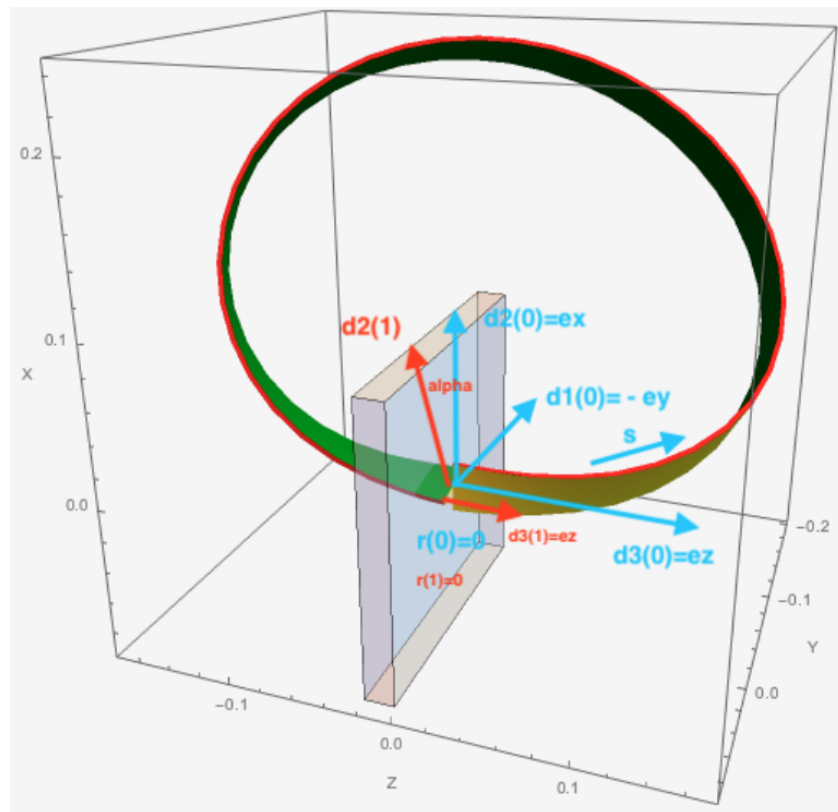


Figure 1: Clamped-clamped ribbon with imposed rotation.

2. Developable and extensible ribbons

Ribbons are flexible band-shaped structures and are widely present in our daily environment. Examples are found in cable plies, fashion accessories, and hair ringlets. In industry, ribbons are present in graphene applications, the design of multi-stable tape springs for the aerospace industry, and flexible wheels for robots. There is recently a renewed interest in understanding and modeling these structures, even if their mechanical study was initiated back in the 1930s [2]. We limit ourselves to the case of a rectangular ribbon, composed of isotropic and linearly elastic material. The thickness of the ribbon remains negligible in comparison to its width, the latter being itself negligible in comparison to its length. We illustrate our methods with the computation of the shape of the Möbius band [1], see Figure 2.

Some models use an inextensibility hypothesis in which the ribbon possesses a developable surface. Developability implies that the surface cannot be stretched nor sheared, but deforms by pure bending. We introduce yet another ribbon model in which extensibility is allowed, and we discuss how equilibrium solutions are modified by the presence of extensibility [3].

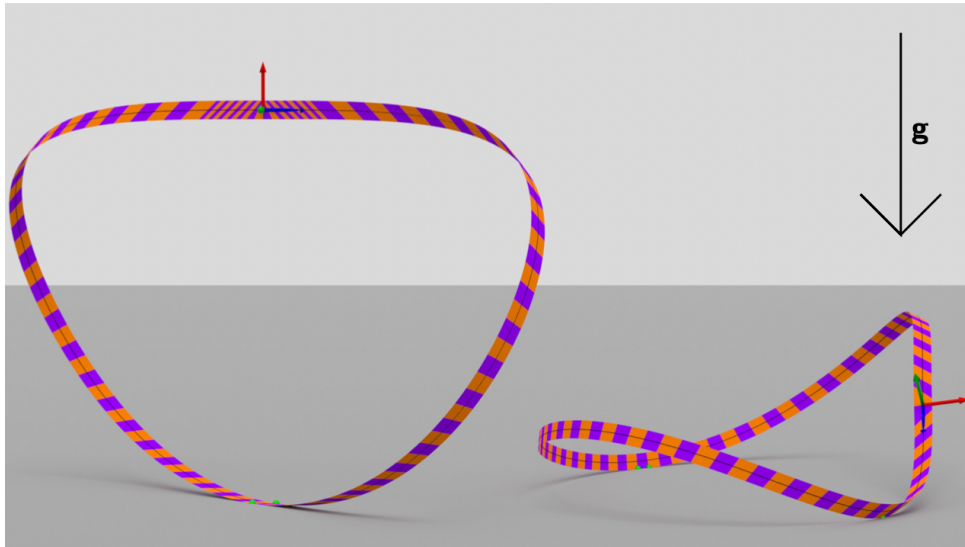


Figure 2: Moebius configurations of a heavy ribbon resting on a support. The ribbon may either stand up (left) or fall on its side (right).

References

- [1] F. A. Moebius. Über die Bestimmung des Inhaltes eines Polyeders (On the determination of the volume of a polyhedron). *Ber. Verh. Sächs. Ges. Wiss.*, 17:31–68, 1865. See also *Gesammelte Werke*, Band II (Collected Works, vol. II), p. 484. Hirzel, Leipzig (1886).
- [2] M. Sadowsky. Die Differentialgleichungen des Moebiuschen Bandes. *Jahresbericht der Deutschen Mathematiker-Vereinigung*, 39:49–51, 1929.
- [3] B. Audoly and S. Neukirch. A one-dimensional model for elastic ribbons: A little stretching makes a big difference. *Journal of the Mechanics and Physics of Solids*, 153:104457, 2021.

Indirect shape adaptation of compliant arches using active supports

András A. Sipos¹, Péter L. Várkonyi²,

¹ Department of Morphology and Geometric Modeling, Budapest University of Technology and Economics, siposa@eik.bme.hu

² Department of Mechanics, Materials, and Structures, Budapest University of Technology and Economics, varkonyi.peter@epk.bme.hu

Keywords: Elastica, shape adaptation, stability, bifurcation

1. Adaptive structures and funicularity

Adaptive structures have active components varying geometric or mechanical properties. Adaptivity is common for biological systems, such as plant shoots responding to light by modulation of intrinsic curvature. Engineered adaptive structures include robotic arms, and adaptive metamaterials [1]. Adaptivity is less common in architectural scale. Nevertheless, active supports and dampers are used to reduce vibration caused by dynamic effects [2] or to optimize a structure under varying quasi-static loads. Natural ways of adaptation for slender structures include modulation of lengths, and support conditions. Modulation of intrinsic curvature is less common, due to difficulty of implementation.

We believe that adaptivity offers high benefits in the case of *funicular structures* such as arches and cables. Funicular geometry ensures that the external loads generate axial internal forces, yielding exceptional material-efficiency [3]. Funicular design is however limited by time-dependent loads, calling for adaptation of structural shape to variations of funicular geometry. Our recent paper investigated adaptive funicularity via direct modulation of intrinsic curvature of cantilevers [4]. However the curved shape of a structure can also be modulated indirectly by varying boundary conditions.

2. Shape adaptation by active supports

We aim to explore quasi-static shape adaptation by active supports. We investigate an incompressible, unsharable, 2D, prismatic elastica rod of length L , and bending stiffness k , parametrized by arclength $0 \leq s \leq L$, using a geometrically exact rod theory. The intrinsic curvature is 0, however curved shapes are enforced by non-conform, statically indeterminate boundary conditions: the two endpoints are fixed at points A, and B at distance $L - \Delta L$ from each other (Fig. 1, left). The tangent angles α and β at the two endpoints are fixed by actuators. The external load is a quasi-static vertical, distributed force $qQ(s)$ where q is an intensity parameter, and $Q(s)$ is normalized load distribution function with $L^{-1} \int_0^L Q(s)^2 ds = 1$.

Our ultimate goal is to maximize the critical load intensity q_{crit} associated with the failure of the structure if q is increased while $Q(s)$ is fixed. This is achieved by adaptation of α and β to $Q(s)$. Failure criteria may

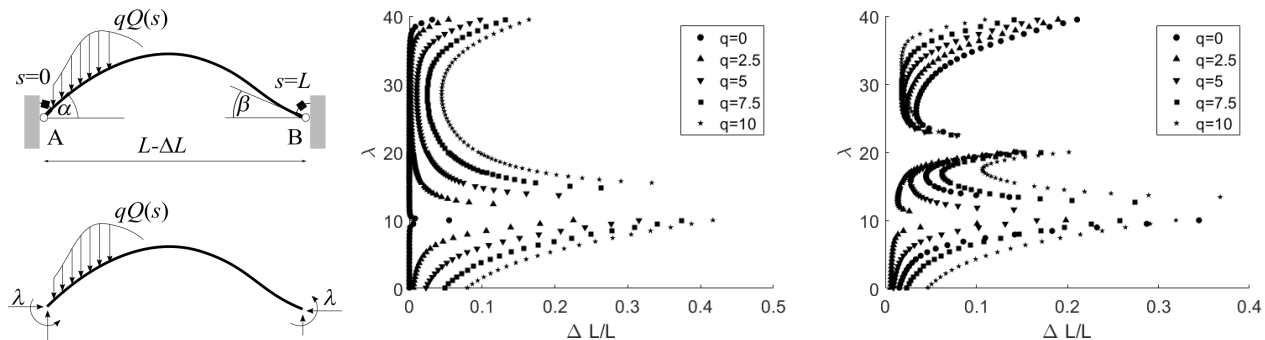


Figure 1: Left: sketch (top) and free body diagram (bottom) of elastica arch with active supports. Center: bifurcation diagrams for $Q(s) = 1$, $L = 2$, $k = 1$ and $\alpha = \beta = 0$ Right: bifurcation diagram for modified terminal angles $\alpha = 0.4$, $\beta = 0.2$.

include (1) *sudden dynamic motion* due to loss of instability (like snap-through of flat arches); or some function of equilibrium shape, for example *the curvature of the bar reaching a critical value*, corresponding to structural damage. The known advantageous properties of funicular design, suggest that optimal shapes are similar to funicular shapes corresponding to $Q(s)$. Perfect match is however unlikely as the system is underactuated, i.e. only a limited set of shapes can be enforced by the two control parameters α and β .

3. Bifurcation diagrams of deformed shapes

Bifurcations of a related model without a transverse load ($q = 0$) have been studied by [5]. We extend that investigation to non-zero external load intensity q . A numerical solver has been implemented using the nonlinear BVP solver of the *Chebfun Toolbox* in Matlab [6] to traverse the equilibrium paths as the horizontal reaction force λ is varied.

Figure 1 shows bifurcation diagrams for two different combinations of the angles α, β if the load distribution is constant. Instead of using q as bifurcation parameter, we project solutions to a plane spanned by a dimensionless parameter $\Delta L/L$ depending on the distance between the two supports, and λ . These diagrams show similarity to bifurcation diagrams of classical Euler buckling. For $\alpha = \beta = 0$, and $q = 0$, we recover the classical pitchfork bifurcation diagram of a buckling column with fixed endpoints. The first bifurcation occurs at $\lambda_{crit} = 4L^{-2}\pi^2$ and further bifurcations at $4n^2L^{-2}\pi^2$ for all integers $n > 1$. The equilibrium paths for $q > 0$ can be viewed as perturbed versions of this equilibrium path (Fig.1, center). A symmetric rotation of the supports $\alpha = \beta = 0.4$ creates a highly similar bifurcation diagram with largely unchanged critical values of λ albeit the pitchfork bifurcation occurs at a non-zero value of the vertical load $2.5 < q_{critical} < 5$ (not shown in the figure). An asymmetric rotation of the supports $\alpha = 0.4, \beta = 0.2$ again leaves $\lambda_{critical}$ of the first bifurcation point largely unchanged with a non-zero critical value $2.5 < q_{critical} < 5$ of the vertical load. At the same time, the second and third critical points of λ are shifted considerably (Fig.1, right). These observations help to understand qualitative features of deformed shapes despite non-integrability of the elastica equations.

4. Towards autonomous shape adaptation

The numerical solution method outlined above can be used to find equilibrium paths for any load distribution, which allows the identification of optimal shapes corresponding to a given load distribution and a failure criterion. Further efforts are needed to design an appropriate control policy in order to synthesize an autonomous, adaptive system. The main challenge to be solved is the difficulty of sensing the actual distribution $Q(s)$ directly. Our ongoing work aims to identify simple, easy-to-measure parameters of the curved shape, which allow for the efficient estimation of $Q(s)$. This problem has been solved successfully in the case of direct curvature adaptation of a discrete model of a cantilever [4], and it is subject to ongoing work for the problem outlined here.

Acknowledgments

This project has received funding from the National Research, Development, and Innovation Office of Hungary under grant 143175.

References

- [1] C. Jiang, F. Rist, H. Wang, J. Wallner, H. Pottmann. *Shape-morphing mechanical metamaterials*, CAD Computer Aided Design, 143 (2022) 103146.
- [2] W. Sobek. *Ultra-lightweight construction*, International Journal of Space Structures, 31 (2016) 74–80
- [3] D. Veenendaal, P. Block. *An overview and comparison of structural form finding methods for general networks*, International Journal of Solids and Structures, 49 (2012) 3741–3753
- [4] A. F. Guerra Riano, P. L. Várkonyi. *Shape control of adaptive funicular structures*, In review.
- [5] M. Liu, M. Gomez, D. Vella. *Delayed bifurcation in elastic snap-through instabilities*, Journal of the Mechanics and Physics of Solids, 151 (2021) 104386
- [6] T. A. Driscoll, N. Hale, L. N. Trefethen eds. *Chebfun Guide*, Pafnuty Publications, Oxford, (2014)

MS-1: Constitutive modelling for flexible slender structures

An Energy Stable Discontinuous Galerkin Approach for the Geometrically Exact Intrinsic Beam Model

Christian Bleffert¹, Lukas Dreyer², Melven Röhrig-Zöllner³

¹ Deutsches Zentrum für Luft- und Raumfahrt (German Aerospace Center), christian.bleffert@dlr.de

² Deutsches Zentrum für Luft- und Raumfahrt (German Aerospace Center), lukas.dreyer@dlr.de

³ Deutsches Zentrum für Luft- und Raumfahrt (German Aerospace Center), melven.roehrig-zoellner@dlr.de

Keywords: Flexible Beams, Discontinuous Galerkin, Discretization, Numerical Simulation, Energy Stable

1. Introduction

With the Versatile Aeromechanic Simulation Tool (VAST), the German Aerospace Center is developing a software framework for the simulation of rotary wing aircraft. One challenge consists of simulating the dynamic behaviour of rotor blades. For this purpose we are investigating the Geometrically Exact Intrinsic Beam Model [1] and its discretization. In [2] we derive an energy stable discretization for the governing equations of the model using Discontinuous Galerkin techniques.

2. The underlying Model

As a theoretical basis for our approach we use the Geometrically Exact Intrinsic Theory for Dynamics of Curved and Twisted Anisotropic Beams (Intrinsic Beam Model), which was developed by Hodges in 2003 [1]. It allows for the modelling of anisotropic and initially curved beams, making it well suited for rotor blades. Furthermore, in contrast to other well-known beam models like Euler-Bernoulli or Timoschenko, the intrinsic beam model contains non-linearities and is geometrically exact. Considered beams are idealized by a one dimensional reference line so that the governing equations of the model can be formulated as system of partial differential equations (PDE) in one space dimension and a time dimension. The solution of the PDE consists of internal forces and moments as well as linear and angular velocities each in three dimensions so that there are 12 unknowns in total. If they are known, these intrinsic variables can be integrated to obtain displacements and rotations of the modelled beam. We use a practical representation of the PDE as a system of linear hyperbolic balance laws to derive boundary conditions that describe the mechanical setup of a clamped-free beam. From these boundary conditions, we also show that they are sensible from a mathematical point of view. Further, we use the energy method to show that the model is energy conserving in general and energy stable when applying the boundary conditions and potential external forces and moments along the modelled beam. In particular, we derive an estimation for the solution's energy which shows that for bounded external forces and moments and zero boundary data, the energy can not grow faster than quadratically in time.

3. Spatial Discretization

As the underlying PDE can be understood as a linear hyperbolic system of balance laws, an appropriate choice for the spatial discretization of the underlying problem is a Discontinuous Galerkin (DG) Approach. The DG approach not only has the advantage that it is very efficient and helps minimizing the degrees of freedom in the computationally intensive process of simulating helicopters. It is also able to depict discontinuities, which may enable us to take jumps in material parameters into account which are not unusual within helicopter rotor blades. As numerical flux we use a slightly modified version of the well-known Lax-Friedrichs flux which contains a so called upwind parameter. With the help of this DG discretization, we derive a semi-discrete formulation of the problem that still continuously depends on the time variable. We further analyse the energy of this semi-discrete problem and derive an estimation for it, that mimics the estimation for the energy of the original problem's solution. That is, also the semi-discrete energy can not increase faster than quadratically in time and the DG discretization is in fact energy stable. The energy of the numerical solution emerging from the semi-discrete problem has, however, additional numerical dissipation whose amount can be controlled by the upwind parameter of the numerical flux.

4. Numerical Experiments

To implement our theoretical considerations, we use the simulation framework Trixi [3]. To obtain a fully discrete problem, we use an explicit fourth order Runge-Kutta scheme for the discretization of the semi-discrete formulation which is represented by an ordinary differential equation in time. In our numerical experiments, we investigate an exemplary case of the intrinsic beam model and use the techniques of manufactured solutions to verify the convergence of the numerical solution resulting from our discretization scheme. The results show an optimal convergence rate, i.e. the empirical order of convergence reaches the degree of the polynomials that are used in the DG approach for the spatial discretization. Moreover, we experimentally verify our predictions concerning the energy of the semi discrete solution. That is, for example that a simulated beam that is not exposed to any external influences like external boundary data or external forces and moments along the beam has a non-increasing energy. Additionally, we verify that the amount of numerical dissipation, i.e. the amount by which the discrete energy decreases in that case is determined by the upwind parameter of the numerical flux. Another point that is investigated in our numerical experiments is the post processing that is needed in order to obtain the displacements and rotations of the one dimensional reference line representing the beam.

5. Conclusion and Outlook

Our results confirm that the DG approach suits the problem of the intrinsic beam model well. Our theoretical investigations as well as our numerical experiments show that the discretization scheme is numerically stable. Moreover, we could verify the convergence of the resulting numerical solution to the exact solution at an optimal convergence rate. What remains to be investigated is the correctness of our simulation results by comparing them to experimental data and other existing results. Often the available data consists of steady state cases, which leads to another question that will be investigated in the future: Can the Intrinsic Beam Model together with the DG discretization be united with a damping model? That will not only be interesting for the comparison of simulation data with experimental data and exact steady state solutions but also for the actual application on helicopter rotor blades. An example of how damping models can be integrated into the intrinsic beam model is to find in [4], where Artola, Wynn and Palacios derive a damped version of the intrinsic beam model using Generalised Kelvin-Voigt damping. Currently, we are investigating the compatibility of the damped model with our considerations on the DG discretization so far.

References

- [1] D. Hodges. *Geometrically Exact, Intrinsic Theory for Dynamics of Curved and Twisted Anisotropic Beams*, AIAA Journal, 41 (2003) 1131-1137
- [2] C. Bleffert. *An Energy Stable Discontinuous Galerkin Discretization Approach for the Geometrically Exact Intrinsic Beam Model*, Master's Thesis, University of Cologne, 2022.
- [3] M. Schlottke-Lakemper et al. *Trixi.jl: Adaptive high-order numerical simulations of hyperbolic PDEs in Julia*, <https://github.com/trixi-framework/Trixi.jl>, 2021.
- [4] M. Artola, A. Wynn, R. Palacios. *A Generalised Kelvin-Voigt Damping Model for Geometrically-Nonlinear Beams*, AIAA Journal, 59 (2021) 356-365

Modeling the Mechanical Behavior of Unshielded Twisted Pair Cables Including Frictional Contact

Muhannad Hawwash¹, Vanessa Dörlich¹, Joachim Linn¹

¹ Mathematics for the Digital Factory
Fraunhofer Institute for Industrial Mathematics (ITWM)
Fraunhofer-Platz 1, 67663 Kaiserslautern, Germany
[muhannad.hawwash, vanessa.doerlich, joachim.linn]@itwm.fraunhofer.de

Keywords: Mechanical Behavior, Multi-axial Load, Contact Model, Finite Beam Element, Twisted Pair Cable

1. Introduction

Cables in modern cars act like the nervous system by linking electronic components and sensors to electronic control units. Depending on the specific application, the cable structure, such as the parameters of the conductor, insulation material and its thickness, is adapted. This work focuses on unshielded twisted pairs (UTP), which are designed to transmit higher frequency signals with minimal interference. UTP are constructed by intertwining two conductors with a specified pitch length, i.e. the distance in which one of the cables completes one revolution, see Figure 1. This pitch length is maintained by the regularity of the twists along the cable and can be disrupted if the cable is subjected to mechanical deformation, such as torsion or locally small bending radii. This can cause the cable's electrical performance to deteriorate, such as an increase in cross talk or impedance [1, 2]. Thus, it is important to investigate the behavior of UTPs under mechanical load in simulations.

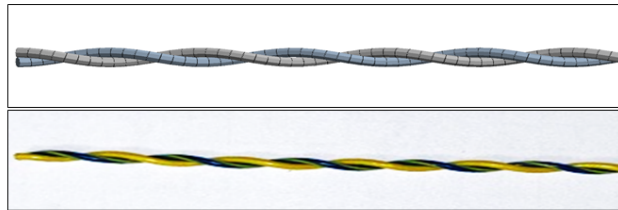


Figure 1: Example of a twisted pair. Top: FE mesh using two helices discretized with beam elements to implement the double wire strand. Bottom: Photograph.

2. Finite Element Models for UTP

This work focuses on utilizing a numerical model to simulate the mechanical behavior of UTP under combined bending and torsion loads, using finite beam elements that take into account the impact of friction on the deformation behavior. The multi-wire FE model presented in [3], specifically the double wire strand model, is used to simulate twisted pairs. In order to capture the nonlinear phenomena in the simulation, we model the two conductors using finite beam elements with quadratic shape functions. Contact between cables is taken into account using a Coulomb friction model with pure penalty formulation. We avoid superposition of geometrical and material nonlinearities by restricting the material model to linear elasticity. The correct parameter identification, i.e. determination of the effective Young's modulus of the two conductors, from experiments is crucial, but not straightforward in this case and will be discussed in the contribution.

We simulate a geometrically nonlinear bending load case (Figure 2), as described in [4] for bending a strand of three parallel elastic wires, to investigate UTPs and validate our numerical model by comparing the predictions to experimental data. This allows for the investigation of the effect of friction and geometry on the simulation results.

The versatility of the presented approach allows for the investigation of various loading conditions including multi-axial loads. Bending of UTP under pre-twisting is for example a test case, where coupling between

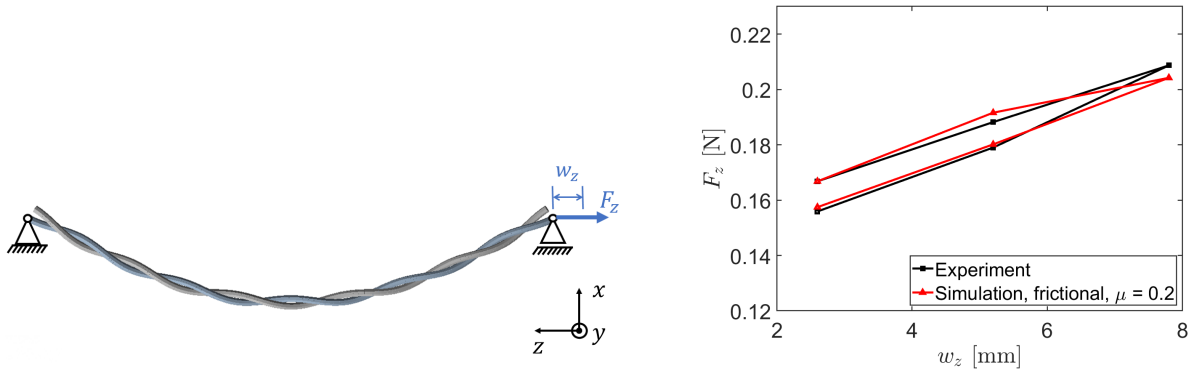


Figure 2: Boundary condition for geometrically nonlinear bending of a twisted pair: The specimen is clamped on both ends with a roller support on one end and a pinned support on the other. A cyclic loading is conducted by applying a displacement w_z on one end and the reaction force F_z is measured (left). Comparison of experimental and simulation results (right).

bending and torsion can be examined. Thus, we apply the FE modeling approach to simulate such deformations and investigate the influence of pre-twisting on the bending behavior of the UTP.

2.1. Results

A first comparison of experimental and simulation results for bending of UTP (Figure 2 (right)) shows that the virtual and physical experiments agree acceptably well. The similar size of the areas under the respective hysteresis indicates that the simulation captures the influence of frictional contact well. Based on the fact that the hysteresis in the FE simulation only stems from friction between the cables and inelastic material effects are not taken into account, it can be concluded that geometry and friction are the main contributions to the inelastic behavior of UTP under bending. Despite the large spatial displacements of the UTP specimen, the local material deformations of the two conductors are comparatively small due to their helix shape. Thus, material inelastic effects such as plasticity do not contribute to the inelastic response of the UTP.

3. Conclusions

In this work, we use a commercial FEM tool to simulate UTP cables and compare simulation results to those from corresponding experiments. Thus, the effect of frictional contact on the deformation behavior taking into account different geometrical models, is investigated. The versatility of the approach allows for the investigation of more advanced load cases, such as bending under pre-twisting which enables the investigation of coupling effects between bending and torsion.

References

- [1] Belden Electronics Division. The Impact of Installation Stresses On Cable Performance. TB66, (2001).
- [2] H. W. Ott. *Electromagnetic Compatibility Engineering*. John Wiley & Sons, 2009.
- [3] M. Hawwash, V. Dörlich, J. Linn, R. Müller and R. Keller. Effective Inelastic Bending Behavior of Multi-Wire Cables Using Finite Elements Accounting for Wire Contact. In *ECCOMAS Thematic Conference on Multibody Dynamics*, pp. 369 – 379, Budapest, 2021.
- [4] M. Hawwash, V. Dörlich, J. Linn, R. Keller and R. Müller. Modeling the Effective Inelastic Behavior of Multi-Wire Cables Under Mechanical Load Using Finite Elements. In *ECCOMAS Congress 2022-8th European Congress on Computational Methods in Applied Sciences and Engineering*, Oslo, 2022.

Nonlinear computation of cable structures with anisotropic plasticity using high-order solid elements

André Hildebrandt-Raj¹, Prateek Sharma², Stefan Diebels², Alexander Düster¹

¹Numerical Structural Analysis with Application in Ship Technology (M-10), Hamburg University of Technology

²Applied Mechanics, Saarland University

Keywords: anisotropy, elastoplasticity, high-order FEM, cables, slender structures

1. Introduction

With the increasing electrification of almost every aspect of our modern civilisation the use of cables has increased considerably. One example is the transition from combustion driven to electric cars. But also in other industrial realms e.g. robots are used to replace or assist workers during manufacturing. Here cables are used for both, signal transmission and provision of electric energy, being exposed to regularly changing mechanical loads. Another aspect is the increasing electrification of the North and Baltic sea by placing offshore wind turbines or other power generating/storing facilities into the sea, connected through undersea cables to the mainland. Thus, apart from the electric properties, their mechanical characterisation is of increasing importance. The aim of our work is to advance the possibilities in simulating cables and other slender structures efficiently.

2. Theory and modelling

In order to model the cables efficiently and accurately at the same time, the finite element method is used with hexahedral elements based on high-order hierarchic shape functions combined with quasi-regional mapping. For the hierarchic ansatz space an anisotropic choice is used, that has different ansatz orders in different directions depending on the structure and load case [1]. To improve the accuracy for local phenomena like plastic fronts or contact regions of the cable the adaptive *hp*-refinement [2] is utilised.

Cables are usually a composition of many layers of different materials. A coaxial cable, for example, is composed of an inner core of copper conductors, an insulation layer, a second layer of copper conductors, and a final protective jacket on the outside. The different materials, the many single parts and their interaction between each other creates a complex overall behaviour [3]. To reduce the complexity of the computation, the interactions and different materials are substituted by an effective material that is able to represent the resulting macroscopic behaviour. Due to the displacement based hexahedral element formulation a large variety of strain energy density function based material models are available. To this end an orthotropic elastoplastic material model [5] was chosen. While the anisotropy enables a different behaviour for the different fibre directions, the elastoplastic behaviour represents lasting changes of the inner structure like reordering of the parts.

The material model is characterised by the three fibre directions ${}_i\mathbf{v}$, for $i = 1, 2, 3$ in the reference configuration. They construct a set of structural tensors ${}_i\mathbf{M} = {}_i\mathbf{v} \otimes {}_i\mathbf{v}$, which define six strain invariants $J_i = \text{tr}[\mathbf{M}\mathbf{C}_e]$ and $J_{i+3} = \text{tr}[\mathbf{M}\mathbf{C}_e^2]$, with the elastic right Cauchy–Green tensor $\mathbf{C}_e = \mathbf{F}_e^T \mathbf{F}_e$. Here the deformation gradient is split multiplicatively $\mathbf{F} = \mathbf{F}_e \mathbf{F}_p$ into elastic and plastic parts. The invariants combined with material parameters α_j , $j = 1, \dots, 12$ define the elastic strain energy density function

$$\Psi_e = \sum_{i=1}^3 \left[\alpha_i J_i + \frac{1}{2} \alpha_{i+3} J_i^2 + \alpha_{i+9} J_{i+3} \right] + \alpha_7 J_1 J_2 + \alpha_8 J_1 J_3 + \alpha_9 J_2 J_3. \quad (1)$$

Since the inelastic behaviour is also anisotropic, the yielding exhibits a similar anisotropy. The structural tensors are used to create six invariants from an Eshelby like stress tensor $\mathbf{\Xi} = 2\rho_0 \mathbf{C} \mathbf{F}_p^{-1} \frac{\partial \Psi_e}{\partial \mathbf{C}_e} \mathbf{F}_p^{-T}$, where \mathbf{C} is the right Cauchy–Green tensor. The stress invariants are then $I_i = \text{tr}[\mathbf{M}_i \text{dev} \mathbf{\Xi}]$ and $I_{i+3} = \text{tr}[\mathbf{M}_i (\text{dev} \mathbf{\Xi})^2]$ for $i = 1, 2, 3$. Combined with the material parameters β_j for $j = 1, \dots, 9$, which represent the yield stresses an equivalent stress

$$\chi = \sum_{i=1}^3 \left[\beta_i I_i^2 + \beta_{i+6} I_{i+3} + \frac{1}{2} \sum_{j=1}^3 \beta_{i+j+1} I_i I_j \right], \quad (2)$$

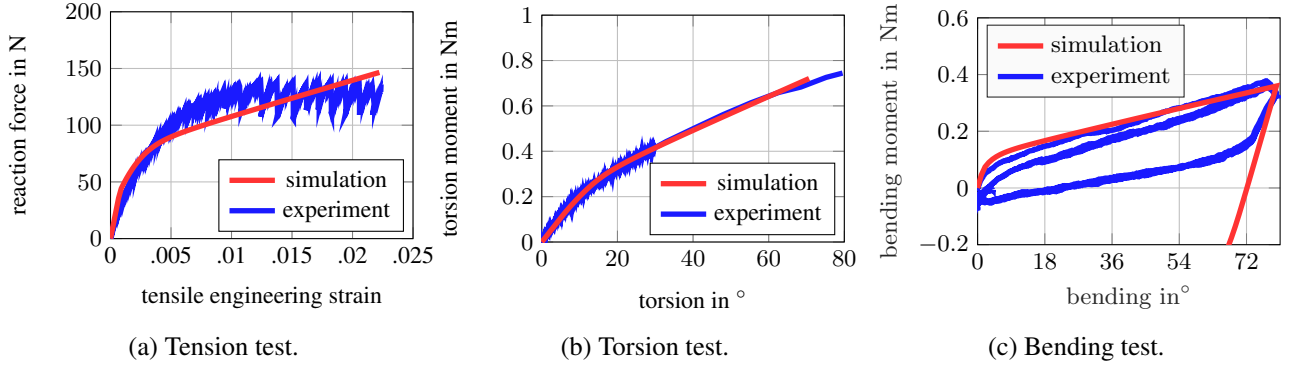


Figure 1: The left and middle picture show the identification simulations and corresponding experimental curves used for the identification. On the right the validation experiment and simulation for free bending is shown [4].

is computed, that defines the yielding in $\Phi = \sqrt{\frac{2}{3}} (\sigma_{11}^0 \sqrt{\bar{\chi}} - (\sigma_{11}^0 - Y))$, with the nonlinear isotropic hardening Y and yield stress σ_{11}^0 . A detailed explanation of the constitutive and kinematic equations used can be found in [4, 5].

Since the model is based on the macroscopic behaviour of the cable, the material parameters have to be identified by experimental tests. To this end the particle swarm optimisation algorithm is used to identify the set of effective material parameters. As an input the experimental results of a tension and a torsion test are used.

3. Numeric simulations and results

The described procedure of the previous section is applied on a coaxial cable of 90.5 mm length and 8.4 mm diameter. In Fig. 1a and 1b the simulations using the identified material parameters show a good agreement with the experimental results. A similar observation can be made for the free bending results (Fig. 1c) of the validation experiment and simulation with the limitation to the loading cycle and the elastic part of the unloading. The inelastic behaviour in the unloading is currently not captured by the model. A possible improvement could be the usage of kinematic hardening instead of isotropic hardening, which has some similarities with the observed behaviour.

In addition, local contact of the cable with hp -refinement is investigated to offer high accuracy for large local strains. In a next step the extension towards twisted cable structures through helix like oriented fibre directions is investigated.

Acknowledgments

The support of the DFG (German Research Foundation) under grant number DU 405/14-2 and DI 430/43-2 is gratefully acknowledged.

References

- [1] A. Hildebrandt, P. Sharma, A. Düster, S. Diebels. *Experimental and numerical investigation of the deformation behaviour of cables and thin beam-like structures under multi-axial loading*, Mathematics and Mechanics of Solids, 27(10) (2022), 2314-2337.
- [2] N. Zander, T. Bog, S. Kollmannsberger, D. Schillinger, E. Rank. *Multi-Level hp -Adaptivity: High-Order Mesh Adaptivity without the Difficulties of Constraining Hanging Nodes*, Computational Mechanics, 55(3) (2015), 499-517.
- [3] V. Dörlich, J. Linn, S. Diebels. *Flexible beam-like structures-experimental investigation and modeling of cables*, Advances in Mechanics of Materials and Structural Analysis: In Honor of Reinhold Kienzler, 27-46, 2018.
- [4] A. Hildebrandt, A. Düster. *Numerical Investigation of High-Order Solid Finite Elements for Anisotropic Finite Strain Problems*, International Journal of Computational Methods, 19(05) (2022), 2250007.
- [5] C. Sansour, I. Karšaj, J. Sorić. *A formulation of anisotropic continuum elastoplasticity at finite strains. Part I: Modelling*, International journal of plasticity, 22(12) (2006), 2346-2365.

Static and dynamic analysis of geometrically and materially nonlinear spatial frame like structures

Sudhanva Kusuma Chandrashekhara ¹, Dejan Zupan ²,

¹ Faculty of Civil and Geodetic Engineering, University of Ljubljana, skusuma@fgg.uni-lj.si

² Faculty of Civil and Geodetic Engineering, University of Ljubljana, dejan.zupan@fgg.uni-lj.si

Keywords: Material softening, localization of deformation, strong discontinuity, three-dimensional rotations

1. Introduction

Modeling the mechanical response of flexible slender structures undergoing complex deformations in post-critical regime pose serious challenges in the adopted numerical methods especially while describing demanding phenomenon such as material softening. The focus of the present work is on the phenomenon of strain localization in beam like structural elements which occurs when a material and stress dependent critical condition is reached at some material point of the solid body. The onset of the critical condition results in concentration of strains in the localized region that accelerates damage within a thin narrow band. In the present work a fully consistent geometric and material nonlinearities are considered for both quasi-static and dynamic response of the structure undergoing localized plastic deformation due to material softening using novel energy preserving velocity based formulation by Zupan and Zupan [1]. The typical problems associated with rotational degrees of freedom is completely avoided here with a convenient representation of tangent space using velocities and angular velocities expressed in suitable reference frames. The model is extended with efficient and robust evaluation of stress resultants and cross-sectional tangent modulus [2] to take material nonlinearity into account. The onset of the critical condition resulting in localization of strains is obtained with short low-order elements where the peak like response of the strains are constant over the short segment.

2. Methodology

The system of governing equations for the Cosserat beam is a set of nonlinear partial differential equations which are as follows[1]:

$$\mathbf{n}' + \tilde{\mathbf{n}} = \rho A \dot{\mathbf{v}}, \quad (1)$$

$$\mathbf{M}' + \mathbf{K} \times \mathbf{M} + (\mathbf{\Gamma} - \mathbf{\Gamma}_0) \times \mathbf{N} + \hat{\mathbf{q}}^* \circ \tilde{\mathbf{m}} \circ \hat{\mathbf{q}} = \mathbf{\Omega} \times \mathbf{J}_\rho \mathbf{\Omega} + \mathbf{J}_\rho \dot{\mathbf{\Omega}}, \quad (2)$$

where prime(\prime) denotes the derivative with respect to x and dot ($\dot{\cdot}$) denotes the derivative with respect to time, $\tilde{\mathbf{n}}$ and $\tilde{\mathbf{m}}$ are the external distributed force and moment vectors per unit length, ρ is the mass density and \mathbf{J}_ρ is the mass moment of inertia of the cross section, \mathbf{v} and $\mathbf{\Omega}$ are the velocities and angular velocities, $\hat{\mathbf{q}}$ is the rotational quaternion, $\mathbf{\Gamma}$ and \mathbf{K} are the vectors of translational and rotational strains, respectively. Assuming that the cross-sections suffers only from rigid rotations while undergoing deformation and the longitudinal strains are linearly distributed over the cross-section, we assume that the longitudinal stress (σ) in the material fibre (y, z) is given by a rate independent nonlinear function of the longitudinal strain (ϵ):

$$\sigma(y, z) = \mathcal{F}(\epsilon(y, z)). \quad (3)$$

The assumption that the localization of deformation is primarily driven by the longitudinal stress is still valid for several type of materials like reinforced concrete. The longitudinal components of the stress resultants \mathbf{N} and \mathbf{M} are then obtained by the integration of the stress field over the cross-section, while the components of shear resultants are assumed to be linearly dependent on the corresponding strains:

$$[N_1^C \quad M_2^C \quad M_3^C]^T = [\iint \sigma(\epsilon) dy dz \quad -\iint z\sigma(\epsilon) dy dz \quad \iint y\sigma(\epsilon) dy dz]^T, \quad (4)$$

$$[N_2^C \quad N_3^C \quad M_1^C]^T = [GA_2\Gamma_2 \quad GA_3\Gamma_3 \quad GJ_t K_1]^T, \quad (5)$$

where G is the shear modulus, A_2 and A_3 are effective shear areas and J_t is the torsional moment of inertia. The set of governing equations (1)-(2) are nonlinear partial differential equations that needs to be discretized in

space and time. The discretization in time is based on midpoint rule and the resulting discrete equations are:

$$\mathbf{n}'^{[n+1/2]} + \tilde{\mathbf{n}}^{[n+1/2]} - \frac{\rho A}{h} \left(\mathbf{v}^{[n+1]} - \mathbf{v}^{[n]} \right) = \mathbf{0}, \quad (6)$$

$$\begin{aligned} \mathbf{M}'^{[n+1/2]} + \mathbf{K}^{[n+1/2]} \times \mathbf{M}^{[n+1/2]} + \left(\mathbf{\Gamma}^{[n+1/2]} - \mathbf{\Gamma}_0 \right) \times \mathbf{N}^{[n+1/2]} \\ + \hat{\mathbf{q}}^{*[n+1/2]} \circ \tilde{\mathbf{m}}^{[n+1/2]} \circ \hat{\mathbf{q}}^{[n+1/2]} - \mathbf{\Omega}^{[n+1/2]} \times \mathbf{J}_\rho \mathbf{\Omega}^{[n+1/2]} - \frac{\mathbf{J}_\rho}{h} \left(\mathbf{\Omega}^{[n+1]} - \mathbf{\Omega}^{[n]} \right) = \mathbf{0}, \end{aligned} \quad (7)$$

where $h = t_{n+1} - t_n$ is the step size, the upper index $[n+1/2]$ denotes the quantities at the midtime $t_{n+1/2} = t_n + h/2$. The spatial discretization is based on Galerkin finite element method where the velocities and angular velocities at midtime are the interpolated variables. Using the method of weighted residuals and the midpoint discretization in time, we get the final discretized equations:

$$\int_0^L \left[\frac{\rho A}{h} \left(\mathbf{v}^{[n+1]} - \mathbf{v}^{[n]} \right) P_i + \mathbf{n}^{[n+1/2]} P_i' - \tilde{\mathbf{n}}^{[n+1/2]} P_i \right] dx - \delta_p \mathbf{f}_e^{[n+1/2]} = \mathbf{0}, \quad (8)$$

$$\begin{aligned} \int_0^L \left[\frac{\mathbf{J}_\rho}{h} \left(\mathbf{\Omega}^{[n+1]} - \mathbf{\Omega}^{[n]} \right) P_i + \mathbf{\Omega}^{[n+1/2]} \times \mathbf{J}_\rho \mathbf{\Omega}^{[n+1/2]} P_i - \mathbf{K}^{[n+1/2]} \times \mathbf{M}^{[n+1/2]} P_i + \mathbf{M}^{[n+1/2]} P_i' \right. \\ \left. - \left(\mathbf{\Gamma}^{[n+1/2]} - \mathbf{\Gamma}_0 \right) \times \mathbf{N}^{[n+1/2]} P_i - \left(\hat{\mathbf{q}}^{*[n+1/2]} \circ \tilde{\mathbf{m}}^{[n+1/2]} \circ \hat{\mathbf{q}}^{[n+1/2]} \right) P_i \right] dx - \delta_p \mathbf{M}_e^{[n+1/2]} = \mathbf{0}, \end{aligned} \quad (9)$$

where $\delta_p \mathbf{f}_e$ and $\delta_p \mathbf{M}_e$ are the external point forces and moments. In the above equations, the quantities in the fixed basis are denoted in lower case notations and vice versa. The choice of velocities and angular velocities as primary unknowns provides a convenient representation of tangent space with numerical advantages of additive type update procedure and consistency of standard Lagrange type interpolation functions to be used when expressed in suitable reference frame.

In the quasi-static analysis, the stress resultants are reduced in the post-critical regime where the material exhibits softening response and thus requires a robust and efficient path following scheme which is adopted here. The modified path-following constraint in the perspective of velocity based formulation is read as:

$$\xi \left(\mathbf{W}^{[n+1/2]}, \lambda^{[n+1]} \right) = h^2 \mathbf{W}^{[n+1/2]T} \mathcal{D} \mathbf{W}^{[n+1/2]} + \left(\lambda^{[n+1]} - \lambda^{[n]} \right)^2 \mathbf{P}_e^T \mathcal{H} \mathbf{P}_e - h^2 = 0, \quad (10)$$

where $\mathbf{W}^{[n+1/2]} = [\mathbf{v}^{[n+1/2]}, \mathbf{\Omega}^{[n+1/2]}]^T$, $\lambda^{[n+1]}$ is the load parameter, \mathcal{D} and \mathcal{H} are arbitrary symmetric scaling matrices. The proposed path-following constraint fits naturally into the original formulation and additionally considers rotational parameters without the need for any additional special treatment. However, for the dynamic analysis with non-monotonic loading, a standard practice in plasticity is followed where the irreversible nature of the plastic strains are captured by means of loading / unloading conditions derived from the Kuhn-Tucker relations [3]. The proposed methodology is fully consistent, computationally efficient, robust and exhibits no loss of convergence while preserving the advantages of the original formulation. The effectiveness of the proposed methodology will be demonstrated using several numerical examples.

Acknowledgments

This project has received funding from the European Union's Horizon 2020 research and innovation programme under the Marie Skłodowska-Curie grant agreement No. 860124.

References

- [1] E. Zupan and D. Zupan, On conservation of energy and kinematic compatibility in dynamics of nonlinear velocity-based three-dimensional beams, *Nonlinear Dynamics*, Vol. **95**, (2019) pp. 1379–1394.
- [2] D. Zupan and M. Saje, Analytical integration of stress field and tangent material moduli over concrete cross-sections. *Computers and Structures*, Vol. **83**, (2005) pp. 2368-2380.
- [3] J.C. Simo, T.J.R. Hughes. *Computational Inelasticity*, Springer, Pasadena, 1994.

Inelastic Constitutive Behaviour and Hysteresis Operators - Modelling and Simulations for 2D Cosserat Rods

Davide Manfredò^{1,2}, Vanessa Dörlich¹, Joachim Linn¹ Martin Arnold²

¹ Fraunhofer ITWM, Fraunhofer-Platz 1, 67663, Kaiserslautern, Germany,
 [davide.manfredo, vanessa.doerlich, joachim.linn]@itwm.fraunhofer.de

² Institute of Mathematics, Martin Luther University Halle-Wittenberg, Theodor-Lieser-Str. 5, 06120 Halle
 (Saale), Germany, martin.arnold@mathematik.uni-halle.de

Keywords: Slender structures, Cosserat rods, Inelastic constitutive behaviour, Hysteresis operators, Plane bending experiments

1. Introduction

Due to their complex structure and different materials used, electric cables behave inelastically and open hysteresis loops arise, with noticeable difference between the first load cycle and the following ones. In this regard, the mathematical theory of hysteresis represents a good choice to model and describe such complex behaviour. In this contribution, we present a procedure to include an inelastic constitutive law formulated in terms of a suitable hysteresis operator in a 2D Cosserat rod model to perform quasi-static simulations.

2. Continuous and discrete 2D Cosserat rod model

A 2D Cosserat rod of length L is described by its centreline $[x(s), y(s)]^T$ and its rotation angle $\alpha(s)$, with $s \in [0, L]$. In the continuous case, the bending curvature $K(s)$ and the shear-extensional strain $\mathbf{\Gamma}(s)$ are given by

$$\mathbf{\Gamma}(s) = \mathbf{R}^T(s) \cdot \begin{bmatrix} x'(s) \\ y'(s) \end{bmatrix} - \begin{bmatrix} 1 \\ 0 \end{bmatrix}, \quad K(s) = \alpha'(s), \quad \text{with } \mathbf{R}(s) = \begin{bmatrix} \cos(\alpha(s)) & -\sin(\alpha(s)) \\ \sin(\alpha(s)) & \cos(\alpha(s)) \end{bmatrix}.$$

If we assume a linear elastic constitutive behaviour for both forces and moment, we can express them respectively as $\mathbf{F}(s) = \mathbf{C}_{\mathbf{\Gamma}} \cdot \mathbf{\Gamma}(s)$ with $\mathbf{C}_{\mathbf{\Gamma}} = \text{diag}([EA], [GA])$ and $M(s) = [EI] \cdot K(s)$. The parameters $[EA]$, $[GA]$, $[EI]$ are respectively the effective tension, shear and bending stiffness. As shown in [1], the static equilibrium can be obtained by minimising the elastic potential energy

$$W = \frac{1}{2} \int_0^L \mathbf{\Gamma}^T(s) \cdot \mathbf{C}_{\mathbf{\Gamma}} \cdot \mathbf{\Gamma}(s) ds + \frac{1}{2} \int_0^L [EI] \cdot K^2(s) ds.$$

A discrete 2D Cosserat rod model can be derived from the continuous one by considering a staggered grid made of vertices $[x_i, y_i]^T$ for $i = 0, \dots, N$ and edge-centred rotation matrices $\mathbf{R}(\alpha_{i+1/2})$ for $i = 0, \dots, N-1$. For further details, see [2].

3. The Prandtl-Ishlinskii (P-I) operator

As shown in [3], hysteresis operators are a well-studied topic with a variety of applications and the P-I operator \mathcal{P} plays a relevant role in modelling the input-output relation in phenomena showing hysteretic behaviour and can be expressed as a superposition of elementary stop operators \mathcal{S}_r multiplied by a suitable weight function $\omega(r)$, which is assumed to vanish for large values of r . We aim at expressing the bending moment vs. bending curvature in terms of P-I operator as a discretised version of

$$M(t) = \mathcal{P}[K](t) = \int_0^{+\infty} \omega(r) \mathcal{S}_r[K](t) dr.$$

The stop operator \mathcal{S}_r can be defined recursively. For a comprehensive analysis, we refer to [3]. By superimposing different elementary stop operators, one is able to model more complex hysteretic effects taking into account the history of the process.

4. Pure bending simulation of a Cosserat rod with inelastic constitutive law

The procedure foresees, firstly, to identify a suitable hysteresis operator able to capture the inelastic relation between bending moment and bending curvature. In our case, we assume the M vs. K constitutive relationship to be described via a P-I operator with weight function given by $\omega(r) = 0.005e^{-0.2r}$ and 15 equidistant thresholds in the interval $[0, 20]$.

Secondly, we define a series of boundary conditions or constraints for each discrete time node $t = 0, \dots, T$, generally expressed in terms of positions and angles at both ends of the rod, while allowing for a translation of one end in x -direction. Starting from an initial approximation of the bending stiffness $[EI]_i^{(t=0)}$, at each simulation step we update the bending stiffness value by means of the hysteresis operator $M_{i,\text{Hyst}}^{(t)} = \mathcal{P}_r[K_i^{(t)}]$

$$[EI]_i^{(t)} = \frac{M_{i,\text{Hyst}}^{(t)} - M_{i,\text{Hyst}}^{(t-1)}}{K_i^{(t)} - K_i^{(t-1)}} \quad \text{for } t = 1, \dots, T.$$

The value of the simulated bending moment is then updated as $M_i^{(t)} = M_i^{(t-1)} + [EI]_i^{(t)} \cdot (K_i^{(t)} - K_i^{(t-1)})$.

As depicted in Fig. 1, starting from a straight configuration, the cable is bent by imposing different angles at both ends of the rod. On one hand, the curvature remains constant along the specimen, as demonstrated by the colours in Fig. 1 right, as well as the bending moments. On the other hand, the M vs. K diagram shows a very good agreement with the assumed inelastic behaviour described by a hysteresis operator of P-I type.

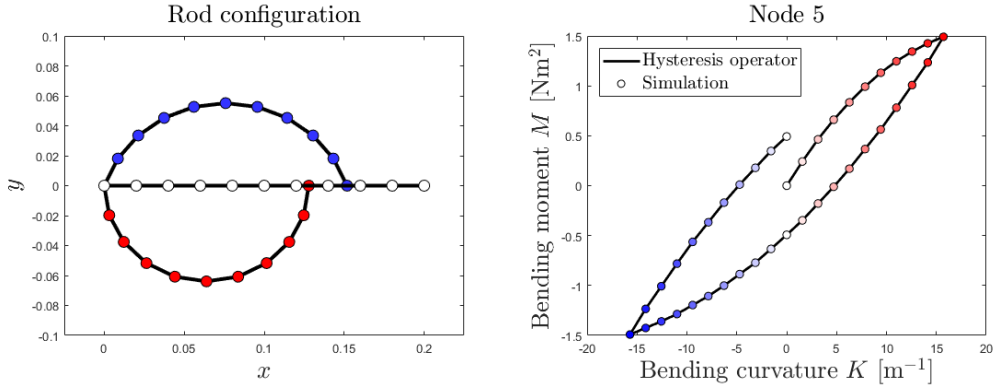


Figure 1: Pure bending simulation results. *Left:* Rod configuration for different boundary conditions. White: straight initial configuration, $K = 0 \text{ m}^{-1}$. Red: $K = 15.71 \text{ m}^{-1}$. Blue: $K = -12.57 \text{ mm}^{-1}$. *Right:* Bending moment vs. bending curvature diagram relative to the fifth node. The scattered plot corresponds to the simulated moments while the solid line depicts the P-I operator. Different colours in the simulated results represent different curvature values.

In conclusion, the Cosserat rod theory seems a good framework for the inclusion of a hysteretic constitutive law. Future plans foresee the identification of such an inelastic law by means of specifically designed pure bending experiments and the implementation of more complex boundary conditions and the validation with real plane bending experiments, such as the MeSOMICS test rig [2].

Acknowledgments

This project has received funding from the European Union's Horizon 2020 research and innovation programme under the Marie Skłodowska-Curie grant agreement No 860124.



References

- [1] J. Linn *et al.*, *Kinetic aspects of discrete Cosserat rods based on the difference geometry of framed curves*, ECCOMAS Thematic Conference on Multibody Dynamics, 2017.
- [2] T. Zhao *et al.*, *Simulating Nonlinear Elastic Behaviour of Cables Using an Iterative Method*, ECCM, 2022.
- [3] K. Kuhnen, *Kompensation komplexer gedächtnisbehafteter Nichtlinearitäten in Systemen mit aktiven Materialien*, Shaker-Verlag, Aachen, Place of Publication, 2008.

Constrained optimization for part-through crack computation

Sébastien Jean Michel¹, András Á. Sipos²,

¹ Dept. Of Morphology and Geometric Modeling, Budapest University of Technology and Economics,
 Budapest, Hungary, sebastien.michel@edu.bme.hu

² MTA-BME Morphodynamics Research Group, Budapest University of Technology and Economics,
 Budapest, Hungary, siposa@eik.bme.hu

Keywords: Variational brittle fracture, Energetic formulation, Euler-Bernoulli beam, Geometric modeling.

1. Introduction

Predicting the failure of structures and describing where and when cracks will occur has immediate relevance in engineering applications, be it for dimensioning, life-time assessment, or cost optimization. The complexity of the elasticity equations makes the sole resolution of a problem complex, even for simple geometry. Ever since the seminal paper of Griffith [5] anchoring the problem in an energy minimization framework, a considerable amount of work has been devoted to expanding the theory [8]. It is only very recently that the equilibrium of a body allowed to crack has been formulated in the modern variational setup [1,2]. The rigorous deduction of the single-dimensional equations for a slender body from the equations of elasticity in the three-dimensional setting proves still challenging and is still currently researched [3,6]. In particular, the active interplay between the varying geometry of the cracking body and the stress resultants is yet to be revealed, despite recent attempts to give a rigorous description of these fields when the slender body possesses a developed crack [4].

2. Problem formulation

In this study we will focus on the effect of bending for an initially straight beam of rectangular cross-section $[-\frac{h}{2}, \frac{h}{2}] \times [-\frac{b}{2}, \frac{b}{2}]$ whose length is L and where the current position on the beam is z . The variable geometry of the beam is modeled by assigning to each cross-section two geometric fields $d^+(z), d^-(z)$ modeling the depth of penetration of the cracks on each side of the beam. We postulate the bending moment in a section to be the product of the variation of the intrinsic curvature of the beam with the section bending stiffness: $M = EI(d^+, d^-)w_{zz}$. The moment of inertia of any section $I(d^+, d^-)$ is adequately computed considering both the surface reduction and the change in the section centroid position. A dissipation term depending on the material fracture toughness G is included, accounting for the energy cost of creating new cracks surfaces. Higher gradients addition ensures the problem is regularized [2]. A characteristic length ℓ is introduced that controls the speed of variation of the geometric fields. For a beam subject to a distributed load $p_t(z)$, the energy to be minimized F with respect to the transversal displacement field w and the geometric fields d^+, d^- reads:

$$F = \int_0^L \frac{EI(d^+, d^-)}{2} w_{zz}^2 - p_t(z)w \, dz + \int_0^L \left\{ \frac{Gb}{4\ell} \left(\left(\frac{d^+}{h} \right)^2 + \left(\frac{d^-}{h} \right)^2 \right) + Gb\ell \left(\left(\frac{d_z^+}{h} \right)^2 + \left(\frac{d_z^-}{h} \right)^2 \right) \right\} dz. \quad (1)$$

In addition, the unknown fields satisfy the boundary conditions adapted to the problem at-hand.

3. Resolution

The computation of the fields follows the operator splitting procedure of [7]. The load $p_t(z)$ is incremented and the geometric and displacement fields are computed in a staggered scheme. At fixed damage fields, the displacement field is uniquely defined, and its computation is straightforward from the functional's stationarity equations and prescribed boundary conditions. At fixed displacement field, the damage fields have to minimize the energy functional. The stationarity equations yield a system of nonlinear differential equation in d^+, d^- and have to be solved under additional constraints. On one hand, the cracks penetration depths have to be compatible with the original height h of the beam cross-section:

$$0 \leq \frac{d^+}{h} \leq 1, \quad 0 \leq \frac{d^-}{h} \leq 1, \quad 0 \leq \frac{d^+ + d^-}{h} \leq 1. \quad (2)$$

On the other hand, the damage fields cannot decrease thus the fields d^+ , d^- have to satisfy the Unilateral Stationarity constraint [2]. Additional constraints ensure crack development on the beam tensiled side.

4. Results

We compare the results of our model with that of the widely accepted variational brittle fracture for a clamped-clamped beam (Fig 1.) and a simple cantilever with a double point load. The results are found to be in good agreement with the variational damage fields models, despite a very strong smearing of the cracks zones. The cracking zones are clearly defined and there is no need for additional treatment to decide what is a crack interface. Crack initiation occurs at position of the computed maximum of the bending moment, and simultaneous cracking is observed if the moment diagram possesses many extrema of same amplitude.

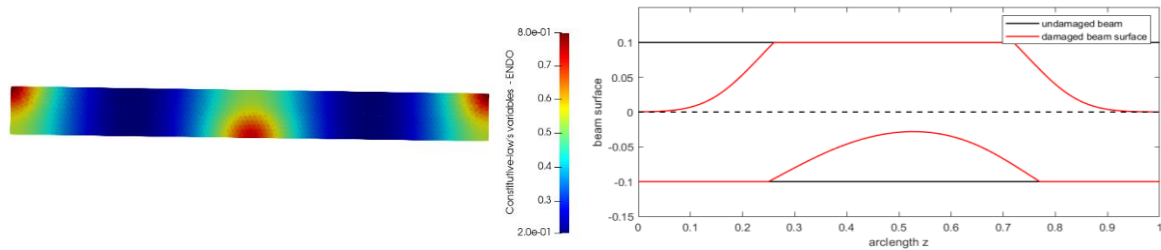


Figure 1. Computed damage field for a clamped-clamped beam under a vertical point load in the middle of the beam. On the left the solution from the variational damage field model figuring in red the most damaged zones. On the right the solution geometric fields d^+ , d^- are in red and the undamaged beam surface is figured in black.

Acknowledgements

This research was supported by the UNKP-22-3 New National Excellence Program of the Ministry for Innovation and Technology from the source of the National Research, Development and Innovation Fund of Hungary.

References

- [1] Amor, H., Marigo, J. J., & Maurini, C. (2009). Regularized formulation of the variational brittle fracture with unilateral contact: Numerical experiments. *Journal of the Mechanics and Physics of Solids*, 57(8), 1209-1229.
- [2] Bourdin, B., Francfort, G. A., & Marigo, J. J. (2008). The variational approach to fracture. *Journal of elasticity*, 91, 5-148.
- [3] Christides, S., Barr, A. D. S. (1984). One-dimensional theory of cracked Bernoulli-Euler beams. *International Journal of Mechanical Sciences*, 26(11-12), 639-648.
- [4] Corsi, G., Favata, A., & Vidoli, S. (2023). A coarse-grained constitutive law for fracturing beams based on a sharp interface crack representation. *International Journal of Solids and Structures*, 112224.
- [5] Griffith, A. A. (1921). VI. The phenomena of rupture and flow in solids. *Philosophical transactions of the royal society of london. Series A, containing papers of a mathematical or physical character*, 221(582-593), 163-198.
- [6] Lai, W., Gao, J., Li, Y., Arroyo, M., & Shen, Y. (2020). Phase field modeling of brittle fracture in an Euler-Bernoulli beam accounting for transverse part-through cracks. *Computer Methods in Applied Mechanics and Engineering*, 361, 112787.
- [7] Miehe, C., Hofacker, M., & Welschinger, F. (2010). A phase field model for rate-independent crack propagation: Robust algorithmic implementation based on operator splits. *Computer Methods in Applied Mechanics and Engineering*, 199(45-48), 2765-2778.
- [8] Tanné, E., Li, T., Bourdin, B., Marigo, J. J., & Maurini, C. (2018). Crack nucleation in variational phase-field models of brittle fracture. *Journal of the Mechanics and Physics of Solids*, 110, 80-99.

Finite element beams based on non-linear micropolar theory

L. P. Obrezkov¹, M. K. Matikainen¹, R. Kouhia²

¹ Mechanical Engineering, LUT University, Yliopistonkatu 34, 53850, Lappeenranta, Finland

² Faculty of Built Environment, Tampere University, Korkeakoulunkatu 7, 33720, Finland

Keywords: Absolute nodal coordinate, Micropolar continuum, Cosserat continua, Size effect

1. Introduction

Experiments of torsion and bending have shown the effects unexplained within classical theories, e.g., size-effect. There, the rigidity depends on the object dimensions, and smaller samples respond stiffer than larger ones from the same material. One can attribute the difference to the microstructure influence. Including the microstructure is possible within the extended continuum theories, such as the micropolar or Cosserat elasticity theory [1]. The difference between the classical and micropolar media is the presence of the particle orientation in the latter. In classical theory, the point has only a position.

The inclusion of the micropolar theory can be beneficial in many aspects: description of the stresses' singularities in contact areas, strain localization computations, micro-scaled structures, presentation of multilayer structures, etc [2]. Therefore, the combination of micropolar theory and the most common engineering approach – finite element analysis – was expected. However, the implementation concerned only 3D solid elements, and it cannot be considered an efficient formulation for many structures, such as beams. The authors present the possible combination of the continuum beam formulation and the micropolar media to fulfill this gap.

2. Micropolar beam element kinematic

The kinematic description for the micropolar beam element based on the absolute nodal coordinate formulation, and all details one can find detail in [2]. The difference from the standard formulation is the inclusion of degrees of freedom components for approximating the microrotational field $\boldsymbol{\theta}$. In this work, we use a three-noded element, where the i -th node has the following set degrees of freedoms:

$$\mathbf{q}_i = \left[\mathbf{r}^{i^T} \mathbf{r}_{,y}^{i^T} \mathbf{r}_{,z}^{i^T}, \mathbf{r}_{,yy}^{i^T} \mathbf{r}_{,yz}^{i^T} \mathbf{r}_{,zz}^{i^T}, \boldsymbol{\theta}^{i^T} \boldsymbol{\theta}_{,y}^{i^T} \boldsymbol{\theta}_{,z}^{i^T} \boldsymbol{\theta}_{,yy}^{i^T} \boldsymbol{\theta}_{,yz}^{i^T} \boldsymbol{\theta}_{,zz}^{i^T} \right]^T, \mathbf{r}_{,\alpha}^i = \frac{\partial \mathbf{r}^i}{\partial \alpha}, \alpha = \{y, z\}. \quad (1)$$

Then, assuming \mathbf{N}_m is the shape matrix, the approximation of position and microrotational fields are :

$$\{\mathbf{r}, \boldsymbol{\theta}\} = \mathbf{N}_m(\xi, \eta, \zeta) \mathbf{q}(t), \quad (2)$$

3. Micropolar media description

The balance of equations for micropolar media gives the following set of equations:

$$\begin{aligned} \nabla_X \cdot \mathbf{t} + \mathbf{f} &= \boldsymbol{\theta}, \\ \nabla_X \cdot \mathbf{m} + \boldsymbol{\varepsilon} : \mathbf{m} + \mathbf{c} &= \boldsymbol{\theta}. \end{aligned} \quad (3)$$

where ∇_X is the covariant differentiation operator in the reference coordinate system. \mathbf{t} and \mathbf{m} are stress and couple stress tensors, respectively. They can be obtained as follows.

$$\begin{aligned} \mathbf{t} &= \lambda \text{tr}(\mathbf{H}) \mathbf{I} + (\mu + k) \mathbf{H} + \mu \mathbf{H}^T, \\ \mathbf{m} &= \alpha \text{tr}(\boldsymbol{\Gamma}) \mathbf{I} + \beta \boldsymbol{\Gamma} + \gamma \boldsymbol{\Gamma}^T. \end{aligned} \quad (4)$$

$\lambda, \mu, \kappa, \alpha, \beta, \gamma$ are elastic constants, \mathbf{H} and $\boldsymbol{\Gamma}$ are material strain and microcurvature tensors, respectively. Assuming that $\boldsymbol{\Omega}$ is the skew-symmetric of $\boldsymbol{\theta}$, and θ is the magnitude of $\boldsymbol{\theta}$, then:

$$\begin{aligned} \boldsymbol{\Gamma} &= -\frac{1}{2} \boldsymbol{\varepsilon} : (\mathbf{R}^T \nabla_X \mathbf{R}), \\ \mathbf{H} &= \mathbf{U} - \mathbf{I}, \mathbf{U} = \mathbf{F}^T \mathbf{R}, \\ \mathbf{R} &= \exp(\boldsymbol{\Omega}) = \left(\mathbf{I} + \frac{\sin \theta}{\theta} \boldsymbol{\Omega} + \frac{1 - \cos \theta}{\theta^2} \boldsymbol{\Omega} \boldsymbol{\Omega} \right), \end{aligned} \quad (5)$$

where \mathbf{F} is the deformation gradient, $\boldsymbol{\varepsilon}$ is the third-order Levi-Civita tensor.

4. Numerical results

Let us consider the bending cantilever beam, where the dimension sizes are regulated by the size-effect coefficient k , which will proportionally change the load and beam's dimensions. The initial geometrical dimensions are $L = 0.03$ m, $H = 0.01$ m, $W = 0.002$ m, the applied force is $F = 500$ N, and material parameters are from [2]. We provide solutions obtained with solid element from [3] for comparison. We also consider elements within the classical theory to present the difference between them.

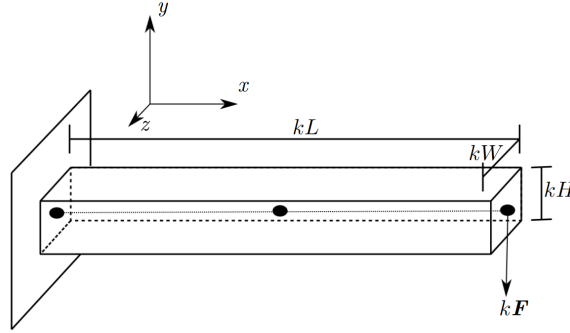


Figure 1: Task set up with the size-coefficient k .

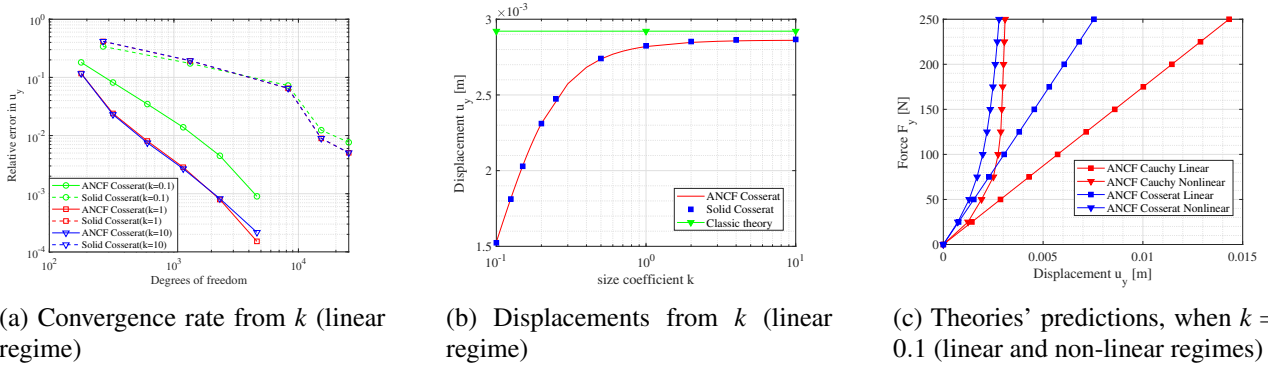


Figure 2: The presentation of the size-dependency for different theories in linear and non-linear regimes, from [2].

5. Conclusion

This work presents the beam element suitable for dealing with the micropolar continuum and using it even in the non-linear regime. Thus, it fully accounts for the differences between the two media descriptions and is a more efficient formulation for beam-like structures.

Acknowledgments

This project has received funding from the Academy of Finland (Application No. 299033 for funding of Academy Research Fellow).

References

- [1] E. Carrera, V. V. Zozulya. Carrera unified formulation (CUF) for the micropolar beams: Analytical solutions, *Mechanics of Advanced Materials and Structures*, 28 (2021) 583-607
- [2] L. Obrezkov, M. K. Matikainen, R. Kouhia. Micropolar beam-like structures under large deformation, *International Journal of Solids and Structures*, 254–255 (2022) 111849
- [3] V. A. Eremeyev, A. Skrzat, F. Stachowicz. On Finite Element Computations of Contact Problems in Micropolar Elasticity, *Advances in Materials Science and Engineering*, (2016) 1-9

Vibrations of an inclined cable with a lumped mass

Moritz Patreider^{1 2 *}, Markus Wenin², Thomas Furtmüller¹, Christoph Adam¹

¹ Universität Innsbruck, Unit of Applied Mechanics

² CPE

* e-mail: moritz.patreider@cphysics.com

Keywords: cables(mechanical), equations of motion, eigenvalue problem, nonlinear dynamical systems, vibrations

1. Introduction

Cables are widely used in engineering applications. Depending on various system parameters they show complex vibratory behavior. An exact analytical description can improve the understanding of these phenomena and be used as benchmark solutions for numerical simulations. The lumped mass alters the dynamics of an inclined cable drastically.

2. Equations of motion

The differential equations governing the in-plane dynamic behavior of an inclined cable with a lumped mass attached to the cable between two immovably fixed supports are given by

$$\frac{\partial}{\partial s} \left[(T + \tau) \left(\frac{d\xi}{ds} + \frac{\partial \mu}{\partial s} \right) \right] + \rho(s)g \sin \vartheta - \rho(s) \frac{\partial^2 \mu}{\partial t^2} = 0 \quad (1)$$

$$\frac{\partial}{\partial s} \left[(T + \tau) \left(\frac{d\eta}{ds} + \frac{\partial \nu}{\partial s} \right) \right] + \rho(s)g \cos \vartheta - \rho(s) \frac{\partial^2 \nu}{\partial t^2} = 0 \quad (2)$$

Here T is the static cable tension, ϑ the angle of inclination and g the gravitational acceleration. ξ, η describe the static parametric solution, μ, ν are the displacements from equilibrium (μ longitudinal and ν normal direction), τ is the additional cable tension, and $\rho(s)$ is the cable density per unit length. The variable s is the Lagrangian coordinate that measures the distance along a static inextensible cable starting from the left support. The cable density ρ including the lumped mass m at position s_m reads as

$$\rho(s) = \rho_0 + m\delta(s - s_m) \quad (3)$$

where ρ_0 is the uniform cable density per unit length and δ the Dirac delta distribution. The lumped mass splits the system into two domains with separate equations and boundary conditions.

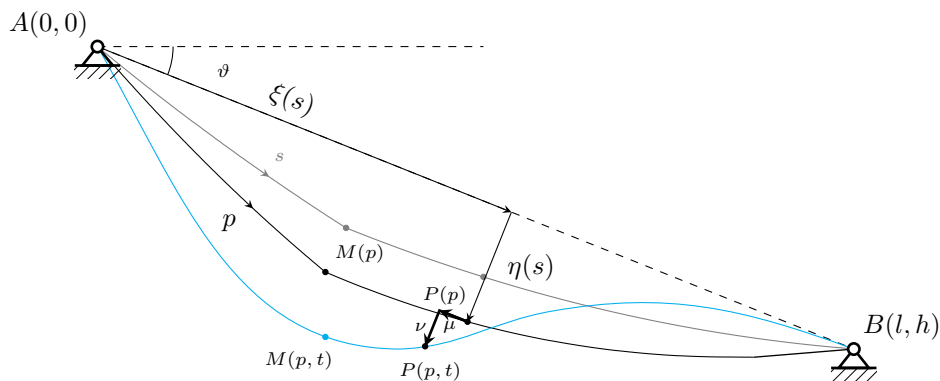


Figure 1: Definition diagram for cable vibrations.

3. Analytical solution of the eigenvalue problem

The equations (1) and (2) are simplified by neglecting terms of second order or higher and removing the static equilibrium terms. After a Fourier-transform, an eigenvalue problem results. Since the longitudinal vibrations

μ will always be smaller than the transverse vibrations v , equation (1) can be discarded and instead we use the linearized cable equation

$$\frac{\chi}{EA} \left(\frac{ds}{d\xi} \right)^3 = \frac{d\mu}{d\xi} + \frac{d\eta}{d\xi} \frac{dv}{d\xi} \quad (4)$$

as an expression for μ . Here E is Young's modulus, A is the cross-section of the cable and χ is the change in cable tension in the ξ -direction ($\chi = \tau \frac{d\xi}{ds}$). It provides the compatibility between the changes in cable tension and cable geometry when the cable is displaced from equilibrium.

The linearized version of equation (2) reads

$$X(\xi) \frac{d^2v}{d\xi^2} - \rho_0 g \sin \vartheta \frac{dv}{d\xi} + \rho_0 \omega^2 v = -\chi \frac{d^2\eta}{d\xi^2} \quad (5)$$

where X is the chordwise component of the static cable tension (different in the two domains and no longer constant due to the inclination of the cable). The solution of this equation is a linear combination of Bessel functions that can be approximated by trigonometric functions with good accuracy. In the solution one assumes that χ is piecewise constant in the two domains to the left and right of the point load. Combining the cable equations for both domains, as well as using the equation of motion describing the movement of the point load in μ -direction, one obtains a system of two equations for the two unknown changes in tension χ_l and χ_r . The nontrivial solutions require the determinant of the 2×2 -matrix to vanish, which can be used to find the eigenfrequencies of the system. The resulting equation is complex and long, and thus not reproduced here. The modeshapes can then be obtained from the solution of equation (5). The approximate solution for μ can be found by integrating equation (4).

4. Validation of the Analytical Expressions

The results presented here were validated by comparing them to numerical simulations of the linearized equations (1) and (2). The accordance between the analytical and numerical results was very good. The theory also reproduces the results found in the paper of Chu [2] that investigated the vibrations of an inclined cable without a lumped mass load (for $m = 0$ in $\rho(s)$).

5. Conclusion

The presented analytical method finds the frequencies and mode shapes for an inclined cable with a point load to good accuracy. The theory is a natural progression of the results presented by Irvine [1] almost 50 years ago and their successor by Chu [2] for an inclined cable. It reproduces these known results and extends the results of the paper by Wenin [3] for a horizontal cable. The extension of this theory to any number of point loads is straightforward.

Acknowledgments

This project has received funding from the Amt für Innovation, Forschung und Universität of the Province of Bolzano (IT) under the grant agreement No 5499/22.

References

- [1] H. M. Irvine, T. K. Caughey. *The linear theory of free vibrations of a suspended cable*, Proc. R. Soc. Lond., A 341 (1974) 299-315
- [2] X. Zhou, S. Yan, F. Chu. *In-Plane Free Vibrations of an Inclined Taut Cable*, J. Vib. Acoust., 133(3) (June 2011) 031001-1-031001-8
- [3] M. Wenin. *Analytical solution of the eigenvalue problem for the elastic cable loaded with a mass point*, Ar. Appl. Mech., 92 (2022) 3649-3660

On the bending of spiral strands

Mohammad Ali Saadat¹, Damien Durville¹

¹ Laboratoire de Mécanique Paris-Saclay, Université Paris-Saclay, Centrale Supélec, ENS Paris-Saclay, CNRS, LMPS, 3 rue Joliot-Curie, Gif-sur-Yvette, 91190, France
[mohammad-ali.saadat,damien.durville]@centralesupelec.fr

Keywords: Spiral strands, Computational homogenization, Rheological models, Offline homogenization

1. Introduction

Frictional interactions between steel wires within spiral strands used as mooring lines for offshore platforms induce a complex mechanical response of these strands when subjected to a bending load under tension. Due to these internal frictional interactions, the mechanical behavior of the strand at the macroscopic scale is dissipative, and the bending stiffness, which is governed by interwire slippage, evolves nonlinearly with respect to curvature and tension. It is possible to simulate the effects of interwire friction using finite element simulation by considering all the individual wires that make up the rope. However, this approach cannot be applied to spiral strands used as mooring lines for offshore platforms due to their size, both in terms of the number of wires and the length considered. This study aims to develop an alternative approach, using computational homogenization, to efficiently calculate not only the macroscopic, but also the microscopic response of spiral strands.

2. Direct numerical simulation (DNS) [1]

In DNS, all wires and frictional contact interactions are modeled using finite element simulation. As can be seen in Figure 1, the obtained axial-bending response of the four-layer spiral strand is in good agreement with the experimental results.

3. Mixed stress-strain driven computational homogenization [2]

To reduce the computational cost of modeling of spiral strands, a mixed stress-strain driven computational homogenization is developed. In this approach, the moment-curvature response of a spiral strand is extracted from a short sample of the strand, called representative volume element (RVE). Using the RVE responses, the axial-bending response of the strands is calculated, and as can be seen in Figure 2, the response obtained from the homogenization is in good agreement with the DNS.

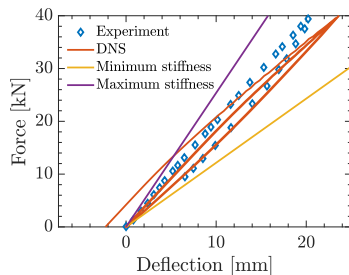


Figure 1: A comparison of the axial-bending response of the four-layer spiral strand obtained from DNS with experimental data.

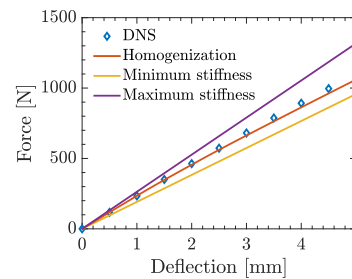


Figure 2: The force-deflection response of a strand under bending with constant axial force obtained through the DNS, homogenization, and theoretical stiffnesses, for the two-layer RVE.

4. Rheological models

In order to reduce the computational cost of homogenization, rheological models are proposed to replace the solution of the RVE boundary value problem to perform offline homogenization. As can be seen in Figure 3, these models, consisting of springs and sliders, predict the biaxial bending response of spiral strands under variable axial force with good accuracy.

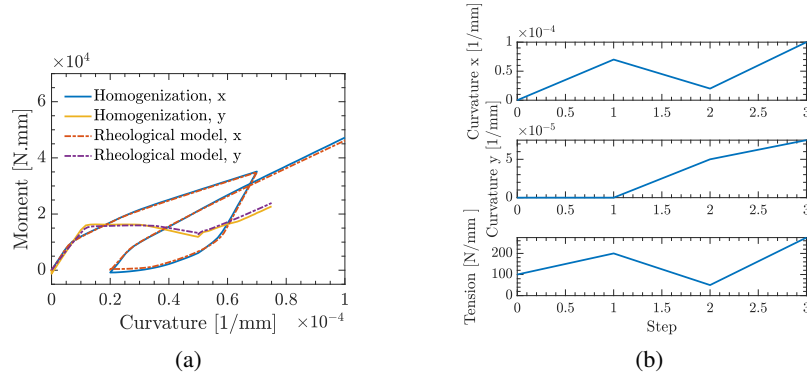


Figure 3: A comparison of the biaxial bending response of spiral strands obtained from homogenization and the rheological models. a, the two-layer strand; b, the loading history.

5. The axial force of individual wires

The axial force in individual wires is required to perform fatigue life estimation for spiral strands. For this purpose, since the bending induced axial force is due to interlayer friction, the friction increment is obtained from the homogenized monotonic axial bending response of the strands as a function of the bending curvature increment. These frictional forces are then integrated to obtain the axial force of the wires. A comparison of the axial force of wires of a two-layer spiral strand obtained from homogenization and the proposed approach is shown in Figure 4.

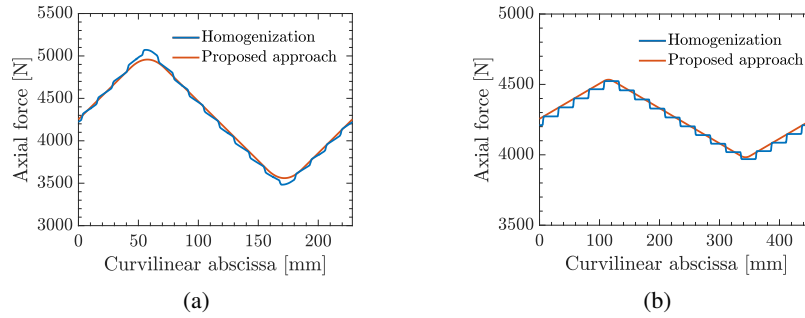


Figure 4: A comparison of the unbalanced axial force caused by bending of spiral strands obtained from homogenization and the proposed model. a, a wire of the first layer; b, a wire of the second layer.

6. Conclusions

As it can be observed, using the proposed framework for modeling spiral strands, the macroscopic and microscopic responses are captured while reducing the computational cost by several orders of magnitude.

Acknowledgments

This work has received funding from the European Union's Horizon 2020 research and innovation programme under the Marie Skłodowska-Curie grant agreement No 860124.



References

- [1] D. Durville, Contact-friction modeling within elastic beam assemblies: an application to knot tightening, *Computational Mechanics* 49 (2012) 687–707.
- [2] M. A. Saadat, D. Durville, A mixed stress-strain driven computational homogenization of spiral strands, *Computers & Structures* 279 (2023) 106981.

On the number of congruent hinges of masonry arches at failure

András A. Sipos^{1,2}

¹ Dept. Morphology and Geometric Modeling, Budapest University of Technology and Economics, Hungary

² MTA-BME Morphodynamics Research Group, Hungary, siposa@eik.bme.hu

Keywords: masonry arch, failure mechanism, thrust line, geometrically exact rod equations

1. Introduction

Structural failure of masonry arches is not with a dominantly material origin: occurring hinges transform the structure into a mechanism and lead to collapse. Nonetheless, the hinges form because of the limited tensile capacity of the voussoir interfaces, called *joints*. The classical approach introduced by J. Heyman [1] adopts a simple, nonlinear constitutive law for the joints. The Heymanian framework carries out the structural analysis of an arch in a geometric manner: the *thrust line*, connecting the intersection points between the voussoir interfaces and the internal reaction force should be contained inside the boundaries of the structure to guarantee equilibrium. The distribution of the external loads, the shape of the arch, and the support conditions mutually determine the structure's safety. Assuming vanishing movements at the supports, the *admissible global geometry* [2, 3] and the role of the cutting pattern of the building elements, called *stereotomy* [4] are extensively studied.

This talk aims to study the maximal number of congruent hinges that can form in the arch. First, the classical governing equations of a *geometrically exact rod* [5], are readily applied to describe the equilibrium of the arch. While a rod is a model of a flexible, one-dimensional continuum, the arches investigated here are structures built of rigid blocks connected with joints characterized by limited tensile capacity. In the case of the rod, the equilibrium of the internal and external loads is attained on the deformed shape. In the case of the arch, the rigid voussoirs, the motionless supports, and the Heymanian assumptions result in vanishing deformations. Hence, the geometry is known *a-priori*, but the internal tractions are prone to unilateral constraints, as the position of the thrust line, should be contained inside the body of the structure.

2. The model in a nutshell

The number of hinges forming in masonry arches with zero tensile strength along the joints is investigated with the help of the equilibrium equations of a geometrically exact rod. Let s denote the arc length of the reference line, and fix the domain as $s \in \Omega := [s_1, s_2]$. Let $\mathbf{r} : \Omega \rightarrow \mathbb{R}^3$ denote the *reference line* of the arch. In general the thrust line, denoted to \mathbf{f} , is also a spatial curve and it is also parametrized with respect to s (see Fig. 1). In the model *stereotomy* is a bijective map between \mathbf{r} and \mathbf{f} , in specific it is characterized by the vector field \mathbf{j} , where

$$\mathbf{j}(s) := \mathbf{f}(s) - \mathbf{r}(s), \quad s \in \Omega. \quad (1)$$

The first derivative of any function $f(x)$ with respect to the argument x is denoted as $f_{,x}$. The governing equations of the new model are based on the geometrically exact rod equations [5]:

$$\mathbf{p}_{,s} + \mathbf{q} = \mathbf{0}, \quad (2)$$

$$\mathbf{m}_{,s} + \mathbf{r}_{,s} \times \mathbf{p} + \mathbf{g} = \mathbf{0}, \quad (3)$$

where $\mathbf{q}(s)$ and $\mathbf{g}(s)$ are the distributed external load and moments, respectively. $\mathbf{p}(s)$ and $\mathbf{m}(s)$ are the vector fields of the internal forces and moments and \times denotes the cross product in 3-space. In rod theoretic problems, both the deformed shape \mathbf{r} and the internal actions \mathbf{p} and \mathbf{m} are unknowns. Constitutive relations and boundary conditions are needed to make the problem well-posed [6].

In the case of the arch, the $\mathbf{p}(s)$ vector field of the internal loads is associated with the moment free thrust line \mathbf{f} , and the external distributive moments vanish. Concentrated loads or moments are not allowed. In this case, exploiting $\mathbf{m} = \mathbf{j} \times \mathbf{p}$ and $\mathbf{g} \equiv \mathbf{0}$ the equilibrium equations (2) and (3) above read

$$\mathbf{p}_{,s} + \mathbf{q} = \mathbf{0}, \quad (4)$$

$$(\mathbf{r}_{,s} + \mathbf{j}_{,s}) \times \mathbf{p} + \mathbf{j} \times \mathbf{p}_{,s} = \mathbf{0}. \quad (5)$$

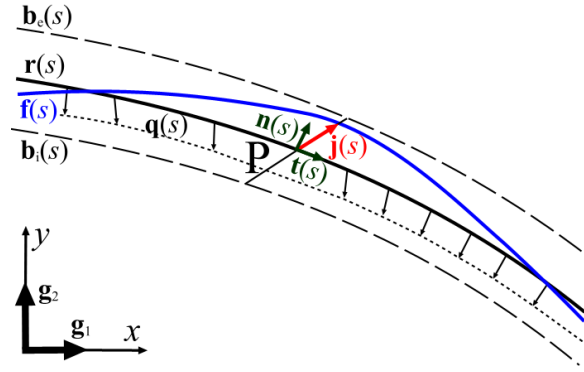


Figure 1: At point P of the arch defined by the reference line \mathbf{r} the stereotomy is given by \mathbf{j} . The curve \mathbf{f} is the thrust line that corresponds to the distributed load \mathbf{q} .

3. Results

After exact definition of the \mathbf{b}_e and \mathbf{b}_i boundaries of the arch, exploiting the governing equations in (4) and (5), the following theorems are proved, affirming the numerical results of the literature [7]:

Theorem 1. Among planar arches loaded by self-weight, for any prescribed stereotomy function $\hat{\mathbf{j}} \in C^1(\Omega \rightarrow \mathbb{R})$ there exists a \mathbf{r} reference line such that $\mathbf{r} + \hat{\mathbf{j}}$ is the thrust line of the structure.

Theorem 2. In a pointed, planar arch, obtained by reflecting a circular segment to a vertical axis crossing the segments higher end, the maximum number of hinges is $C = 7$ under self-weight if the stereotomy of the arch

1. is vertical and the arch is with constant thickness in stereotomy direction;
2. is vertical and the arch has a constant thickness in normal direction;
3. is radial and the arch has a constant thickness in normal direction.

4. Conclusions

The new model, applied to planar problems in this talk, can readily be utilized for the in-depth study of spatially curved masonry arches. Although such structures are less common in traditional construction, a theory of spatial curves made of rigid blocks and tension-less joints might lead to the erection of optimized masonry structures. Building spatial arches is within reach nowadays as automated, robotic construction spreads quickly.

Acknowledgments

The research was supported by the NKFIH Grant 143175 and by the TKP2021-BME-NVA-02 program.

References

- [1] J. Heyman. Safety of masonry arches. *Int. J. Mech. Sci.*, 11:363–385, 1969.
- [2] G. Cocchetti, G. Colasante, and E. Rizzi. On the analysis of minimum thickness in circular masonry arches. *Appl. Mech. Rev.*, 64(5):050802, 2012.
- [3] H. Alexakis and N. Makris. Minimum thickness of elliptical masonry arches. *Acta Mech.*, 224:2977–2991, 2013.
- [4] O. Gáspár, A. A. Sipos, and I. Sajtos. Effect of stereotomy on the lower bound value of minimum thickness of semi-circular masonry arches. *Int. J. Arch. Herit.*, 12(6):899–921, 2018.
- [5] S.S. Antman. *Nonlinear Problems in Elasticity*. Springer-Verlag, NY, 2nd edition, 2005.
- [6] T. J. Healey and P. G. Mehta. Straightforward computation of spatial equilibria of geometrically exact cosserat rods. *Int. J. Bifur. Chaos*, 15(3):949–965, 2005.
- [7] D. Nikolić. Thrust line analysis and the minimum thickness of pointed masonry arches. *Acta Mech.*, 228(6):2219–2236, 2017.

Homogenised stiffness coefficients of unloaded endoscope shafts

Martina Stavole¹, Rodrigo T. Sato Martín de Almagro¹, Vanessa Dörlich², Sigrid Leyendecker¹

¹ Institute of Applied Dynamics, Friedrich-Alexander-Universität Erlangen-Nürnberg,
Immerwahrstrasse 1, D-91058 Erlangen, Germany
martina.stavole@fau.de rodrigo.t.sato@fau.de sigrid.leyendecker@fau.de

² Mathematics for the Digital Factory, Fraunhofer Institute for Industrial Mathematics (ITWM)
Fraunhofer-Platz 1, 67663 Kaiserslautern, Germany
vanessa.doerlich@itwm.fraunhofer.de

Keywords: Homogenisation, Composite Materials, Experimental characterisation, Endoscopes

1. Introduction

In order to characterise the mechanical behaviour of slender structures we need to determine their stiffness parameters. These allow us to translate the behaviour of the real-world object to a mathematical model. However, when these structures are made out of composite materials, obtaining analytic expressions for the effective or homogenised stiffness parameters from those of single materials is very difficult due to the numerous uncertainties and interactions involved. In this work, we aim to identify a homogenisation procedure for the stiffness coefficients of circular multi-layered beam cross-sections. Our aim is to streamline the material characterisation of flexible unloaded endoscope shafts when modelled as beams. An experimental campaign was carried out at Fraunhofer ITWM in order to evaluate the torsional and bending stiffness coefficients of such devices. Experimental results will be shown and used to build a proper cross-section model.

2. Description of the endoscope samples and the cross-section model

The mechanical behaviour of flexible endoscopes is governed by the external structure, denominated *unloaded shaft*. Thus, the internal cavity, where the instruments are housed, is not taken into account in this study. The unloaded shafts have a complex structure characterised by a hollow slender cylindrical geometry, shown in Figure 1, and made out of composite materials, i.e. starting from the outer side, two layers of plastic, one layer of stainless steel mesh, and one inner layer of stainless steel coil.

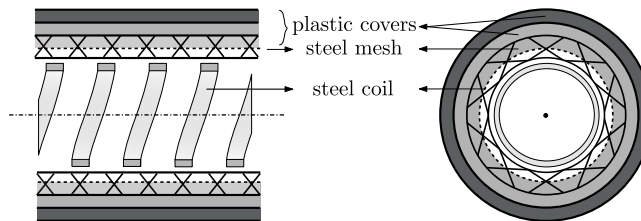


Figure 1: Longitudinal (left) and transversal (right) sections of an unloaded shaft

Since the coil is only attached to the overall structure at the ends of the shaft and can move relative to the other layers, its contribution to the mechanical properties of the cross-section can be considered as additive on top of the rest. We will disregard its effect in this work. Thus, one can model the shaft as a fused three-layered cross-section, see Figure 2. One can distinguish the hollow interior (considered as layer 1) and a steel mesh as layer 2. Due to difficulties in properly characterising and differentiating the two outermost layers of plastic, they are considered as a single one (layer 3).

3. Homogenisation of the cross-section stiffnesses parameters

Assuming linear material behaviour, the stiffness coefficients to be determined are the axial, shear, bending and torsional stiffnesses. In the case of a single isotropic material, these parameters are EA , κGA , EI and GJ respectively, where A is the cross-sectional area, I is the second moment of area, $J = 2I$ is the polar moment of inertia, E is Young's modulus, $G = E/[2(1 + \nu)]$ is the shear modulus, ν is Poisson's ratio, and κ is a

shear correction factor [1]. In the case of cylindrical beams made out of composite materials welded together with different Poisson's ratios, the homogenisation procedure to obtain the stiffness coefficients is complex due to coupling effects at the interface level between the layers [2, 3]. In this work, we also obtain analytical homogenised stiffness coefficients for axisymmetric bars of piecewise-isotropic materials.

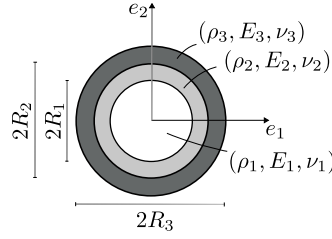


Figure 2: Three-layers piecewise homogeneous cross-section model

4. Data-fitting problem

Bending and torsional experiments were performed at Fraunhofer ITWM where MeSOMICS was developed for the characterisation of mechanical properties of such materials. In this fitting problem, we take into account three different shaft models provided by Karl Storz Video Endoscopy Estonia (KSEE). The bending EI_{exp}^j and torsional GJ_{exp}^j average values evaluated on several experiments, are used to identify optimised variables E_3 , ν_3 , γ and δ in a data-fitting problem in Eq. 1. Here, E_3 and ν_3 are material properties of the outer layer composed by a mixture of treated plastics (layer 3), and γ and δ are correction factors introduced to better represent the contribution of the mesh (layer 2).

$$\min_{[E_3, \nu_3, \gamma, \delta]} f(E_3, \nu_3, \gamma, \delta) = \min_{[E_3, \nu_3, \gamma, \delta]} \left[\sum_j \left(EI_{exp}^j - C_1^j(E_3, \gamma) \right)^2 + \sum_j \left(GJ_{exp}^j - C_3^j(E_3, \nu_3, \delta) \right)^2 \right] \quad (1)$$

Here, C_1 and C_3 denote the bending and torsional effective stiffnesses for the j -th endoscope model

$$\begin{aligned} C_1 &= E_1 I_1 + \gamma \frac{R_2 - R_1}{R_3} E_2 I_2 + E_3 I_3 \\ C_3 &= G_1(E_1, \nu_1) J_1 + \delta G_2(E_2, \nu_2) J_2 + G_3(E_3, \nu_3) J_3 \end{aligned} \quad (2)$$

5. Conclusion and discussion

Performing experiments on composite materials is fundamental to better understand their mechanical behaviour. Thus, we experimentally characterise the mechanical properties of unload endoscope shafts in order to investigate the complexity of their behaviour due to their structure and the many influencing factors, such as production process. Moreover, in this work, we aim to obtain an analytical model to predict effective stiffness coefficients of similar endoscope models.

Acknowledgments

This project has received funding from the European Union's Horizon 2020 research and innovation programme under the Marie Skłodowska-Curie grant agreement No 860124.



References

- [1] G. R. Cowper. The Shear Coefficient in Timoshenko's Beam Theory. *Journal of Applied Mechanics*, Vol. 33, 2:335-340, 1966.
- [2] N. I. Muskhelishvili. Some basic problems of the mathematical theory of elasticity. *Fundamental equations, plane theory of elasticity, torsion and bending*, translated from the fourth, corrected and augmented Russian edition by J. R. M. Radok. Noordhoff International Publishing, Vol. 15, 1977.
- [3] D. Ieşan. *Classical and generalized models of elastic rods*. CRC Press, Boca Raton, FL, 2009.

Experimentally validated conservative nonlinear modes of highly flexible structures by phase resonance testing and effect of damping

O. Thomas[‡], M. Debeurre[‡], C. Giraud-Audine[‡], A. Grolet[‡], S. Benacchio[‡]

[‡]LISPEN, Arts et Metiers Institute of Technology, HESAM Université, Lille, France

[‡]LE2P, Arts et Metiers Institute of Technology, University of Lille, HESAM Université, Lille, France

Keywords: Nonlinear modes, nonlinear frequency response, phase resonance testing, damping estimation

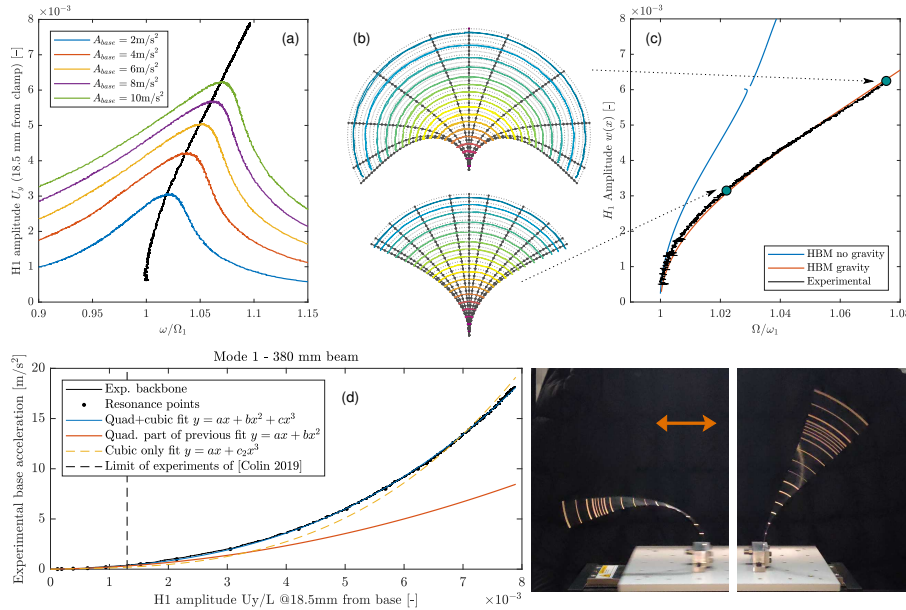


Figure 1: (a) Experimental frequency response of the first mode of a cantilever beam, obtained by phase lock loop. (b,c) Theory vs. experiments for the backbone curve & nonlinear mode shapes. (d) Estimation of the damping evolution as a function of the amplitude along the backbone curve.

1. Introduction

We consider in this article the vibrations of a highly flexible slender structure around one of its resonances. In this case, one can obtain very high displacements in the transverse (low rigidity) direction for moderate external force. A canonical example, considered in the present paper, is a cantilever beam subjected to a prescribed transverse base displacement, for which, as shown in Fig. 1, deformations with rotations of the tip cross-section of more than $\pi/2$ are easily reached.

This paper addresses the measurement of the frequency response of such a structure and especially its nonlinear modes, the so-called backbone curves, that shows the evolution of the free oscillation frequency of a given vibration mode as a function of the amplitude of the motion. We consider here the nonlinear modes of the equivalent conservative system, also known as the Lyapunov invariant manifolds of the phase space [1]. These backbone curves are of primary interest since they are independent of the damping in the system and are thus an efficient mean to validate a model. We address this point by comparing our experimental results to those of a geometrically exact beam model numerically solved in the frequency domain with the Harmonic Balance Method and an Asymptotic Numerical Method for continuation of periodic solutions, as explained in [2]. Additionally, since our experiments are performed in open air as well as because of the geometrical nonlinearities, complex and nonlinear damping phenomena are at play (internal damping in the beam as well as interaction with the surrounding air [3]). We show first that using a phase resonance experiment (as in [4]) enables exact measurement of the conservative backbone curve and, at the same time, it enables to estimate the evolution of damping as a function of the amplitude of the motion of the nonlinear mode.

Comparisons between theoretical results and experiments are scarce in the case of highly flexible structures in

the frequency domain, apart from [5], in which the measurements are performed in a vacuum to avoid the air damping, but without specific considerations of the nonlinear modes.

2. Theory & results

We consider the following discrete model for the structure:

$$M\ddot{x} + D\dot{x} + Kx + f_d(x, \dot{x}) + f_c(x) = f_e, \quad (1)$$

where $x(t)$ gathers the unknown degrees of freedom, M , D , K are inertia, damping and stiffness matrices, f_d and f_c are the internal dissipative and conservative parts of the nonlinear internal force vector and f_e is an external forcing vector.

It is possible to prove that a dissipative force of the form $f_d(x, \dot{x})$ is necessarily an odd function of \dot{x} and that in this case, a forcing vector f_e which is periodic with each of its harmonics in phase quadrature with the corresponding harmonic of $x(t)$ (a phase resonance) perfectly cancels the damping part of the equations, meaning that the structure is vibrating as if it were in free conservative vibrations, thus vibrating on a conservative nonlinear mode [6, 7].

Figure 1 gathers some of the results. In experiments, using a control loop to prescribe the phase between $f_e = f_0 \cos \Omega t$ and x allows for measurement of both frequency responses (with a phase sweep at constant forcing amplitude f_0) and the backbone curve (with a forcing amplitude sweep at constant phase), (Fig. 1(a)). Then, using a camera with stroboscopy, the nonlinear deformed shape can be measured and compared to the ones obtained numerically, with a perfect match (Fig. 1(b)). The experimental backbone curve also perfectly match its theoretical counterpart, in which the effect of gravity is evident, as explained in [8] (Fig. 1(c)). Finally, by plotting the amplitude of the forcing (the acceleration of the shaking table) as a function of the amplitude on the backbone curve, the effect of the damping can be estimated (Fig. 1(d)). In particular, a linear response would be characteristic of a linear damping; here, on the contrary, both quadratic and cubic damping dependencies are observed, probably due to the fluid structure interaction as well as geometrically nonlinear internal damping.

Acknowledgments: This project has received funding from the EU’s Horizon 2020 research and innovation programme under the Marie Skłodowska-Curie grant agreement No. 860124.



References

- [1] C. Touzé, A. Vizzaccaro, and O. Thomas. Model order reduction methods for geometrically nonlinear structures: a review of nonlinear techniques. *Nonlinear Dynamics*, 105:1141–1190, 2021.
- [2] M. Debeurre, A. Grolet, B. Cochelin, and O. Thomas. Finite element computation of nonlinear modes and frequency response of geometrically exact beam structures. *Journal of Sound and Vibration*, 548:117534, 2023.
- [3] M. Colin, O. Thomas, S. Grondel, and É. Cattan. Very large amplitude vibrations of flexible structures: Experimental identification and validation of a quadratic drag damping model. *Journal of Fluids and Structures*, 97:103056, 2020.
- [4] V. Denis, M. Jossic, C. Giraud-Audine, B. Chomette, A. Renault, and O. Thomas. Identification of nonlinear modes using phase-locked-loop experimental continuation and normal form. *Mechanical Systems and Signal Processing*, 106:430–452, 2018.
- [5] H. Farohki, Y. Xia, and A. Erturk. Experimentally validated geometrically exact model for extreme nonlinear motions of cantilevers. *Nonlinear dynamics*, 107(457-475), 2022.
- [6] C. Grenat. *Nonlinear Normal Modes and multi-parametric continuation of bifurcations : Application to vibration absorbers and architected MEMS sensors for mass detection*. PhD thesis, INSA de Lyon, France, 2018.
- [7] M. Peeters, G. Kerschen, and J. C. Golinval. Dynamic testing of nonlinear vibrating structures using nonlinear normal modes. *Journal of Sound and Vibration*, 330(3):486–509, 2011.
- [8] M. Debeurre, A. Grolet, and O. Thomas. Extreme nonlinear dynamics of cantilever beams: effect of gravity and slenderness on the nonlinear modes. *Nonlinear Dynamics*, 2023. submitted.

Investigation of the influence of the inner structure on the stiffness of a cable under pure torsion

C. Tsegouog¹, P. Sharma¹, V. Dörlich², J. Linn², S. Diebels¹

¹Applied Mechanics, Saarland University, carole.tsegouogkue@uni-saarland.de

²Department Mathematics for the Digital Factory, Fraunhofer ITWM,
vanessa.doerlich@itwm.fraunhofer.de

Keywords: pure torsion experiments, nonlinear behaviour, multi-wire structure, anisotropic torsion

1. Introduction

Cable bundles and harnesses are used for better cable management in vehicles. Each cable bundle is made up of several cables which in turn are formed by different layers. Analysing in detail the behaviour of a single cable when subjected to loading is a necessary process to understanding the behaviour of a cable bundle. Dörlich et al. [1] as well as Hildebrandt et al. [2] have studied the behaviour of a cable experimentally. Based on the results, they suggested a Cosserat rod and an elasto-plastic continuum models respectively. Burger et al. [3] presented an estimation tool for linear elastic model parameters for cable bundles based on bundle parameters using Gaussian Process regression. However, the effect of internal structure on mechanical properties has not been investigated. In this work, we aim at the prediction of nonlinear behaviour of cables and lay the foundation by investigating the behaviour of cables under torsion. Experiments based on pure torsion are carried out and the influence of the direction of rotation on the stiffness of the cable is investigated.

2. Experimental method and results

Cable specimens clamped at both ends using collet chuck are subjected to an angular deformation. During the rotation, forces normal to the cross section of the sample are compensated allowing a pure torsion. Subjected to a torsion up to a twist of 15 rad/m, the cables experience four successive cycles of loading and unloading. As shown in Figure 1a, the first cycle is the pre-loading that the cable requires in order to reach a stable state. The stiffness is then determined on the following cycles (Figure 1b). A linear fit up to a twist of 1.5 rad/m is used to determine the stiffness for small deformations.

2.1. Determining a representative length

The manufacturing process and the different ways of transporting the cable bundle influence the internal structure and shape of the cables [4]. Different lengths of the same cable may have different mechanical properties because of their internal structure and boundary effects of the clamping. In order to determine a representative specimen length, three lengths, namely 70 mm, 100 mm and 140 mm, were subjected to a torsion angle of 60°, 85.7° and 120° respectively so as to obtain the same twist of 15 rad/m for all cable lengths.

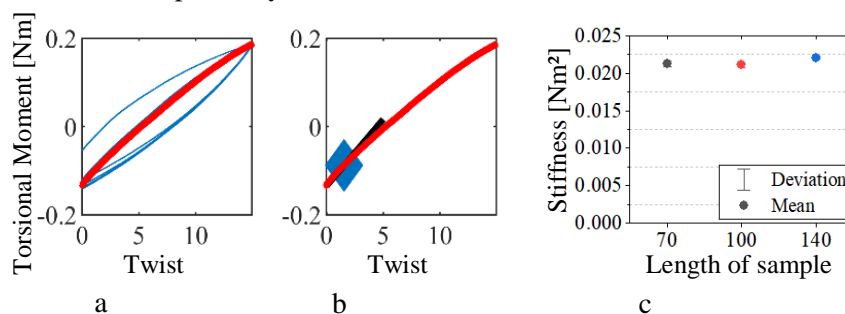


Figure 1. Result of 4-cycle torsion test (a), stiffness determination using a linear fit (b) and mean value of the stiffness for a deformation up to a twist of 1,53 rad/m of 5 samples per length twisted in the winding direction of the wires (c).

The results (Figure 1c) show that for the three lengths, the stiffness does not change. Therefore, 70 mm can be considered to be a representative length and used for further investigations.

2.2. Effect of direction

To analyse the effect of the direction five samples are twisted in clockwise direction and 5 samples in counter-clockwise direction. The clockwise direction corresponds to the wrapping direction of the wires, see figure 3c. The moment versus twist and the average stiffness of the 5 samples according to the direction of the applied angle are shown in figure 2a-b.

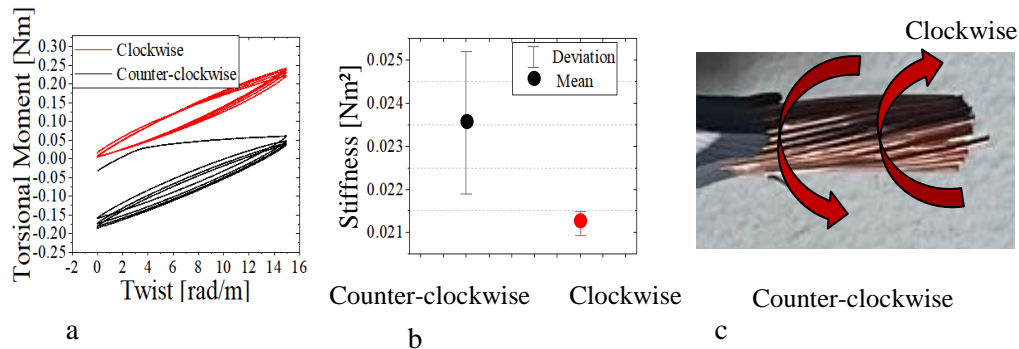


Figure 2. Result of the 4-cycle torsion test for $l=70$ mm in the wire winding direction (clockwise) and in the anti-winding direction (counter-clockwise) (left) and average stiffness value of 5 twisted samples (middle).

The results show that the stiffness in the clockwise direction is ca. 10% less than the stiffness in counter clockwise direction. However, the scattering in the measurement for the counter-clockwise direction is approximately 7%. Therefore, a reproducible effect in the clockwise direction is observed, which is not the case in counter-clockwise direction. A stochastic effect is observed for the counter-clockwise direction and the scattering interval is much bigger than clockwise direction.

3. Conclusions

A study of the influence of the cable length and the direction of the applied loading on the cable was analysed. For this purpose, a pure torsion was performed and a representative length of 70 mm was determined. In a second step the effect of direction on stiffness for a length of 70 mm of cable was presented. The difference in stiffness between the two directions is less than 10%. However, the samples twisted in the clockwise direction show a more reproducible effect during loading and unloading and the scattering interval is small in comparison to counter-clockwise direction. The authors will present similar investigations for the influence of the direction of torsion on the stiffness at higher twist and consider the observed effects in a modelling approach.

Acknowledgements

This project has received funding from the German Research Foundation [Di 430/37-1].

Reference

- [1] V. Dörlich, S. Diebels and J. Linn. *Towards Viscoplastic constitutive models for Cosserat Rods*, Archive of Mechanical Engineering, LXIII (2016) 215-230.
- [2] A. Hildebrandt, P. Sharma, A. Düster, S. Diebels. *Experimental and numerical investigation of the deformation behaviour of cables and thin beam-like structures under multi-axial loading*, Mathematics and Mechanics of solids, 27(10) (2022) 2314-2337.
- [3] L. Burger, V. Dörlich, J. Linn, F. Schneider. *Estimation of Cable Bundle Stiffness Based on Gaussian Process Regression*, Progress in Industrial Mathematics at ECMI 2021, Springer International publishing, 329-336, 2022.
- [4] M. Roof and T. Davies. *Determination of the bending stiffness for a spiral strand*. Journal Strain Analysis, 39 (2004) 1-13.

Simulation and Parameterization of Nonlinear Elastic Behavior of Cables

Tian Zhao^{1,2}, Fabio Schneider-Jung¹, Joachim Linn¹, Ralf Müller²

¹ Fraunhofer Institute for Industrial Mathematics ITWM, Fraunhofer-Platz 1, 67663 Kaiserslautern, Germany, [tian.zhao, fabio.julian.schneider-jung, joachim.linn]@itwm.fraunhofer.de

² Technical University of Darmstadt, Franziska-Braun-Straße 7, 64287 Darmstadt, Germany, ralf.mueller@mechanik.tu-darmstadt.de

Keywords: Cable Simulation, Nonlinear Elasticity, Cosserat Rod

1. Introduction

In recent years, there has been an increasing demand for fast and realistic simulations of flexible slender structures such as cables and hoses in the automotive industry. For some complex slender flexible structures, a nonlinear constitutive bending behavior can be clearly observed during cyclic pure bending [2] and MeSOMICS bending experiments [3]. In this work, we present an iterative method for the simulation of such nonlinear elastic behavior, where in each iteration step, only a linear elastic constitutive behavior is used. Furthermore, we formulate an inverse problem to determine the nonlinear elastic behavior from given measured data. We also investigate an alternative method to determine the bending stiffness characteristic based on the balance equations for rods.

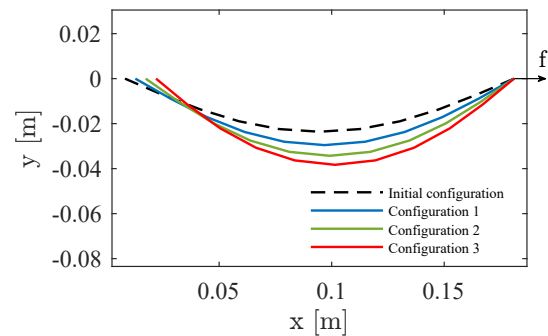


Figure 1: Left: Top-view of MeSOMICS [3] bending experiment. Right: Schematic representation of experimental procedure for MeSOMICS bending measurements. At the left clamping point, horizontal displacements are stepwise applied, resulting in different bending configurations. At the right clamping point, the resulting horizontal reaction force is measured.

2. Iterative method to simulate nonlinear elastic bending behavior

Fig. 1 shows bending experiments performed on a cable using the MeSOMICS measurement machine. To simulate this experiment, a Cosserat rod in two-dimensional space is utilized, where the static equilibrium state of the cable is obtained by minimizing the potential energy (consisting of potential bending energy, potential shear- and tension energy) [1]. While this model is geometrically exact, it only considers linear constitutive behavior, namely a constant bending stiffness $[EI]$. The potential bending energy is formulated as $W_B = \frac{1}{2} \int_0^L [EI] \cdot (K(s) - K_0)^2 ds$, where L is the length of cable, $K(s)$ is the curvature at arc length s and K_0 is a constant pre-curvature specifying the force- and moment-free reference configuration.

For nonlinear elasticity, which is represented by a state-dependent bending stiffness $f_{EI}(\kappa)$, the corresponding potential bending energy is formulated as $\tilde{W}_B = \int_0^L \int_{K_0}^{K(s)} \int_{K_0}^{\xi} f_{EI}(\kappa) d\kappa d\xi ds$. However, directly using this formulation in the energy minimization is computationally expensive. To simulate nonlinear elastic behavior while maintaining the efficiency of the method in [1], we propose an iterative method. In each iteration, only constant stiffness parameters are used and set according to the current cable state and a given bending stiffness characteristic. The new equilibrium is computed by minimizing the potential energy, and we proceed iteratively until the cable state converges.

To validate the proposed iterative method, we use a fictive state-dependent bending stiffness characteristic

$f_{EI}(\kappa)$, simulate the above presented bending test and compare the results with a reference solution. The latter is generated by directly solving the energy minimization problem with \tilde{W}_B . Fig. 2 shows very good agreement of the horizontal reaction force from the iterative method and the reference solution.

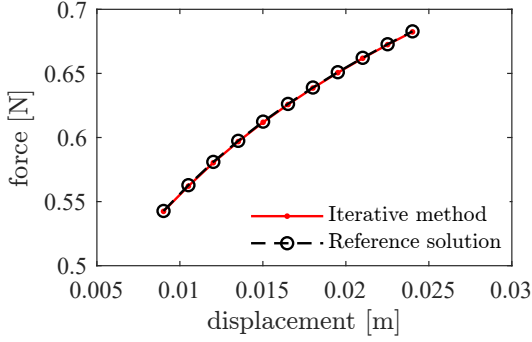


Figure 2: Horizontal reaction force obtained at the fixed end point, resulting from varying displacements.

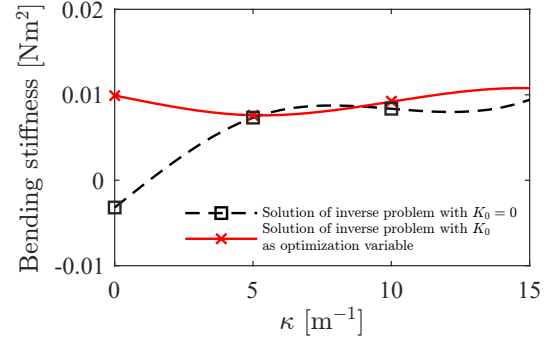


Figure 3: Identified bending stiffness characteristic using experimentally measured data.

3. Identification of state-dependent bending stiffness characteristic

Besides enabling the simulation with nonlinear elastic bending behavior, we also investigate how to determine characteristic from given measurement results. To this end, we formulate an inverse problem to find a state-dependent bending stiffness characteristic $f_{EI}(\kappa)$, such that the difference between the simulated force and the measured force is minimized. Using measured reaction forces from real cable experiments and assuming vanishing pre-curvature K_0 , we first identified a characteristic with negative stiffness for low curvatures (cf. black dashed line in Fig. 3). Considering pre-curvature K_0 as additional optimization variable provides a more realistic characteristic (red curve in Fig. 3), and identified pre-curvature $K_0 \approx 3 \text{ m}^{-1}$.

To assess the resulting characteristic, besides the data-driven inverse problem, we investigate an alternative model-based approach, which utilizes the balance equations for rods: $\partial_t \mathbf{f} = \mathbf{0}$ and $\partial_t \mathbf{m} + \partial_s \mathbf{r} \times \mathbf{f} = \mathbf{0}$. Together with measured data, this allows to derive a $(\kappa, f_{EI}(\kappa))$ -graph. Our current research is focused on comparisons of both approaches.

4. Conclusions

In summary, the proposed iterative method efficiently simulates the nonlinear elastic behavior. By solving the corresponding inverse problem with including pre-curvature as an optimization variable, we can identify a plausible bending stiffness characteristic from experimentally measured data. However, for a better understanding, we aim to complement the inverse problem with a model-based approach, based on the balance equations. Current research focuses on how to properly treat pre-curvature in the model-based approach.

References

- [1] J. Linn, T. Hermansson, F. Andersson, and F. Schneider. Kinetic aspects of discrete Cosserat rods based on the difference geometry of framed curves. In: M. Valasek, et al. (eds) Proceedings of the ECCOMAS Thematic Conference on Multibody Dynamics, 163-176. Prague, Czech Republic, 2017.
- [2] V. Dörlich, J. Linn, S. Diebels. Flexible beam-like structures - experimental investigation and modeling of cables. In: Altenbach, et al. (eds) Advances in Mechanics of Materials and Structural Analysis. Advanced Structured Materials, Springer, Cham, 80:27-46, 2018.
- [3] *MeSOMICS: Measurement System for the Optically Monitored Identification of Cable Stiffnesses*. Homepage: www.mesomics.eu

MS-2: Contact and friction in mechanics of flexible slender structures

Geometrically exact beam-to-beam contact interactions embedded in a finite volume-based discretisation framework

Seevani Bali ^{1,a}, Željko Tuković ², Philip Cardiff ^{1,c}, Alojz Ivanković ^{1,d}, Vikram Pakrashi ^{1,e}

¹ School of Mechanical and Materials Engineering, University College Dublin, Ireland

² Faculty of Mechanical Engineering and Naval Architecture, University of Zagreb, Croatia

^aseevani.bali@ucdconnect.ie, ^bzeljko.tukovic@fsb.hr, ^cphilip.cardiff@ucd.ie, ^dalojz.ivankovic@ucd.ie, ^evikram.pakrashi@ucd.ie

Keywords: beam-to-beam contact, friction, penalty method, finite volume method, geometrically-exact beam

1. Introduction

This research extends the work by Bali et al. [1] to include contact interactions between geometrically exact Simo-Reissner (SR) type beams in a finite volume (FV) discretisation framework. The possibilities of point-to-point and line-to-line frictionless contact [2] scenarios between slender beams and a frictional point contact interaction are investigated in this work. For frictionless contact, penalty and augmented Lagrangian constraint methods are implemented for beams with multiple-point contact possibilities. A Coulomb-based friction law and the analogy of rigid plasticity are adopted to model the stick and slip regions of friction between beams. The primary motivation to use FV methods instead of conventional finite element techniques is to allow fluid-structure interactions in a single FV framework and to expand the domain of numerical problems solved using the FV approach.

2. Mathematical model

Conventional beam kinematic relations (deformed mean centroid \mathbf{r} and rotation matrix $\mathbf{\Lambda}$ attached to beam cross-section) are used here. Volume integral equations are used as balance laws instead of constructing the variational form of governing force and moment equations. The primary displacement (\mathbf{w}) and rotation vectors ($\boldsymbol{\psi}$) are solved for all the (volume) cell centres of the beam that typically lie on the deformed centroid line. Generally, for computing arc-length derivatives, a central finite-difference method is used; however, for the contact formulation, Hermite spline polynomials are used to ensure C^1 -continuity of derivatives and smoother contact point detections. After appropriate linearisation (see Eq. [1]), the contact force is added to the system as a Neumann boundary condition via the penalty/augmented Lagrangian method. In Eq. [1], $L[(n_c)]$ is the linearised contact force (magnitude n_c) about its previous converged configuration \mathbf{n}_c^i , g_n is the normal gap, $\hat{\mathbf{d}}$ is a unit normal vector in the direction of force and, Δg_n , $\Delta \hat{\mathbf{d}}$ are variations of normal gap and unit normal vector respectively. For frictional contributions, the tangential gap function as per Litewka et al. [3] is defined, and frictional contact moments due to the transfer of surface friction forces to the beam-centreline are ignored.

$$L[n_c] = \mathbf{n}_c^i + \frac{\partial n_c}{\partial g_n} \Delta g_n \hat{\mathbf{d}} + n_c(g_n) \Delta \hat{\mathbf{d}} \quad (1)$$

3. Numerical results and conclusions

Two numerical test cases are presented here. Figure [1a] presents the contact force between two beams when they are twisted about each other by an angle of 2π radians. Figure [1b] provides a comparison of contact forces for the discretisation of 25 beam control volumes (CVs) and penalty stiffness $p_n = 1000 \text{ N/m}^2$ developed using the FV method and the reference FE values adapted from Meier et al. [2]. Figure [2a] shows the deformed configuration of two orthogonal steel beams sliding over each other by values, $w_x = -w_z = 0.05 \text{ m}$, superimposed with a normal displacement of $w_y = -0.12 \text{ m}$ by the upper beam on the beam aligned with x -axis. Slip-gap values for the same test case for different friction coefficients are presented in Figure. [2b] that clearly shows a full stick condition for the coefficient of friction, $\mu = 1$ and tangent penalty stiffness, $p_t = 1 \times 10^6 \text{ N/m}$.

Acknowledgments

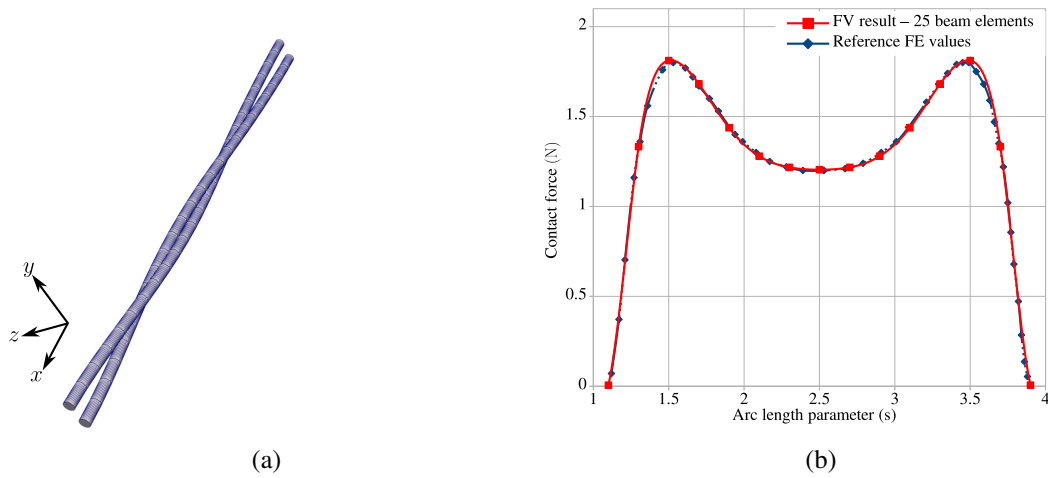


Figure 1: Twisting of two beams (length, $L = 1$ m, equal radius $R = 0.01$ m) - (a) Deformed beam configuration for twisting of two beams, (b) Variation of contact force over the beam length.

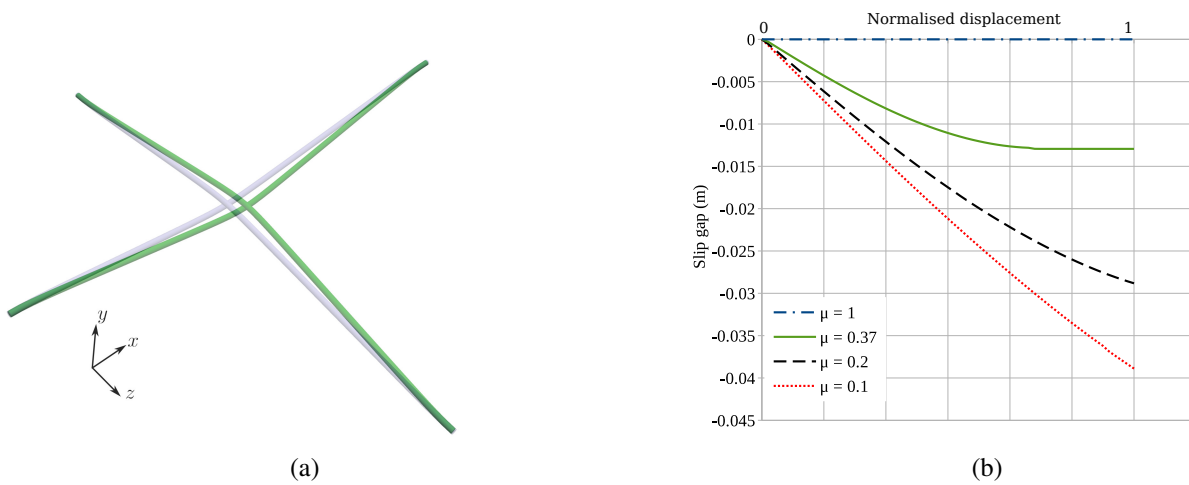


Figure 2: Sliding of two perpendicular beams - (a) Beam deformed configuration for frictionless contact (blue) and with friction (green, $\mu = 1$), (b) slip gap values for the beam aligned with x-axis for different μ values.

This work is conducted with the financial support of Science Foundation Ireland (SFI) under Grant number RC2302_2. Financial support from the Irish Research Council, grant number IRCLA/2017/45 is gratefully acknowledged. Additionally, the authors want to acknowledge project affiliates, Bekaert, through the Bekaert University Technology Centre (UTC) at University College Dublin, I-Form, funded by SFI Grant Number 16/RC/3872, co-funded under European Regional Development Fund and by I-Form industry partners. Vikram Pakrashi would like to acknowledge SFI, NexSys project 21/SPP/3756.

References

- [1] Bali, S., Tuković, Ž., Cardiff, P., Ivanković, A., & Pakrashi, V. *A cell-centered finite volume formulation of geometrically exact Simo-Reissner beams with arbitrary initial curvatures*. *International Journal for Numerical Methods in Engineering*, 123.17 (2022): 3950-3973.
- [2] Meier, C., Popp, A., & Wall, W. A. *A finite element approach for the line-to-line contact interaction of thin beams with arbitrary orientation*. *Computer Methods in Applied Mechanics and Engineering*, 308 (2016): 377-413.
- [3] Litewka, P., & Wriggers, P. *Frictional contact between 3D beams*. *Computational Mechanics*, 28.1 (2002), 26-39.

On the Evaluation of the Tangential Slip Increment in Quasi-static Beam-to-Beam Contact Problems

Olivier Brùls¹ and Armin Bosten^{1,2}

¹ Department of Aerospace and Mechanical Engineering, University of Liège
 {o.bruls, a.bosten}@uliege.be

² Department of Mathematics for the Digital Factory, Fraunhofer Institute for Industrial Mathematics ITWM

Keywords: Geometrically exact beams, Nonsmooth contact mechanics, Friction, special Euclidean group SE(3)

1. Introduction

Frictional contact models between beams are relevant for the numerical simulation of beam assemblies in various applications such as wiring harnesses, cable bundles or textile manufacturing processes. An essential ingredient of the contact model is the kinematic description of the relative motions of the material particles in the contact zone. In particular, frictional contact models require a quantification of the relative slip motion between the two bodies. This work addresses the definition of the tangential slip increment between geometrically exact beams using the special Euclidean group formalism. This geometric setting guarantees the frame invariance of the results and enables an accurate treatment of complex contact behaviours, such as rolling without slipping interactions.

2. Contact model

In contact mechanics, the normal and tangential contact forces λ_N and λ_T can be expressed as inclusions

$$\lambda_N \in \partial \psi_{\mathbb{R}^+}(g_N), \quad \lambda_T \in \partial \psi_{\mathcal{C}(\lambda_N)}(\mathbf{u}_T) \quad (1)$$

where g_N is the *normal gap*, \mathbf{u}_T is the *tangential slip velocity*, $\psi_{\mathbb{R}^+}$ is the indicator function of the set of positive real numbers and $\mathcal{C}(\lambda_N)$ is the Coulomb disk defined as

$$\mathcal{C}(\lambda_N) = \{\lambda_T \in \mathbb{R}^2 : \|\lambda_T\| \leq \mu \lambda_N\} \quad (2)$$

In a quasi-static analysis, this contact model can still be considered provided that the slip velocity \mathbf{u}_T is substituted by a *tangential slip increment* $\Delta \mathbf{g}_T(t - \Delta t, t)$ over the pseudo-time interval Δt evaluated as

$$\Delta \mathbf{g}_T(t - \Delta t, t) = \int_{t-\Delta t}^t \mathbf{u}_T(\tau) \, d\tau \quad (3)$$

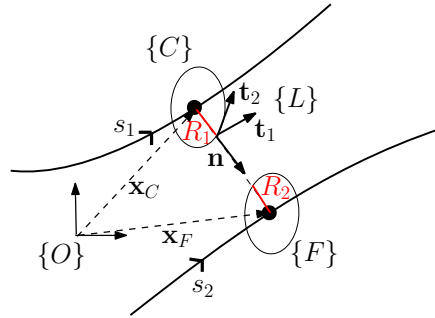


Figure 1: Kinematics of the beam-to-beam contact

3. Contact kinematics

Let us consider two beams with circular cross-sections of radii R_1 and R_2 (see Fig. 1). At each point of the centerline, the position and orientation of the cross-section shall be treated as an element of the special Euclidean group $SE(3)$ [1]. Furthermore, we assume that the deformation of the cross-section as well as the shear

deformation can be neglected in the contact kinematics. One of the beam is qualified as the slave and the other one as the master. For the slave beam, the centerline is parameterized using the material coordinate s_1 , the section-attached frame at point s_1 is denoted as $\{C\}$ (with origin C), and the first axis \mathbf{e}_{C1} is pointing in the tangential direction to the slave centerline. For a given point s_1 on the slave beam, an orthogonal projection is applied to define the potential contact section on the master beam, which is represented by the frame $\{F\}$ with origin F at the material coordinate s_2 . By construction, this frame $\{F\}$ is such that the vector joining C and F is orthogonal to \mathbf{e}_{C1} and the first axis \mathbf{e}_{F1} is pointing in the tangent direction to the master centerline.

On each beam, one additional frame is defined at the potential contact point on the external contour of the cross-section. On the slave beam, the frame $\{L\}$ at the potential contact point is defined such that (i) the normal vector $\mathbf{n} = \mathbf{e}_{L1}$ is along the directed line joining C to F , (ii) the tangent vector $\mathbf{t}_1 = \mathbf{e}_{L2}$ is equal to \mathbf{e}_{C1} and the tangent vector $\mathbf{t}_2 = \mathbf{e}_{L3}$ completes the orthonormal basis, (iii) the origin L is localized on the external contour of the slave cross-section (i.e., at a distance R_1 of C) and on the directed line joining C to F . On the master beam, the frame $\{K\}$ at the potential contact point is defined such that its three axes coincide with \mathbf{n} , \mathbf{t}_1 and \mathbf{t}_2 and its origin K is localized on the external contour of the master cross-section (i.e., at a distance R_2 of F) and on the directed line joining F to C .

The relative configuration is then obtained as a 4×4 matrix $\mathbf{H}_{LK} \in SE(3)$ and the *normal gap* is simply

$$g_N = [\mathbf{H}_{LK}]_{11} \quad (4)$$

From now, the frames $\{L\}$ and $\{K\}$ are considered as material frames attached to the material points on the contour of the cross-sections. The relative velocity is represented by a 6×1 twist vector \mathbf{v}_{LK}^K with components in the frame $\{K\}$. The *tangential slip velocity* is then obtained as a two dimensional vector

$$\mathbf{u}_T = \begin{bmatrix} [\mathbf{v}_{LK}^K]_2 \\ [\mathbf{v}_{LK}^K]_3 \end{bmatrix} \quad (5)$$

4. Tangential slip increment

For quasi-static problems, we propose to define the tangential slip increment by assuming a constant relative velocity over the pseudo-time interval Δt . The 6×1 *relative motion increment* is then introduced as

$$\Delta \mathbf{y}_{LK}^K(t - \Delta t, t) = \int_{t-\Delta t}^t \mathbf{v}_{LK}^K(\tau) \mathbf{d}\tau = \mathbf{v}_{LK}^K(t) \Delta t \quad (6)$$

This motion increment is related to the change of \mathbf{H}_{LK} by the finite difference formula

$$\Delta \mathbf{y}_{LK}^K(t - \Delta t, t) \simeq \log(\mathbf{H}_{LK}^{-1}(t - \Delta t) \mathbf{H}_{LK}(t)) \quad (7)$$

where \log is the logarithm map on $SE(3)$. Then, the *tangential slip increment* is obtained from the components

$$\Delta \mathbf{g}_T = \begin{bmatrix} [\Delta \mathbf{y}_{LK}^K]_2 \\ [\Delta \mathbf{y}_{LK}^K]_3 \end{bmatrix} \quad (8)$$

which can be interpreted as a geometrically consistent finite difference approximation of \mathbf{u}_T scaled by Δt .

To the best of our knowledge, the definition of the finite slip increment $\Delta \mathbf{g}_T$ based on a finite difference on $SE(3)$ has not been presented in the literature. In the presentation, the formulation will be illustrated using quasi-static simulations of beam-to-beam frictional contact problems.

Acknowledgments

This project has received funding from the European Union's Horizon 2020 research and innovation programme under the Marie Skłodowska-Curie grant agreement No 860124. The present paper only reflects the author's view. The European Commission and its Research Executive Agency (REA) are not responsible for any use that may be made of the information it contains.



References

- [1] V. Sonnevile, A. Cardona, and O. Brüls. *Geometrically exact beam finite element formulated on the special Euclidean group $SE(3)$* , Computer Methods in Applied Mechanics and Engineering, 268 (2014) 451–474.

An arbitrary Lagrangian-Eulerian geometrically exact beam formulation applied to reeving systems

O. Devigne, O. Bruls

University of Liège, Belgium, o.devigne@uliege.be

Keywords: Lie group, beam, ALE, multibody system

1. Introduction

Reeving systems generally consist of a cable and one or several pulleys and can be modeled as a multibody system, *i.e.*, as an assembly of rigid or flexible bodies linked by joints. In such applications, a special attention should be paid to the cable model, which must account for two main aspects: the cable deformation, and frictional contact due to the interaction between the cable and the pulley.

2. Flexible cable model

A cable is a typical example of a highly flexible and slender structure where nonlinearities could arise. Cables are often modeled as beams and most nonlinear finite element beams are formulated based on distinct translation and rotation coordinates. Another approach is to formulate the beam on the special Euclidian group $SE(3)$ where rotations and translations are inherently coupled. This formulation has already been used for beam modeling [1] or more recently for nonsmooth beam-to-beam contact [2]. The advantages of using an $SE(3)$ formulation are diverse. No global set of coordinates is needed since the motion variables are inherent to the mathematical objects used in the formulation. Moreover, with the wisely chosen representation of derivatives, a frame-invariant formulation is obtained. A local parametrization of motion is then applied on motion increments. The continuous equations to be solved in a quasi-static setting are obtained by the variation of the internal potential energy as

$$\delta_{\text{spatial}}(\mathcal{W}_{\text{int}}) = \int_0^L \delta_{\text{spatial}}(\boldsymbol{\epsilon})^T \mathbf{K} \boldsymbol{\epsilon} ds \quad (1)$$

where $\boldsymbol{\epsilon}$ is the 6×1 strain vector and \mathbf{K} is the 6×6 sectional stiffness matrix.

3. Arbitrary Lagrangian-Eulerian formulation

Sometimes, the cable comes into contact with a structure, for instance when it travels around a pulley. In this scenario, there is a need for a fine finite element discretization of this specific portion of the cable in order to accurately represent the frictional contact conditions. Because the cable is moving around the pulley, small elements must often be used along the whole cable length. One remedy to this problem is to use an arbitrary Lagrangian-Eulerian (ALE) formulation of the cable, which permits a dissociation between the mesh and the material points of the cable. In [3], an ALE formulation based on a continuous variational framework is proposed, where a remeshing of the discretized structure provides an optimal energy solution. In multibody dynamics, an ALE formulation was applied in a fully discrete setting in [4], where a joint ALE-ANCF approach for a beam element is developed to model reeving systems. In multibody systems, ideal kinematic joints between different bodies are modeled using bilateral constraints. In this work, the approach proposed by [3] is applied to model cables as Timoshenko beam elements on $SE(3)$ starting from a continuous form of the equations. In this ALE formulation, the connection between the cable and another body such as the pulley can be modelled using bilateral constraints. An equation taking into account the flow of material along the centerline is thus added to Eq. (1):

$$\delta_{\text{material}}(\mathcal{W}_{\text{int}}) = \frac{1}{2} \int_0^L \delta_{\text{material}}(F) (\boldsymbol{\epsilon}^T \mathbf{K} \boldsymbol{\epsilon} - 2\mathbf{f}^T \mathbf{K} \boldsymbol{\epsilon}) ds \quad (2)$$

where F represents the flow of material coordinate and \mathbf{f} is the deformation gradient.

4. Test case

The example of a cable slipping around a fixed pulley illustrates the advantages of an $SE(3)$ beam formulation (with traction, bending, shearing and torsion energy) and a simpler bar formulation (with only traction energy). Firstly, large traction cables might have a non-negligible bending stiffness which cannot be modeled in bar elements. Secondly, the $SE(3)$ formulation can exactly represent the curvature of the beam around the pulley. In Fig. 1 preliminary results are proposed with a unidimensional bar formulation. A displacement of -40 [mm] in x_1 is imposed at the bottom end of the cable, while the other end has an imposed displacement of 20 [mm] in x_1 , so that internal forces are developed. The nodes initially present on the pulley are constrained to their initial positions. A flow of the material coordinate s is thus observed. The retrieval of the contact forces between the cable and the pulley is done directly through the evaluation of the constraint reaction forces. Assuming a purely slipping contact, a slipping friction force $T = \mu N$ is then added to every node lying on the pulley, where μ is the friction coefficient and N is the normal contact force.

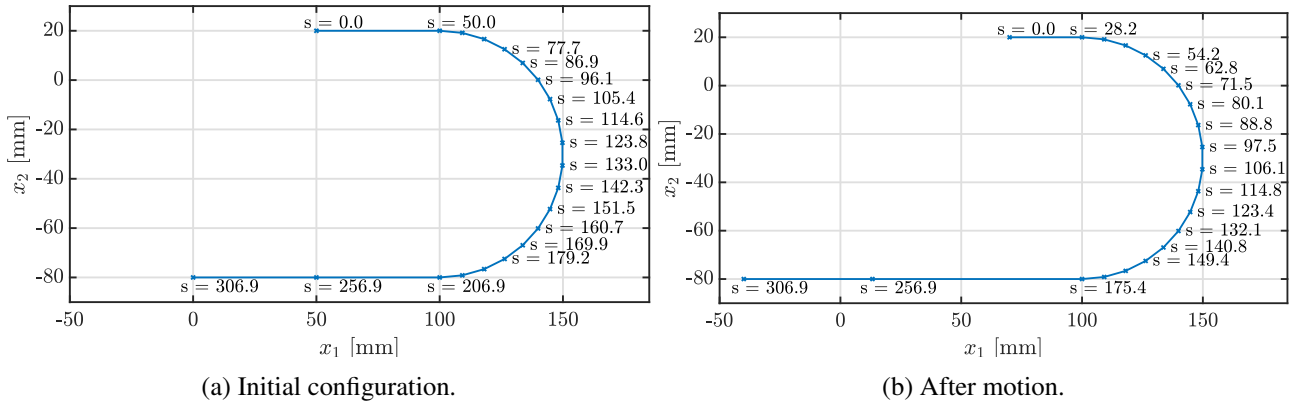


Figure 1: ALE simulation of a cable around a pulley using bar elements.

5. Conclusions

In this work, a geometrically exact beam model formulated on $SE(3)$ is developed in an ALE framework. It couples the advantages of using an $SE(3)$ beam, such as the avoidance of a global parametrization of rotations and a local frame formulation, with the perks of the ALE formulation, permitting to model a closed and sliding contact as a bilateral constraint and to directly recover the contact forces. In this scenario, a slipping friction force can be considered in the simulation without further changes in the solver.

Acknowledgments

This project has received funding from the European Union's Horizon 2020 research and innovation programme under the Marie Skłodowska-Curie grant agreement No 860124.



This work has been partly funded by the Robotix Academy project of the Greater Region.

References

- [1] Sonnevile, V., Cardona, A., Brüls, O., *Geometrically exact beam finite element formulated on the special Euclidean group $SE(3)$* , Computer Methods in Applied Mechanics and Engineering, 268 (2014), 451-474.
- [2] Bosten, A., Cosimo, A., Linn, J., Brüls, O., *A mortar formulation for frictionless line-to-line beam contact*, Multibody System Dynamics, 54(1) (2022), 31-52.
- [3] Kuhl, E., Askes, H., Steinmann, P., *An ALE formulation based on spatial and material settings of continuum mechanics. Part 1: Generic hyperelastic formulation*, Computer Methods in Applied Mechanics and Engineering 193, (2004), 4207-4222. numerical methods in engineering 74(7) (2008), 1162-1197.
- [4] Escalona, J.L., *An arbitrary Lagrangian-Eulerian discretization method for modeling and simulation of reeving systems in multibody dynamics*, Mechanism and Machine Theory 112 (2017), 1-21.

Numerical analysis of the rope-sheave contact interaction using the Arbitrary Lagrangian-Eulerian approach

José L. Escalona ¹

¹ Dept. of Mechanical and Manufacturing Engineering, University of Seville, escalona@us.es

Keywords: Frictional contact, ALE discretization, reeving systems, rope-sheave contact

1. Introduction

The Arbitrary Lagrangian-Eulerian (ALE) discretization method can be efficiently applied to the numerical analysis of the dynamics of reeving systems [1-3]. In the work published so far in this topic, specific modeling assumptions, like the no-slip condition, have been taken to avoid the detailed modeling of the rope-sheave contact analysis. The reason is that contact conditions have little influence in the overall dynamics of the mechanisms. However, some important industrial applications, like elevator or crane safety analysis, require the detailed analysis of the rope-sheave interaction. This paper presents a model that can be used to this end.

2. Free span elements and rope-contact elements

The ALEM [2-3] method for the modeling of rope free spans in reeving systems combines three types of coordinates in the kinematic description of the ropes: (1) absolute position coordinates of the ends of the span, \mathbf{q}_a , (2) arc-length coordinates of the nodal points within the rope, \mathbf{q}_s , and (3) modal coordinates for the description of transverse and axial deformation of the ropes, \mathbf{q}_m . However, these elements are not appropriate to model the rope-sheave contact zone. In this research, new *rope-contact elements* have been specifically defined to model this zone. Figure 1 shows part of a reeving system and a detail of a rope wound in a sheave. In the detail, the free-span elements, a and b , and the rope-contact elements, $c_1 - c_4$, can be observed.

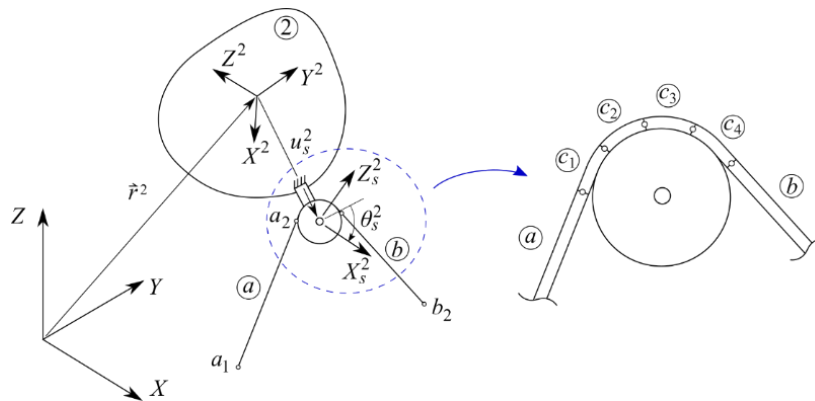


Figure 1. Part of a reeving system.

The rope-contact elements c_i are equivalent to the cubic ALE-ANCF elements defined in [1]. They do not require modal coordinates. The nodal coordinates of this ALE element are: $\mathbf{q} = \left[\mathbf{q}_a^T \quad \mathbf{q}_s^T \right]^T$ with :

$$\mathbf{q}_a = \left[\mathbf{r}_1^T \quad \mathbf{r}_1'^T \quad \mathbf{r}_2^T \quad \mathbf{r}_2'^T \right], \quad \mathbf{r}_i' = \frac{\partial \mathbf{r}_i}{\partial s}, \quad i = 1, 2. \quad (1)$$

However, the ALE rope-contact element does not include modal coordinates because they are considered needless. Therefore, the ALE rope-contact element includes $12 + 2 + 2 = 16$ nodal coordinates.

3. Contact simulation

For the contact simulation, a bristle model is used. The bristles are assumed to be located at the ends of a set of equally spaced segments in the rope. The rope-sheave contact simulation includes three phases: (1) Contact search, when the exact location of the contact forces is determined, (2) calculation of the normal contact forces, using a penetration-based model and, (3) calculation of the tangential contact forces, with prior calculation of the stick or slip contact condition.

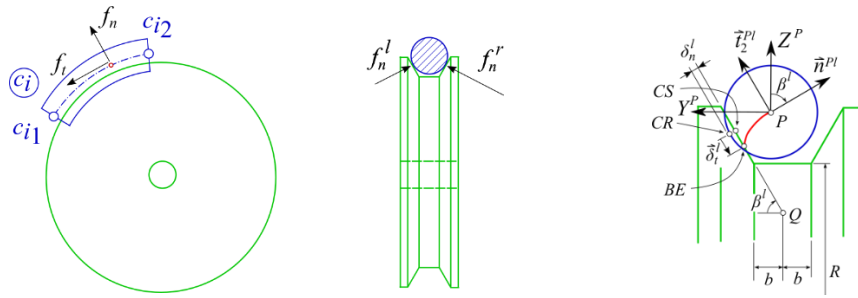


Figure 2. Rope-sheave contact. Left: contact in V-shape groove. Right: geometry of the contact analysis

In this research, the detailed 3D contact geometry of the sheave groove is considered, as can be observed in Fig. 2. That means that at each rope cross section more than one contact zone may appear, as shown in the figure.

4. The double mesh

In the ALE formulation the nodal points of the finite element mesh are not necessarily connected to material points. This is an important difficulty when modeling stick-slip tangential contact. The stick or slip conditions are related to the relative tangential velocity of the sheave and rope contact points. These are of course material points. It makes no sense to analyze stick-slip conditions working with non-material points. In other words, the bristles cannot be attached to the nodal points in the ALE formulation. This is the reason for using a double mesh for the contact analysis. Figure 3 shows the ALE nodal points using white circles and the *Lagrangian knots*, where the bristles are assumed to be attached, using blue circles. Nodes move along the rope, but knots do not. Contact forces at the rope are applied at the bristle's free ends.

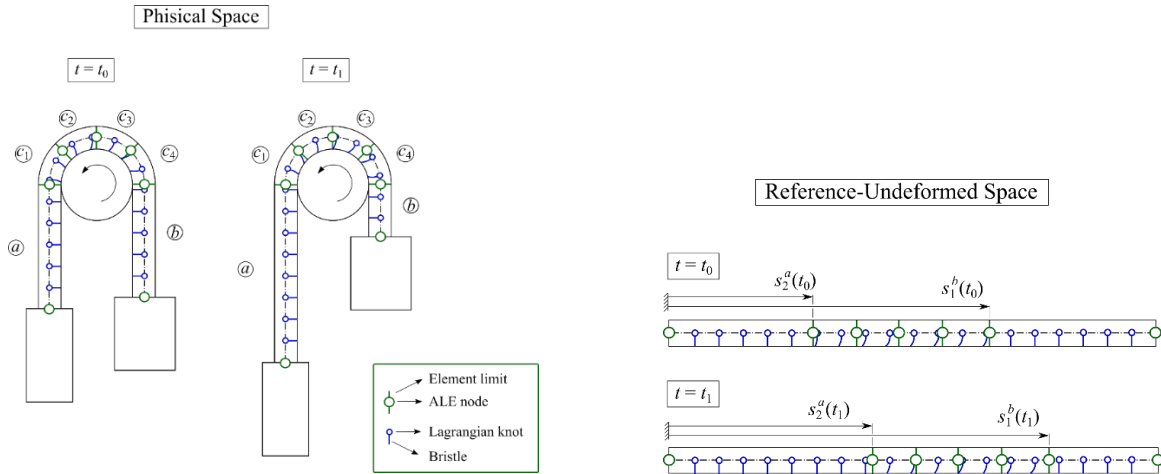


Figure 3. Double mesh for rope discretization. Left: meshes in physical space. Right: meshes in reference space.

5. Simulation results

The simulation of a 1:1 suspension elevator is used to show the validity of the presented model.

Acknowledgements

This project has received funding from the European Union's Horizon 2020 research and innovation programme under the Marie Skłodowska-Curie grant agreement No 860124.



References

- [1] Escalona, J.L. "An arbitrary Lagrangian–Eulerian discretization method for modeling and simulation of reeving systems in multibody dynamics". *Mechanism and Machine Theory*, 112, pp.1-21, 2017.
- [2] Escalona, J.L., Orzechowski, G. and Mikkola, A.M. "Flexible multibody modeling of reeving systems including transverse vibrations". *Multibody System Dynamics*, 44(2), pp.107-133, 2018.
- [3] Escalona, J.L., Mohammadi, N. "Advances in the modeling and dynamic simulation of reeving systems using arbitrary Lagrangian-Eulerian modal method". *Nonlinear Dynamics*, 108, pp. 3985–4003 2022.

A total Lagrangian Petrov–Galerkin $SE(3)$ Cosserat rod finite element formulation

Simon R. Eugster¹, Jonas Harsch¹, Simon Sailer¹

¹ Institute for Nonlinear Mechanics, University of Stuttgart, eugster@inm.uni-stuttgart.de

Keywords: rod finite elements, Petrov–Galerkin, $SE(3)$, objectivity, locking

1. Introduction

A chief difficulty in position/orientation-based rod finite element formulations is to formulate an objective interpolation to approximate the rod’s centerline and cross-section orientations. The choice of the interpolation leads directly to the approximation of the strains. Interpolations that cannot fulfill shear-rigidity and inextensibility constraints exactly are prone to shear and membrane locking. Sonnevile et al. [1] extended the idea of interpolating the nodal orientations using relative rotation vectors [2] to the interpolation of nodal Euclidean transformation matrices using relative twists. This is an objective interpolation strategy where positions and orientations are intrinsically coupled resulting in an element-wise constant strain approximation. Consequently, the formulation is intrinsically locking-free. Exclusively working on the Lie group $SE(3)$, the authors [1] applied a Bubnov–Galerkin projection where the generalized virtual displacements are given by the variation of the nodal values.

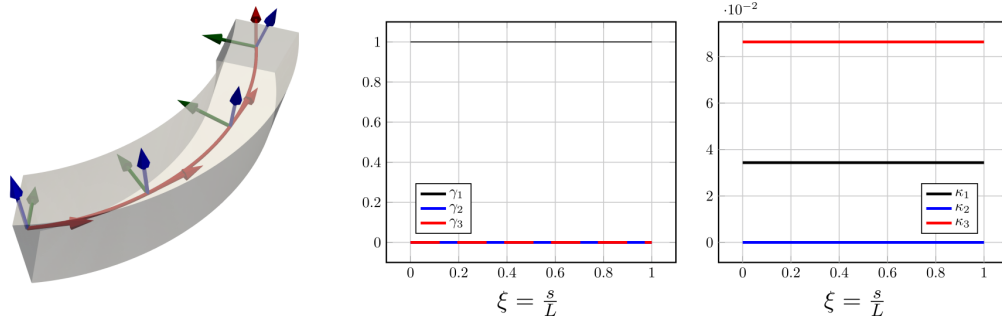


Figure 1: A single two-node $SE(3)$ -element can exactly represent a quarter helix.

Applying a Petrov–Galerkin projection method, we present a total Lagrangian, objective and intrinsically locking-free rod finite element formulation [3], where the virtual displacements and rotations as well as the translational and angular velocities are interpolated instead of using the consistent variations and time-derivatives of the introduced interpolation formula. Lie group solvers are avoided by opting for an arbitrary but explicit orientation parameterization.

2. Continuous rod kinematics

Let $\xi \in \mathcal{J} = [0, 1] \subset \mathbb{R}$ denote the centerline parameter, the motion of the Cosserat rod is described by the centerline point ${}^I\mathbf{r}_{OP}$ at (ξ, t) with respect to an inertial basis I . The respective cross-section orientation for time t is captured by the transformation matrix $\mathbf{A}_{IK}(\xi, t) \in SO(3)$. Using homogenous coordinates, the rod kinematics can be rewritten in such a way that the entire motion of the rod is represented by the Euclidean transformation matrix

$$\mathbf{H}_{\mathcal{J}\mathcal{K}}(\xi, t) = \begin{pmatrix} \mathbf{A}_{IK}(\xi, t) & {}^I\mathbf{r}_{OP}(\xi, t) \\ \mathbf{0} & 1 \end{pmatrix} \in SE(3) \quad (1)$$

which transforms the coordinates of a point in the \mathcal{K} -frame to the coordinates in the \mathcal{J} -frame, see [4].

3. Nodal kinematics

The rod is discretized by n_{el} two-node finite elements. For a given node e , the nodal transformation matrix $\mathbf{A}_{IK_e} = \text{Exp}_{SO(3)}(\boldsymbol{\Psi}_e)$ is parameterized in terms of the nodal total rotation vector $\boldsymbol{\Psi}_e(t) \in \mathbb{R}^3$. Hence the nodal

generalized coordinates are given by a minimal number of six position coordinates $\mathbf{q}_e(t) = ({}_I\mathbf{r}_{OP_e}(t), \boldsymbol{\psi}_e(t)) \in \mathbb{R}^6$. The nodal generalized velocities $\mathbf{u}_e(t) = ({}_I\mathbf{v}_{P_e}(t), {}_{K_e}\boldsymbol{\omega}_{IK_e}(t)) \in \mathbb{R}^6$ are given by the nodal translational velocity ${}_I\mathbf{v}_{P_e}$ and the angular velocity ${}_{K_e}\boldsymbol{\omega}_{IK_e}$ represented in the cross-section fixed coordinate system K_e . The nodal kinematic differential equation

$$\dot{\mathbf{q}}_e = \begin{pmatrix} {}_I\dot{\mathbf{r}}_{OP_e} \\ \dot{\boldsymbol{\psi}}_e \end{pmatrix} = \begin{pmatrix} \mathbf{1}_{3 \times 3} & \mathbf{0}_{3 \times 3} \\ \mathbf{0}_{3 \times 3} & \mathbf{T}_{SO(3)}^{-1}(\boldsymbol{\psi}_e^e) \end{pmatrix} \begin{pmatrix} {}_I\mathbf{v}_{P_e} \\ {}_{K_e}\boldsymbol{\omega}_{IK_e} \end{pmatrix} = \mathbf{B}_e(\mathbf{q}_e)\mathbf{u}_e \quad (2)$$

ouples the generalized nodal velocities with the time-derivative of the position coordinates. Possible singularities in dynamic simulations are circumvented by employing the concept of the complement rotation vector. Similar to the nodal generalized velocities, we introduce the nodal generalized virtual displacements $\delta\mathbf{s}_i^e = ({}_I\delta\mathbf{r}_{P_e, K_e}, \delta\boldsymbol{\phi}_{IK_e}) \in \mathbb{R}^6$ representing the virtual displacement of the nodal centerline point ${}_I\mathbf{r}_{P_e}$ and the virtual rotation of the nodal cross-section orientation ${}_{K_e}\delta\boldsymbol{\phi}_{IK_e}$.

4. Petrov–Galerkin projection

The nodal virtual displacements and rotations are interpolated by linear Lagrangian polynomials N_i^e in agreement with

$${}_I\delta\mathbf{r}_P(\xi, \delta\mathbf{s}) = \sum_{e=0}^{n_{el}-1} \chi_{\mathcal{J}^e}(\xi) \sum_{i=0}^1 N_i^e(\xi) {}_I\delta\mathbf{r}_{P_{e+i}}, \quad {}_K\delta\boldsymbol{\phi}_{IK}(\xi, \delta\mathbf{s}) = \sum_{e=0}^{n_{el}-1} \chi_{\mathcal{J}^e}(\xi) \sum_{i=0}^1 N_i^e(\xi) {}_{K_{e+i}}\delta\boldsymbol{\phi}_{IK_{e+i}}, \quad (3)$$

where we have used the characteristic function $\chi_{\mathcal{J}^e}: \mathcal{J} \rightarrow \{0, 1\}$, which is one for $\xi \in \mathcal{J}^e = [\xi^e, \xi^{e+1})$ and zero elsewhere. In order to obtain a constant and symmetric mass matrix, the velocities are considered as independent fields and are interpolated also linearly.

5. SE(3)-interpolation

Using the $SE(3)$ -structure of the rod, we apply the interpolation of [1], such that the Euclidean transformations of the rod are approximated by

$$\mathbf{H}_{\mathcal{J}\mathcal{K}}(\xi, \mathbf{q}) = \sum_{e=0}^{n_{el}-1} \chi_{\mathcal{J}^e}(\xi) \mathbf{H}_{\mathcal{J}\mathcal{K}_0^e}(\mathbf{q}) \mathbf{H}_{\mathcal{K}_0^e\mathcal{K}}(\xi, \mathbf{q}), \quad \text{with } \mathbf{H}_{\mathcal{K}_0^e\mathcal{K}}(\xi, \mathbf{q}) = \text{Exp}_{SE(3)}(N_1^e(\xi) \boldsymbol{\theta}_{01}^e(\mathbf{q})), \quad (4)$$

where $\boldsymbol{\theta}_{01}^e = \text{Log}_{SE(3)}(\mathbf{H}_{\mathcal{J}\mathcal{K}_0^e}^{-1} \mathbf{H}_{\mathcal{J}\mathcal{K}_1^e})$ denotes the relative twist between the two nodal Euclidean transformations.

6. Equations of motion

The equations of motion of the discretized rod directly follow from inserting all approximations into the principle of virtual work of the continuous Cosserat rod and is given by a set of first order differential equations in the form

$$\dot{\mathbf{q}} = \mathbf{B}(\mathbf{q})\mathbf{u}, \quad \dot{\mathbf{u}} = \mathbf{M}^{-1}(\mathbf{f}^{\text{gyr}}(\mathbf{u}) + \mathbf{f}^{\text{int}}(\mathbf{q}) + \mathbf{f}^{\text{ext}}(\mathbf{q})). \quad (5)$$

References

- [1] V. Sonnevile, A. Cardona, and O. Brüls. Geometrically exact beam finite element formulated on the special Euclidean group $SE(3)$. *Computer Methods in Applied Mechanics and Engineering*, 268:451–474, 2014.
- [2] M. A. Crisfield and G. Jelenić. Objectivity of strain measures in the geometrically exact three-dimensional beam theory and its finite-element implementation. *Proceedings: Mathematical, Physical and Engineering Sciences*, 455(1983):1125–1147, 1999.
- [3] J. Harsch, S. Sailer, and S. R. Eugster. A total Lagrangian, objective and intrinsically locking-free Petrov–Galerkin $SE(3)$ Cosserat rod finite element formulation. *International Journal for Numerical Methods in Engineering*, 2023. Accepted article in production, preprint: arXiv:2301.05595.
- [4] S. R. Eugster and J. Harsch. A family of total Lagrangian Petrov–Galerkin Cosserat rod finite element formulations. *GAMM-Mitteilungen*, submitted 2023.

Efficient simulation of ropeway systems with multibody systems

Johannes Gerstmayr¹, Konstantina Ntarladima¹

¹Department of Mechatronics
Universität Innsbruck
Technikerstrasse 13, 6020 Innsbruck, Austria
[johannes.gerstmayr, konstantina.ntarladima]@uibk.ac.at

Keywords: ropeway system, computational methods, contact and friction

1. Introduction

Due to their ability to provide mass transportation and the small spatial requirement of stations, ropeway systems are suitable as a means of transportation in urban environments, running at low energy costs and emissions. Proper and efficient design of these systems urges the need for a dynamic model for ropeway systems, which is not available so far. While there already exist computational frameworks for the computation of the static configuration, the dynamic problem of the rope with cabins in contact with sheaves and rollers is not straightforward. The multibody system model has the potential to investigate and predict its dynamic behavior in the design phase, which allows ropeway manufacturers to increase comfort in urban applications. This work aims to develop a planar dynamic model with physical parameters including contact between rope and sheaves and cabins attached which can be simulated using an implicit time integrator.

Few studies exist on the full-scale modeling and simulation of ropeway systems, using a dynamic and fully nonlinear model of the rope. Existing literature is focusing on the dynamic effects of cross-wind and other influences, [1]. A few recent works are studying the dynamic response of roller batteries, [2]. However, very limited research has been conducted on the detailed numerical modeling and efficient simulation of the dynamics of the rope interacting with the dynamics of the cabins and in contact with sheaves and rollers.

2. Mechanical and Numerical Modeling

We are modeling the system using a special finite element for the rope and a multibody dynamics framework which allows to directly embed the cabins and the roller batteries, see Figure 1. The numerical modeling of the rope is based on the Absolute Nodal Coordinate Formulation (ANCF), [3]. An alternative approach would be the ALE ANCF beam element proposed in [4], which can be used for ropeway systems with masses distributed along the rope.

As a crucial part of the simulation model, an efficient contact detection and computation between sheaves or rollers and the rope has to be performed. As a main part of the efficient contact implementation, we use boxed search for more than 100 rollers and 1000s of beam elements to model the rope. Contact between the rollers in roller batteries and the rope is modeled through a normal contact model based on the penalty formulation and a regularized Coulomb friction model. The special geometry of the system which consists of cubic polynomials that interpolate the nodes of the rope and circular objects allows us to compute the contact points of the two bodies as the numerical solution of the exact geometrical problem. For the contact of the rope with the sheaves, the modeling of the friction is crucial for the transmission of the motion from the driving sheave to the system. A so-called bristle model, has been previously used for reeving systems [5].

3. Ropeway System Simulation

The ropeway system of Figure 1 is simulated in the multibody dynamics code EXUDYN [6]. Because the major part of the relevant system components moves in a plane, we reduce the system to a planar model. Sheaves A and B are used to model the upper and lower station, however, the axis of sheaves A and B are rotated by 90° around X, as in reality the sheaves' axes would coincide with coordinate Y, see Figure 1(a). Cabins are modeled as rigid bodies connected to the rope through revolute joints. For the dynamic simulation, an according initial (static) configuration is needed, considering the rope and cabins under gravity as well as the contact with rollers

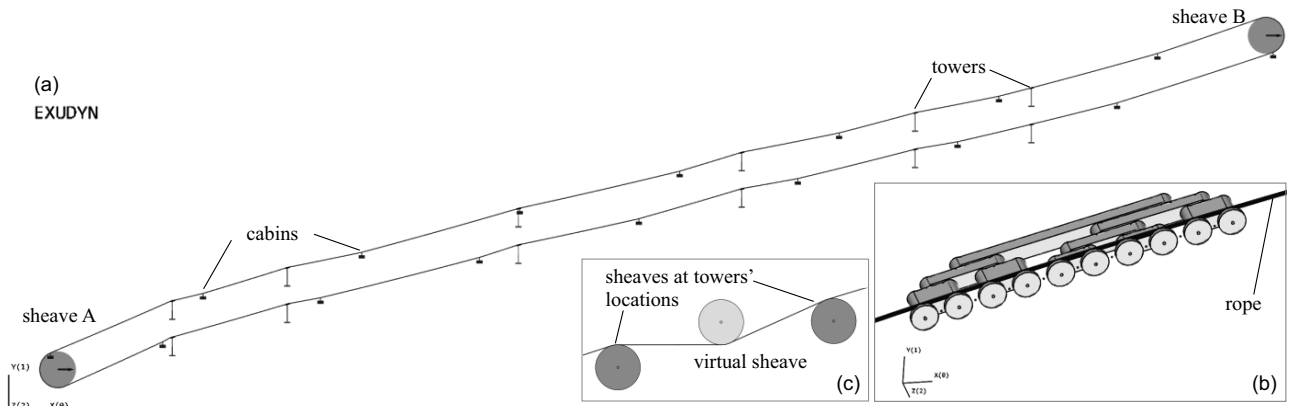


Figure 1: (a) Simulated ropeway system. (b) Detailed figure of roller battery (without a tower drawn) used during simulation. (c) Reaving system consisted of sheaves at the location of the towers (in dark grey) and virtual sheaves (in light grey).

and sheaves within a nonlinear static problem. For this static problem, an initial static guess is needed, as well. As a simplified but robust initialization, we use the geometry of a simplified reaving system without gravity and one circle for contact at each tower instead of the detailed roller batteries. In order to speed up the computation, the contact computation as well as the computation of rigid bodies and ANCF beams is performed in parallel, using multithreaded parallelization.

In the presentation we will show parameter variations of rope velocity and cabin masses, being important design parameters in the system. The full scale simulation and parameter variation allow determining critical operation modes during the design phase.

Acknowledgments

This project has received funding from the European Union’s Horizon 2020 research and innovation programme under the Marie Skłodowska-Curie grant agreement No 860124. This publication reflects only the author’s view and the Research Executive Agency is not responsible for any use that may be made of the information it contains.



References

- [1] Klaus Hoffman. Oscillation effects of ropeways caused by cross-wind and other influences. *FME Transactions*, 37(4):175–184, 2009.
- [2] Andrea Arena, Biagio Carboni, Fabio Angeletti, Mathieu Babaz, and Walter Lacarbonara. Ropeway roller batteries dynamics: Modeling, identification, and full-scale validation. *Engineering Structures*, 180:793–808, 2019.
- [3] Ahmed A Shabana. An absolute nodal coordinate formulation for the large rotation and deformation analysis of flexible bodies. *Technical Report, Department of Mechanical Engineering, University of Illinois at Chicago*, 1996.
- [4] Michael Pieber, Konstantina Ntarladima, Robert Winkler, and Johannes Gerstmayr. A Hybrid Arbitrary Lagrangian Eulerian Formulation for the Investigation of the Stability of Pipes Conveying Fluid and Axially Moving Beams. *Journal of Computational and Nonlinear Dynamics*, 17(5):051006 (13 pages), 2022.
- [5] Urbano Lugrís, José Luis Escalona, Daniel Dopico Dopico, and Javier Cuadrado. Efficient and accurate simulation of the rope-sheave interaction in weight-lifting machines. *Proceedings of the Institution of Mechanical Engineers, Part K: Journal of Multi-body Dynamics*, 225(4):331–343, 2011.
- [6] Johannes Gerstmayr. Exudyn – A C++ based Python package for flexible multibody systems. preprint, Research Square, <https://www.researchsquare.com/article/rs-2693700/v1>, 2023.

An Invariant Bézier FE-formulation for the Analysis of Slender Beams

L. Greco¹, D. Castello¹, M. Cuomo¹

¹ Department of Civil Engineering and Architecture (DICAR), University of Catania, Italy

Keywords: Invariant formulation, Kirchhoff-Love rod, G^1 -continuity, Mixed formulation, Slender structures

1. Introduction

A new invariant Finite Element (FE) formulation for the geometrically non linear static analysis of the slender beams is presented. The proposed FE formulation is based on the Kirchhoff-Love (KL) beam model as in [1] in which an ad-hoc rotation decomposition (i.e. the Smallest Rotation (SR) map, see [6]) is introduced in order to account the cross section orthogonality constraint. On this way the configuration space for the proposed KL beam model splits in the cartesian product $\mathbb{R}^3 \times \mathbf{S}^2 \times \mathbf{S}^1$ characterized by the two kinematic descriptors: the centroid curve \mathbf{p} and an angle ϕ in order to correct the orientation of the cross section around the centroid curve.

2. Numerical formulation

The weak formulation for the KL beam model present a variational index equal to 2, then G^1 -conforming FE's are need. Following [2, 3] the G^1 -conforming FE formulation can be designed introducing the rotation at the ends of the FE with the aim to map the second and the second last control points. Furthermore, an Hellinger-Reissner type mixed formulation is adopted in order to avoid the several locking pathologies and improve the computational strategy. In order to achieve the objectivity of the strain interpolations, with respect to the G^1 -conforming formulation proposed in [2, 3] in this contribute a new hierarchic interpolation for the kinematic descriptor ϕ is proposed. The same Bézier interpolations for both the two kinematic descriptors of the model are considered. The proposed invariant FE formulation is very simple with regard to the others present in the literature, see for instance [4, 5].

3. Numerical investigations

3.1. Objectivity test

Following [5], on the end A of a quarter circular cantilever pre-twisted beam is applied a rotation $\omega_y = 20\pi$ about the y-direction. In figure 1(a) the initial (orange) and several deformed configurations (gray) are depicted for the angle $\omega_y = \frac{2\pi}{5}, \frac{4\pi}{5}, \frac{6\pi}{5}$ and $\frac{8\pi}{5}$ respectively. In figure 1(b) the logarithm of the computed strain energy versus the imposed rotation ω_y for the polynomial degrees $p = 3, 4$ and 5 is shown.

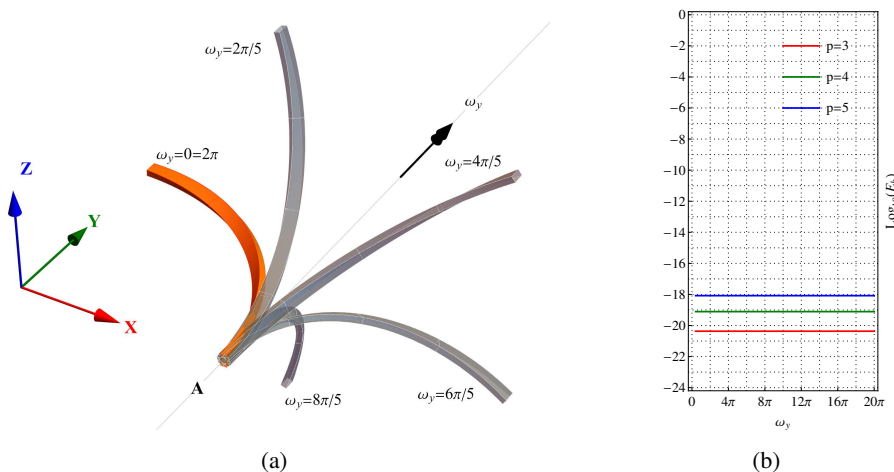


Figure 1: Objectivity test: (a) geometry and deformed configurations, (b) $\log_{10}(E_h)$ versus the angle ω_y .

3.2. Shallow arch

Following [7] a plane shallow slender arch is considered, due to the symmetry only an half of the structure is modeled. Two geometries are examined, for both the two cases the span of the half-arc is $L = 5\text{ m}$ while the heights are $f = 0.5\text{ m}$ and $f = 0.75\text{ m}$ while the two loads are 500 kN and 2000 kN respectively. The cross section is $0.2 \times 0.2\text{ m}^2$ the Young modulus $E = 3 \times 10^4\text{ MPa}$. In figure 2(a) the problem set up is shown, while in figure 2(b) and 2(c) the fundamental equilibrium paths are depicted for the two geometries considered. A mesh of only 3 FE's with $p = 5$ is adopted. The Crisfield's path following algorithm is adapted to the proposed invariant G^1 -conforming formulation.

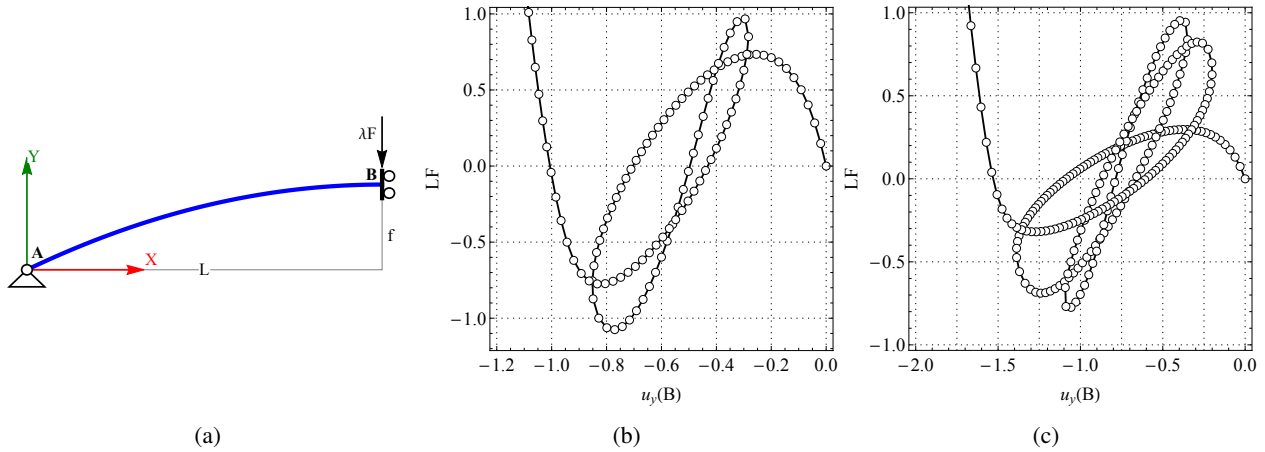


Figure 2: Shallow arch: (a) geometry and equilibrium paths for the case (b) $f = 0.5\text{ m}$ with $F = 500\text{ kN}$ and (c) $f = 0.75\text{ m}$ with $F = 2000\text{ kN}$ respectively.

4. Conclusions

A new invariant Bézier G^1 -conforming FE formulation based on the Kirchhoff-Love beam model is presented. HR-like mixed formulation is adopted in order to reduce the computational effort of the numerical resolution strategy. The proposed formulation can be extended to the IGA.

References

- [1] L. Greco, M. Cuomo. *B-Spline interpolation of Kirchhoff-Love space rods*, Computer Methods in Applied Mechanics and Engineering, 256 (2013) 251-269.
- [2] L. Greco, A. Scrofani, M. Cuomo. *A non-linear symmetric G^1 -conforming Bézier finite element formulation for the analysis of Kirchhoff beam assemblies*, Computer Methods in Applied Mechanics and Engineering, 387 (2021) 114176.
- [3] L. Greco, M. Cuomo, A. Scrofani, D. Castello. *An updated Lagrangian Bézier finite element formulation for the analysis of slender beams*, Mathematics and Mechanics of Solids, 27(10) (2022) 2110-2138.
- [4] C. Meier, A. Popp, W.A. Wall. *Geometrically exact finite element formulations for curved slender beams: Kirchhoff-Love theory vs Simo-Reissner theory*, Archives of Computational Methods in Engineering, 26 (2019) 163–243.
- [5] A. Borković, G. Gfrerer, B. Marussig. *Geometrically exact isogeometric Bernoulli-Euler beam based on the Frenet-Serret frame*, Computer Methods in Applied Mechanics and Engineering, 405 (2023) 115848.
- [6] M. A. Crisfield, *Non-linear Finite Element Analysis of Solids and Structures*, John Wiley & Sons, Place of Publication, 1997.
- [7] A. Borković, B. Marussig, G. Radenković. *Geometrically exact static isogeometric analysis of an arbitrarily curved spatial Bernoulli-Euler beam*, Thin-Walled Structures, 170 (2022) 108539.

Rotation parametrization and interpolation strategies for Petrov–Galerkin rod finite elements – a family of Cosserat rod formulations

Jonas Harsch¹, Simon R. Eugster¹

¹ Institute for Nonlinear Mechanics, University of Stuttgart, Germany, harsch@inm.uni-stuttgart.de

Keywords: rod finite elements, Petrov–Galerkin, locking, $SO(3)$, $SE(3)$

1. Introduction

The development of rod finite elements poses two significant challenges: the first being the need for a singularity-free description of the cross-sectional orientation, and the second involving the objective interpolation of the kinematic descriptors. This talk provides an in-depth discussion of both challenges and presents a Petrov–Galerkin discretization approach. Specifically, this approach involves the interpolation of virtual displacements differently from the kinematic descriptors, resulting in a finite element formulation that is independent of the chosen parametrization or interpolation strategy. As a result, a family of Cosserat rod finite element formulations [1] is obtained.

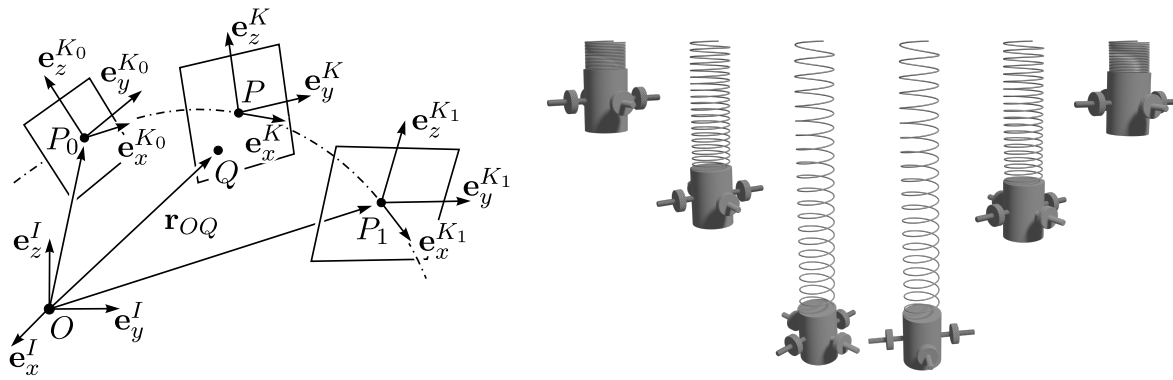


Figure 1: Kinematics of the Cosserat rod (left). Application of rod finite elements (right).

2. Kinematics

Let $\xi \in \mathcal{J} = [0, 1] \subset \mathbb{R}$ denote the centerline parameter, the kinematics of the Cosserat rod is described by the centerline point r_{OP} at (ξ, t) with respect to an inertial basis I . The respective cross-section orientation is captured by the transformation matrix $\mathbf{A}_{IK} \in SO(3)$.

3. Rotation parametrization

For a given node i of finite-element e , the corresponding transformation matrix $\mathbf{A}_{IK_i^e}$ has to be parametrized. A first possibility is given by the Rodrigues' formula

$$\mathbf{A}_{IK_i^e} = \text{Exp}_{SO(3)}(\boldsymbol{\psi}_i^e) = \mathbf{1}_{3 \times 3} + \frac{\sin(\|\boldsymbol{\psi}_i^e\|)}{\|\boldsymbol{\psi}_i^e\|} \tilde{\boldsymbol{\psi}}_i^e + \frac{1 - \cos(\|\boldsymbol{\psi}_i^e\|)}{\|\boldsymbol{\psi}_i^e\|^2} (\tilde{\boldsymbol{\psi}}_i^e)^2 \in SO(3) \quad (1)$$

in terms of the nodal total rotation vectors $\boldsymbol{\psi}_i^e(t) \in \mathbb{R}^3$. Alternatively, the nodal unit quaternions $\mathbf{P}_i^e(t) = (p_0, \mathbf{p}) \in \mathbb{R}^4$ can be used to parametrize the orientation in accordance with

$$\mathbf{A}_{IK_i^e} = \mathbf{1} + 2(p_0 \tilde{\mathbf{p}} + \tilde{\mathbf{p}}^2). \quad (2)$$

4. Interpolation strategies

\mathbb{R}^{12} -interpolation: Following [2, 3], both the centerline and the cross-section orientations are approximated by the piecewise interpolation with p -th order Lagrangian polynomials $N_i^{p,e}$, which can be written as

$$r_{OP}(\xi, \mathbf{q}) = \sum_{e=0}^{n_{el}-1} \chi_{\mathcal{J}^e}(\xi) \sum_{i=0}^p N_i^{p,e}(\xi) r_{OP_i^e}, \quad \mathbf{A}_{IK}(\xi, \mathbf{q}) = \sum_{e=0}^{n_{el}-1} \chi_{\mathcal{J}^e}(\xi) \sum_{i=0}^p N_i^{p,e}(\xi) \mathbf{A}_{IK_i^e}(\mathbf{q}), \quad (3)$$

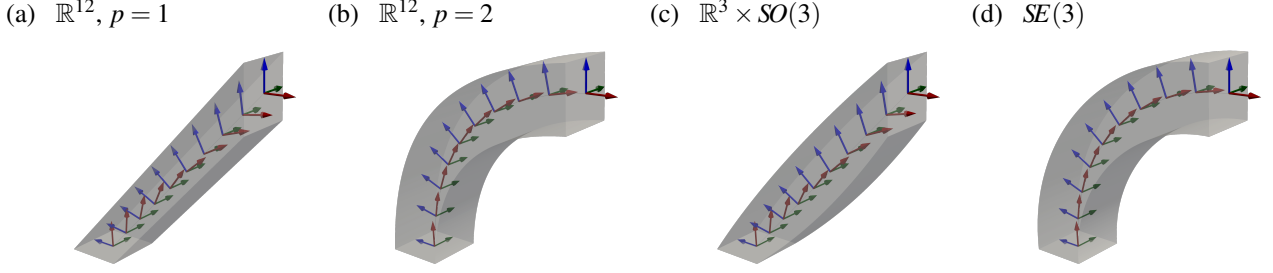


Figure 2: Different interpolation strategies applied to a quarter circle deformation.

where we have used the characteristic function $\chi_{\mathcal{J}^e}: \mathcal{J} \rightarrow \{0, 1\}$, being one for $\xi \in \mathcal{J}^e = [\xi^e, \xi^{e+1})$ and zero elsewhere.

$\mathbb{R}^3 \times SO(3)$ -interpolation: Originally proposed by Crisfield and Jelenić [4], the centerline is discretized by the piecewise interpolation (3) and the orientation is interpolated by the ansatz

$$\mathbf{A}_{IK}(\xi, \mathbf{q}) = \sum_{e=0}^{n_{el}-1} \chi_{\mathcal{J}^e}(\xi) \mathbf{A}_{IK_0^e}(\mathbf{q}) \mathbf{A}_{K_0^e K}(\xi, \mathbf{q}), \quad \mathbf{A}_{K_0^e K}(\xi, \mathbf{q}) = \text{Exp}_{SO(3)} \left(\sum_{i=1}^p N_i^{p,e}(\xi) \boldsymbol{\psi}_{0i}^e \right), \quad (4)$$

with the relative rotation vector $\boldsymbol{\psi}_{0i}^e = \text{Log}_{SO(3)}(\mathbf{A}_{IK_0^e}^T \mathbf{A}_{IK_i^e})$. For simplicity, we restricted ourselves on the reference orientation $\mathbf{A}_{IK_0^e}$.

$SE(3)$ -interpolation: In [5, 6], the idea from the $\mathbb{R}^3 \times SO(3)$ -interpolation is extended to the interpolation of nodal Euclidean transformation matrices

$$\mathbf{H}_{\mathcal{J} \mathcal{K}_i^e} = \begin{pmatrix} \mathbf{A}_{IK_i^e} & i \mathbf{r}_{OP_0^e} \\ \mathbf{0} & 1 \end{pmatrix} \quad (5)$$

with the aid of relative twists $\boldsymbol{\theta}_{0i}^e = \text{Log}_{SE(3)}(\mathbf{H}_{\mathcal{J} \mathcal{K}_0^e}^{-1} \mathbf{H}_{\mathcal{J} \mathcal{K}_i^e})$. This leads to a highly nonlinear interpolation strategy that couples the interpolations of centerline points and cross-section orientations. Again, we have chosen the reference Euclidean transformation matrix $\mathbf{H}_{\mathcal{J} \mathcal{K}_0^e}$, although the sophisticated choice of [4] can be applied. Only the two-node formulation ($p = 1$) leads to constant strain measures, hence, without further adaptations, higher order schemes will suffer from membrane and shear locking.

References

- [1] S. R. Eugster and J. Harsch. A family of total Lagrangian Petrov–Galerkin Cosserat rod finite element formulations. *GAMM-Mitteilungen*, submitted 2023.
- [2] P. Betsch and P. Steinmann. Frame-indifferent beam finite elements based upon the geometrically exact beam theory. *International Journal for Numerical Methods in Engineering*, 54(12):1775–1788, 2002.
- [3] I. Romero and F. Armero. An objective finite element approximation of the kinematics of geometrically exact rods and its use in the formulation of an energy-momentum conserving scheme in dynamics. *International Journal for Numerical Methods in Engineering*, 54:1683–1716, 2002.
- [4] M. A. Crisfield and G. Jelenić. Objectivity of strain measures in the geometrically exact three-dimensional beam theory and its finite-element implementation. *Proceedings: Mathematical, Physical and Engineering Sciences*, 455(1983):1125–1147, 1999.
- [5] V. Sonnevile, A. Cardona, and O. Brüls. Geometrically exact beam finite element formulated on the special Euclidean group $SE(3)$. *Computer Methods in Applied Mechanics and Engineering*, 268:451–474, 2014.
- [6] J. Harsch, S. Sailer, and S. R. Eugster. A total Lagrangian, objective and intrinsically locking-free Petrov–Galerkin $SE(3)$ Cosserat rod finite element formulation. *International Journal for Numerical Methods in Engineering*, 2023. Accepted article in production, preprint: arXiv:2301.05595.

Accurate contact detection and response in fibre assemblies with friction.

Emile Hohnadel, Octave Crespel, Thibaut Métivet, Florence Bertails-Descoubes

Univ. Grenoble Alpes, Inria, CNRS, Grenoble INP, LJK, emile.hohnadel@inria.fr

Keywords: thin elastic rods, high-order contact detection, frictional contact, numerical simulation

1. Introduction

Simulating dry interacting fibres is relevant to a diverse set of applications, ranging from the fundamental understanding of fibre entanglement [1] to the realistic animation of hair in special effects [4, 6] and the virtual prototyping and design of a wide set of new rod-based materials in the fields of engineering [5]. Since the 2000's, a number of numerical models for fibres subject to frictional contact has therefore been developed both in Computer Graphics and Mechanical Engineering, with variability across the validity range, computational performance, and predictability. While the former community has focused on the simulation of extremely complex scenes (thousands to millions long interacting fibres under large displacements), often at the expense of little quantitative validation, the latter has generally favoured much simpler scenarios (small deflection of beams, low number of fibres and contact points, regularised friction laws) albeit with extensive care for predictability.

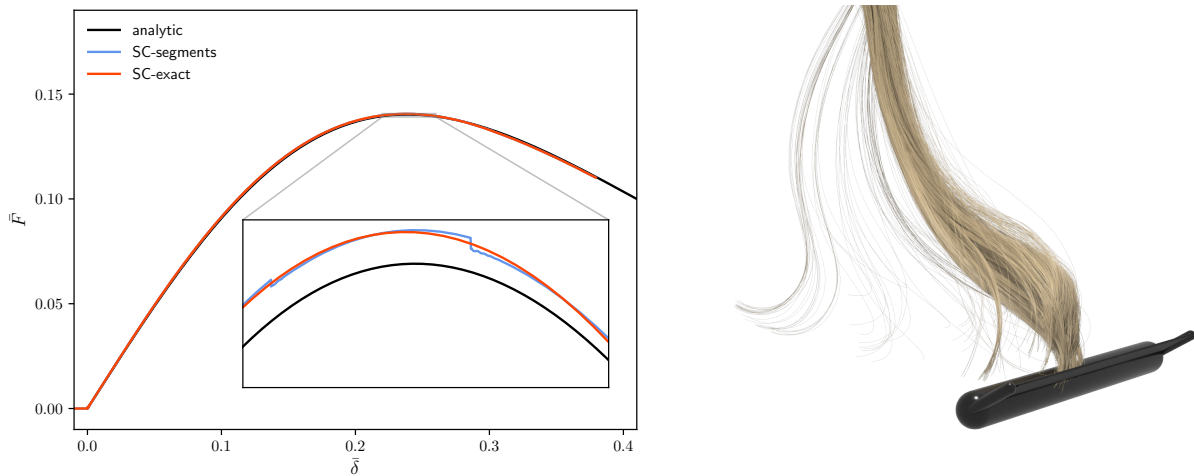


Figure 1: (Left) Comparison of the normalised force \bar{F} as a function of the normalised displacement $\bar{\delta}$ in the frictionless three-point-bending test using a 2D implementation of the *Super-Helix* model to simulate the rod. Two detections schemes are compared, segments discretisation and exact distance computation, to the analytic solution. (Right) Application of our full pipeline to the challenging simulation of a comb passing into a wisp of hair: 2025 tightly contacting super-helices are simulated with dry friction, resulting in 33100 contacts on average, which are accurately detected using our new curve-curve detection algorithm [3] and resolved precisely with our non-smooth Coulomb friction contact solver so-bogus [4].

The goal of this work is to explore novel algorithms to enhance the predictability of fibre assembly simulators, without sacrificing the complexity of the target scenarios. Our present study is precisely aimed at evaluating and improving the accuracy of the *forces* computed among fibre assemblies. Computing frictional contact forces emerging from fibre systems in an accurate manner is indeed fundamental to the proper understanding of micro-mechanisms at the origin of macro-behaviours such as adhesion or crackling in fibre assemblies, which still remain poorly understood nowadays [1, 8]. On an applicative point of view, predicting forces correctly would further allow to enhance considerably the predictability of material design, especially for systems requiring high-fidelity restitution of some target properties like the strength, feasibility and sustainability of the design [7], but also the user sensorial experience related to touch or audio sense of reality [10].

2. Contribution

Our work relies on the super-helix [2] curvature-based discrete model for Kirchhoff elastic rods, coupled with contact and friction through the non-smooth so-bogus solver [4]. This coupled simulator has been carefully validated *geometrically* in 2D and 3D configuration, against the dimensionless cantilever and pinning tests [9].

When analysing the contact forces yielded by this numerical model on the classical three-point-bending test, for which an analytical law can be derived, we note the occurrence of spurious jumps which, to the best of our knowledge, were never reported before. We demonstrate that these artifacts are actually directly linked to the *low-order contact detection* being used between the fibre and the obstacles. Low-order detection, based on segment proxys, is classically used due to its simplicity of treatment, even for fibre models possessing a higher-order geometry like super-helices. We show that spurious artifacts occur whatever the fibre model and contact response solver used, as soon as a segment-segment detection scheme is employed.

To remove such numerical artifacts in the force profile, which can accumulate to yield large force errors, we introduce an efficient high-order detection algorithm [3]. Our method aims at finding the closest point between a pair of curves, with respective centreline parametric equations $a(s)$ and $b(s)$, by looking for the two curvilinear abscissa s_1 and s_2 that minimise the distance fonction $D(s_1, s_2) \equiv \frac{1}{2} \|a(s_1) - b(s_2)\|^2$.

In the 2D case, we show that there exists an analytic solution to our problem. In the general 3D case, the problem becomes non-convex and challenging to solve: we devise a branch-and-bound approach to find pairs of closest points in an accurate and efficient way. Our algorithm proves to be particularly well-suited to super-helices, but can be adapted to other family of curves, provided there is a bound on their second derivative. We combine that narrow phase detection to a broad phase that prunes obvious cases and add a final pass that merges close contact at the junction between discretised elements.

We demonstrate the validity of our detection algorithm on the 2D three-point bending test (see Figure 1, left), and the scalability and robustness of our method on a challenging 3D scenario involving tens thousands of frictional contacts (Figure 1, right).

References

- [1] I. Andrade-Silva, T. Godefroy, O. Pouliquen, J. Marthelot. *Cohesion of bird nests*, APS March Meeting Abstracts, jan. 2021.
- [2] F. Bertails, B. Audoly, M.-P. Cani, B. Querleux, F. Leroy, J.-L. L ev eque. *Super-Helices for Predicting the Dynamics of Natural Hair*, ACM Trans. Graph., 25 (2006).
- [3] O. Crespel, E. Hohnadel, T. Metivet, F. Bertails-Descoubes. *Contact detection between fibres: high order makes a difference*, submitted.
- [4] G. Daviet, F. Bertails-Descoubes, L. Boissieux. *A hybrid iterative solver for robustly capturing coulomb friction in hair dynamics*, ACM Trans. Graph., 139 (2011).
- [5] D. Durville, *Contact-friction modeling within elastic beam assemblies: an application to knot tightening*, Comput. Mech., vol. 49, num. 6 (2012).
- [6] D. Kaufman, R. Tamstorf, B. Smith, J.-M. Aubry, E. Grinspun. *Adaptive Nonlinearity for Collisions in Complex Rod Assemblies*, ACM Trans. Graph., 33 (2014).
- [7] J. Panetta, M. Konakovi c-Lukovi c, F. Isvoranu, E. Bouleau, M. Pauly. *X-Shells: A New Class of Deployable Beam Structures*, ACM Trans. Graph., 38 (2019).
- [8] S. Poincloux, M. Adda-Bedia, F. Lechenault. *Crackling dynamics in the mechanical response of knitted fabrics*, Phys. Rev. Lett., 121 (2018).
- [9] V. Romero, M. Ly, A.-H. Rasheed, R. Charrondi re, A. Lazarus, S. Neukirch, F. Bertails-Descoubes. *Physical validation of simulators in Computer Graphics: A new framework dedicated to slender elastic structures and frictional contact*, ACM Trans. Graph., 40 (2021).
- [10] E. Schweickart, D. James, S. Marschner. *Animating Elastic Rods with Sound*, ACM Trans. Graph., 36 (2017).

A numerical bending study of sandwiched beams with a mortar line-to-line contact formulation

Amol V. Kulkarni¹, Armin Bosten^{1,2}, Vanessa Dörlich², Olivier Brüls¹, Joachim Linn²

^{1,2,4} Department of Aerospace and Mechanical Engineering, University of Liège,
avkulkarni@uliege.be, a.bosten@uliege.be, o.bruls@uliege.be

^{3,5} Dept. of Mathematics for Vehicle Engineering, Fraunhofer Institute for Industrial Mathematics ITWM,
vanessa.doerlich@itwm.fraunhofer.de, joachim.linn@itwm.fraunhofer.de

Keywords: Odin, Mortar Method, Bending, Finite Elements, Contact

1. Introduction

Nowadays, flexible beam-like structures have found extensive use in the automobile and the aerospace domain. With the implementation of fly-by-wire systems in the the aerospace industry and drive-by-wire in modern electric vehicles, these flexible slender structures of wire bundles, cables or hoses play a vital role in the functioning of these systems. IPS Cable Simulation is a commercial simulation tool developed at Fraunhofer ITWM which is capable of real-time simulations of flexible cables deformations. It is based on a geometrically exact rod model where the constitutive model is formulated based on the sectional quantities of the rod. Thus, the internal mechanical response of the individual wires in the cable and their interactions are not explicitly incorporated. This project aims at a deeper understanding of such finer scales.

Mechanical experiments for flexible slender structures can be performed in order to understand the constitutive model of the cable bundle [3]. However, only the global quantities such as the displacement at the boundary and the sectional forces can be measured through the experiments. The contact forces between the individual wires and the exact knowledge of the geometric rearrangements are not measured. Therefore, some results from the experiments cannot be interpreted with certainty such as the hysteresis in the load displacement curves. Although some commercial simulation software can simulate such cable bundles [2], the results are highly sensitive to numerical parameters of the contact model, whose tuning is particularly cumbersome. The alternative to using commercial software is to use a research simulation code, such as Odin [4].

The contact mechanics between highly flexible slender structures is still an active field of research. Our current hypothesis to explain the hysteresis effect is that it originates in the frictional interactions between the individual fibres. This motivates the development of a research simulation framework with advanced beam models, constitutive laws and custom solvers for the simulation of multibody systems with contact conditions. Odin includes many recently developed functionalities and relevant test cases are needed to ascertain the results. The investigation of the mechanical phenomena and the numerical behaviour of line-to-line contact formulations implemented in Odin motivates the present study of the bending response of sandwiched beams.

2. Sandwiched Beams Bending Test

In this simulation, geometrically exact beams based on the special Euclidean group SE(3) theory represent the two beams. The beams have a radius $r = 0.001$ m with length $l = 0.3$ m and the material properties are referenced from [7] ($E = 200$ GPa, $\nu = 0.2$). The beams are discretized into 10 elements. The master beam is superposed over the slave beam and a mortar line-to-line contact discussed in [6] is defined between the two beams. A quasi-static uniformly distributed load $P = 1$ N/m is applied on the upper surface of the master beam. Both beams are clamped on the left end and are free on the right end. The total time of simulation is 5 s, with a time-step size of $h = 0.01$ s. Figure 1a shows the boundary conditions and the uniformly distributed load applied over the upper beam.

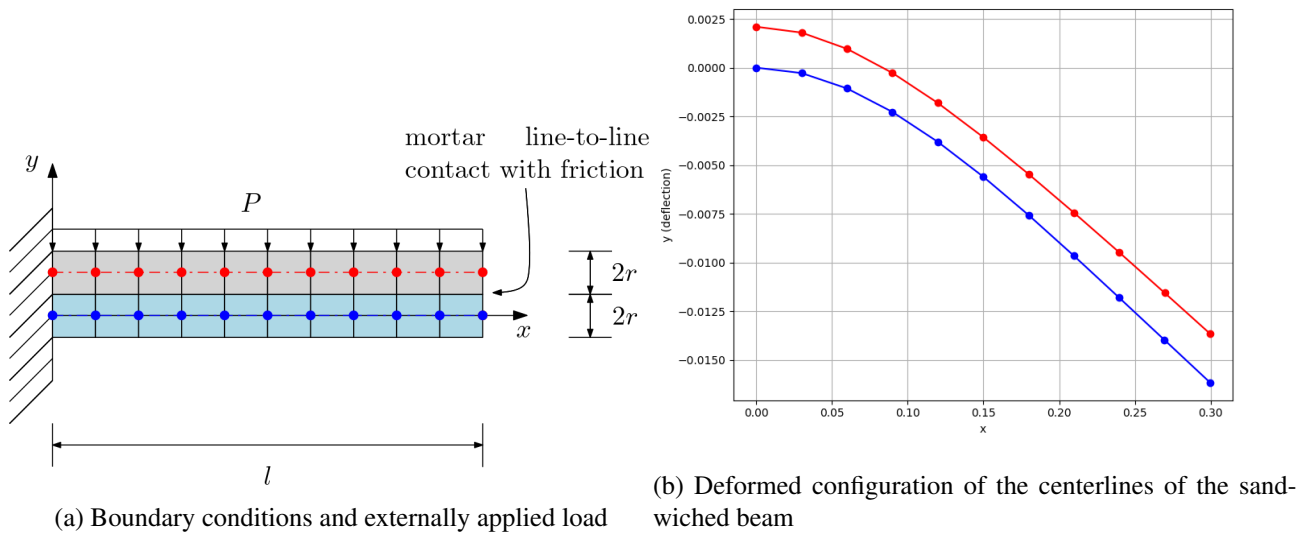


Figure 1: Load case and final deformed configuration of the sandwiched beam

The final deformation configuration of the sandwiched beams is shown in Figure 1b. This figure shows the deflection of the lower beam under the contact pressure due to the contact force. A minimal sliding between the beams is observed as the nodes are getting misaligned during the bending process. In the talk, the distribution of the normal and tangential contact forces and the sliding of the nodes during the bending will be analysed in detail.

Acknowledgments

This project has received funding from the European Union’s Horizon 2020 research and innovation program under the Marie Skłodowska-Curie grant agreement No 860124.

References

- [1] J. Linn, K. Dreßler. *Discrete Cosserat rod models based on the difference geometry of framed curves for interactive simulation of Flexible Cables*, Math for the Digital Factory, Springer International Publishing, 2017.
- [2] M. Hawwash, V. Dörlich, J. Linn, R. Keller, R. Müller. *Modelling the effective inelastic behavior of multi-wire cables under mechanical load using finite elements*, ECCOMAS Congress 2022.
- [3] V. Dörlich, P. Češarek, J. Linn, S. Diebels. *Experimental investigation and numerical modeling of resultant-based bending plasticity in cables*, ECCOMAS Thematic Conference on Multibody Dynamics, 2017.
- [4] A. Cosimo and O. Brüls. Odin. GitLab repository. <https://gitlab.uliege.be/am-dept/odin>, 2022.
- [5] V. Sonneville, A. Cardona, O. Brüls. *Geometrically exact beam finite element formulated on the special Euclidean group $SE(3)$* , Computer Methods in Applied Mechanics and Engineering, Volume 268, Pages 451-474, 2014.
- [6] A. Bosten, A. Cosimo, J. Linn, O. Brüls. *A mortar formulation for frictionless line-to-line beam contact*. Multibody System Dynamics 54, 31–52, 2022.
- [7] B. Bozorgmehri, X. Yu, M. Matikainen, A. Harish, A. Mikkola. *A study of contact mechanics in application of large deformation dynamics*, Nonlinear Dyn 103:581–616, 2021.

Investigating the compaction of open ring stacks through real and numerical experiments

Thibaut Metivet ¹, Emile Hohnadel ¹, Tomohiko G. Sano ², Toshiyuki Kawata ²,
 Florence Bertails-Descoubes ¹

¹ Univ. Grenoble Alpes, Inria, CNRS, Grenoble INP, LJK, Grenoble, France, thibaut.metivet@inria.fr

² Department of Mechanical Engineering, Keio University, Yokohama, Japan, sano@mech.keio.ac.jp

Keywords: thin elastic rods, frictional contact, 2D open rings, mechanical metamaterials, snap-fits

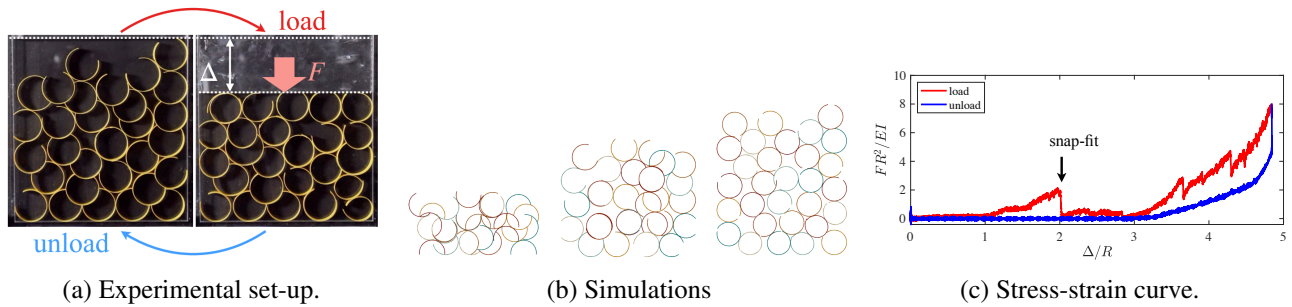


Figure 1: (a) Experimental set-up with 30 open rings. (b) Simulation of 30 rings with different opening angles. (c) Stress-strain curve for one compression cycle, illustrating the shell-shell snap-fit events leading to force drops.

Mechanical metamaterials remarkably exploit large-displacement phenomena, such as the buckling instabilities of slender structures or the coupling between elasticity and friction, as mechanical energy transducers able to achieve designed functionalities [2, 3]. While such systems have recently met large interest owing to the progress in fabrication technology and computational modelling, they often rely on the careful manufacturing of controlled structures, and the effect of randomness or defects in the components are seldom quantified nor accounted for.

This work investigates the mechanical response of a random stack of bidimensional flexible open rings [1a] subject to compression cycles, by the means of experiments and simulations [1]. We leverage the curvature-based super-helix [4] numerical model to simulate the open rings as two-dimensional Kirchhoff rods, and fully account for frictional interaction between the rings with a geometrically-exact contact detection algorithm coupled to frictional contact constraints [5]. This fully high-order framework allows for robust and scalable simulations, notably removing the spurious discretisation-based artefacts in the force response that occur with low-order models.

Our numerical model is carefully validated against theoretical predictions for the snap-fit of a single ring onto a cylinder [6], demonstrating the particularly accurate account of Coulomb friction with our non-smooth approach [2]. The excellent agreement obtained between our simulations and experiments for the 30 rings assembly compression cycles, in particular regarding the snap-fit force drops and cycle hysteresis, allows to rely on the numerical model to further investigate the impact of the friction coefficient and the opening angle of the rings [1b] on the mechanical behaviour of the system. In particular, we find that such a system, which acts as a disordered mechanical metamaterial, can absorb and store mechanical energy upon compression in a controlled way by exploiting large displacement and relocation of rings, snap-fits, and friction [3].

References

- [1] Sano T. G., Hohnadel E., Kawata T., Metivet T., Bertails-Descoubes F. *Randomly stacked open-cylindrical shells as a functional mechanical device*, arXiv 2301.07867, <https://arxiv.org/abs/2301.07867>, 2023.
- [2] Holmes, D.P. *Elasticity and stability of shape-shifting structures*, Current opinion in colloid and interface science, 40, pp.118-137, 2019.

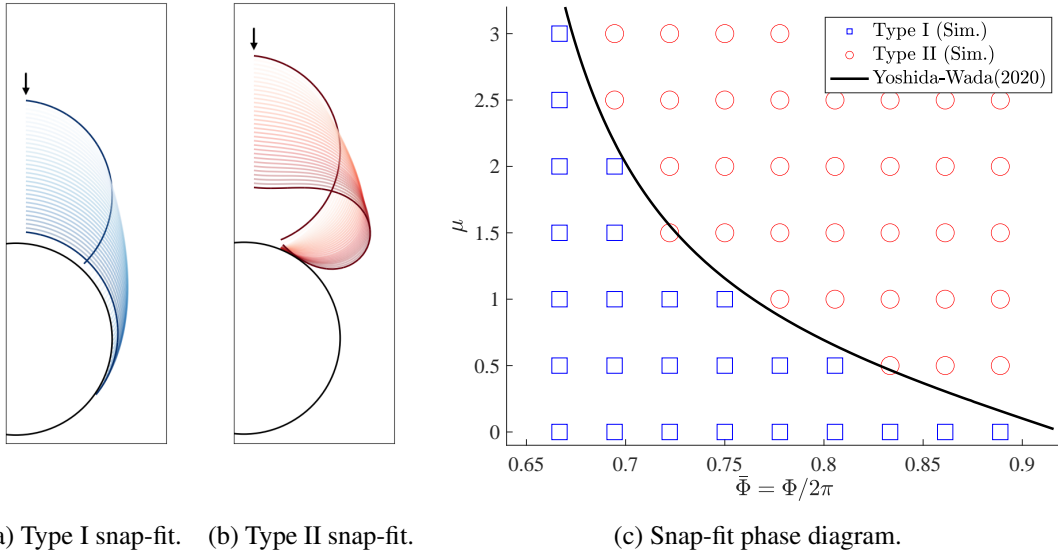


Figure 2: (a,b) Simulations of sliding (type I) or sticking (type II) snap-fit of a 2D cylindrical shell onto a rigid cylinder. The snap-fit regime depends on the opening angle of the ring Φ and the friction coefficient μ between the ring and the cylinder. (c) Simulated and theoretical phase diagram for type I or II snap-fitting in (Φ, μ) space.

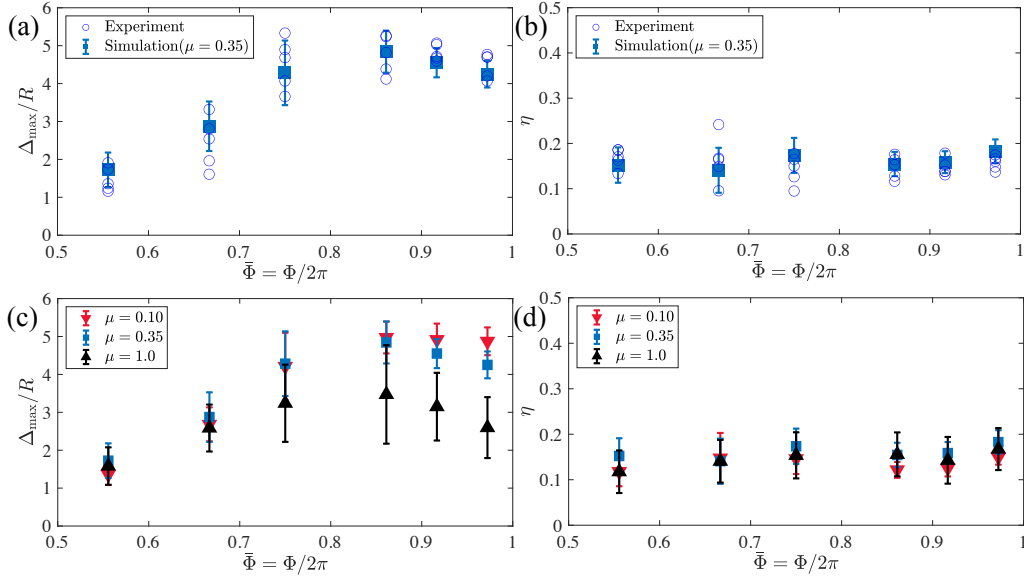


Figure 3: The maximum relative displacement $\Delta_{\max} \equiv \frac{H_0}{H_f}$ (with H_0 and H_f the initial and final heights of the stack during the compression cycle) and energy absorption ratio, $\eta \equiv \frac{\int_{\text{cycle}} F d\Delta}{F_{\max} \Delta_{\max}}$ as a function of the ring opening Φ and the friction coefficient μ .

[3] Reis, P.M. *A perspective on the revival of structural (in) stability with novel opportunities for function: from buckliphobia to buckliphilia*, Journal of Applied Mechanics, 82(11), p.111001, 2015.

[4] Bertails F., Audoly B., Cani M.-P., Querleux B., Leroy F., L ev eque J.-L.. *Super-Helices for Predicting the Dynamics of Natural Hair*, ACM Transactions on Graphics, 25:3: 1180-1187, 2006.

[5] Daviet G., Bertails-Descoubes F., Boissieux L.. *A hybrid iterative solver for robustly capturing Coulomb friction in hair dynamics*, ACM Transactions on Graphics, 30, Article 139: 1-12, 2011.

[6] Yoshida K., Wada H.. *Mechanics of a Snap Fit*, Physical Review Letters, 125, 194301, 2020.

Real-time co-simulation of wire-rope systems

Narges Mohammadi¹, Asko Rouvinen², Pasi Korkealaakso², José L. Escalona¹

¹ University of Seville, narges@us.es

² Mevea LTD., asko.rouvinen@mevea.com

³ Mevea LTD., pasi.korkealaakso@mevea.com

⁴ University of Seville, escalona@us.es

Keywords: Reeving systems, mobile harbor cranes, real-time co-simulation, ALEM method

1. Introduction

The dynamics of complex industrial machines can be modeled using recently-developed sophisticated software. These software can well model common mechanical parts such as elastic bodies or rigid bodies. However, for slender structures such as wire ropes, a tailored method is often required to model their large motions as well as their small deformations. The Arbitrary Lagrangian-Eulerian Modal (ALEM) approach [1] has recently been developed as an efficient method for wire ropes with a minimal number of finite elements. To be able to apply this formulation in the corresponding industrial applications, this study models an industrial mobile harbor crane by a co-simulation approach. Moreover, real-time simulation as one of the challenges in the wire-rope modeling is achieved in this study for a 3D wire-rope system under 1D hoisting motion.

2. Problem definition

The system under consideration is an industrial mobile harbor crane, as illustrated in Figure 1. The dimensions and mechanical characteristics of the system are based on those of a real mobile harbor crane that is used for simulators. The system is kinetically actuated by a motor installed on the reel to raise or lower the payload. The payload system is modeled as Subsystem 1, while the wire-rope system is modeled as Subsystem 2. The corresponding inputs and outputs of Subsystem 1 are defined as:

$$\mathbf{u}^{s1} = [\mathbf{F}^{WR1} \quad \mathbf{F}^{WR6}]^T, \quad \mathbf{y}^{s1} = [(\mathbf{q}^{s1})^T \quad (\dot{\mathbf{q}}^{s1})^T]^T \quad (1)$$

where the vector \mathbf{F}^{WRi} ($i = 1, 6$) is the wire-rope force exerted on the payload that can be computed by extracting the first three elements of the wire-rope elastic force, gravity force, and quadratic-velocity inertia force [1]. On the other hand, \mathbf{q}^{s1} and $\dot{\mathbf{q}}^{s1}$ are the generalized coordinates and velocities of the Subsystem 1, which are the rigid-body coordinates and velocities. Regarding Subsystem 2, the corresponding inputs and outputs can be defined as:

$$\mathbf{u}^{s2} = [(\mathbf{q}^{s1})^T \quad (\dot{\mathbf{q}}^{s1})^T]^T, \quad \mathbf{y}^{s2} = [\mathbf{F}^{WR1} \quad \mathbf{F}^{WR6}]^T \quad (2)$$

The resulting equations of motion of Subsystem 1 are the Ordinary Differential Equations (ODE) that have been solved using the Runge-Kutta method. However, the equations of motion of Subsystem 2 are Differential Algebraic Equations (DAE) that has been solved using the Generalized Alpha method. Both subsystems are modeled in a MATLAB environment.

3. Results and discussion

The wire-rope system is modeled based on an explicit co-simulation method based on the Gauss-Seidel scheme. To evaluate the effects of the extrapolation method on the accuracy of the results, Figure 2 depicts the co-simulation results obtained based on the Zero-Order Hold (ZOH), First-Order Hold (FOH), and Second-Order Hold (SOH) extrapolation methods with the same micro time steps as the macro time step as $\Delta T = 25$ ms. The co-simulated results are compared with a reference monolithic approach with the time step equal to $\Delta t = 50$ ms. According to Figure 2, it can be observed that the implementation of a higher-order extrapolation can significantly increase the accuracy of the results; however, the difference between FOH and SOH extrapolation

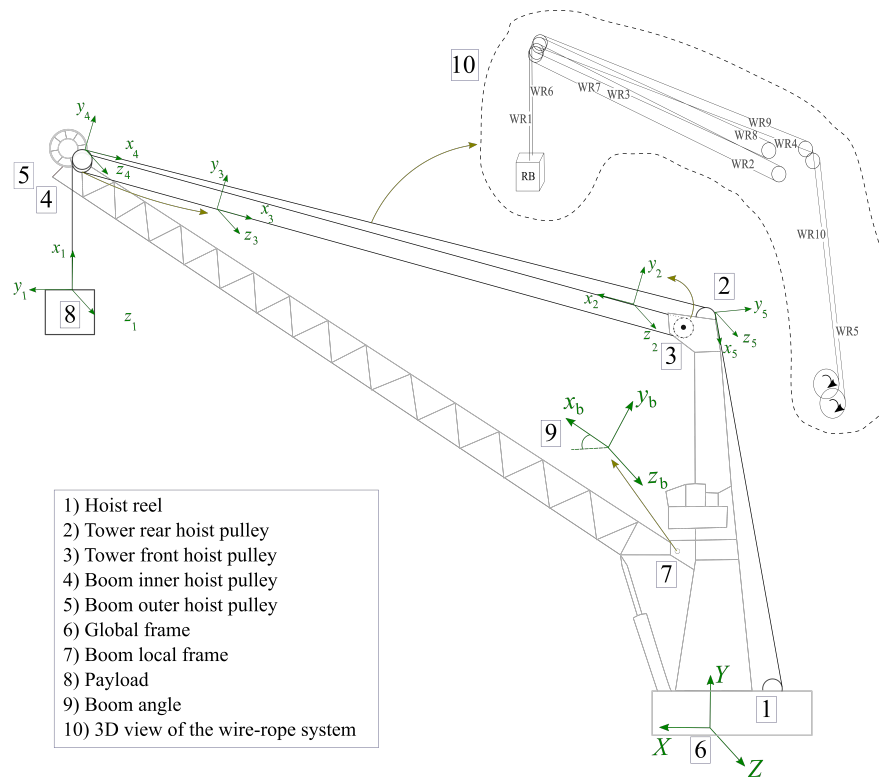


Figure 1: The configuration of mobile harbor crane

methods is not significant. The resulting simulation time for the wire-rope subsystem using the current macro time step is approximately 8.8 (s) for a 9 (s) ride. These results can demonstrate the accuracy and efficiency of the given formulation for real-time applications which was a question in recent studies.

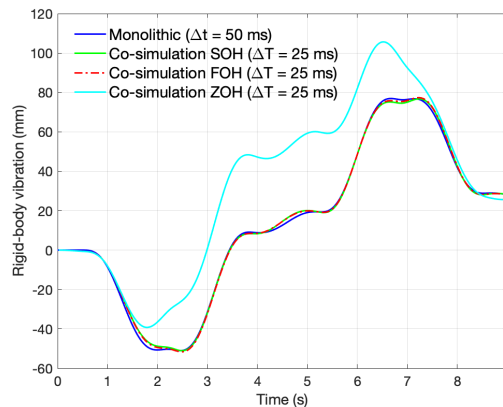


Figure 2: Comparison of the vibration of the rigid body with respect to the extrapolation method

Acknowledgements

This project has received funding from the European Union’s Horizon 2020 research and innovation programme under the Marie Skłodowska-Curie grant agreement No 860124, THREAD.



References

[1] J.L. Escalona, and N. Mohammadi. *Advances in the modeling and dynamic simulation of reeving systems using the arbitrary Lagrangian–Eulerian modal method*. *Nonlinear Dynamics*, 108(4), 3985-4003, 2022.

Optimal Control for locomotion of contractile slender bodies on frictional substrates

A. Bijalwan ¹, J.J. Muñoz ²

¹ Universitat Politècnica de Catalunya (UPC), Centre Internacional de Mètodes Numèrics en Enginyeria (CIMNE)

² Universitat Politècnica de Catalunya (UPC), Laboratori de Càlcul Numèric (LaCàN), Centre Internacional de Mètodes Numèrics en Enginyeria (CIMNE), Institut de Matemàtiques de la UPC (IMTech), j.munoz@upc.edu

Keywords: Optimal Control, Adjoint Method, Locomotion, Elastodynamics, Friction

1. Introduction

Body locomotion of slender organisms has been studied experimentally [4] and computationally [1]. However, due to the lack of information on the muscle activity and the frictional parameters, which may vary in time and space, it is not yet possible to reproduce the observed motion. Some recent works outline the necessity of non-reciprocal trajectories in the parameter space for swimming organisms [1] and the need of non-isotropic friction for locomotion on substrates [3].

We here aim at replicating their locomotion by computing the optimal contractility profile for different body geometries and strategies: (i) an inchworm with different top and bottom contractility, (ii) a maggot with a constricting wave, and (iii) a *C. elegans* type with different left-right contractions. The first two types have different forward-backward friction, while the latter exploits the different friction in normal and tangential directions. Figure 1 shows the three types of bodies and illustrates their deformations during their propulsion.

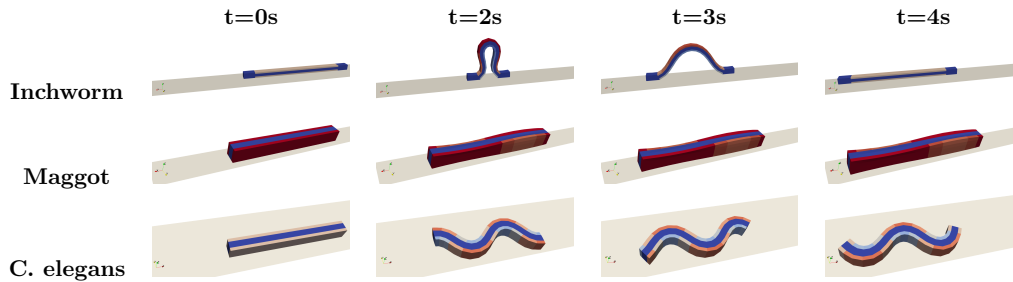


Figure 1: Three body types analysed and four snapshots of their locomotion strategy.

2. Methods

2.1. Mechanical Model

The organisms are modelled as non-linear elastic bodies occupying a domain $\Omega \subset \mathbb{R}^3$. They have the ability to constrict in different subdomains at different times. More specifically, the deformation gradient $\mathbf{F} = \frac{\partial \mathbf{x}}{\partial \mathbf{X}}$ of each body is decomposed into an elastic and contractile part, i.e. $\mathbf{F} = \mathbf{F}_e \mathbf{F}_c$, with $\mathbf{F}_c = u(t)\mathbf{I}$ a time dependent imposed uniform isotropic deformation. After neglecting inertial forces, the following equilibrium equations are then solved

$$\begin{aligned} \nabla \cdot \boldsymbol{\sigma} &= \mathbf{0}, \forall \mathbf{x} \in \text{int}(\Omega) \\ \boldsymbol{\sigma} \mathbf{n} &= \mathbf{0}, \forall \mathbf{x} \in \Gamma_0 \\ \boldsymbol{\sigma} \mathbf{n} &= \boldsymbol{\eta} \dot{\mathbf{x}}, \forall \mathbf{x} \in \Gamma_s \end{aligned}$$

with $\boldsymbol{\sigma} = J_e^{-1} \mathbf{F}_e \mathbf{S}_e \mathbf{F}_e^T$ the Cauchy stress-tensor, and $\mathbf{S}_e = \frac{\partial W}{\partial \mathbf{E}_e}$ the second Piola stress tensor, $\mathbf{E}_e = (\mathbf{F}_e^T \mathbf{F}_e - \mathbf{I})/2$ the Green-Lagrange strain tensor, and W the elasticity function, which is here assumed as Neo-Hookean. The boundary Γ_s is the bottom surface, where a velocity dependent frictional condition is imposed, and $\Gamma_0 = \partial\Omega \setminus \Gamma_s$.

The finite element discretisation of the equilibrium equations yields the following set of non-linear equations,

$$\dot{\mathbf{x}} = \mathbf{g}(\mathbf{x}(t), \mathbf{u}(t)). \quad (1)$$

Vector \mathbf{u} contains all the elemental values of the contractility in the relevant subdomains for the type of body being modelled. In order to deduce the form in (1), a small amount of friction is imposed in all the nodal values.

2.2. Optimal Control

We aim at computing the optimal contractility $\mathbf{u}(t)$ that minimises a measure of the translation of the centre of mass of body Ω , $\mathbf{x}_{cm} = \int_{\Omega} \mathbf{x} d\Omega / \int_{\Omega} d\Omega$, subjected to the discretised equilibrium equations in (1). We thus aim to solve the following minimisation problem (time t is omitted for clarity),

$$\begin{aligned} \min \int_0^T j(\mathbf{x}, \mathbf{u}) dt \\ \text{s.t. } \dot{\mathbf{x}} = \mathbf{g}(\mathbf{x}, \mathbf{u}), \mathbf{x}(0) = \mathbf{x}_0 \end{aligned} \quad (2)$$

with $\|\mathbf{x}_{cm} - \mathbf{x}_d\|^2 + \alpha \|\mathbf{u}\|^2$ the cost function, and \mathbf{x}_d a given target position. Parameter α weights the cost of the active deformation given by \mathbf{u} . After defining the Hamiltonian function $H(\mathbf{x}, \mathbf{u}) = j(\mathbf{x}, \mathbf{u}) + \lambda^T \mathbf{g}(\mathbf{x}, \mathbf{u})$, with $\lambda(t)$ a set of adjoint variables, the optimality conditions of problem in (2) may be written as the following two-point boundary value problem [2],

$$\dot{\mathbf{x}} = \nabla_{\lambda} H, \quad \dot{\boldsymbol{\lambda}} = -\nabla_{\mathbf{x}} H, \quad \mathbf{0} = \nabla_{\mathbf{u}} H \quad (3)$$

Figure 2(left) shows the evolution of \mathbf{x}_{cm} when solving system (1) for a given sinusoidal $\mathbf{u}(t)$, and using the undulatory gait with different ratios of normal vs. tangential friction, while 2(right) shows this evolution for the optimal locomotion.

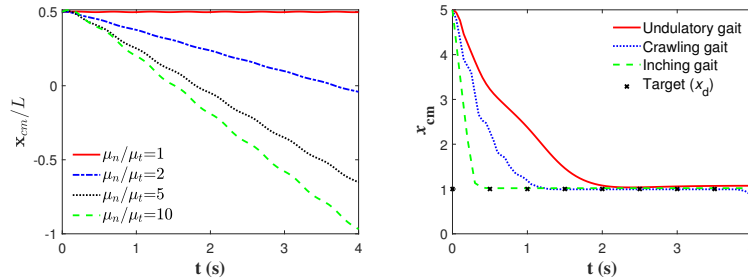


Figure 2: Evolution of the displacement of centre of mass \mathbf{x}_{cm} .

Acknowledgments

AB and JJM have been funded by the Spanish Ministry of Science and Innovation under grants PID2020-116141GB-I00 and CEX2018-000797-S, and JJM has been also financially supported by the local government Generalitat de Catalunya with grant 2021 SGR 01049.

References

- [1] F. Alouges a, A. DeSimone b, L. Giraldi a, M. Zoppello. *Self-propulsion of slender micro-swimmers by curvature control: N-link swimmers*. Int. J. Non-Linear Mech. 56:132-141, (2013).
- [2] A. Bijalwan, J.J. Muñoz. *A control Hamiltonian-preserving discretisation for optimal control*. Multibody System Dynamics. Accepted (2023) DOI: 10.1007/s11044-023-09902-y
- [3] J.J. Muñoz, L. Condamin, D. Doste. *On the net displacement of contact surface centroid in contractile bodies*. Mechanics Research Communications, 119:103809 (2022).
- [4] Stephens, G., Johnson-Kerner, B., Bialek, W., Ryu, W.: *Dimensionality and dynamics in the behavior of C. elegans*. PLOS Comp. Biol. 4, e1000028 (2008)

Coupling of bending and axial motion in highly flexible axially moving beams modeled with ALE

Konstantina Ntarladima¹, Johannes Gerstmayr¹

¹Department of Mechatronics
 Universität Innsbruck
 Technikerstrasse 13, 6020 Innsbruck, Austria
 [konstantina.ntarladima, johannes.gerstmayr]@uibk.ac.at

Keywords: Flexible beams, Arbitrary Lagrange Eulerian

1. Abstract

For the numerical modeling of slender structures that are characterized by an axial motion and transient oscillations, i.e. belt drives, conveyor belts and ropeway systems, mixed Lagrange Eulerian descriptions have been developed, see i.e. [1, 2, 3]. An approach based on the Arbitrary Lagrange Eulerian (ALE) formulation where the beam finite element discretization is based on the Absolute Nodal Coordinate Formulation (ANCF) has been introduced in Ref. [4]. In the latter approach, the ANCF beam element was extended by an additional independent coordinate, s_E , which models the overall motion of mass in the axial direction of the beam. However, in the numerical investigations performed in Ref. [4] some of the s_E -dependent terms were neglected. These terms appear in the virtual work of elastic forces:

$$\delta W_e = \int_0^L (EA(\varepsilon(q_i, s_E) - \varepsilon_0) \delta \varepsilon(q_i, s_E) + EI(K(q_i, s_E) - K_0) \delta K(q_i, s_E)) d\bar{x}, \quad (1)$$

and the virtual work of viscous damping forces:

$$\delta W_{ve} = \int_0^L d_\varepsilon \dot{\varepsilon}(q_i, s_E) \delta \varepsilon(q_i, s_E) + d_K \dot{K}(q_i, s_E) \delta K(q_i, s_E) d\bar{x}. \quad (2)$$

In Eqs. (1) and (2), L is the element's length, EA and EI are the axial and flexural rigidity respectively, ε is the axial strain, ε_0 is the (pre-)stretch of the beam, K is the curvature, K_0 denotes the curvature of the beam in the reference configuration, $\dot{\varepsilon}$ and \dot{K} are the total time derivatives of ε and K and d_ε , d_K are damping parameters. Note that the axial strain, ε , depends both on the nodal coordinates, q_i , and the Eulerian coordinate, s_E . Therefore, in Eq. (1) the variations $\delta \varepsilon$ and δK include the terms $\frac{\partial \varepsilon}{\partial s_E} \delta s_E$ and $\frac{\partial K}{\partial s_E} \delta s_E$ respectively, which were neglected in Ref. [4]. Likewise, in Eq. (2) the time derivatives $\dot{\varepsilon}$, \dot{K} include an Eulerian part which arises from the total time derivative of the position vector $\mathbf{v} = \frac{d\mathbf{r}}{dt} = v_E \frac{\partial \mathbf{r}}{\partial \bar{x}} + \frac{\partial \mathbf{r}}{\partial t}$, with \mathbf{r} being the position vector and v_E the Eulerian velocity, \dot{s}_E . This Eulerian part was also neglected in the numerical investigations performed in Ref. [4].

In this work, we investigate the influence of the above-described additional terms in Eqs. (1) and (2) through numerical examples which have also been reproduced using the ANCF beam element for comparison. The obtained results showed good agreement as well as convergence to an available analytical solution.

2. Numerical example

We model a rope of length L being wound around a pulley of radius R as shown in Figure 1. The right tip of the belt is fixed on the pulley, while we apply a force, F , on the left tip. The pulley was modeled as a rigid body while for the contact between the belt and the pulley we use the contact modeling described in [5]. When modeling the belt using the ALE element described above we fix the rotation of the pulley and we model the axial motion of the belt through the Eulerian coordinate, s_E , using a constant velocity $v_E = \frac{s_E}{t}$, which is chosen adequately small for avoiding dynamic effects. When modeling the system with the ANCF beam element the pulley rotates with a prescribed angular velocity, $\omega = \frac{v_E}{R}$. We measure the torque applied to the pulley. We compare the results obtained by the extended ALE element with those obtained using the ANCF element. Furthermore, we deactivate the newly added terms in the implementation in order to examine their influence.

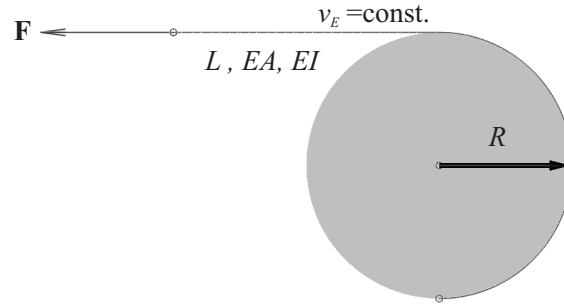


Figure 1: A belt is wound around a pulley. The right tip of the belt is fixed on the pulley while a force, $F = -10\text{N}$, is applied to the left tip.

Finally, we examine the convergence to the analytical solution for the torque required for bending a belt into a circular curve, $\tau = \frac{EI}{2R}$, see Table 1.

Table 1: Force responsible for bending the belt.

Method	Result (N)		
Analytical solution	$-10.533 (F + \tau/R)$		
ANCF beam [5]	-10.543 (32 elements)		
ALE beam [4]	-10.002 (32 elements)		
ALE beam extended	8 elements -10.386	16 elements -10.431	32 elements -10.533

The present numerical example shows that the extended ALE beam element complies with the analytical solution and the results obtained by the ANCF beam modeling which shows us that the inclusion of the above-described terms allows us to model systems which involve change in the curvature of the belt. Other numerical examples for investigating the influence of s_E -dependent terms in $\dot{\epsilon}$ and \dot{K} in Eq. (2) will be included in the presentation.

Acknowledgments

This project has received funding from the European Union’s Horizon 2020 research and innovation programme under the Marie Skłodowska-Curie grant agreement No 860124. This publication reflects only the author’s view and the Research Executive Agency is not responsible for any use that may be made of the information it contains.



References

- [1] Yury Vetyukov. Non-material finite element modelling of large vibrations of axially moving strings and beams. *Journal of Sound and Vibration*, 414:299–317, 2018.
- [2] Difeng Hong and Gexue Ren. A modeling of sliding joint on one-dimensional flexible medium. *Multibody System Dynamics*, 26:91–106, 2011.
- [3] José L Escalona and Narges Mohammadi. Advances in the modeling and dynamic simulation of reeving systems using the arbitrary Lagrangian–Eulerian modal method. *Nonlinear Dynamics*, 108:3985 – 4003, 2022.
- [4] Michael Pieber, Konstantina Ntarladima, Robert Winkler, and Johannes Gerstmayr. A Hybrid Arbitrary Lagrangian Eulerian Formulation for the Investigation of the Stability of Pipes Conveying Fluid and Axially Moving Beams. *Journal of Computational and Nonlinear Dynamics*, 17(5):051006 (13 pages), 2022.
- [5] Konstantina Ntarladima, Michael Pieber, and Johannes Gerstmayr. Contact modeling between axially moving beams and sheaves. Submitted to *Nonlinear Dynamics*.

Towards a complete Riemannian metric on the space of elastic rods

Elias Döhrer *, Philipp Reiter *, Henrik Schumacher *

* Chemnitz University of Technology

{elias.doehrer, philipp.reiter, henrik.schumacher}@mathematik.tu-chemnitz.de

Keywords: Kirchhoff–Love model, Riemannian metrics, tangent-point energy, self-contact

1. The Kirchhoff–Love model

Imagine a piece of springy wire, form a knot out of it and clamp its endpoints. Which shape will it take? Besides general curiosity, the answer to this question is of some relevance to modeling long slender objects on quite different length-scales—which match the concept of an unsharable impermeable ‘elastic’ rod.

Following [1, 2] we may characterize equilibria as critical points of a linear combination of bending and twisting energy. In total, we consider the functional

$$E[\mathbf{u}; \mathbf{b}] = \frac{c_b}{2} \int_0^L \kappa^2 ds + \frac{c_t}{2} \int_0^L \beta^2 ds, \quad (1)$$

where $\mathbf{u} : [0, L] \rightarrow \mathbb{R}^3$ is a curve with a normal field $\mathbf{b} : [0, L] \rightarrow \mathbb{S}^2$ and κ, β denote the curvature and twist rate, respectively. The bending and torsion rigidities $c_b > 0$, $c_t \geq 0$ are determined by the Lamé coefficients of the material and geometrical properties of the rod (\mathbf{u}, \mathbf{b}) .

The shape of ‘stable’ equilibria, i.e., local minimizers, of E is determined by some trade-off between bending and twisting energy depending on c_b, c_t . Experiments indicate a complex energy landscape; see [3] and references therein.

However, a gradient descent for (1) is likely to show physically meaningless self-penetrations of the curve. In order to incorporate impermeability of matter and to produce more realistic simulations such as the one shown in Figure 1 below we have to pass to a more refined model.

2. Modeling impermeability

The general idea of a *repulsive functional* is to define a ‘measure of embeddedness’ which blows up if an embedding degenerates. In the case of closed curves this occurs if a sequence of embedded curves converges to a curve with a self-intersection. Thus a repulsive functional erects infinite barriers between different topology types.

From the numerical point of view, the *tangent-point potential* TP_q is a particularly convenient example of a repulsive functional on a (closed) curve $\mathbf{u} : [0, L] \rightarrow \mathbb{R}^3$. For any $q > 2$ it amounts to the L^q norm of the reciprocal tangent-point radius at two given points $x, y \in [0, L]$, namely the (unique) radius of a circle passing through $\mathbf{u}(x)$ and $\mathbf{u}(y)$ while being tangential to \mathbf{u} at $\mathbf{u}(x)$. For an arclength parametrized curve \mathbf{u} it amounts to

$$TP_q[\mathbf{u}] = \int_0^L \int_0^L \frac{|\mathbf{u}'(x) \wedge (\mathbf{u}(x) - \mathbf{u}(y))|^q}{|\mathbf{u}(x) - \mathbf{u}(y)|^{2q}} dx dy. \quad (2)$$

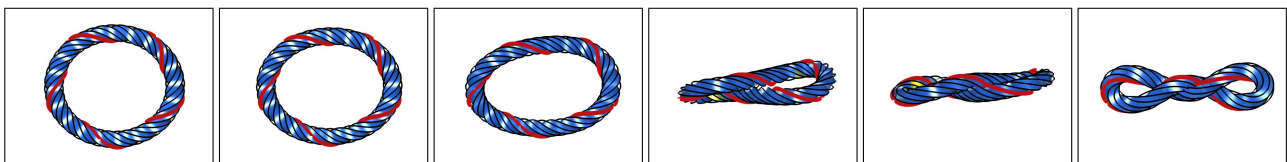


Figure 1: Snapshots of the gradient descent of an ‘elastic’ rod: The initial configuration is a round circle twisted by five full rotations. Relaxing its total energy leads to a significant reduction of the twisting energy at the expense of ‘coiling’. This simulation is based on a gradient descent for (3) as described in [3].

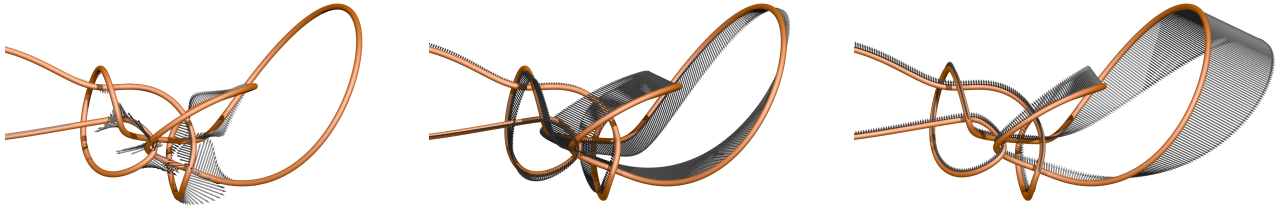


Figure 2: Gradients of a repulsive functional; cf. [5]. The gradient field defined by the L^2 metric (on the left-hand side) is pathologically concentrated on regions of near self-contact. Consequently, one has to pick tiny step sizes to prevent self-collision. Passing to a Sobolev metric (middle) produces a gradient field which is more uniformly distributed along the curve. However, this can still be improved considerably by adding a lower order term to the inner product that discourages movement in regions of near self-contact (right-hand side).

Regularizing the functional E from (1) by the tangent-point potential yields the new total energy

$$E_{\vartheta}[\mathbf{u}; \mathbf{b}] = \frac{c_b}{2} \int_0^L \kappa^2 ds + \frac{c_t}{2} \int_0^L \beta^2 ds + \vartheta \text{TP}[\mathbf{u}], \quad (3)$$

where the regularization parameter $\vartheta > 0$ may be interpreted as the ‘thickness’ of the rod. Choosing $c_t = 0$ we recover the case of so-called ‘elastic knots’; see [3, 4].

3. Finding the shortest path between two rods

Based on a repulsive energy we can define a metric on the manifold of embedded curves and rods. Here the choice of that metric really matters. As illustrated in Figure 2, a careful definition which exploits the structure of the problem may prevent self-interpenetrations even when taking relatively large time steps; cf. [5].

This approach paves the way not only to a more efficient implementation of the gradient descent for (3). In fact, we may now aim for studying geodesics and finding the shortest path between two rods belonging to the same topology class by extending an approach for embedded curves [6].

References

- [1] Joel Langer and David A. Singer. Lagrangian aspects of the Kirchhoff elastic rod. *SIAM Rev.*, 38(4):605–618, 1996.
- [2] Heiko von der Mosel. Minimizing the elastic energy of knots. *Asymptot. Anal.*, 18(1–2):49–65, 1998.
- [3] Sören Bartels and Philipp Reiter. Numerical solution of a bending-torsion model for elastic rods. *Numer. Math.*, 146(4):661–697, 2020.
- [4] Henryk Gerlach, Philipp Reiter, and Heiko von der Mosel. The elastic trefoil is the doubly covered circle. *Arch. Ration. Mech. Anal.*, 225(1):89–139, 2017.
- [5] Philipp Reiter and Henrik Schumacher. Sobolev Gradients for the Möbius Energy. *Arch. Ration. Mech. Anal.*, 242(2):701–746, 2021.
- [6] Elias Döhrer, Philipp Reiter, and Henrik Schumacher. On a complete Riemannian metric on the space of embedded curves. In preparation.

Untangling the physics of self-locking in tight knots

Alexandre T. da Silva, Thibaut Metivet, Victor Gramegna, Melina Skouras, Florence Bertails-Descoubes

Univ. Grenoble Alpes, Inria, CNRS, Grenoble INP, LJK, alexandre.teixeira-da-silva@inria.fr

Keywords: tight knot, self-locking, elastic rod, frictional contact, numerical simulation

1. Introduction

Thanks to the simplicity in their form, knots are commonly used in day-to-day lives like in shoelaces as a most basic example. Just by tying a rope in a certain configuration, we are able to firmly attach structures thanks to some self-locking effect of the rope. Found in activities such as hiking, fishing or knitting, knot tight tying shows utility in multiple scales and forms. However, despite their usefulness and apparent simplicity, knots have only recently been deeply studied in the fields of physics and mechanics. Although there are multiple mathematical models to describe the topology of different kinds of knots, a mechanical model capable of capturing some core behaviors, like self-locking, is still absent.

A first model was developed by Audoly et al.[3], addressing the mechanics of knots in in loose configurations. This approach is derived from an inextensible Kirchhoff rod model that is tied in a simple overhand configuration at the limit of a vanishing thickness. Because it assumes the rod to be inextensible, the model diverges in tight knots configurations. Since the core utility of knots are found in their tight forms, it is fundamentally important to understand how each physical and geometrical parameter interact with one another. Baek et al.[2] and Durville[4] have explored the tight knot configuration with volumetric effects, and in particular the deformation of the cross-section of the rod. While these approaches allow, for the first time, to capture the geometry and forces of tight knots, they are restricted to a particular choice of physical parameters, and none of them studies the mechanism of self-locking.

Our work proposed here aims at expanding previous studies to multiple sets of parameters in order to characterise some core behaviours still poorly understood, in particular the self-locking property in tight knots.

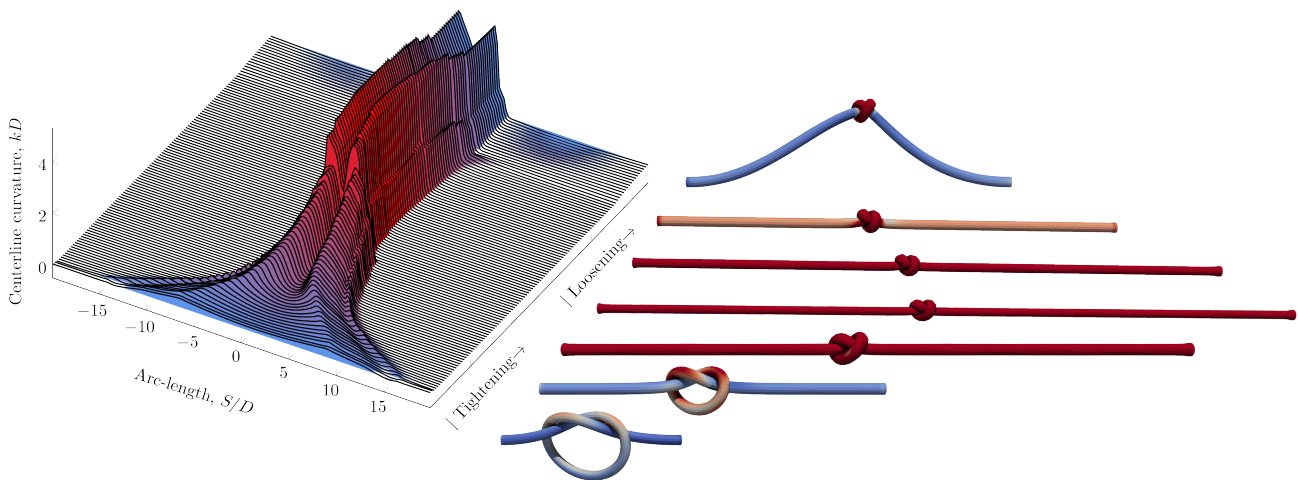


Figure 1: On the left, multiple snapshots of the rod centerline curvature are plotted to exhibit the self-locking behavior. The knot is first tightened and then loosened; As the tightened state surpasses the critic locking value of the end-to-end shortening $\bar{\epsilon}$, the centerline curvature remains constant, which indicates a locking effect. On the right, snapshots of the knot are shown to illustrate the state of deformation of the knot alongside the centerline curvature. We note that given the locking of the knot, the structure buckles itself with the imposed displacements on both ends of the rod.

2. Contribution

We analyse the self-locking mechanism in tight knots using an open-source, full 3D FEM simulator [5]. Our protocol is based on two steps: first, a thin rod is tied in an overhand knot form and tightened by imposing the displacement on both ends; then, by imposing a displacements towards the center of the knot to loosen it, the tensile force is relaxed.

Given a set of physical and geometrical features, namely the Young Modulus (E), Poisson's ratio (ν), friction coefficient (μ), diameter of the rod (D), length of the straight rod without the knot (L_0), and end-to-end shortening $\bar{\epsilon} = (L - L_0)/D$, we find a critical dimensionless locking parameter beyond which self-locking indeed occurs, as illustrated in Figure 1. In contrast, below this threshold, no locking appear and the knot gets untied (see Figure 2).

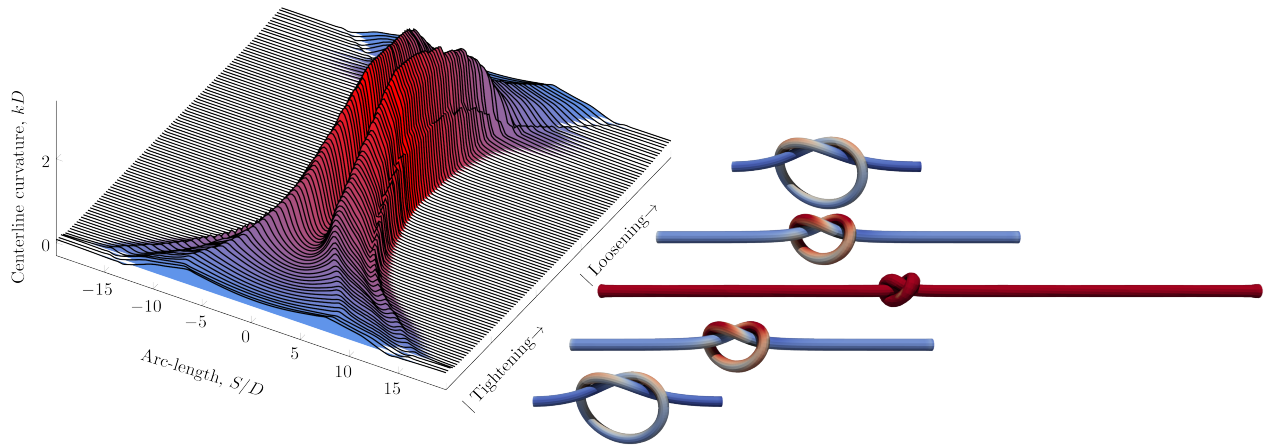


Figure 2: Since the knot is not tight enough, it gets untied and recovers its initial form.

By combining simulations and experiments, we are able to validate our numerical approach and further leverage it to explore systematically the respective impacts of geometrical and mechanical parameters involved in the self-locking phenomena.

References

- [1] P. Johanns, P. Grandgeorge, C. Baek, T. G. Sano, J. H. Maddocks. *The shapes of physical trefoil knots*, Extreme Mechanics Letters, 43:101172, 2021.
- [2] C. Baek, P. Johanns, T. G. Sano, P. Grandgeorge, P. M. Reis. *Technical brief: Finite element modeling of tight elastic knots*, Journal of Applied Mechanics, 88(2), 2021.
- [3] B. Audoly, N. Clauvelin, S. Neukirch. *Elastic knots*, Physical Review Letters, 99(16): 164301, 2007.
- [4] D. Durville. *Contact-friction modeling within elastic beam assemblies: an application to knot tightening*, Computational Mechanics, 49(6): 687–707, 2012.
- [5] T. Schneider, J. Dumas, X. Gao, M. Botsch, D. Panozzo, and D. Zorin. *Poly-spline finite-element method*, ACM Transactions on Graphics (TOG), 38. (3):1–16, 2019a.

Unbiased line-to-line contact method for static frictionless beam-to-beam contact

Jan Tomec ¹, Gordan Jelenić ²

¹ University of Rijeka, Faculty of Civil Engineering, jan.tomec@uniri.hr

² University of Rijeka, Faculty of Civil Engineering, gordan.jelenic@uniri.hr

Keywords: Line-to-line contact, unbiased formulation, mortar method, penalty method, Lagrange multipliers

1. Introduction

Beam-to-beam contacts are complicated phenomena due to the beam's simplified mathematical model with a rigid cross-section. This requires careful treatment of the subject by developing appropriate formulation for a specific use. The most general and also computationally the most costly are the mortar methods [1, 2]. In this work, we explore a new parametrization that eliminates the need for distinguishing or favouring one side of the contact when selecting the master and slave sides of the beam. This formulation is then solved using the Lagrange multipliers and the penalty method and compared with the mortar method and its penalty variant.

2. Contact between beams

A beam is characterised by the position of its centreline \mathbf{x} to which an oriented rigid cross-section is attached. For the presented contact formulations, only the position of the centreline is required.

A line-to-line contact describes a configuration where the contact force is distributed along the length of the contact zone. Using g as a measure of the gap between beams and the Lagrange-multiplier field λ to represent the negative distributed contact force results in the following additional constraints to the system:

$$g \geq 0 \quad (1)$$

$$-\lambda \geq 0 \quad (2)$$

$$g\lambda = 0. \quad (3)$$

These constraints are pointwise, while the mortar method distributes them along the contact using a weak relationship.

Denoting beams in contact as 1 and 2, the contact virtual work is

$$\delta\Pi_N = \int_{\Gamma_c} \delta\lambda g + (\delta\mathbf{x}_1 - \delta\mathbf{x}_2)^T \mathbf{n}\lambda + (\mathbf{x}'_1 \delta s_1 - \delta\mathbf{x}'_2 \delta s_2)^T \mathbf{n}\lambda ds, \quad (4)$$

where $\mathbf{n} = (\mathbf{x}_1 - \mathbf{x}_2)/\|\mathbf{x}_1 - \mathbf{x}_2\|$ is the contact normal. At this point, the relationship between \mathbf{x}_1 and \mathbf{x}_2 is still undetermined. The additional projection constraint comes from the specific formulation.

3. Mortar and unbiased method

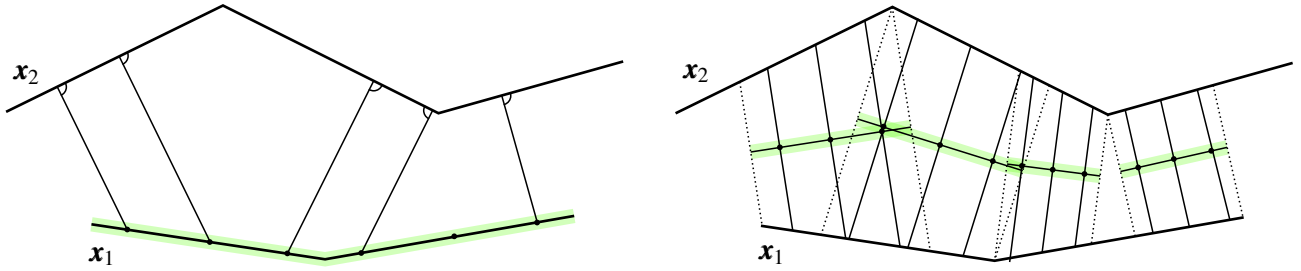
The mortar method discretises the contact along one of the beams by using its finite element discretisation. The unbiased formulation combines each pair of beam finite elements using a specially developed parametrisation. Both formulations are developed side by side for comparison. See also Figure 1

	Mortar	Unbiased
Projection	$\mathbf{n}^T \mathbf{x}'_2 = 0$	$\mathbf{n}^T (\mathbf{x}'_1 + \mathbf{x}'_2) = 0$
Parametrisation	$s = s_1$	$s = (s_1 + s_2)/2$
Integration boundaries	$[0, L_1]$	$[\max_i(s _{s_i=-1}), \min_i(s _{s_i=1})]$

4. Lagrange multipliers and penalty method

The Lagrange multipliers field can be discretised using the standard shape function

$$\lambda = \Phi^T \Lambda. \quad (5)$$



(a) Mortar method: Bottom beam is selected as slave side. Green shadow indicates the integration zone, which is conducted using Gauss quadrature in black dots. Perpendicular projection is computed to master side (globally) which requires integration across discontinuities. Some points might not have a valid projection and their contribution is neglected.

(b) Unbiased method: Each pair of beam elements produces a contact element as indicated with green shadow. The integral is evaluated using Gauss quadrature in black dots. There, an unbiased projection is computed to both beams. Contact domain is discontinuous but converges towards continuity when the contact forces straighten the beams.

Figure 1: Discretisation and integration of contact

While the mortar methods allows continuous multipliers across elements and thus a connected mesh, the unbiased method requires element-wise discretisation. Optimally, the field is approximated using constant interpolation as a higher order interpolation leads to over-constraint and consequentially to instabilities.

The penalty method can be implemented through

$$\lambda = \varepsilon g, \quad \varepsilon = \begin{cases} \varepsilon_0 & \text{if } g < 0 \\ 0 & \text{otherwise,} \end{cases} \quad (6)$$

where ε_0 is the penalty parameter.

5. Conclusions

The unbiased formulation achieves objectivity by employing suitable projection functions and parametrisation techniques. However, higher interpolation orders result in over-constraint, requiring to combine this method with either constant interpolation or the penalty approach. The unbiased method explores the potential of utilising various projection functions and parametrisations within the mortar method, known for its stability and robustness. Further investigations are needed to improve the method's performance concerning over-constraint and parametrisation.

Acknowledgments

This project has received funding from the European Union's Horizon 2020 research and innovation programme under the Marie Skłodowska-Curie grant agreement No 860124 and from the Croatian science foundation under the research project FIMCOS (HRZZ IP 2018-01-1732).



References

- [1] Armin Bosten, Alejandro Cosimo, Joachim Linn, and Olivier Brüls. A mortar formulation for frictionless line-to-line beam contact. *Multibody System Dynamics*, 54(1):31–52, 2022.
- [2] Jan Tomec and Gordan Jelenić. Analysis of static frictionless beam-to-beam contact using mortar method. *Multibody System Dynamics*, 2022.

Sliding flexible rods: non-material finite elements and configurational forces

Yury Vetyukov ¹, Alexander Humer ²

¹ Technische Universität Wien, Getreidemarkt 9, 1060 Vienna, Austria, yury.vetyukov@tuwien.ac.at

² Johannes Kepler University Linz, Altenberger Straße 69, 4040 Linz, Austria, alexander.humer@jku.at

Sliding rods, axially moving structures, ALE, configurational force

1. Introduction

The body of literature devoted to flexible structures, which move axially across a given control domain is steadily growing, see the recent review paper [1]. Also problems featuring thin elastic rods, partially sliding within a rigid or flexible channel (sleeve) are receiving more and more attention in the recent years, see [2, 3, 4]. From a practical point of view, such mechanical systems may represent deployable space structures, concentric tube robots used in modern surgery as well as a broad range of other mechanisms – or the vibrating tail end of the spaghetti when being sucked into one’s mouth too fast. Besides practical importance and sometimes counter-intuitive behavior (as for the dancing rod problem considered in [4, 5]), the class of problems at hand is barely accessible for mathematical modelling with traditional methods of structural mechanics, featuring conventional material (Lagrangian) kinematic description because the material particles move between qualitatively different domains on the constant basis. The resulting solution-dependent discontinuities of the curvature of the axis of the rod are difficult to resolve using standard approximation techniques, which promotes the use of various kinds of the Arbitrary Lagrangian-Eulerian formulations with a finite element discretization of a non-material parameter domain, see e.g. [6, 7]. In particular, the transformation of the principle of virtual work for a part of a rod in a control domain to a non-material variational equation is presented in [8]. The subsequently derived Lagrange equations of motion for large vibrations of an axially transported rod feature nodal unknowns of the approximation of the deformed state in terms of a Eulerian coordinate.

The specific feature of the sliding rod problems is that the relative motion between the rods is not prescribed in advance, but rather belongs to the set of unknowns. The respective work conjugate generalized force is related to the energy release rate and shall be classified as Eshelby-like or configurational force [2, 3, 4]. The distinctive feature of the benchmark problem, considered in the present contribution is that it allows for a static analysis, which allows obtaining the solution both using the finite element approach and semi-analytically by integrating the boundary value problem. Furthermore, it helps elaborating on the nature of the configurational force acting between two flexible rods by comparing the solution of the geometrically nonlinear problem to the analytic expression of the energy release rate in a simple geometrically linear setting.

2. Problem formulation

Consider two beams in the field of gravity, simply supported at the outer ends and sliding one inside another without friction in the middle part of the flexible mechanism as shown in Fig. 1. Which of the beams plays the role of a sleeve and which one is inside is irrelevant as we consider both beams having the same bending stiffness a and mass density per unit length ρ . The beams are inextensible, and each of them has the same length ℓ , while the distance between the supports $H < 2\ell$ to enable contact in the overlapping region. Because of the weight load, the beams bend and partially slide out of each other, the overlapping region is getting shorter.

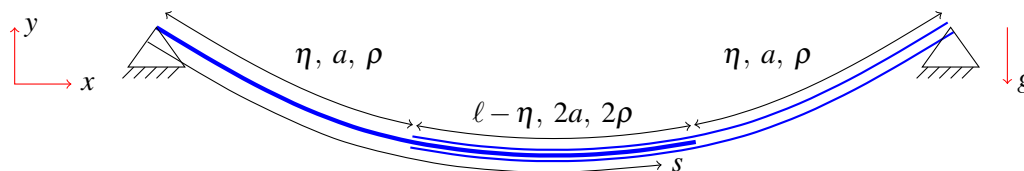


Figure 1: Compound beam, simply supported at both ends with sliding in the overlapping domain

The symmetric setting comprises three segments. The first and the third one are the outer segments, both of the length η . The single beam here has the bending stiffness a and the mass per unit length ρ . The second region,

where both beams overlap, has the length $\ell - \eta$. Here the compound beam has the bending stiffness $2a$ and the mass per unit length 2ρ . It is important that the length of each non-overlapping region η belongs to the unknowns of the problem and needs to be determined both in the static as well as in the dynamic analysis.

3. Analysis methods

The numerical approach to finding static equilibrium features the finite element discretization of the deformed configuration of the compound rod $x(s), y(s)$ by re-parametrizing the material coordinate s in all three segments via a non-material one, which varies in a fixed range independent from η . Particular attention needs to be paid to the continuity of the approximation at the transition points $s = \eta$ and $s = \ell$. Minimizing the total potential energy (the strain energy of bending plus the potential in the field of gravity) with respect to the finite element degrees of freedom and η we obtain equilibrium configurations, which depend on the gravity load factor g . Interestingly, the equilibria exist only until η is sufficiently large: for the considered parameter set with $\ell = 1$, $H = 1.4$, $a = 2666.67$, $\rho = 3.12$ the limiting value of the load is approximately $g = 6.433$, which corresponds to $\eta = 0.517$. At larger g the frictionless connection between the rods cannot withstand the loading.

A semi-analytical solution for the considered benchmark problem justifies the numerical results. For each fixed value of η the boundary value problem

$$\begin{aligned} Q'_x = 0, \quad Q'_y - \rho_{\text{eff}}(s)g = 0, \quad M' + Q_y \cos \theta - Q_x \sin \theta = 0, \quad a_{\text{eff}}(s)\theta' = M, \quad x' = \cos \theta, \quad y' = \sin \theta, \\ s = 0: \quad M = 0, \quad x = 0, \quad y = 0; \quad s = (\ell + \eta)/2: \quad Q_y = 0, \quad \theta = 0, \quad x = H/2 \end{aligned} \quad (1)$$

with symmetry boundary conditions in the middle produces the static deformed shape as if sliding was restricted. The effective bending stiffness a_{eff} and effective mass density ρ_{eff} change from a, ρ to $2a, 2\rho$ at $s = \eta$; $Q_{x,y}, M$ are components of the force and the bending moment in a cross-section; θ is the rotation angle. The actual value of η , which minimizes the total potential energy obtained by integrating the boundary value problem Eq. (1), stands in perfect correspondence with the finite element solution.

4. Configurational force

Both the FE and the semi-analytical solutions show that the longitudinal component of the tension force $Q_t = Q_x \cos \theta + Q_y \sin \theta$ at the transition points is related to the local complementary strain energy: $Q_t|_{s=\eta} = 3M^2/(4a^2)|_{s=\eta}$. A simple consideration of the energy release rate in a geometrically linear setting confirms this observation and allows to identify this force as work conjugate to η , revealing its configurational nature.

References

- [1] J. Scheidl, Y. Vetyukov. *Review and perspectives in applied mechanics of axially moving flexible structures*, Acta Mech. (2023), 1-34
- [2] A. Humer, I. Steinbrecher, L. Vu-Quoc. *General sliding-beam formulation: A non-material description for analysis of sliding structures and axially moving beams*, J. Sound Vib. 480 (2020) 115341
- [3] S. Han, O.A. Bauchau. *Configurational forces in variable-length beams for flexible multibody dynamics*, Multibody Syst. Dyn. (2022), 1-24
- [4] C. Armanini, F. Dal Corso, D. Misseroni, D. Bigoni. *Configurational forces and nonlinear structural dynamics*, J. Mech. Phys. Solids 130 (2019) 82–100
- [5] Y. Vetyukov, A. Humer. *Dancing rod problem in the context of Lagrangian mechanics*, Eurodyn XII International Conference on Structural Dynamics, 2023.
- [6] A. Pechstein, J. Gerstmayr. *A Lagrange–Eulerian formulation of an axially moving beam based on the absolute nodal coordinate formulation*, Multibody Syst. Dyn. 30 (2013), 343-358
- [7] J.L. Escalona. *An arbitrary Lagrangian–Eulerian discretization method for modeling and simulation of reeving systems in multibody dynamics*, Mech. Mach. Theory 112 (2017), 1-21
- [8] Y. Vetyukov. *Non-material finite element modelling of large vibrations of axially moving strings and beams*, J. Sound Vib. 414 (2018), 299-317

MS-3: Geometric integration methods for non-linear structural dynamics

Test equations for Lie group time integration

Martin Arnold

Institute of Mathematics, Martin Luther University Halle-Wittenberg
06099 Halle (Saale), Germany, martin.arnold@mathematik.uni-halle.de

Keywords: Lie group time integration, stability, test equation

1. Introduction

Nonlinear configuration spaces with Lie group structure have become a quasi-standard for modelling highly flexible slender structures with large rotations [1]. Lie group time integration methods [2, 3] have been studied in great detail with respect to (local) error [2, 4] and zero-stability [4] but there is not much known about their numerical stability for larger time step sizes. Simple but non-trivial test equations can be a first step towards a better understanding of the stability on coarse time grids.

We start with a test problem from rigid body dynamics: a (damped) torsional spring being attached to a homogeneous rigid ball that rotates around a fixed axis in \mathbb{R}^3 . On $\text{SO}(3)$, the local parametrization based approach of Munthe-Kaas [2] is shown to result in Runge-Kutta Lie group integrators that share for this test problem the stability properties of their classical counterparts being applied to a (damped) oscillator in a linear space.

The test problem from mechanics motivates the definition of a test equation for Lie group time integration methods in the general Lie group setting. The practical relevance of this approach will be discussed in view of the non-commutativity of rotations in 3D.

2. Linear time-invariant second order systems

Linear time-invariant second order systems

$$\mathbf{M}\ddot{\mathbf{x}} + \mathbf{K}\mathbf{x} = \mathbf{r}(t) \quad (1)$$

with symmetric positive definite mass matrix $\mathbf{M} \in \mathbb{R}^{n \times n}$ and symmetric, positive semi-definite stiffness matrix $\mathbf{K} \in \mathbb{R}^{n \times n}$ may be decoupled into n scalar equations using an orthogonal transformation $\mathbf{M} = \mathbf{U}_M \mathbf{\Lambda}_M \mathbf{U}_M^\top$ with diagonal matrix $\mathbf{\Lambda}_M = \text{diag}_i m_i$ followed by a second orthogonal transformation $\mathbf{\Lambda}_M^{-1/2} \mathbf{U}_M^\top \mathbf{K} \mathbf{U}_M \mathbf{\Lambda}_M^{-1/2} = \mathbf{U}_\Omega (\mathbf{\Lambda}_M^{-1/2} \mathbf{\Lambda}_K \mathbf{\Lambda}_M^{-1/2}) \mathbf{U}_\Omega^\top$ with $\mathbf{\Lambda}_K = \text{diag}_i k_i$:

$$m_i \ddot{\xi}_i + k_i \xi_i = \rho_i(t), \quad (i = 1, \dots, n), \quad (2)$$

with $(\xi_1, \dots, \xi_n)^\top = \mathbf{\Lambda}_M^{-1/2} \mathbf{U}_\Omega^\top \mathbf{\Lambda}_M^{1/2} \mathbf{U}_M^\top \mathbf{x}$ and $(\rho_1, \dots, \rho_n)^\top = \mathbf{\Lambda}_M^{1/2} \mathbf{U}_\Omega^\top \mathbf{\Lambda}_M^{-1/2} \mathbf{U}_M^\top \mathbf{r}$. Damped systems with Rayleigh damping, i.e., $\mathbf{M}\ddot{\mathbf{x}} + \mathbf{D}\dot{\mathbf{x}} + \mathbf{K}\mathbf{x} = \mathbf{r}(t)$ with damping matrix $\mathbf{D} = c_M \mathbf{M} + c_K \mathbf{K}$ and constants $c_M, c_K \geq 0$, may be diagonalized in the same way resulting in scalar equations $m_i \ddot{\xi}_i + d_i \dot{\xi}_i + k_i \xi_i = \rho_i(t)$ with non-negative damping parameters d_i , $(i = 1, \dots, n)$.

3. Test problem: Rotating ball with (damped) torsional spring

In a Lie group setting, the natural counterpart to the scalar system $m\ddot{\xi} + d\dot{\xi} + k\xi = 0$ is a (damped) torsional spring being attached to a rigid ball with homogeneous mass distribution that has its centre in the origin and rotates around a fixed axis $\mathbf{n} \in \mathbb{R}^3$, $\|\mathbf{n}\|_2 = 1$. In $\text{SO}(3)$, the orientation of the body is given by $\mathbf{R} = \exp_{\text{SO}(3)}(\alpha \tilde{\mathbf{n}})$ with $\alpha \in \mathbb{R}$ denoting the angle of rotation and the skew symmetric matrix $\tilde{\mathbf{n}} \in \mathbb{R}^{3 \times 3}$ that represents the vector product in the sense of $\tilde{\mathbf{n}} \mathbf{w} = \mathbf{n} \times \mathbf{w}$, $(\mathbf{w} \in \mathbb{R}^3)$. The exponential map is invertible in a neighbourhood of the origin and defines an inverse map $\log_{\text{SO}(3)} : \text{SO}(3) \rightarrow \mathbb{R}^3$ with $\log_{\text{SO}(3)}(\exp_{\text{SO}(3)}(\tilde{\boldsymbol{\theta}})) = \boldsymbol{\theta}$.

The ball's inertia tensor $\mathbf{J} = m\mathbf{I}_3$ results in gyroscopic terms that vanish identically: $\boldsymbol{\omega} \times \mathbf{J}\boldsymbol{\omega} = m \boldsymbol{\omega} \times \boldsymbol{\omega} = \mathbf{0}$. Here, $\boldsymbol{\omega} \in \mathbb{R}^3$ denotes the angular velocity that is parallel to the axis of rotation: $\boldsymbol{\omega} = v \mathbf{n}$ with $v \in \mathbb{R}$. With these notations, the torsional spring is characterized by a torque vector $-(d\boldsymbol{\omega} + k \widetilde{\log_{\text{SO}(3)}}(\mathbf{R})) = -(dv + k\alpha) \mathbf{n}$ with damping and stiffness parameters d, k and yields equations of motion [1, Section 2.1]

$$\dot{\mathbf{R}} = \mathbf{R} \tilde{\boldsymbol{\omega}}, \quad \mathbf{J} \dot{\boldsymbol{\omega}} + d \boldsymbol{\omega} + k \widetilde{\log_{\text{SO}(3)}}(\mathbf{R}) = \mathbf{0} \quad (3)$$

in the tangent bundle $T\text{SO}(3)$. For the local parametrization based approach of Munthe-Kaas [2, Section 3], we consider incremental rotation vectors $\boldsymbol{\theta}_r(t) \in \mathbb{R}^3$ that parametrize $\mathbf{R}(t) = \exp_{\text{SO}(3)}(\tilde{\boldsymbol{\theta}}_r(t)) \mathbf{R}(t_r)$ and solve a locally defined initial value problem

$$\dot{\boldsymbol{\theta}}_r(t) = (T_{\text{SO}(3)}(\boldsymbol{\theta}_r(t)))^{-1} \boldsymbol{\omega}(t), \quad \boldsymbol{\theta}_r(t_r) = \mathbf{0} \quad (4)$$

with the tangent operator $T_{\text{SO}(3)}$ of $\exp_{\text{SO}(3)}$, see [3]. This operator represents the $\text{dexp}_{\tilde{\boldsymbol{\theta}}_r}$ operator [2] in matrix form. Taking into account that $T_{\text{SO}(3)}(s(t)\mathbf{n})(\dot{s}(t)\mathbf{n}) = \dot{s}(t)\mathbf{n}$ for any scalar function $s(t)$, the solution of (4) with $\boldsymbol{\omega}(t) = v(t)\mathbf{n}$ is given by $\boldsymbol{\theta}_r(t) = s_r(t)\mathbf{n}$ with $\dot{s}_r(t) = v(t)$ and $s_r(t_r) = 0$, i.e., $\mathbf{R}(t) = \exp_{\text{SO}(3)}(\alpha(t)\tilde{\mathbf{n}})$ with $\dot{\alpha}(t) = \dot{s}_r(t) = v(t)$, $\dot{\alpha}(t)\mathbf{n} = \boldsymbol{\omega}(t)$, $\ddot{\alpha}(t)\mathbf{n} = \dot{\boldsymbol{\omega}}(t)$ and $0 = m\ddot{\alpha} + dv + k\alpha = m\ddot{\alpha} + d\dot{\alpha} + k\alpha$, see (3).

Time step $t_r \rightarrow t_{r+1} = t_r + h$ of a Runge-Kutta Munthe-Kaas method [2] defines $\boldsymbol{\omega}_{r+1} = \boldsymbol{\omega}_r^+ = \boldsymbol{\omega}_r + h \sum_j b_j \dot{\boldsymbol{\omega}}_{rj}$ and $\mathbf{R}_{r+1} = \exp_{\text{SO}(3)}(\tilde{\boldsymbol{\theta}}_r^+) \mathbf{R}_r$ with $\boldsymbol{\theta}_r^+ = h \sum_j b_j \dot{\boldsymbol{\theta}}_{rj}$. The stages are $\boldsymbol{\omega}_{ri} = \boldsymbol{\omega}_r + h \sum_j a_{ij} \dot{\boldsymbol{\omega}}_{rj}$, $\boldsymbol{\theta}_{ri} = h \sum_j a_{ij} \dot{\boldsymbol{\theta}}_{rj}$,

$$\dot{\boldsymbol{\omega}}_{ri} = -\mathbf{J}^{-1}(d\boldsymbol{\omega}_{ri} + k\widetilde{\log}_{\text{SO}(3)}(\mathbf{R}_{ri})), \quad \mathbf{R}_{ri} = \exp_{\text{SO}(3)}(\tilde{\boldsymbol{\theta}}_{ri}) \mathbf{R}_r, \quad \dot{\boldsymbol{\theta}}_{ri} = (T_{\text{SO}(3)}(\boldsymbol{\theta}_{ri}))^{-1} \boldsymbol{\omega}_{ri}, \quad (i = 1, \dots, s). \quad (5)$$

As for the analytical solution $(\boldsymbol{\theta}_r(t), \boldsymbol{\omega}(t))$ and its time derivative, we see that all stage vectors $\boldsymbol{\theta}_{ri}, \dot{\boldsymbol{\theta}}_{ri}, \boldsymbol{\omega}_{ri}, \dot{\boldsymbol{\omega}}_{ri}$, $(i = 1, \dots, s)$, are parallel to \mathbf{n} resulting in numerical solutions $\mathbf{R}_{r+1} = \exp_{\text{SO}(3)}(\alpha_{r+1}\tilde{\mathbf{n}})$, $\boldsymbol{\omega}_{r+1} = v_{r+1}\mathbf{n}$ with (α_{r+1}, v_{r+1}) being the result of a classical Runge-Kutta step for the first order system $\dot{\alpha} = v$, $m\dot{v} = -dv - k\alpha$ starting from (α_r, v_r) . For this test problem, the Runge-Kutta Lie group integrator shares one-by-one the well known stability properties of its classical counterpart applied to the second order problem in linear spaces.

4. Test equation for Lie group time integration


In linear spaces, the analysis of the scalar test problem (2) characterizes the stability of time integration methods for the linear time-invariant system (1) as well since the vector valued problem is just a super-position of n decoupled scalar problems, see Section 2. In the Lie group setting of $\text{SO}(3)$, the results for low dimensional test problems, see Section 3., are less universal than in linear spaces since rotations in 3D do not commute.

As a straightforward generalization of the $\text{SO}(3)$ test problem of Section 3. to general Lie groups, we may consider the test equation

$$\dot{q}(t) = DL_{q(t)}(e) \cdot \lambda \log q(t) \quad (6)$$

with a real parameter $\lambda < 0$. Its solution is given by $q(t) = \exp(e^{\lambda(t-t_0)} \log q(t_0))$ and tends to the neutral element $e \in G$ for $t \rightarrow \infty$. In (6), we used the notations of [3] and the map $\log : G \rightarrow \mathfrak{g}$, the inverse of the exponential $\exp : \mathfrak{g} \rightarrow G$. It is well defined in a neighbourhood of the neutral element e and satisfies $\log(\exp(\tilde{\mathbf{v}})) = \tilde{\mathbf{v}}$, $(\mathbf{v} \in \mathbb{R}^n)$. Again, the local parametrization based approach of Munthe-Kaas is seen to result in Runge-Kutta Lie group methods that share one-by-one the stability properties of their classical counterparts from linear spaces.

Acknowledgments

The author acknowledges gratefully fruitful discussions with Elena Celledoni, Ergys Çokaj, Brynjulf Owren (Trondheim) and Denise Tumiotto (Halle) on contractivity of Lie group time integration methods. That research has been part of the THREAD project, see <https://thread-etn.eu/>, that has received funding from the European Union's Horizon 2020 research and innovation programme under the Marie Skłodowska-Curie grant agreement No 860124. 

References

- [1] O. Brüls, A. Cardona, M. Arnold. Lie group generalized- α time integration of constrained flexible multi-body systems. *Mechanism and Machine Theory*, 48:121–137, 2012.
- [2] A. Iserles, H.Z. Munthe-Kaas, S. Nørsett, A. Zanna. Lie-group methods. *Acta Numerica*, 9:215–365, 2000.
- [3] O. Brüls, A. Cardona. On the use of Lie group time integrators in multibody dynamics. *ASME J. Comput. Nonlinear Dynam.*, 5:031002 (13 pages), 2010.
- [4] M. Arnold, O. Brüls, A. Cardona. Error analysis of generalized- α Lie group time integration methods for constrained mechanical systems. *Numerische Mathematik*, 129:149–179, 2015.

Lie group integrators for mechanical systems and their stability

Martin Arnold¹, Elena Celledoni², Ergys Çokaj², Andrea Leone², Davide Murari², Brynjulf Owren²,
 Denise Tumiotto¹

¹ Institute for Mathematics, Martin-Luther-University Halle-Wittenberg, Halle (Saale), Germany,
 [martin.arnold, denise.tumiotto]@mathematik.uni-halle.de

² Department of Mathematical Sciences, Norwegian University of Science and Technology, Trondheim,
 Norway, [elena.celledoni, ergys.cokaj, andrea.leone, davide.murari, brynjulf.owren]@ntnu.no

Keywords: numerical integration of ODEs, Lie group integrators, numerical stability, contractivity.

1. Introduction

Classically, numerical integration of ordinary differential equations (ODEs) [1] is associated with solving initial value problems evolving on \mathbb{R}^N ,

$$\dot{\mathbf{y}} = F(t, \mathbf{y}), \quad t \geq 0, \quad \mathbf{y}(0) = \mathbf{y}_0, \quad \mathbf{y}(t) \in \mathbb{R}^N, \quad (1)$$

where F is a vector field on $\mathbb{R}^+ \times \mathbb{R}^N$. Well-known numerical integrators, such as Runge-Kutta and multistep methods, exist, which are formulated using a set of 'basic motions' given by translations on \mathbb{R}^N .

In many physical problems, the configuration space is not linear but consists of a collection of rotations and translations. A simple well known example is that of the free rigid body whose configuration space consists of rotations in 3D. Mathematically, the structure of such problems is more accurately described as a manifold. Choosing manifolds as configuration spaces makes it possible to express important geometric attributes of the underlying differential system, such as conservation laws, symmetries, or symplectic structure. Such a choice leads to interesting numerical advantages, in particular, to slower error accumulation. A popular family of integrators used to simulate the dynamics of systems evolving on manifolds are Lie group integrators, see [2] and references therein. In this approach, the model and the numerical integrator are expressed entirely in terms of a Lie group and its action on the phase space. In [3], we discuss different ways of applying Lie group integrators to simulate the dynamics of mechanical multibody systems. Our work is motivated by applications in the modeling and simulation of slender structures like rods and beams.

2. Lie group integrators

Solving differential equations whose solutions evolve on a manifold M means that we seek a curve $\mathbf{y}(t) \in M$ whose tangent at any point coincides with a vector field $F \in \mathfrak{X}(M)$, where $\mathfrak{X}(M)$ denotes the set of smooth vector fields defined on M , and passes through a given initial value \mathbf{y}_0 at $t = t_0$,

$$\dot{\mathbf{y}}(t) = F|_{\mathbf{y}(t)}, \quad \mathbf{y}(t_0) = \mathbf{y}_0. \quad (2)$$

A convenient way of representing the vector field F , originally presented in [4], is to furnish M with a transitive action $\psi : G \times M \rightarrow M$ by some Lie group G of dimension $d \geq \dim M$. We denote the action of $\mathbf{g} \in G$ on $\mathbf{m} \in M$ as $\mathbf{g} \cdot \mathbf{m}$, i.e. $\mathbf{g} \cdot \mathbf{m} = \psi(\mathbf{g}, \mathbf{m})$. Let \mathfrak{g} be the Lie algebra of G , and denote by $\exp : \mathfrak{g} \rightarrow G$ the exponential map. We define $\psi_* : \mathfrak{g} \rightarrow \mathfrak{X}(M)$ to be the infinitesimal generator of the action, i.e.,

$$F_{\xi}|_{\mathbf{m}} = \psi_*(\xi)|_{\mathbf{m}} = \left. \frac{d}{dt} \right|_{t=0} \psi(\exp(t\xi), \mathbf{m}), \quad \xi \in \mathfrak{g}. \quad (3)$$

The transitivity of the action now ensures that $\psi_*(\mathfrak{g})|_{\mathbf{m}} = T_{\mathbf{m}}M$ for any $\mathbf{m} \in M$, such that any tangent vector $\mathbf{v}_{\mathbf{m}} \in T_{\mathbf{m}}M$ can be represented as $\mathbf{v}_{\mathbf{m}} = \psi_*(\xi_{\mathbf{v}})|_{\mathbf{m}}$ for some $\xi_{\mathbf{v}} \in \mathfrak{g}$. Consequently, for any vector field $F \in \mathfrak{X}(M)$ there exists a map $f : M \rightarrow \mathfrak{g}$ such that

$$F|_{\mathbf{m}} = \psi_*(f(\mathbf{m}))|_{\mathbf{m}}, \quad \text{for all } \mathbf{m} \in M. \quad (4)$$

Example 1. *The implicit Lie-Euler method*

Given the initial value problem (1), the well known implicit Euler method is defined as

$$\mathbf{y}_{n+1} = \mathbf{y}_n + \tau F(\mathbf{y}_{n+1}), \quad (5)$$

for some stepsize τ . One can think of (5) as the τ -flow of the constant vector field $F_{\mathbf{y}_{n+1}}(\mathbf{y}) = F(\mathbf{y}_{n+1})$, that is

$$\mathbf{y}_{n+1} = \exp(\tau F_{\mathbf{y}_{n+1}}) \mathbf{y}_n. \quad (6)$$

Method (6) makes sense also when F is replaced by a vector field on some manifold. In this case, it is known as the implicit Lie-Euler method.

In [3], we consider the two classes of methods known as Runge-Kutta-Munthe-Kaas (RKMK) methods and Commutator-free Lie group methods. As the name suggests, in contrast to the former group, the latter one does not include commutators in the scheme. Both groups of methods have been tested on simulating the dynamics of a chain of pendula and the dynamics of two quadrotors transporting a mass point. The Lie group setting of both examples is presented and properties such as the rate of convergence, the preservation of the configuration manifold and phase space are tested.

3. Investigation of stability

While the stability and the contractivity of classical numerical integrators have been studied in detail, for Lie group integrators, they are to be investigated. In the present work, we investigate stability, global error estimation, and convergence for simple Lie group integrators. The engine for this study is the use of Riemannian metrics for measuring distance on a manifold. A starting point is the article [5] where some Grönwall estimates are given in this setting. Compared to the usual situation in linear spaces, on the estimates they obtained, the norm is replaced by a Riemannian distance function, and the Lipschitz constant is replaced by the operator norm of the Riemannian connection. The operator norm of the Riemannian connection can actually be replaced by a bound for a logarithmic norm that might be useful when strongly damped or stiff systems on manifolds are to be considered. We show an alternative proof to a one-sided Lipschitz condition obtained via the logarithmic norm and we derive a bound for the global error. We consider how analytical contractivity results for simple Lie group integrators applied to contractive systems can be derived. Numerical experiments are performed to better illustrate the theory.

4. Conclusions

Contractivity is a desired property for numerical methods which integrate stiff systems and such methods exist in the Euclidean case. Since many stiff systems evolve on manifolds, e.g., Lie Groups, Riemannian manifolds, etc., Lie group integrators have been developed to integrate such systems. The goal of this work is to prove the contractivity of such integrators.

Acknowledgments

This project has received funding from the European Union's Horizon 2020 research and innovation programme under the Marie Skłodowska-Curie grant agreement No 860124.



References

- [1] E. Hairer, Ch. Lubich, and G. Wanner. *Geometric numerical integration*. Springer, Heidelberg, 2010.
- [2] A. Iserles, H. Z. Munthe-Kaas, S. P. Nørsett, and A. Zanna. Lie-group methods. *Acta Numerica*, 9:215–365, 2000.
- [3] E. Celledoni, E. Çokaj, A. Leone, D. Murari, and B. Owren. Lie group integrators for mechanical systems. *International Journal of Computer Mathematics*, 99(8):1–31, 2021.
- [4] H. Munthe-Kaas. High order Runge-Kutta methods on manifolds. *Acta Applicandae Mathematicae*, 29:115–127, 1999.
- [5] M. Kunzinger, H. Schichl, R. Steinbauer, and J. A. Vickers. Global Gronwall estimates for integral curves on Riemannian manifolds. *Revista Matemática Complutense*, 19(1):133–137, 2006.

Computing normal forms of quadratic differential algebraic equations

A. GROLET¹, A. VIZZACCARO², M. DEBEURRE¹, O. THOMAS¹

¹ Arts et Métiers Institute of Technology, Lille, France. aurelien.grolet@ensam.eu

² University of Bristol, Bristol, UK. alessandra.vizzaccaro@bristol.ac.uk

Keywords: Normal Form, Differential-Algebraic Equation (DAE), Quadratic Recast, Model Reduction

1. Introduction

We consider nonlinear dynamical systems arising in engineering, such as when modelling slender structures in large amplitude vibration. In this paper, we consider reduced order model construction and solution approximation through the computation of a normal form up to a given order [1, 2, 3]. Usually, the normal form method is presented by considering a system with only polynomial nonlinearities (or a Taylor expansion of the nonlinearities), but this reduces the precision of the results. To increase the generality of the normal form, we propose to consider that the initial dynamical system is under the form of a differential-algebraic equation (DAE) with quadratic nonlinearities only. This is the same hypothesis as that of the Manlab package, which allows for application of the Asymptotic Numerical Method on a wide variety of systems [4]. Although this seem restrictive, it can be shown that most nonlinear systems can be written under this form, provided that one includes enough auxiliary variables in the so-called quadratic recast [4]. In this paper, we present a general method to compute the (reduced) normal form of a quadratic DAE up to any order. To present the computation, we rely on multivariate polynomials theory with a focus on linear operations such as derivation and multiplication. The resulting homological equation and the solving strategy is presented. The presented method is quite general and can be applied to many different systems provided it can be written under the form of a quadratic DAE.

2. Method

We consider the following quadratic DAE: $A\dot{y} = Ly + Q(y, y)$, where y is the vector of unknowns containing N generalized positions, N generalized velocities and M auxiliary variables (Lagrange multipliers from mechanical constraints or auxiliary variables arising from the quadratic recast). A is the mass matrix (of size $2N + M$, possibly singular), L is a linear operator (matrix of size $2N + M$) and Q a quadratic operator. For the normal form computation, we are searching for:

- (i) : a change of coordinates $y = W(z)$ where $z \in \mathbb{C}^n$ is a set of (complex) normal variables with n elements (n even, and usually $n \ll 2N$)
- (ii): a (reduced) dynamic function $f(z) \in \mathbb{C}^n$ for the normal variables, such that: $\dot{z} = f(z)$

Substituting the expression for the normal dynamics and the change of variable into the original DAE leads to the following homological equation: $A(\nabla_z W)f = LW + Q(W, W)$. In this study, both the change of coordinates (W) and the reduced dynamics (f) are considered to be (multivariate) polynomials of given degree d , so that they can be written as:

$$\begin{aligned} W(z) &= \sum W_i z^{\alpha_i}, \text{ with } W_i \in \mathbb{C}^{2N+M}, \\ f(z) &= \sum f_i z^{\alpha_i}, \text{ with } f_i \in \mathbb{C}^n. \end{aligned}$$

The computation of the normal form then reduces to finding the vectors of coefficients W_i and f_i for each monomial z^{α_i} up to degree d . This is realized by balancing the coefficients of each monomial z^{α_i} in the homological equation, resulting in the following series of equations:

$$(A\sigma_i(f) - L)W_i + A\Lambda(W)f_i = R_i(W). \quad (1)$$

Note that a closed form for the expression of $R_i(W)$, $\Lambda(W)$ and $\sigma_i(f)$ can easily be obtained if one considers derivation and multiplication as linear operations in the vector space of multivariate polynomials. The resolution is sequential, by increasing degree. At first order, the equations are associated to the linear monomials $z^{\alpha_i} = z_k$ and can be solved using the (complex) linear eigenmodes of the system (λ, Y) defined by $\lambda AY = LY$. The results yield the linear part of the change of variable and of the reduced dynamics under the form:

$$y = \sum_{k=1}^n Y_k z_k, \text{ and } \dot{z}_k = \lambda_k z_k. \quad (2)$$

At higher orders, one has to solve an equation of the form:

$$(A\sigma_i(f) - L)W_i + A \sum_{k=1}^n Y_k f_{i,r} = R_i(W). \quad (3)$$

Note that the functions $R_i(W)$, and $\sigma_i(f)$ depend only on terms associated to monomials of lower degree, and are therefore known at this point. The idea is to have a reduced dynamic under its simplest form, so most of the coefficients f_i should be zero and the equation should be solved by the change of variable W_i . However, if it happened that $A\sigma_i(f) - L$ is singular then the component of $R_i(W)$ parallel to the kernel cannot be generated by the term $[A\sigma_i(f) - L]W_i$. As a result, some terms in the reduced dynamics must be included by keeping the vectors generating the kernel (i.e the resonant modes): $\sum_{r \in \text{Res. Modes}} Y_r f_{i,r}$. The coefficients associated to the non-resonant modes can be set to zero, i.e. $f_{i,r} = 0$ if $r \notin \text{Res. Modes}$. Finally one sets the part of W_i parallel to the kernel to be zero, i.e. $X_r^T W_i = 0$ for $r \in \text{Res. Modes}$ (where X^T are the left eigenvectors). To summarize, the coefficients of the monomial z^{α_i} can be obtained by solving the following linear system of equations:

$$\begin{pmatrix} A\sigma_i - L & AY_{r \in \text{Res. Modes}} & 0 \\ X_{r \in \text{Res. Modes}}^T & 0 & 0 \\ 0 & 0 & I \end{pmatrix} \begin{pmatrix} W_i \\ f_{i,s \in \text{Res. Modes}} \\ f_{i,s \notin \text{Res. Modes}} \end{pmatrix} = \begin{pmatrix} R_i \\ 0 \\ 0 \end{pmatrix}. \quad (4)$$

This system is solved for each monomial of a given degree and the operation is repeated iteratively for the monomials of the next degree until the maximum degree d has been reached.

3. Examples

Fig.1 (left) depicts the backbones curves of a Duffing oscillator obtained with the normal form for several orders, along with the exact result using Jacobi elliptic functions. As the order of the normal form increases, a very good agreement can be observed with the exact results. Fig. 1 (right) depicts the same kind of results for a cantilever beam modelled with geometrically exact beam elements.

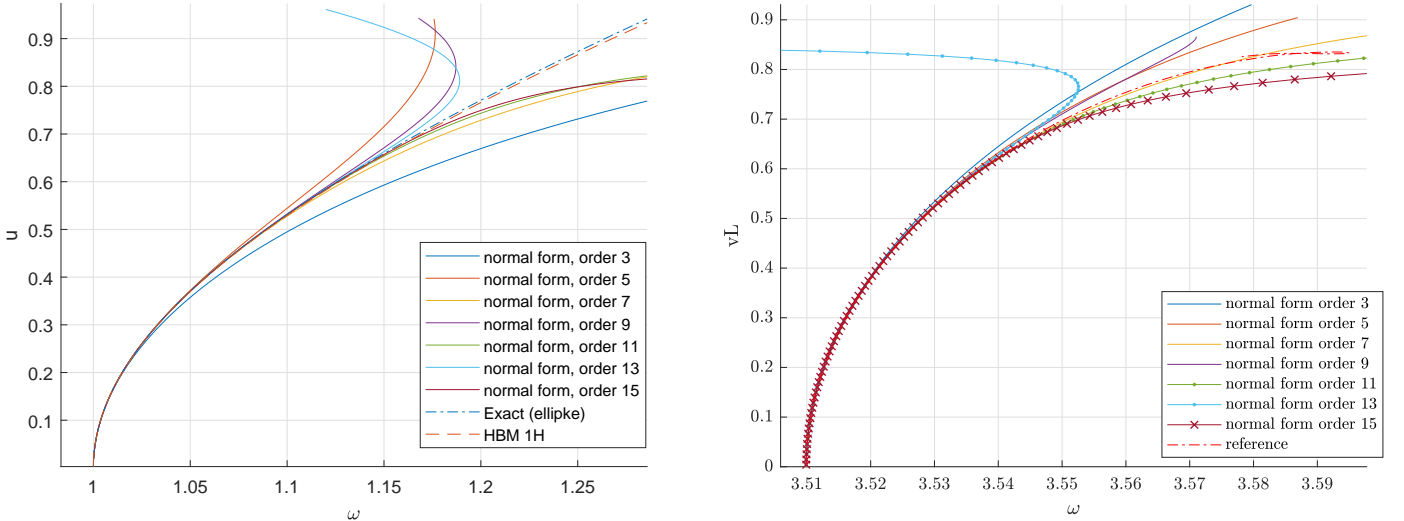


Figure 1: Comparison between normal form solution and reference solution. Left: Duffing oscillator, right: cantilever beam.

References

- [1] Vizzaccaro A., Shen Y., Salles L., Blahoš J., and Touzé C. Direct computation of nonlinear mapping via normal form for reduced-order models of finite element nonlinear structures. *Computational Methods in Applied Mechanical Engineering*, 2021.
- [2] Vizzaccaro A., Opreni A., Salles L., Frangi A., and Touzé C. High order direct parametrisation of invariant manifolds for model order reduction of finite element structures: application to large amplitude vibrations and uncovering of a folding point. *Nonlinear Dynamics*, 2021.
- [3] Touzé C., Thomas O., and Chaigne A. Hardening/softening behaviour in non-linear oscillations of structural systems using non-linear normal modes. *Journal of Sound and Vibration*, (273):77–101, 2004.
- [4] Guillot L., Cochelin B., and Vergez C. A generic and efficient Taylor series–based continuation method using a quadratic recast of smooth nonlinear systems. *International Journal of Numerical Methods in Engineering*, 119(4):261–280, 2019.

Higher Order Fractional Variational Integrators

Fernando Jiménez¹, Khaled Hariz-Belgacem², Sina Ober-Blöbaum³

¹ Technical University of Madrid, fernando.jimenez.alburquerque@upm.es

² Paderborn University, hariz@math.upb.de

³ Paderborn University, sinaober@math.upb.de

Keywords: Convolution quadrature, fractional variational integrators, restricted calculus of variations.

1. Introduction

Fractional dissipation is a powerful tool to study non-local physical phenomena such as damping models. The design of geometric, in particular, variational integrators for the numerical simulation of such systems relies on a variational formulation of the model. In [4] a new approach is proposed to deal with dissipative systems in a variational way for both, the continuous and discrete setting. It is based on the doubling of variables and their fractional derivatives. In this contribution we derive higher-order fractional variational integrators based on convolution quadratures and study the numerical properties of those integrators.

1.1. Fractional integrals and convolution quadrature method

Let $\alpha \in [0, 1]$ and $f : [0, T] \rightarrow \mathbb{R}$ be a AC^2 - function. The Riemann-Liouville α -fractional integrals of f are

$$I_-^\alpha f(t) = \frac{1}{\Gamma(\alpha)} \int_0^t \frac{f(\tau)}{(t-\tau)^{1-\alpha}} d\tau, \quad t \in (0, T], \quad I_+^\alpha f(t) = \frac{1}{\Gamma(\alpha)} \int_t^T \frac{f(\tau)}{(\tau-t)^{1-\alpha}} d\tau, \quad t \in [0, T). \quad (1)$$

Focusing on the *retarded* fractional integral, $I_-^\alpha f(t)$, it is easy to see that it may be written as a convolution

$$I_-^\alpha f(t) = \left(\kappa^{(\alpha)} * f \right) (t) := \int_0^t \kappa^{(\alpha)}(t-\tau) f(\tau) d\tau, \quad \text{where} \quad \kappa^{(\alpha)}(t) = \frac{t^{\alpha-1}}{\Gamma(\alpha)}. \quad (2)$$

The Laplace transform of this convolution kernel $\kappa^{(\alpha)}$ is given by $K^{(\alpha)}(s) = s^{-\alpha}$. An approximation of the convolution integral (2) was introduced by [1, 2, 3] using the so-called convolution quadrature method. This method numerically approximates the integral (2) based on a special quadrature rule with the help of the Laplace transformed function and a linear multistep method. The discrete convolution is defined by

$$\left(\kappa^{(\alpha)} * f \right) (t_k) \approx \mathfrak{J}_-^\alpha f_k := \sum_{n=0}^k \omega_n(h) f_{k-n} = \sum_{n=0}^k \omega_{k-n}(h) f_k, \quad (h \in \mathbb{R}_+ \text{ the time step}). \quad (3)$$

The *convolution quadrature weights* ω_n are defined as the coefficients of the generating power series

$$K^{(\alpha)} \left(\frac{\gamma(z)}{h} \right) = \sum_{n=0}^{\infty} \omega_n z^n, \quad |z| \text{ small}, \quad (4)$$

where $\gamma(z)$ is the quotient of the generating polynomials of a linear multistep method for $y' = f(y)$.

The important properties of this CQ are semi-group and asymmetric integration, which allows us to derive the fractional variational integrators. A convolution quadrature determined by the coefficients $\omega_n^{(\alpha)}$ is convergent of order p (to I_σ^α) if

$$I_\sigma^\alpha t^{\beta-1} - \mathfrak{J}_\sigma^\alpha t^{\beta-1} = O(h^\beta) + O(h^p), \quad \text{for all } \beta \in \mathbb{C}, \beta \neq 0, -1, -2, \dots. \quad (5)$$

Therefore, for a fixed $\beta > 0$, we expect the saturation of the convergence order at $\min(\beta, p)$, i.e., the error is still limited to the order $O(h^\beta)$ even for a larger p . A technique to obtain the correct order for functions $f(t) = t^{\beta-1} g(t)$, $g(t)$ smooth, was introduced in [1] by adding a correction term in approximation (3).

To illustrate the saturation, we make a log-plot of h versus the error $e(h)$ in Figure 1, which is defined as usual in the literature by means of the maximum norm.

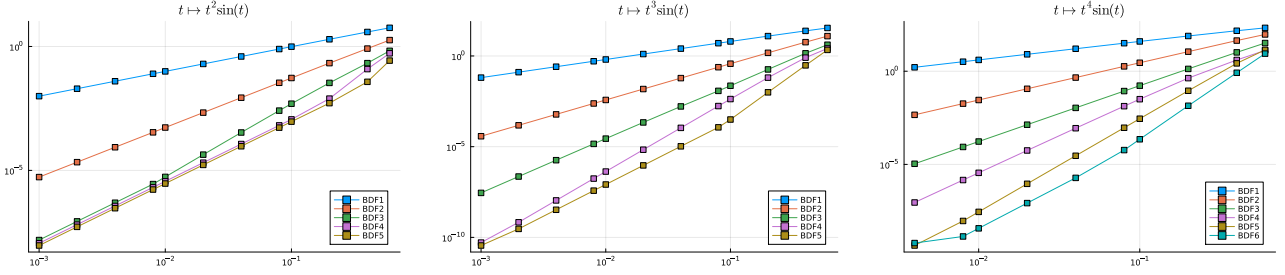


Figure 1: Log-log plot of h versus the error $e(h)$ with $\alpha = -1/2$ corresponds to the half Caputo fractional derivative. As expected, the convergence starts to saturate at $p = 3$ (left), $p = 4$ (middle) and $p = 5$ (right), respectively.

2. Fractional Variational integrators with CQ

A *restricted calculus of variations* [4] is used to obtain the dynamics of a fractional damping Lagrangian system. In particular, the *fractional variational integrators* have been derived with order 1 approximation for the fractional derivatives.

Let I_-^α and I_+^β be the Caputo fractional operators, we define the following action:

$$\mathcal{L}(x, y) = \mathcal{L}^{\text{con}}(x, y) + \mathcal{L}^{\text{frac}}(x, y) = \int_0^T (L(x, \dot{x}) + L(y, \dot{y})) dt - \rho \int_0^T I_-^\alpha x(t) I_+^\beta y(t) dt. \quad (6)$$

For a higher-order approximation, we choose a quadrature rule $(b_i, c_i)_{i=1}^r$ for the conservative part \mathcal{L}^{con} and a convolution quadrature for the fractional integrals involved in $\mathcal{L}^{\text{frac}}$. For that, we take into account two discrete series $x_d = \{x_k\}_{0, \dots, N} \in (\mathbb{R}^d)^{N+1}$, $y_d = \{y_k\}_{0, \dots, N} \in (\mathbb{R}^d)^{N+1}$ and $s + 1$ inner nodes $\{x_k^v\}_{0, \dots, s} \in (\mathbb{R}^d)^{s+1}$ in each interval $[k, k + 1]$ such that $x_k^s = x_{k+1}^0$ (equiv. for y). Namely

$$\mathcal{L}_d(x_d, y_d) = \mathcal{L}_d^{\text{con}}(x_d, y_d) + \mathcal{L}_d^{\text{frac}}(x_d, y_d) = \sum_{k=0}^{N-1} (L_d(x_k) + L_d(y_k)) - \rho h \sum_{k=0}^N \tilde{\mathfrak{J}}_-^\alpha x_k \tilde{\mathfrak{J}}_+^\beta y_k, \quad (7)$$

where $L_d(x_k) = \sum_{i=1}^r b_i L(x_d(c_i h; k), \dot{x}_d(c_i h; k))$ (equiv. for $L_d(y_k)$) is the piecewise polynomial on $[k, k + 1]$ (equiv. for $y_d(t; k)$). The restricted calculus of variations lead to the so-called fractional variational integrators

$$D_{s+1} L_d(x_{k-1}^0, \dots, x_{k-1}^s) + D_1 L_d(x_k^0, \dots, x_k^s) - \rho h \tilde{\mathfrak{J}}_-^{-(\beta+\alpha)} x_k^0 = 0, \quad k = 1, \dots, N-1, \quad (8)$$

$$D_i L_d(x_k^0, \dots, x_k^s) = 0, \quad k = 0, \dots, N-1, \quad i = 2, \dots, s, \quad (9)$$

$$D_{s+1} L_d(y_{k-1}^0, \dots, y_{k-1}^s) + D_1 L_d(y_k^0, \dots, y_k^s) - \rho h \tilde{\mathfrak{J}}_+^{-(\alpha+\beta)} y_k^0 = 0, \quad k = 1, \dots, N-1, \quad (10)$$

$$D_i L_d(y_k^0, \dots, y_k^s) = 0, \quad k = 0, \dots, N-1, \quad i = 2, \dots, s. \quad (11)$$

These equations correspond to discretized dynamics of a Lagrangian systems subject to fractional damping in forward (equations (8)-(9)) and backward time (equations (10)-(11)), see also [4]. In this contribution we will study convergence properties of the fractional variational integrators, saturation effects due to the approximation of the fractional derivatives and discuss ideas how to improve the accuracy. Furthermore, we will also apply Runge-Kutta convolution quadrature and compare the resulting integration methods.

References

- [1] C. Lubich. *Discretized fractional calculus*, SIAM J. Math. Anal., 17(3) (1983) 704-719.
- [2] C. Lubich. *Convolution quadrature and discretized operational calculus I and II*, Numer. Math., 52 (1988) 129-145 and 413-425.
- [3] C. Lubich. *On the multistep time discretization of linear initial-boundary value problems and their boundary integral equations*, Numer. Math., 67 (1994) 365-389.
- [4] F. Jiménez and S. Ober-Blöbaum *Fractional Damping Through Restricted Calculus of Variations*, Journal of Nonlinear Science, 31 (2021).

Machine learning applications for mechanical systems

Elena Celledoni ¹, [Andrea Leone](#) ², Davide Murari ³, Brynjulf Owren ⁴,

¹ NTNU, elena.celledoni@ntnu.no ² NTNU, andrea.leone@ntnu.no ³ NTNU, davide.murari@ntnu.no

⁴ NTNU, brynjulf.owren@ntnu.no

Neural networks, Hamiltonian systems, Constrained mechanical systems, Geometric numerical integration, Lie group methods

1. Introduction

There is an increasing interest in data-driven modelling of physical systems with machine learning – in particular deep learning – techniques. In Hamiltonian mechanical systems, the dynamics is fully determined by the Hamiltonian, a scalar function which corresponds to the total energy of the system. As a consequence, multiple approaches have been proposed to approximate this energy function. In this talk, we focus on the task of learning the Hamiltonian of constrained mechanical systems with neural networks, given observations of the solution trajectories [1, 2].

We consider Hamiltonian functions of the form

$$H(q, p) = \frac{1}{2} p^T M^{-1}(q) p + V(q), \quad (1)$$

where $M(q)$ is the mass matrix, possibly depending on the configuration $q \in \mathbb{R}^n$, and $V(q)$ is the potential energy of the system. The solution trajectories are often constrained to evolve on a submanifold of a linear vector space. In particular, we focus on systems that are holonomically constrained on some configuration manifold $\mathcal{Q} = \{q \in \mathbb{R}^n : g(q) = 0\}$ embedded in \mathbb{R}^n , and we model them either by means of Lagrange multipliers or some projection operator. In the first case, we end up with a system of differential algebraic equations, while in the second case the vector field is written in such a way that it directly respects the constraints, without the addition of algebraic equations [3, 4]. We provide a brief account of the different formulations.

2. Method

We assume to be given N training trajectories denoted by

$$\{(x_i, y_i^2, \dots, y_i^M)\}_{i=1, \dots, N}. \quad (2)$$

To obtain an approximation of the Hamiltonian H in (1), we define a parametric model H_Θ and look for a Θ so that the trajectories generated by H_Θ resemble the given ones. In our approach, Θ will collect a factor of the mass matrix and the weights of a neural network. To learn H_Θ , we use some numerical one-step method $\Psi_{X_{H_\Theta}}^{\Delta t}$ to generate the trajectories

$$\hat{y}_i^j(\Theta) := \Psi_{X_{H_\Theta}}^{\Delta t}(\hat{y}_i^{j-1}(\Theta)), \quad \hat{y}_i^1(\Theta) := x_i, \quad j = 2, \dots, M, \quad i = 1, \dots, N, \quad (3)$$

and we optimize a loss function measuring the distance between the given trajectories y_i^j and the generated ones \hat{y}_i^j , defined as

$$\mathcal{L}(\Theta) := \frac{1}{2n} \frac{1}{NM} \sum_{i=1}^N \mathcal{L}_i(\Theta) = \frac{1}{2n} \frac{1}{NM} \sum_{i=1}^N \sum_{j=1}^M \left\| \hat{y}_i^j(\Theta) - y_i^j \right\|^2, \quad (4)$$

where $\|\cdot\|$ is the Euclidean metric of \mathbb{R}^{2n} .

3. Results

We consider systems whose configuration manifold is given by a product of unit sphere in \mathbb{R}^3 . We present in Figure 1 the results obtained in the case of a double spherical pendulum. To train H_Θ , a Lie group method is used

in (3). This gives a final training loss (4) of $1.3 \cdot 10^{-9}$ and an approximation accuracy $\mathcal{E}_1 = 2.05 \cdot 10^{-6}$, where \mathcal{E}_1 , defined in [1, Equation 2], is given by the square of the 2-norm of the difference between the learned trajectories and the given ones (considering both positions and momenta), averaged over the number of trajectories.

Time evolution of the configuration variable for pendulum 1

Time evolution of the configuration variable for pendulum 2

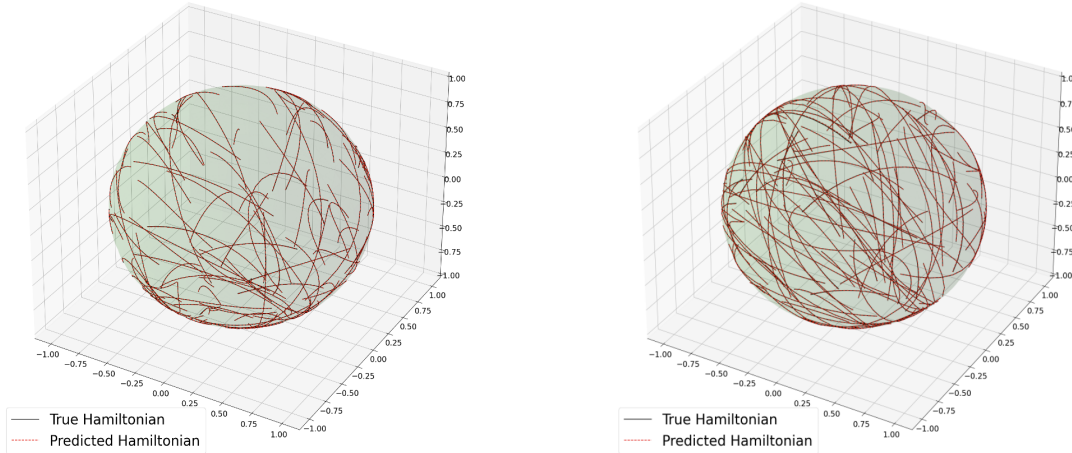


Figure 1: Comparison between 100 test trajectories obtained with the true Hamiltonian H and the predicted one H_Θ .

In general, numerical integrators do not preserve the geometry of the system and there might be a drift from the constrained manifold. Experimentally this does not seem to have a great impact on the quality of the predicted Hamiltonian in most of the cases, while the order of the numerical integrator plays a significant role.

4. Conclusions

Our main contribution is an approach to learn the Hamiltonian for systems defined on the cotangent bundle T^*Q of some manifold Q embedded in a vector space. Under the assumption that T^*Q is homogeneous, we show how to do that while preserving the phase space during the learning procedure with a Lie group method. The influence of the preservation of other geometric properties will be investigated, by using different geometric integrators in (3).

Acknowledgments

This project has received funding from the European Union's Horizon 2020 research and innovation programme under the Marie Skłodowska-Curie grant agreement No 860124. This contribution reflects only the authors' view and the Research Executive Agency and the European Commission are not responsible for any use that may be made of the information it contains.

References

- [1] E. Celledoni, A. Leone, D. Murari, B. Owren. *Learning Hamiltonians of constrained mechanical systems*. Journal of Computational and Applied Mathematics, 417 (2023): 114608.
- [2] M. Arnold, O. Brüls, E. Celledoni, S. Chandrashekhara, E. Çokaj, M. Debeurre, V. Dörlich, G. Jelenić, A. Leone, S. Leyendecker, J. Linn, D. Manfredi, B. Owren, I. Patil, M. Stavole, O. Thomas, J. Tomec, D. Tumiotto, D. Zupan, 2023. *Report on methods (benchmark test) Deliverable D3.3*. EU Horizon 2020 THREAD Project, Grant agreement No. 860124.
- [3] T. Lee, M. Leok., N. H. McClamroch. *Global formulations of Lagrangian and Hamiltonian dynamics on manifolds*. Springer 13 (2017): 31.
- [4] E. Hairer, C. Lubich, G. Wanner. *Geometric numerical integration. Structure-preserving algorithms for ordinary differential equations*. Berlin Heidelberg New York: Springer (2006).

2D Euler elastica in constrained environments

Martina Stavole¹, Rodrigo T. Sato Martín de Almagro¹, Sigrid Leyendecker¹

¹ Institute of Applied Dynamics, Friedrich-Alexander-Universität Erlangen-Nürnberg,
 Immerwahrstrasse 1, D-91058 Erlangen, Germany
 martina.stavole@fau.de rodrigo.t.sato@fau.de sigrid.leyendecker@fau.de

Keywords: Euler Elastica, Contact, Lagrangian mechanics, Endoscopes

1. Introduction

Flexible endoscopes are medical devices that can be modelled as beam-like objects due to their slender geometry. During operation, endoscopes mainly undergo bending and this justifies the choice of a beam model able to capture the behaviour under large bending deformations. In this work, we consider a 2D Euler elastica and assigned boundary conditions, associated to a second-order Lagrangian L . We derive its equations of equilibrium through a variational principle. Moreover, in order to describe the motion of endoscopes in narrow tubes, the contact problem is modelled by an augmented Lagrangian formulation proposed in [1].

2. Euler elastica beam model

An inextensible 2-dimensional Euler elastica can be treated as a constrained second order Lagrangian problem with augmented Lagrangian $L : T^{(2)}Q \times \mathbb{R} \rightarrow \mathbb{R}$, where $Q \cong \mathbb{R}^2$ is its configuration manifold

$$L(q, q', q'', \Lambda) = \frac{1}{2}EI||q''||^2 + \Lambda(||q'||^2 - 1) \quad (1)$$

Here q represents the coordinates of the centerline of the beam, q' and q'' are its first and second spatial derivatives respectively, E is the Young's modulus of the beam, I is the second moment of the cross-section area, Λ is a Lagrange multiplier. Applying Hamilton's principle to the action functional $S = \int_0^l L(q, q', q'', \Lambda) ds$, where length $l > 0$ is the length of the beam, yields the Euler-Lagrange equations

$$EIq^{(4)} = 2(\Lambda q'' + \Lambda' q') \quad ||q'||^2 = 1 \quad (2)$$

subject to boundary conditions $(q(0), q'(0)) = (q_a, q'_a)$ and $(q(l), q'(l)) = (q_b, q'_b)$. The action integral is discretised in N intervals with space steps Δs . For the discrete Lagrangian $L_d : TQ \times TQ \times \mathbb{R} \times \mathbb{R} \rightarrow \mathbb{R}$ we refer to a discretisation proposed in [4] based on the trapezoidal rule.

$$L_d(q_i, q'_i, q_{i+1}, q'_{i+1}, \Lambda_i, \Lambda_{i+1}) = \frac{\Delta s}{2} [L(q_i, q'_i, (q''_i)^\alpha, \Lambda_i) + L(q_{i+1}, q'_{i+1}, (q''_{i+1})^\alpha, \Lambda_{i+1})] \quad (3)$$

Where

$$(q''_i)^\alpha = \frac{[(1 - 3\alpha)q'_{i+1} - (1 + 3\alpha)q'_i] \Delta s + 6\alpha(q_{i+1} - q_i)}{\Delta s^2} \quad (4a)$$

$$(q''_{i+1})^\alpha = \frac{[(1 + 3\alpha)q'_{i+1} - (1 - 3\alpha)q'_i] \Delta s - 6\alpha(q_{i+1} - q_i)}{\Delta s^2} \quad (4b)$$

By applying the discrete Hamilton's principle [5, 3] to the resulting discrete action $S_d = \sum_{i=0}^{N-1} L_d(q_i, q'_i, q_{i+1}, q'_{i+1}, \Lambda_i, \Lambda_{i+1})$, with fixed $(q_0, q'_0) = (q_a, q'_a)$ and $(q_N, q'_N) = (q_b, q'_b)$, we obtain the discrete Euler-Lagrange equations (DEL), which are the discrete equilibrium equations.

$$\begin{aligned} D_1 L(q_i, q'_i, q_{i+1}, q'_{i+1}, \Lambda_i, \Lambda_{i+1}) + D_3 L(q_{i-1}, q'_{i-1}, q_i, q'_i, \Lambda_{i-1}, \Lambda_i) &= 0 \\ D_2 L(q_i, q'_i, q_{i+1}, q'_{i+1}, \Lambda_i, \Lambda_{i+1}) + D_4 L(q_{i-1}, q'_{i-1}, q_i, q'_i, \Lambda_{i-1}, \Lambda_i) &= 0 \\ D_5 L(q_i, q'_i, q_{i+1}, q'_{i+1}, \Lambda_i, \Lambda_{i+1}) + D_6 L(q_{i-1}, q'_{i-1}, q_i, q'_i, \Lambda_{i-1}, \Lambda_i) &= 0 \end{aligned} \quad (5)$$

Results will be shown in terms of internal forces, i.e. normal and shear forces and bending moment, and total energy of the system. Axial force and shear are conserved along the beam due to the translational invariance of L , i.e. under different boundary conditions. Moreover, a convergence study is performed looking at the energy behaviour. The variational integrator is proved to be symplectic and structure preserving method.

3. Augmented Lagrangian formulation for contact problem

The problem of a beam in contact with a rigid wall is described by the augmented Lagrangian \tilde{L} in Eq. 6 [1].

$$\tilde{L} = L - kg\Lambda_c + \frac{p}{2}g^2 - \frac{1}{2p} (\text{dist}(k\Lambda_c - pg, \mathbb{R}^+))^2 \quad (6)$$

Here, k is a scaling factor, g is the gap function w.r.t. the wall, Λ_c is a Lagrange multiplier, and p is a positive penalty coefficient. One can recognise a Lagrange multiplier term, a penalty term and distance term, where $\xi = k\Lambda_c - pg$ is the augmented Lagrange multiplier. The latter can represent two possible scenarios, i.e. for $\xi < 0$ the contact forces are not active, while for $\xi > 0$ the contact is activated.

4. Conclusions and remarks

Figure 1 shows the elastica in a straight tube, where contact points are identified at the interfaces with the two walls. More complex and narrow geometrical shapes are of particular interest when using the presented contact Lagrangian formulation.

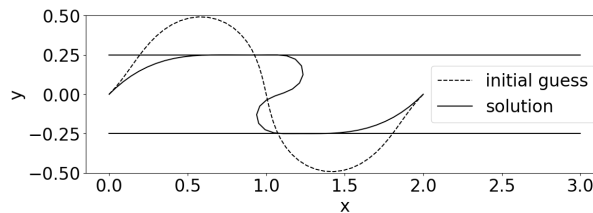


Figure 1: Elastica in a straight tube

Acknowledgments

This project has received funding from the European Union's Horizon 2020 research and innovation programme under the Marie Skłodowska-Curie grant agreement No 860124.



References

- [1] P. Alart, A. Curnier. *A mixed formulation for frictional contact problems prone to Newton like solution methods*, Computer methods in applied mechanics and engineering, vol. 92(3), pp. 353-375, 1991.
- [2] D. A. Singer. *Lectures on elastic curves and rods*, in AIP Conference Proceedings, American Institute of Physics, vol. 1002, pp. 3-32, 2008
- [3] L. Colombo, S. Ferraro, D. Martín de Diego. *Geometric integrators for higher-order variational systems and their application to optimal control*, Journal of Nonlinear Science, vol. 26, pp. 1615-1650, 2016.
- [4] S. J. Ferraro, D. M. de Diego, R. T. Sato Martín de Almagro. *Parallel iterative methods for variational integration applied to navigation problems*, IFAC-PapersOnLine, vol. 54(19), pp. 321-326, 2021.
- [5] J. E. Marsden, M. West. *Discrete mechanics and variational integrators*, Acta numerica, vol. 10, pp. 357-514, 2001.

Energy-momentum conserving time integrator for geometrically exact beam dynamics

Jan Tomec ¹, Gordan Jelenić ²

¹ University of Rijeka, Faculty of Civil Engineering, jan.tomec@uniri.hr

² University of Rijeka, Faculty of Civil Engineering, gordan.jelenic@uniri.hr

Keywords: Geometrically exact beam theory, Numerical time integration, Energy-momentum conservation/decay, Implicit SE(3) interpolation, Lie midpoint rule

1. Introduction

The stability of a time-stepping algorithm for mechanical systems has long been associated with its ability to conserve linear and angular momentum and energy. The same principle can be applied to Cosserat beam problems where the geometrically-exact strains present non-linearities to the system due to the non-commutative properties of the special Euclidean group.

2. Beam kinematics

A beam is characterised by the position of its centreline to which an oriented rigid cross-section is attached. As such, a beam can be placed on the special Euclidean group $SE(3)$ by parametrising its configuration as

$$\mathbf{H} : \mathbb{R} \times [0, L] \subset \mathbb{R} \rightarrow SE(3); (t, s) \mapsto \mathbf{H}(t, s). \quad (1)$$

Traditionally, the position and the orientation have often been considered separately

$$\mathbf{x} \in \mathbb{R}^3, \quad \mathbf{\Lambda} \in SO(3). \quad (2)$$

In $SE(3)$, its configuration can be represented using a configuration matrix, expressed as

$$\mathbf{H} = \begin{bmatrix} \mathbf{\Lambda} & \mathbf{x} \\ \mathbf{0}^T & 1 \end{bmatrix}. \quad (3)$$

The time derivative of \mathbf{H} can be written as

$$\dot{\mathbf{H}} = \mathbf{H}\hat{\mathbf{v}}, \quad (4)$$

where \mathbf{v} is the velocity in the material frame. Strains $\boldsymbol{\varepsilon}$ are obtained through spatial differentiation

$$\mathbf{H}' = \mathbf{H}\hat{\boldsymbol{\varepsilon}}, \quad (5)$$

$$\boldsymbol{\varepsilon} = \boldsymbol{\varepsilon} - \boldsymbol{\varepsilon}_0, \quad (6)$$

where $\boldsymbol{\varepsilon}$ is the configuration spatial derivative in the material frame and index 0 denotes the undeformed configuration.

3. Equation of motion

For a beam of initial length L , the variational formulation of the equilibrium equation in the fixed-pole frame, as presented by Bottasso in [1], can be expressed as follows

$$-\delta\boldsymbol{\eta}(0)^T \mathbf{q}(0) - \delta\boldsymbol{\eta}(L)^T \mathbf{q}(L) + \int_0^L \delta\boldsymbol{\eta}^T (\dot{\mathbf{p}} - \mathbf{q}) + \delta\boldsymbol{\eta}^T \mathbf{f} ds = 0, \quad (7)$$

where $\delta\boldsymbol{\eta}$ are the variations defined as

$$\delta\mathbf{H} = \widehat{\delta\boldsymbol{\eta}}\mathbf{H}, \quad (8)$$

\mathbf{q} denotes external forces, while inertial and internal forces are defined as

$$\mathbf{p} = \mathbf{H}^{-T} \mathbf{M}\mathbf{v}, \quad (9)$$

$$\mathbf{f} = \mathbf{H}^{-T} \mathbf{K}\boldsymbol{\varepsilon}, \quad (10)$$

and \mathbf{M} and \mathbf{K} are the matrices of mass and the stiffness properties of the beam's cross-section.

4. Finite element formulation

Let us define a 2-node $SE(3)$ configuration interpolation as

$$\mathbf{H}(s) = \mathbf{H}_A \exp\left(\frac{s}{L} \hat{\mathbf{d}}\right), \quad \exp(\hat{\mathbf{d}}) = \mathbf{H}_A^{-1} \mathbf{H}_B, \quad (11)$$

where indices A and B indicates nodal values.

An energy-momentum conservative time-stepping algorithm is one that maintains constant total energy, linear momentum, and angular momentum along the solution. It can be showed that the following residual meets these requirements when $\underline{\mathbf{R}}_m = \mathbf{0}$

$$\underline{\mathbf{R}}_m = \int_L \Psi^T (\dot{\mathbf{p}}_m - \mathbf{q}_m) + \Psi'^T \mathbf{f}_m ds, \quad (12)$$

where $\Psi = [\psi_A \mathbf{I} \quad \psi_B \mathbf{I}]$ and ψ_i are the Lagrange polynomial shape functions. The midpoint values (denoted by m) are approximated as

$$\dot{\mathbf{p}}_m = \frac{\mathbf{p}_{n+1} - \mathbf{p}_n}{\Delta t}, \quad (13)$$

$$\mathbf{f}_m = \frac{1}{2} (\mathbf{T}(-\boldsymbol{\eta})^T \mathbf{f}_{n+1} + \mathbf{T}(\boldsymbol{\eta})^T \mathbf{f}_n), \quad (14)$$

where \mathbf{T} is a tangent map in $SE(3)$ [2]. The nodal configuration values are updated from time t_n to t_{n+1} with the time step $\Delta t = t_{n+1} - t_n$ as

$$\mathbf{H}_{n+1} = \exp(\hat{\boldsymbol{\eta}}) \mathbf{H}_n \quad (15)$$

while the integration point velocity values are updated as

$$\text{Ad}_{\mathbf{H}^{-1}}(\boldsymbol{\eta}) = \Delta t \frac{\mathbf{v}_{n+1} + \mathbf{v}_n}{2}. \quad (16)$$

In addition, energy conservation requires interpolation of incremental kinematics and use of the same interpolation functions for the test functions.

5. Conclusions

A new energy-momentum preserving time integration algorithm was developed using beam elements interpolated on the $SE(3)$ Lie group. Conservation of momentum is guaranteed in the absence of external forces using configuration-independent test functions, while conservation of energy is achieved via midpoint approximation of the velocity field and internal forces. An energy decaying algorithm may be obtained by adding an extra term controlled by a damping parameter. The method is easy to implement and can handle large time steps.

Acknowledgments

This project has received funding from the European Union's Horizon 2020 research and innovation programme under the Marie Skłodowska-Curie grant agreement No 860124 and from the Croatian science foundation under the research project FIMCOS (HRZZ IP 2018-01-1732).



References

- [1] Carlo L. Bottasso and Marco Borri. Integrating finite rotations. *Computer Methods in Applied Mechanics and Engineering*, 164(3-4):307–331, 1998.
- [2] V. Sonnevile, A. Cardona, and O. Brüls. Geometrically exact beam finite element formulated on the special euclidean group $se(3)$. *Computer Methods in Applied Mechanics and Engineering*, 268:451–474, 2014.

Implementation and Stability Issues of Lie Group Integrators for Cosserat Rod Models with Constraints

Denise Tumiotto, Martin Arnold

Institute for Mathematics, Martin-Luther-University Halle-Wittenberg, Halle (Saale), Germany
 [denise.tumiotto, martin.arnold]@mathematik.uni-halle.de

Keywords: Numerical Stability, Half-Explicit Lie Group Integrators, Cosserat Rod Model

1. Introduction

An established model for highly flexible slender structures is the Cosserat rod model. It describes the body with a centreline parameter and discrete cross sections along it. To determine the orientation of the cross sections, one needs a parameterization of large rotations without singularities [5]. Typically, the most suitable elements are rotation matrices $SO(3)$ or unit quaternions \mathbb{S}^3 . In particular, the configuration spaces are direct or semi-direct products of the previous sets with \mathbb{R}^3 , equipped with a group operation they are Lie groups (G, \circ) .

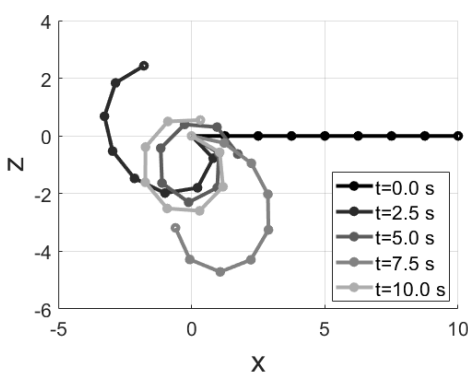
More concerns arise when constraints are introduced. If we consider holonomic constraints, the model includes algebraic variables alongside the differential ones. In fact, the equations describing the constraints are usually coupled with the ODE by the use of Lagrangian multipliers. The approach leads to differential-algebraic equations DAEs, which limit the solution to sub-manifolds of the previous Lie groups [2].

Existing methods include the Lie group version of half-explicit Runge-Kutta methods [1], the Runge-Kutta Munthe-Kaas methods [4], the Lie group generalized- α [2], RATTLie [3]. If the stability for classical Runge-Kutta methods and constrained systems in linear spaces is deeply studied and well known, the numerical stability of the Lie group methods is still an open problem, because nonlinear configuration spaces are involved.

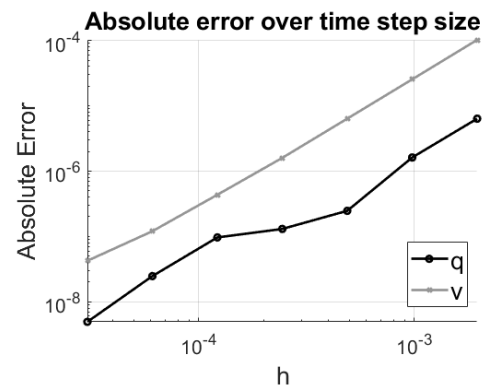
The implementation of the previous methods faces some criticality when introducing the derivative of the exponential map and its inverse. The tangent operator of the exponential map [2] and its derivative may be useful to implement Lie group methods in local parametrization [2, Section 6]. While the tangent operator and its inverse have been inspected and a closed form for the sake of the implementation obtained [3], the evaluation in closed form of the derivative of the tangent operator is an ongoing subject of study. In the present paper, we address the investigation of the stability of the methods in nonlinear settings and the implementation issues for local parametrization of the methods, such as the Lie group half-explicit RK.

2. Numerical results

Typical results involve the discretisation of beam by a staggered grid. On the nodes one may assign the position variable in \mathbb{R}^3 and on the segments' midpoints the rotation variables, unit quaternions \mathbb{S}^3 in our case, see [3]. In Figure 1, we simulate a clamped Cosserat rod subject to a constant momentum on the free extreme. On



(a) Position at multiple times.



(b) Absolute error over the time step h .

Figure 1: Roll-up of a clamped beam.

the left, Figure 1a, we observe snapshots of the beam at different time steps. The time discretisation by the generalized- α Lie group method [2] in the implementation of [3] has second order convergence, see Figure 1b. The plot represents the absolute error of the system variables over the time step size h .

3. Implementation of Lie group integrators

The present paper aims to solve the dynamics of a constrained system of equations using a parametrization of the Lie group in terms of the exponential map. Consider the following equations of motion [2]

$$\dot{q} = DL_q(e) \cdot \tilde{\mathbf{v}}, \quad \mathbf{M}(q)\dot{\mathbf{v}} = -\mathbf{g}(q, \mathbf{v}, t) - \mathbf{B}^\top(q)\boldsymbol{\lambda}, \quad \boldsymbol{\Phi}(q) = \mathbf{0} \quad (1)$$

where the details can be read in [2]. Numerical solutions of the system could be obtained with a Lie group generalized- α scheme as in [2] or with half-explicit Runge-Kutta methods [1]. We here present the latter, starting from the notion that in a neighbourhood of $t = t_m$ any element $q(t) \in G$ is parametrized by elements of the Lie algebra \mathfrak{g} , so that $q(t) = q(t_m) \circ \exp\left(\tilde{\boldsymbol{\theta}}_m(t)\right)$, where $\boldsymbol{\theta}_m(t)$ is the solution of $\dot{\boldsymbol{\theta}}_m(t) = \text{dexp}_{\tilde{\boldsymbol{\theta}}_m(t)}^{-1} \mathbf{v}(t)$, $\boldsymbol{\theta}_m(t_m) = \mathbf{0}$. The first stage is $Q_{m1} = q_m \circ \exp\left(\tilde{\boldsymbol{\Theta}}_{m1}\right)$ with $\boldsymbol{\Theta}_{m1} := \boldsymbol{\theta}_m(t_m) = \mathbf{0}$ and $\mathbf{V}_{m1} = \mathbf{v}_m$, while the following stages are given by

$$Q_{mi} = q_m \circ \exp\left(\tilde{\boldsymbol{\Theta}}_{mi}\right), \quad \boldsymbol{\Theta}_{mi} = h \sum_{j=1}^{i-1} a_{ij} \dot{\boldsymbol{\Theta}}_{mj}, \quad \mathbf{V}_{mi} = \mathbf{v}_m + h \sum_{j=1}^{i-1} a_{ij} \dot{\mathbf{V}}_{mj}, \quad (i = 2, \dots, \bar{s} + 1) \quad (2a)$$

with

$$\dot{\boldsymbol{\Theta}}_{mi} = \text{dexp}_{\tilde{\boldsymbol{\Theta}}_{mi}}^{-1} \mathbf{V}_{mi}, \quad \mathbf{M}(Q_{mi})\dot{\mathbf{V}}_{mi} = -\mathbf{g}(Q_{mi}, \mathbf{V}_{mi}, t_m + c_i h) - \mathbf{B}^\top(Q_{mi})\boldsymbol{\Lambda}_{mi}, \quad (i = 1, \dots, \bar{s}) \quad (2b)$$

The stages for the Lagrange multipliers $\boldsymbol{\Lambda}_{mi}$ are obtained enforcing the constraints (2c) at the velocity level

$$\mathbf{0} = \mathbf{B}(Q_{m,i+1})\mathbf{V}_{m,i+1} = \mathbf{B}(Q_{m,i+1}) \left(\mathbf{v}_m + h \sum_{j=1}^{i-1} a_{i+1,j} \dot{\mathbf{V}}_{mj} + h a_{i+1,i} \dot{\mathbf{V}}_{mi} \right), \quad (i = 2, \dots, \bar{s}) \quad (2c)$$

except for $\boldsymbol{\Lambda}_{m1} := \boldsymbol{\lambda}_m$ for which we apply an explicit stage. The numerical solution at $t = t_{m+1}$ is defined by $q_{m+1} = Q_{m,s+1}$ and $\mathbf{v}_{m+1} = \mathbf{V}_{m,s+1}$ with some $s \leq \bar{s}$, for the Lagrangian multipliers we have $\boldsymbol{\lambda}_{m+1} = \boldsymbol{\Lambda}_{m\bar{s}}$.

4. Conclusions

We are interested in the Lie half-explicit RK methods because of the reduced computational costs and efficient implementation. The study will highlight the efficiency in the implementation and will investigate their stability properties. Given the positive results in the local parametrization, we developed further studies on the implementation of the generalized- α in local coordinates as in [2, Section 6]. Results from both methods will then be compared for the solution of the constrained Cosserat rod model as described by equations (1).

Acknowledgements

This project has received funding from the European Union's Horizon 2020 research and innovation programme under the Marie Skłodowska-Curie grant agreement No 860124.



References

- [1] M. Arnold. *Half-explicit Runge–Kutta methods with explicit stages for differential-algebraic systems of index 2*, BIT Num. Math., Vol. 38 (3) (1998) 415–438.
- [2] O. Brüls, A. Cardona, M. Arnold. *Lie group generalized- α time integration of constrained flexible multi-body systems*, Mechanism and Machine Theory, Vol. 48 (2012) 121–137.
- [3] S. Hante. *Geometric integration of a constrained Cosserat beam model*, PhD thesis, Martin-Luther-Universität Halle-Wittenberg, 2022.
- [4] H. Munthe-Kaas. *Runge-Kutta methods on Lie groups*, BIT Num. Math., Vol. 38 (1) (1998) 92–111.
- [5] I. Romero, M. Arnold. *Computing with Rotations: Algorithms and Applications*, Encyclopedia of Computational Mechanics Second Edition, (2017) 1–27.

MS-4: Teaching the science of modelling and simulation of slender flexible structures for application in industry: A curriculum for early stage researchers

THREAD– Numerical modelling of highly flexible structures for industrial applications. Design of a training programme.

Elena Celledoni¹, Sigrid Leyendecker², Brynjulf Owren¹

¹ Norwegian University of Science and Technology (NTNU), elena.celledoni@ntnu.no,
brynjulf.owren@ntnu.no

² Friedrich-Alexander-Universität, sigrid.leyendecker@fau.de

Keywords: Instructions, Abstract Preparation, Contact Information, Slender Structures (max. five)

1. Introduction

THREAD is a European Training Network (ETN) with funding support from the European Commission addressing modeling and simulation of highly flexible slender structures and their applications.

The mechanical response of slender structures like rods and beams is dominated by very complex phenomena that occur at different spatial and temporal scales. Full-scale 3D models of multimaterial rods based on a detailed representation of their internal structure would imply high complexity and high computational cost. Usual 1D rod models lead to lower-dimensional problems but can hardly reproduce experimental results because of their inadequacy to render local, nonlinear phenomena. On the other hand, geometrically exact 1D beam models (Cosserat rods) provide a faithful representation of the mechanical properties of the slender structures at an acceptable computational complexity.

To understand the geometrical foundations of these models requires however knowledge of differential geometry and Lie groups. This kind of mathematics is taught at universities in advanced courses at master level and it is not part of the standard curriculum in mechanical engineering. The equations are geometric PDEs interesting for their mathematical properties and challenging to approximate with numerical methods. Typically, they require the use of special types of finite element methods to be successfully discretized. The purpose of THREAD is to create a multidisciplinary learning environment of PhD students and senior researchers where mathematicians and mechanical engineers learn and advance together the theory of slender structures for industrial applications. THREAD is a unique network of universities, research organisations and industry from Austria, Belgium, Croatia, France, Germany, Norway, Slovenia and Spain that brings together mechanical engineers and mathematicians around major challenges in industrial applications and simulation software development. It establishes an innovative modelling chain starting from detailed 3D models and experimental measurements to build validated 1D rod models and producing software with outstanding numerical properties.

The 14 Early Stage Researchers (ESRs) benefit from cooperation with twelve industrial partner organisations implementing a comprehensive programme of research secondments and contributing their experience.

2. The training programme of THREAD

With a focus on interdisciplinarity and transferable skills, the THREAD training programme aims at producing candidates that are highly attractive on the job market, in Europe and worldwide.

The training activities of THREAD started in July 2020, with a Summer school on “Fundamentals of beam theory and flexible multibody dynamics” and “Parametrisation of rotations” at the University of Erlangen-Nuremberg, Germany. It comprises 14 network-wide training events organised across Europe and divided in *core research training*, *advanced research training* and *transferable skills training*. The ECOMMAS International Conference on Highly Flexible Slender Structures is the last of the network wide training events. This conference will include special sessions aimed at career perspectives for young researchers.

Acquiring advanced knowledge of Cosserat rod models has been the prime objective of the training programme. The PhD students have been assigned individual research projects and learn through the network wide training activities as well as by discussion with their supervisors and fellow students. Each PhD-project is contributing to address one of the main *industrial challenges* targeted by the THREAD project. The young researchers acquire inter-sectoral experience by working in tight collaboration with the industrial partners and performing

industrial secondments. Particular attention is paid to the training and development of communication skills with numerous, dedicated activities.

The core research training consists of mandatory course work, locally, at each partner institution, and is complemented by advanced and additional research training provided by the consortium via short courses, summer schools, workshops and conferences. The network wide training activities are open for external participation.

The transferable skills training is organised partly locally and partly by the network. The involvement of the industrial partners in the planned training activities is substantial. Each PhD fellow will spend a period of at least three months at one of the partner industries.

3. Conclusions

There is a pressing need of young engineers and mathematicians capable of addressing fundamental questions related with theory and simulation of slender structures. The THREAD project will leverage the training of this new generation of researchers. In this talk I will present the training programme of THREAD, discuss experiences of the practical implementation of the training plans and draw some conclusions about lessons learned and success stories.

Acknowledgments

This project has received funding from the European Union's Horizon 2020 research and innovation programme under the Marie Skłodowska-Curie grant agreement No 860124.

References

- [1] M. Arnold, O. Brüls and J. Linn, *THREAD — Numerical modelling of highly flexible structures for industrial applications*, ECMI Annual report (2019), 20-25.
- [2] O. Brüls, E. Celledoni, J. Gerstmayr and S. Leyendecker, *THREAD — Highly flexible structures for industrial applications*, ECMI Annual report (2021), 43-46.
- [3] <https://thread-etn.eu>

Teaching small and large deformation flexible multibody dynamics

José L. Escalona ¹

¹ Dept. of Mechanical and Manufacturing Engineering, University of Seville, escalona@us.es

Keywords: flexible multibody dynamics, floating frame of reference approach, arbitrary Lagrangian-Eulerian approach, dynamics of reeving systems.

1. Introduction

As part of the THREAD Network Wide Training program, the author had the opportunity to teach the courses:

1. FMBS_FFR: “An introduction to flexible multibody dynamics. The floating frame of reference approach”
2. RV_ALE: “Modeling and simulation of reeving systems using an arbitrary Lagrangian-Eulerian approach”

These two courses correspond to computer techniques for the dynamic analysis of small (FMBS_FFR) and large (RV_ALE) deformation analysis in multibody dynamics. This paper shows the experience and difficulties preparing these courses and the students response.

2. Teaching small deformation analysis in multibody dynamics

The subject of flexible multibody dynamics (FMBS) with the floating frame of reference (FFR) approach is the combination of two computational mechanics fields:

1. Rigid multibody dynamics (MBS) and
2. Linear finite elements (FEM).

Probably all master students in mechanical engineering are educated in FEM. However, MBS are less extended. Instead, students use to have basic knowledge on the theory of machines and mechanisms, but probably not oriented to computer analysis. That is why the FMBS_FFR started with an introduction to MBS. Other topics that the students need to know in advance to follow the course are:

1. Rayleigh-Ritz modeling (modal superposition) of flexible bodies. This technique uses to be covered in medium-level mechanical vibrations course on master level.
2. Analytical mechanics techniques to find the equations of motion of complex dynamics systems, like principle of virtual work in dynamics or Lagrange equations.

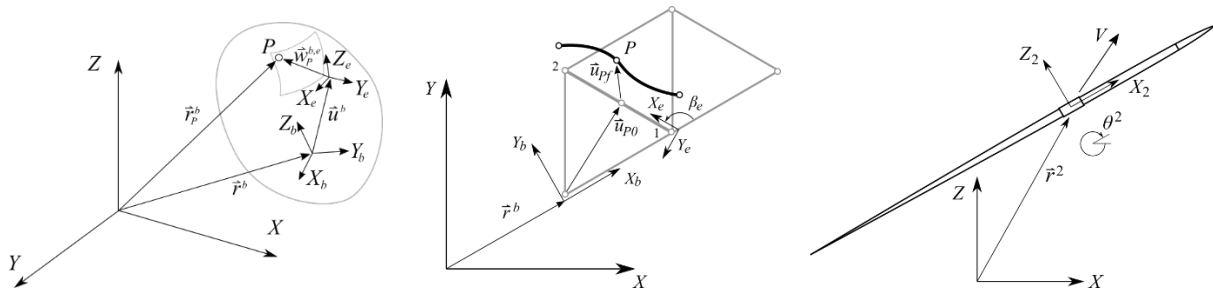


Figure 1. Flexible multibody dynamics. Left: kinematics of the FEM model for large rigid body motion. Middle: 2D truss in space. Right: the flight of a javelin.

In many cases students do not include in their background some of the 4 topics described above. This is a difficulty when teaching FMBS_FFR that is associated with the non-uniformity of the education of the audience. Other difficulties, more related to the contents of the course are:

1. Dealing with many different frames and the required 3D vector and matrix transformation (see Fig. 1).
2. Dealing with the matrix notation.
3. Understanding the calculation, and the importance, of the generalized inertia forces.

The FMBS_FFR included two application examples:

1. The launch of a stone with a catapult, and
2. The free flight of a javelin.

The examples were simple and selected to show the combined analysis of rigid body motion and vibrations, that is the main objective of FMBS. The FMBS_FFR also included a simple, home-made, general purpose Matlab code based on beam models.

The output of the students showed that they got a taste of FMBS and they could understand the concepts used to build the theory and what they can do with it. Following the calculations would require a deep study of the contents of the course.

3. Teaching large deformation analysis in multibody dynamics

While the FMBS_FFR described a well-known, most used method in FMBS, the RV_ALE explained a very specific method of analysis of very flexible mechanical systems. It is clear for the author that the FMBS_FFR was much more important for the education of most of the students than the RV_ALE. However, the RV_ALE brought other benefits, like dealing with very practical large deformable FMBS and advanced modeling techniques under research.

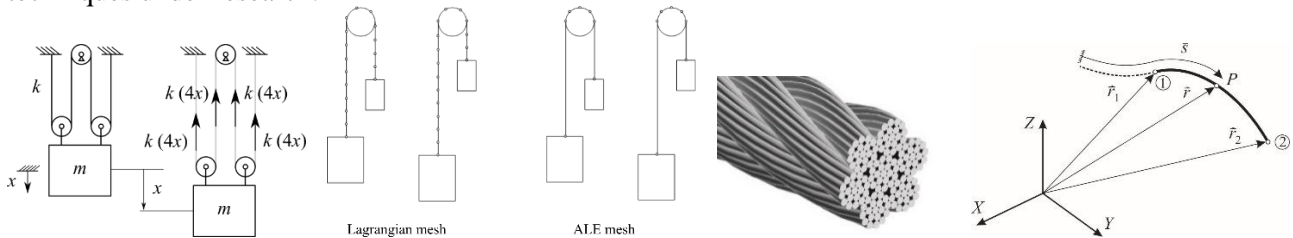


Figure 2. Reeving systems and their modeling with the ALEM approach.

Under the engineering practice point of view, students learnt some insights about how reeving systems work and the mechanical behavior of wire ropes. The specific method for modeling the dynamics of reeving systems is a finite elements method that combines three types of coordinates in the kinematic description of the ropes: (1) absolute position coordinates of the ends of the span, \mathbf{q}_a , (2) arc-length coordinates of the nodal points within the rope, \mathbf{q}_s , and (3) modal coordinates for the description of transverse and axial deformation of the ropes, \mathbf{q}_m . But the most prominent property is the use of an arbitrary Lagrangian-Eulerian description. That means that the finite element nodes are not necessarily attached to material or geometric points. Their position within the flexible body is arbitrary, user defined. The benefits of this approach in dynamic systems where the length of the rope free spans changes continuously are very important, as shown in the 2nd sketch of Fig. 2.

The educational background needed to follow this course was similar than that needed to follow the FMBS_FFR. Main difficulty of RV_ALE was to get familiar with the ALE approach. The used of the arc-length coordinates as nodal coordinates to locate the finite element nodes is not common in computational mechanics. Getting the equations of motion in non-material volumes is also non-conventional in solid mechanics. In comparison with other topics in high deformable flexible bodies, the RV_ALE was original and practical, because:

1. It deals with one of the most common types of mechanism used in machinery that show large deformation and rigid body motion.
2. It deals with a specific structure, the wire rope, that being very important in the industry, does not match the behavior of “classical beams.”
3. It shows a complete methodology and the software that can be used to model any reeving system.

Students found difficulties to follow some of the mathematical derivations. They enjoyed learning practical aspects of the mechanical behavior of reeving systems and wire-ropes.

Acknowledgements

This project has received funding from the European Union's Horizon 2020 research and innovation programme under the Marie Skłodowska-Curie grant agreement No 860124.



References

- [1] Escalona, J.L. “An introduction to flexible multibody dynamics. The floating frame of reference approach”. THREAD NWT1 lecture notes, *Fundamentals of beam theory and flexible multibody dynamics*, online course, June 29-July 3, 2020.
- [2] Escalona, J.L. “Modeling and simulation of reeving systems using an arbitrary Lagrangian-Eulerian approach”. THREAD NWT5 lecture notes, *Summer school on ropes and cables*, Obergurgl, Austria, September 1-5, 2020.

Preparing students for a PhD position in application-oriented research on flexible slender structures.

Joachim Linn¹, Vanessa Dörlich¹

¹Mathematics for the Digital Factory
Fraunhofer Institute for Industrial Mathematics (ITWM)
Fraunhofer-Platz 1, 67663 Kaiserslautern, Germany
[joachim.linn, vanessa.doerlich]@itwm.fraunhofer.de

Keywords: Curriculum, Teaching, Slender structures, Flexible multibody dynamics, Continuum mechanics

1. Introduction

The department Mathematics for the Digital Factory focuses on application-oriented research in the fields of cable simulation and digital human modelling with (flexible) multibody dynamics as the joint methodical core. PhD positions at Fraunhofer ITWM are typically motivated by challenges faced in industrial applications. In the European Training Network THREAD, ITWM contributed to the industrial challenge dealing with virtual product development, digital validation and development of digital twins with a focus on wiring systems in the automotive industry. Specifically, active research topics derived from this challenge include advanced constitutive models for cable systems and hoses as well as mesoscopic effects in multi-wire cables and cable bundles. Doctoral students working on such projects are preferably trained in continuum mechanics in general and specifically in flexible multibody dynamics, constitutive modelling and experimental mechanics.

ITWM contributed to THREAD's core training programme and organised the network wide training (nwt) 2 "Virtual product development with interactive simulation of flexible structures" and nwt 3 "Experimental data acquisition for modelling and validation in industrial applications". The contents of nwt 2 were compiled to achieve two goals in an early stage of the participants' PhD projects: Getting an overview over the daily business in computer-aided design and engineering for flexible structures and thus understanding the motivation for application-driven research. The agenda consisted of practical trainings in IPS Cable Simulation [1], a software for assembly simulation of and validation of cable routing, including typical use cases from automotive industry. The practical sessions were accompanied by theoretical lectures explaining the models and research topics behind different modules of IPS Cable Simulation.

Experimental mechanics are an essential (counter)part of mechanical modelling as they connect theory with reality by determining parameters for a model in the relevant application range using a suitable experiment. The main goal of nwt 3 was to teach the participants the basics of experimental mechanics, data acquisition and model parameter identification specifically for flexible slender objects. This involved teaching the ability to choose the most fitting method to determine model parameters and estimate their range of validity. The training included a practical course on experiments for cables including MeSOMICS[®] measurements [2] and tasks in IPS Cable Simulation.

In this contribution, the authors will describe the background knowledge that potential doctoral students preferably possess to be successful in an application-oriented research topic and give a summary of the contents of THREAD's nwt 2 and nwt 3.

Acknowledgments

This project has received funding from the European Union's Horizon 2020 research and innovation programme under the Marie Skłodowska-Curie grant agreement No 860124.



References

- [1] IPS Cable Simulation, www.flexstructures.com
- [2] www.mesomics.eu

MS-5: Advanced models and numerical formulations for the interaction of beams and the coupling of beams with solids

A note on modeling potential-based interactions between plane beams

Aleksandar Borković¹, Michael H. Gfrerer², Benjamin Marussig³, Roger A. Sauer⁴

¹ Graz University of Technology, aborkovic@tugraz.at; University of Banja Luka

² Graz University of Technology, gfrerer@tugraz.at

³ Graz University of Technology, marussig@tugraz.at

⁴ Gdansk University of Technology, roger.sauer@pg.edu.pl; RWTH Aachen University

Keywords: section-section interaction potential, isogeometric analysis, rotation-free beam model

1. Introduction

Mechanical behavior of various slender bodies at micro- and nano-level is often governed by intermolecular forces. These forces arise from interaction potentials (IP). The examples are electrostatic, steric and van der Waals forces. If the IP law is known, computational modeling of these interactions is rather straightforward using the molecular dynamics approach where an IP between each molecule is taken into account. However, such an approach is computationally expensive for the fine time and spatial resolutions that are often required. The main problem is that the integration has to be done with respect to the volumes of all interacting bodies. In order to accurately and efficiently model these interactions, a *coarse-grained* approach is proposed in the literature [1]. This technique provides a reasonable balance between accuracy and efficiency by coarse-graining and homogenizing the molecular model, and using the well-established continuum mechanics of solid bodies.

A novel method for the modeling of potential-based (PB) interactions between deformable beams has recently been developed [2]. The main idea is to pre-integrate an IP with respect to the cross-sections of interacting beams. The approach is designated as section-section IP (SSIP) and compelling results are obtained [3, 4].

Motivated by the importance of PB interactions between slender bodies, this work further investigates the SSIP approach. IP is modeled using rotation-free Bernoulli-Euler (BE) beam theory and isogeometric analysis (IGA).

2. Methods

Let us consider two beams that represent assemblies of molecules with positions $\bar{\mathbf{r}}_i$. An IP between two molecules, separated by the distance $x = \|\bar{\mathbf{r}}_{12}\| = \|\bar{\mathbf{r}}_2 - \bar{\mathbf{r}}_1\|$, is $\Phi(x)$. Among various IPs, let us focus on the well-known Lennard-Jones IP that is suitable for the modeling of van der Waals attraction and steric repulsion:

$$\Phi_{LJ}(x) = 4\epsilon \left[\left(\frac{\sigma}{x}\right)^{12} - \left(\frac{\sigma}{x}\right)^6 \right] \quad \rightarrow \quad \mathbf{f}_{21} = -\nabla_2 \Phi_{LJ}(x) = -\frac{\partial \Phi_{LJ}(x)}{\partial x} \hat{\mathbf{r}}, \quad \text{with} \quad \hat{\mathbf{r}} = \frac{\bar{\mathbf{r}}_{12}}{\|\bar{\mathbf{r}}_{12}\|}, \quad (1)$$

where $-\epsilon$ is the minimal value of the IP, σ is the distance at equilibrium, and \mathbf{f}_{21} is the force acting on molecule 2. To find the total IP and corresponding force, this potential must be integrated over both assemblies leading to two nested 3D integrals. The SSIP technique allows us to reduce this integral to two nested 1D integrals with respect to the axes of both beams. In order to make SSIP feasible, several assumptions are required, such as an assumption of rigid cross-sections. Furthermore, the utilized SSIP disregards orientation between cross-sections. It is argued in [2, 3] that such a set of assumptions leads to an accurate and efficient formulation.

In this work, an IGA rotation-free BE beam model is utilized [5] and both static and implicit dynamic procedures are implemented. Several issues emerge for PB computational models. For example, the forces that act on each assembly depend on the configurations of both assemblies. This makes the off-diagonal blocks of the coupled stiffness matrix dense. Furthermore, some IPs are short-ranged, meaning that they rapidly decay with distance, see Eq. (1). To save computational time, it is possible to employ a cut-off distance. This significantly reduces computational time but requires an efficient interaction-pair search algorithm.

3. Numerical example

Let us consider a numerical experiment of peeling and pull-off of two fibers with circular cross-sections that interact via the LJ potential, Fig. 1a. Almost all input data is the same as in [3] and no units are specified. Since

this example requires very fine spatial and time discretizations, we have reduced the length to 2 in order to speed up the computation. Each beam is meshed with 20 quartic elements, while 24 integration points per element are employed for integrating the IP. For static analysis, the nonlinear solver struggles to find equilibrium after the pull-off [3]. To alleviate this issue, we have employed dynamic analysis with a mass density of $\rho = 0.001$ and stiffness-proportional viscous damping with $k_c = 0.0025$. The displacement $U_x(t) = 5t$ is prescribed to the supports of the right beam, and the characteristic simulation snapshots are shown in Fig. 1b. Furthermore, the horizontal reaction is plotted in Fig. 1c. The observed behavior is quite complex and in-line with the observations in [3]. Moreover, a brief parametric analysis is done by varying cut-off distances. Fig. 1c shows the corresponding results for $d = 0.1$ and $d = 0.05$. The results are practically the same until the pull-off phase, while the computational time is reduced by a factor of 3.

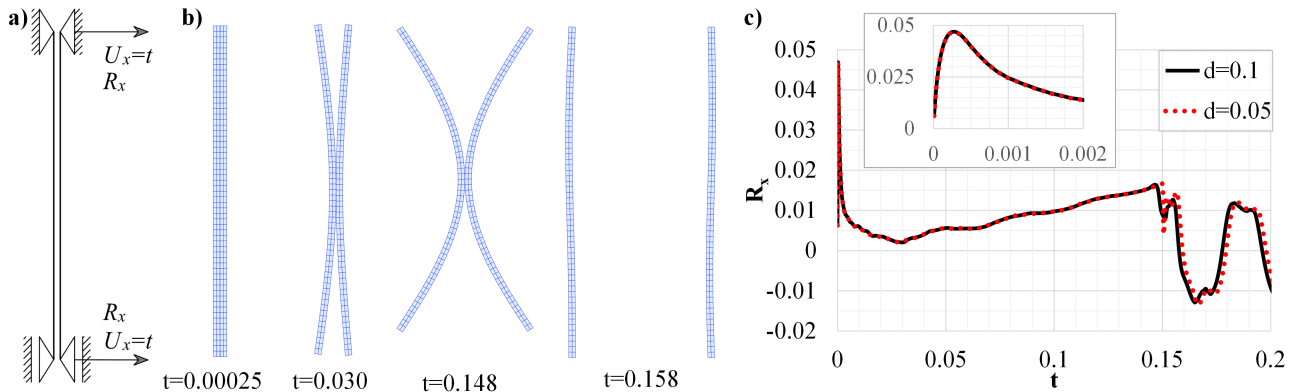


Figure 1: Peeling and pull-off of two fibers. a) Problem setup. b) Characteristic snapshots. c) Reaction force for two values of cut-off distance.

4. Conclusions

The SSIP approach is implemented in the context of IGA using the rotation-free BE model. The dynamic analysis allows for finding equilibrium configurations after the pull-off phase. By a careful selection of the cut-off distance, computational can be significantly reduced. Several new research directions are envisaged, such as consideration of Timoshenko beam, beams with deformable cross-sections and self-interactions.

Acknowledgments

This research was funded in part by the Austrian Science Fund (FWF) P 36019-N. For the purpose of open access, the authors have applied a CC BY public copyright license to any Author Accepted Manuscript version arising from this submission.

References

- [1] R.A. Sauer, S. Li. *A contact mechanics model for quasi-continua*, International Journal for Numerical Methods in Engineering, 71(2007) 931–962
- [2] M.J. Grill, W.A. Wall, C. Meier. *A computational model for molecular interactions between curved slender fibers undergoing large 3D deformations with a focus on electrostatic, van der Waals, and repulsive steric forces*, International Journal for Numerical Methods in Engineering, 121(2020) 2285–2330
- [3] M.J. Grill, C. Meier, W.A. Wall. *Investigation of the peeling and pull-off behavior of adhesive elastic fibers via a novel computational beam interaction model*, The Journal of Adhesion, 97 (2021) 730–759
- [4] C. Meier, M.J. Grill, W.A. Wall. *Generalized Section-Section Interaction Potentials in the Geometrically Exact Beam Theory: Modeling of Intermolecular Forces, Asymptotic Limit as Strain-Energy Function, and Formulation of Rotational Constraints*, preprint at arXiv.org, 2022
- [5] A. Borković, M.H. Gfrerer, B. Marussig. *Geometrically exact isogeometric Bernoulli–Euler beam based on the Frenet–Serret frame*, Computer Methods in Applied Mechanics and Engineering, 405(2022) 115848

An isogeometric three-field mixed finite element formulation of nonlinear beam structures with extensible directors

Myung-Jin Choi ^{1*}, Sauer A. Roger ^{2,3,4}, Sven Klinkel ¹

¹ Chair of Structural Analysis and Dynamics, RWTH Aachen University, Mies-van-der-Rohe Str. 1, 52074 Aachen, Germany

² Aachen Institute for Advanced Study in Computational Engineering Science (AICES), RWTH Aachen University, klinkel@lbb.rwth-aachen.de

³ Faculty of Civil and Environmental Engineering, Gdańsk University of Technology, ul. Narutowicza 11/12, 80-233 Gdańsk, Poland

⁴ Department of Mechanical Engineering, Indian Institute of Technology Guwahati, Guwahati, 781039, Assam, India

* Corresponding author (choi@lbb.rwth-aachen.de)

Keywords: Isogeometric analysis, Beam structures, Extensible directors, Locking, Path independence

1. Introduction

We present an isogeometric mixed finite element formulation for geometrically and materially nonlinear beam structures, based on the three-field Hu-Washizu variational principle. This alleviates not only membrane and transverse shear locking, but also curvature-thickness locking, associated with an artificial cross-sectional stretching by the finite element approximation of the extensible director field. It further significantly improves the stability of the convergence in the Newton-Raphson iteration in the thin beam limit. We employ the B-spline basis functions, to approximate the displacement and director fields along the beam's center axis, which is referred to as *isogeometric* analysis. The higher order continuity of the basis functions eventually gives superior *per-degree-of-freedom* accuracy, in comparison to conventional C^0 finite element analysis (FEA). In several numerical examples, we verify the accuracy and efficiency of the formulation, as well as the path independence of the solution.

2. Three-field mixed variational formulation of beams

The beam kinematics assumes the position vector of an arbitrary point in the cross-section to be a linear function of the transverse coordinates ζ^1 and ζ^2 , as

$$\mathbf{x}_t(\zeta^1, \zeta^2, s) = \boldsymbol{\varphi}(s) + \zeta^1 \mathbf{d}_1(s) + \zeta^2 \mathbf{d}_2(s), \quad (1)$$

where $\boldsymbol{\varphi}(s)$ denotes the position of the beam's center axis, and \mathbf{d}_1 and \mathbf{d}_2 denote the *extensible* directors. s denotes the arc-length coordinate of the initial center axis. This first order beam kinematics can be further generalized to an arbitrary order, see [2]. In the mixed formulation, we obtain the internal virtual work, as

$$G_{\text{int}}^{\text{HW}} := \int_0^L \left[\delta \mathbf{y} \cdot \mathbb{B}_{\text{total}}^T \mathbf{r}_p + \delta \mathbf{r}_p \cdot \underbrace{\{\boldsymbol{\varepsilon}(\mathbf{y}) - \boldsymbol{\varepsilon}_p\}}_{\text{compatibility}} + \delta \boldsymbol{\varepsilon}_p \cdot \underbrace{\{\partial_{\boldsymbol{\varepsilon}_p} \Psi(\boldsymbol{\varepsilon}_p) - \mathbf{r}_p\}}_{\text{constitutive law}} \right] ds, \quad (2)$$

where $\boldsymbol{\varepsilon}_p$ and \mathbf{r}_p denote the arrays of the physical strain and stress resultants of the beam, respectively, and $\boldsymbol{\varepsilon}$ denotes the array of geometrical (compatible) strains. \mathbf{y} denotes the displacement of the center axis and the directors. Ψ denotes the strain energy density function. The strain-displacement operator $\mathbb{B}_{\text{total}}$ for the geometrical strain can be found in [1]. The physical beam strains and stress resultants are considered as independent unknown variables.

3. Numerical examples

The first example shows the superior *per-degree-of-freedom* accuracy of IGA, compared with the conventional FEA (see Fig. 1b). The second example verifies the path independence of the IGA solution, see Fig. 2b for the exactly overlapped deformed beam configuration between every prescribed rotation angle (θ) and its multiples.

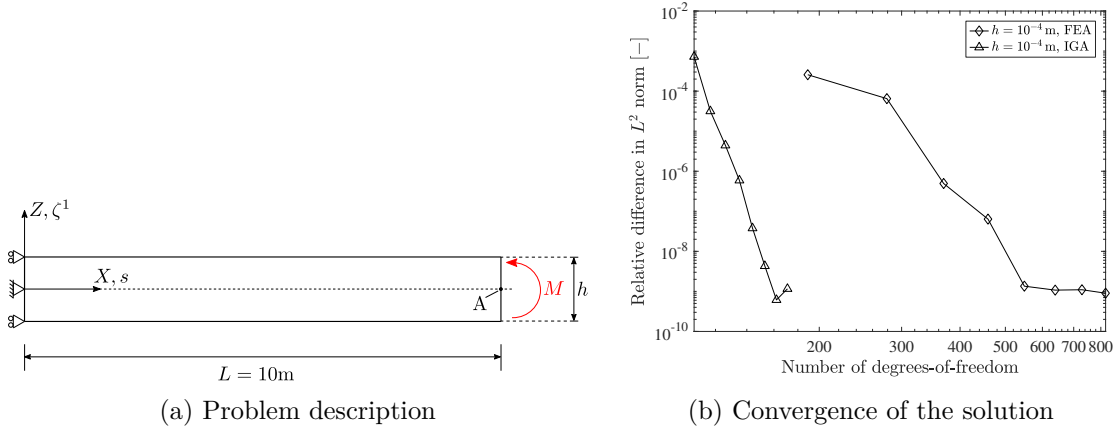


Figure 1: Cantilever beam under end moment. Young’s modulus $E = 1.2 \times 10^7$ Pa, Poisson’s ratio $\nu = 0$, and the slenderness ratio $L/h = 10^5$. For the same number of elements $n_{el} = 10$, every data point in each graph represents the result of using degree of basis functions $p = 2, 3, \dots, 9$.

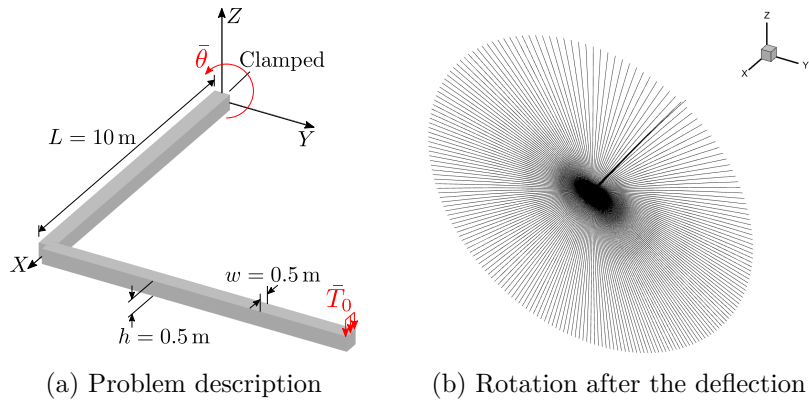


Figure 2: L-shaped beam. Young’s modulus $E = 10^7$ Pa, and the Poisson’s ratio $\nu = 0.3$, and the distributed force $\bar{T}_0 = -200$ N/m.

4. Conclusions

We present an isogeometric mixed finite element formulation for hyperelastic beam structures, based on the three-field Hu-Washizu variational principle. We verify that the developed formulation alleviates the locking effects, and significantly improves the stability in the Newton-Raphson iteration process in thin beam limit. Further, in the numerical examples, we show the superior per-degree-of-freedom accuracy in the isogeometric analysis due to the higher order continuity of basis functions, compared with the conventional FEA.

Acknowledgments

M.-J. Choi would like to gratefully acknowledge the financial support of a postdoctoral research fellowship from the Alexander von Humboldt Foundation in Germany.

References

- [1] M.-J. Choi, R.A. Sauer, and S. Klinkel *An isogeometric finite element formulation for geometrically exact Timoshenko beams with extensible directors*, Computer Methods in Applied Mechanics and Engineering, 385 (2021) 113993
- [2] M.-J. Choi, S. Klinkel, and R.A. Sauer *An isogeometric finite element formulation for frictionless contact of Cosserat rods with unconstrained directors*, Computational Mechanics, 70 (2022), 1107-1144

Nonlinear Dynamics of Complex 3D Rod Assemblies

Rufus Dickinson¹, Alessandro Palmeri¹, Timothy I. Marjoribanks¹

¹ Loughborough University, {R.Dickinson, A.Palmeri, T.I.Marjoribanks}@Lboro.ac.uk

Keywords: Rod assembly, n-pendulum, Nonlinear dynamics, Flow-induced reconfiguration, Fractal structure

1. Introduction

n -pendula with rotational springs have previously been used to describe 2D dynamics of slender structures (e.g., simple beams), but this approach has not so far been generalized to the case of 3D dynamics. The research presents a method for applying a set of inverse and forward dynamics algorithms to this type of highly flexible structural system. The motivation of this method over those using traditional continuum formulations is that the joint-angle coordinate system potentially allows a more efficient simulation of structures that primarily undergo bending, without significant shearing and stretching deformations.

2. Methodology

In Ref. [1], Saha has derived modifications to general equations of 3D multi-body motion, applying distance constraints to serially connect rigid bodies. The resulting equations are written in terms of twist and wrench, i.e., the six-dimensional vectors used in Ball's "screw theory", widely used in robot mechanics (e.g., [2]). Recursive forward and inverse dynamics algorithms are provided with $O(n)$ complexity, where n is the number of rigid bodies. In Ref. [3], Shah extends these algorithms to describe branching (non-serial) assemblies. In this work, the dynamics of branching n -pendula are solved with these algorithms.

Three orthogonal rotary springs are added at each pendulum joint to model material stiffness, akin to how this is achieved in 2D models. Within the algorithms presented by Shah [3], these springs can simply be included as internal (driving) forces. Additionally, an algorithm change is proposed to facilitate the application of spatially and temporally varying external forces. In the original method, a constant vector $\rho = \{0, 0, 0, g, 0, 0\}^T$ for gravity is added to the rate-of-twist of the root node, and the effect of this is propagated over the rigid body network by the inverse dynamics algorithm. In this paper, this step is replaced by adding a new vector $\rho(t, \text{node}_i)$ to the twist-rate of each node i after the propagation step, where ρ is now a function of the time t and the node's physical and kinematic properties and represents the sum of the external forces applied to that node.

In this study, the above modifications have been implemented to dynamically model flexible assemblies with serial and tree topologies, for validation first and then demonstration, respectively. Readers interested in the implementation of looping topologies can find a method for doing so in Ref. [4].

3. Results

3.1. Cantilever Deformation

To validate that the kinematic methods were implemented correctly and appropriately, two tests were performed on a cantilever beam with circular cross section. In Fig. 1(a), the deformed states under two load cases are shown, with their inaccuracy given in comparison to Euler-Timoshenko beam theory. A pendulum with 15 elements was used to model the beam. In Fig. 1(b), an example of 3D behaviour is assessed. Under a perpendicular load, a circular section rod should theoretically deform parallel to the load direction, which the model only fails to reasonably achieve at very low resolutions. Between cardinal directions the error is non-zero, because the rotational springs act independently.

3.2. Complex Assemblies

The nature of the n -pendula model makes it well-suited to describing structures of inhomogeneous geometry and rigidity. The results in Fig. 2(a) demonstrate this capability, by replicating the results of a two-dimensional n -pendula, which was formed and validated experimentally by Marjoribanks & Paul [5]. Two 30 cm cantilevers

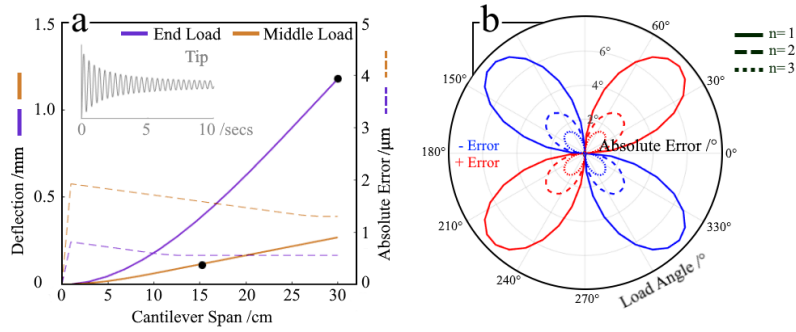


Figure 1: (a) Rest positions for a cantilever under two point loads (Inset, time history of end load oscillation). (b) The variation of error with deformation direction at different pendulum resolutions, in another test.

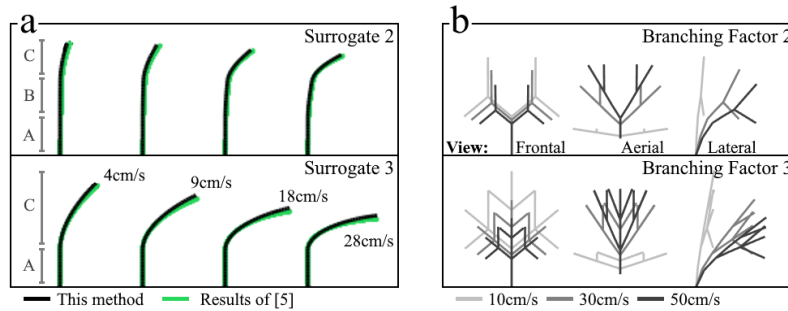


Figure 2: (a) Bending of composite beams under increasing flow speeds. Materials A,B, and C have decreasing rigidity (see Ref. [5] for details). (b) Deformation of two fractal structures under increasing flow speed, from three viewing planes, exhibiting vertical and horizontal compaction.

of varying rigidity are shown deforming under increasing fluid flow speeds, with the effect of the water given by the buoyant force plus a modified drag equation as used in the original study.

In Fig. 2(b), three fractal structures are shown deforming under increasing flow speeds. This demonstrates how the model can be used for complex assemblies, such as multi-stem aquatic plants which, so far, have not been simulated at the scale of individual stems like in the present study.

4. Conclusions

Modifications are made to a set of 3D dynamics algorithms in order to model complex tree structures with flexible, slender components using an n -pendula representation. These modifications, which implement material stiffness and spatially/temporally varying external forces, are shown to be valid for the deformation of a simple cantilever. They are further validated by replication of results for a variable-rigidity cantilever and, finally, are demonstrated on fractal trees to showcase initial results with assemblies of complex topology.

References

- [1] S. K. Saha. Dynamics of serial multi-body systems using the decoupled natural orthogonal complement matrices. *Journal of Applied Mechanics*, 66, 1999.
- [2] H Lipkin and J Duffy. Sir robert stawell ball and methodologies of modern screw theory. *Proceedings of the Institution of Mechanical Engineers, Part C: Journal of Mechanical Engineering Science*, 216(1), 2002.
- [3] S. V. Shah. *Modular Framework for Dynamic Modeling and Analyses of Tree-Type Robotic Systems*. PhD thesis, Indian Institute of Technology Delhi, 2011.
- [4] M. Koul et al. Reduced-order forward dynamics of multiclosed-loop systems. *Multibody System Dynamics*, 31, 2014.
- [5] T. I. Marjoribanks and M. Paul. Modelling flow-induced reconfiguration of variable rigidity aquatic vegetation. *Journal of Hydraulic Research*, 60, 2021.

Transitioning from solids to first-order shear deformable beams

Klarmann S.¹, Wackerfuß J.², Klinkel S.³

¹ Chair of Structural Analysis and Dynamics, RWTH Aachen University, klarmann@lbb.rwth-aachen.de

² Institute of Structural Analysis, University of Kassel, wackerfuss@uni-kassel.de

³ Chair of Structural Analysis and Dynamics, RWTH Aachen University, klinkel@lbb.rwth-aachen.de

Keywords: Beam-Solid coupling, Transition element, Coupled models, Deformable cross-section, Hybrid-mixed finite element formulation

1. Introduction

This contribution presents an approach to couple solid and beam elements such that no spurious stresses occur on the solid side at the transition zone. The proposed element formulation achieves the transition from a solid to a beam displacement field, allowing general cross-sectional deformations, see [1]. One of the key features of the element is that it only requires data of the mesh and the solid material data. Further information, like the warping function, center of gravity, or other cross-sectional information, is not required. This allows the connection of beam elements at any point of the cross-section without additional considerations. Such transition elements are essential in many applications, e.g., substructural modeling or homogenization. In the latter, avoiding spurious stresses at the boundaries is very important to reduce the necessary length of a so-called representative volume element.

2. Assumed Kinematics

The proposed element connects a solid surface to a beam node, achieving the transition from a continuum displacement field \mathbf{u}_S to a beam displacement field $\mathbf{u}_B = \mathbf{u}_{B0} + \xi_2 \mathbf{A}_1 \beta$. Herein, \mathbf{A}_1 is the normal vector on Γ_S and Γ_B , \mathbf{u}_{B0} the displacements on the beam point, β the rotation of that point, and \mathbf{A}_1 and \mathbf{A}_2 represent the local orthonormal basis system of the beam. Additionally, faces Γ_S and Γ_B are identical and only shifted by ℓ in the \mathbf{A}_1 direction. Both faces are initially plane and parallel. The transition is achieved inside the domain Ω_I of the

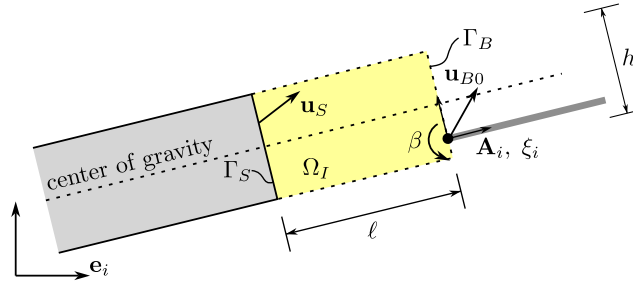


Figure 1: Solid model (gray), connected by transition element (yellow) to beam model (gray line).

transition element; see Figure 1. The domain possesses the same material properties as the solid gray part of the model. The connection point of the beam element is arbitrarily located on the cross-section plane. With this at hand, the displacement field inside the transition zone is a linear interpolation between the displacements of the solid side \mathbf{u}_S and the beam displacements \mathbf{u}_B . In the local coordinate system \mathbf{A}_i , the displacement field reads:

$$\mathbf{u} = \begin{bmatrix} u_1 \\ u_2 \end{bmatrix} = -\frac{\xi_1}{\ell} \begin{bmatrix} \mathbf{A}_1 \cdot \mathbf{u}_S \\ \mathbf{A}_2 \cdot \mathbf{u}_S \end{bmatrix} + \left(1 + \frac{\xi_1}{\ell}\right) \begin{bmatrix} \mathbf{A}_1 \cdot (\mathbf{u}_{B0} - \beta \xi_2 \mathbf{A}_1) \\ \mathbf{A}_2 \cdot \mathbf{u}_{B0} \end{bmatrix}. \quad (1)$$

With eq. (1) the strain state can be defined. Assuming small strains, it reads

$$\begin{bmatrix} \varepsilon_1 \\ \varepsilon_2 \\ 2\varepsilon_{12} \end{bmatrix} = \begin{bmatrix} u_{1,1} \\ u_{2,2} \\ u_{1,2} + u_{2,1} \end{bmatrix} = \begin{bmatrix} \frac{1}{\ell} (\mathbf{u}_{B0} - \beta \xi_2 \mathbf{A}_1 - \mathbf{u}_S) \cdot \mathbf{A}_1 \\ -\frac{\xi_1}{\ell} \mathbf{A}_2 \cdot \mathbf{u}_{S,2} \\ -\frac{\xi_1}{\ell} \mathbf{A}_1 \cdot \mathbf{u}_{S,2} - \left(1 + \frac{\xi_1}{\ell}\right) \beta + \frac{1}{\ell} [\mathbf{u}_{B0} - \mathbf{u}_S] \cdot \mathbf{A}_2 \end{bmatrix}. \quad (2)$$

It is important to note that in eq. (2) the cross-section at the beam node does not deform.

3. Weak form of equilibrium

Based on Figure 1, the weak form of equilibrium can be written as:

$$g = g_S + g_I + g_B = 0. \quad (3)$$

In eq. (3) g_S are the solid, g_B the beam, and g_I the transition zone part of the weak form of equilibrium. The part g_I of the weak form of equilibrium is the actual contribution of this paper. It reads:

$$g_I(\mathbf{u}, \boldsymbol{\sigma}_p, \boldsymbol{\varepsilon}_p, \boldsymbol{\varepsilon}_c, \delta \mathbf{u}, \delta \boldsymbol{\sigma}_p, \delta \boldsymbol{\varepsilon}_p, \delta \boldsymbol{\varepsilon}_c) = \int_{\Omega_I} \left\{ (\delta \boldsymbol{\varepsilon} + \delta \boldsymbol{\varepsilon}_c)^T \boldsymbol{\sigma}_p + \delta \boldsymbol{\sigma}_p^T ((\boldsymbol{\varepsilon} + \boldsymbol{\varepsilon}_c) - \boldsymbol{\varepsilon}_p) + \delta \boldsymbol{\varepsilon}_p^T (\mathbf{C} \boldsymbol{\varepsilon}_p - \boldsymbol{\sigma}_p) \right\} d\Omega. \quad (4)$$

The parts of eq. (4) are the displacements \mathbf{u} , the geometric strains $\boldsymbol{\varepsilon}$ resulting from the symmetric gradient of \mathbf{u} , the independent strains $\boldsymbol{\varepsilon}_p$, the independent stresses $\boldsymbol{\sigma}_p$, and the correction strains $\boldsymbol{\varepsilon}_c$. The correction strains are responsible for the cross-sectional deformations, and their approximation is inspired by [2] and read

$$\boldsymbol{\varepsilon}_c = \begin{bmatrix} \boldsymbol{\omega}_1 & \mathbf{0} & \mathbf{0} \\ \mathbf{0} & \boldsymbol{\omega}_{2,2} & \mathbf{0} \\ \mathbf{0} & \mathbf{0} & \boldsymbol{\omega}_{1,2} \end{bmatrix} \hat{\boldsymbol{\varepsilon}}_c, \quad \text{with} \quad \int_h \boldsymbol{\omega}_1^T d\Gamma_B = \mathbf{0}, \quad \int_h \xi_2 \boldsymbol{\omega}_1^T d\Gamma_B = \mathbf{0}, \quad \text{and} \quad \int_h \boldsymbol{\omega}_2^T d\Gamma_B = \mathbf{0}. \quad (5)$$

The correction strains are specified by general deformation function $\boldsymbol{\omega}_1$ and $\boldsymbol{\omega}_2$ which fulfill the orthogonality condition in eq. (5), and are scaled with their associated values in $\hat{\boldsymbol{\varepsilon}}_c$.

4. Finite Element Formulation

Due to the non-local character of the correction strains, the element formulation is not a standard finite element formulation. It consists of an assembly of all the surface elements of the solid boundary Γ_S and the beam node. The surface displacement field \mathbf{u}_S is approximated with standard local nodal shape functions. Furthermore, the geometry and displacement field interpolation are comparable to the approximation in [3]. The independent stresses and strains are interpolated with shape functions local to a single surface element, thus discontinuous inside the transition element. For the correction strains, the same shape functions as the displacement field \mathbf{u}_S are chosen, but they get extended with a non-local component such that the orthogonality conditions in eq. (5) are satisfied. Further details about the element formulation can be found in [1].

5. Conclusion

The proposed element formulation incorporates cross-sectional deformations based on local degrees of freedom (Dofs). These additional Dofs can be condensed out on the element level such that the element has only displacement degrees of freedom. Thus, connecting classical solid elements with classical beam elements is possible. For the present 2D case, the element possesses exactly three non-zero eigenvalues, which can be related to the beam's tension, bending, and shearing stiffness. The resulting shear stiffness of the element includes the correct shear correction factor. One key feature is that only the mesh and the typical continuum material parameters must be specified. It is not required to compute any additional parameters like warping functions a priori.

References

- [1] S. Klarmann, J. Wackerfuß, S. Klinkel. *Coupling 2D continuum and beam elements: a mixed formulation for avoiding spurious stresses*, Computational Mechanics, 70 (2022) 1145-1166
- [2] J. Wackerfuß, F. Gruttmann. *A nonlinear Hu–Washizu variational formulation and related finite-element implementation for spatial beams with arbitrary moderate thick cross-sections*, Computer Methods in Applied Mechanics and Engineering, 200 (2011) 1671-1690
- [3] T. C. Gmür, R. H. Kauten. *Three-dimensional solid-to-beam transition elements for structural dynamics analysis*, International Journal for Numerical Methods in Engineering, 36 (1993) 1429-1444

Coupling 1D beam elements with 3D solid elements for the modelling of fibre-reinforced composites

Valentin Poussard¹, Camille Gandiolle¹, Damien Durville¹

¹ Université Paris-Saclay, CentraleSupélec, ENS Paris-Saclay, CNRS, LMPS-Laboratoire de Mécanique Paris-Saclay, 91190, Gif-sur-Yvette, France, valentin.poussard@centralesupelec.fr, camille.gandiolle@centralesupelec.fr, damien.durville@centralesupelec.fr

Keywords: 1D-3D coupling, finite elements, overlapping meshes, fibre-reinforced composites

1. Purpose

Specific applications require fibrous structures to be embedded inside a matrix. The penetration of the matrix between the fibres may result in important local stresses, which affect the macroscopic behaviour of the composite. This represents a challenge for numerical simulation, which can be addressed using a full 3D finite elements model. Considering the slenderness of the fibres, a more time-efficient approach consists in using a 1D-3D finite elements model with non-conforming meshes [1]. In the proposed model, coupling is ensured using a pointwise penalty method. Additional 1D structural elements are introduced between fibres when the thickness of the matrix layer is smaller than the 3D solid elements of the matrix mesh, to account for the specific behaviour of such a thin layer.

2. Methodology

The model uses overlapping meshes. The fibres are modelled using 1D elements with enriched kinematics, as described in [2]. The matrix is modelled using a coarse, structured 3D mesh. Both meshes overlap and are coupled with a pointwise penalty method: coupling elements are equally distributed at the surface of the fibres embedded in the matrix (Figure 1). Each coupling element E_i^{F-M} links a fibre particle ξ_i^F to its overlapping matrix particle ξ_i^M in the reference configuration:

$$E_i^{F-M} = (\xi_i^F, \xi_i^M) \mid x^0(\xi_i^F) = x^0(\xi_i^M) = A_i \quad (1)$$

where x^0 refers to the particle position in the reference configuration. The relative displacement of the two particles is penalised by adding a term w_{F-M} to the virtual work:

$$w_{F-M} = K_{F-M} (x(\xi^F) - x(\xi^M), v(\xi^F) - v(\xi^M)) \quad (2)$$

where K_{F-M} represents the coupling element stiffness, x is the current position of the particle and v is its virtual displacement. Whereas standard displacement fields are used to describe the kinematics of the matrix particle ξ^M , beam displacement fields are used to follow the fibre particle ξ^F .

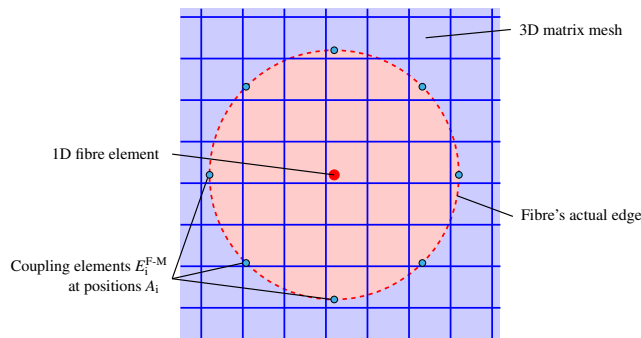


Figure 1: Representation of the fibre-matrix coupling in a fibre cross-section

When the thickness of the matrix is small compared to the dimensions of the 3D elements of the matrix mesh, additional refining 1D bridge elements are introduced between wires to account for the matrix behaviour at

these locations [3]. The bridge elements act as springs, coupling two wires in three directions, as shown in Figure 2. The stiffness of the bridge elements is non-linear, and determined using a full 3D finite elements model of a matrix bridge.

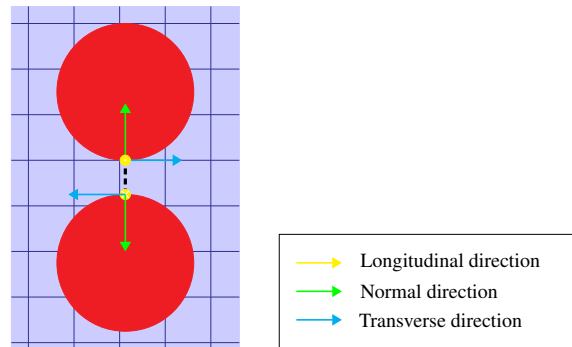


Figure 2: Representation of a 1D bridge element between two fibres and the associated coupling forces directions

3. Results

Simple tests with two fibres were performed to validate the model. It was then used to simulate rubber-embedded metallic cables. Further developments were made to deal with the matrix material incompressibility, especially regarding computation stability. Tensile tests were performed against experimental data to validate the model at the cable scale. More complex loading cases such as cable indentation were then simulated.

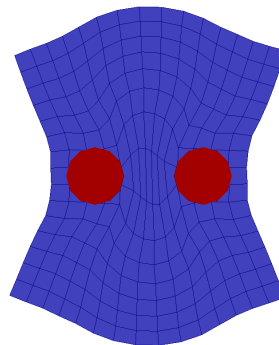


Figure 3: Deformed shape of a two-fibre geometry used to validate the model

References

- [1] I. Steinbrecher, M. Mayr, M. J. Grill, J. Kremheller, C. Meier, A. Popp *A mortar-type finite element approach for embedding 1D beams into 3D solid volumes*, Computational Mechanics, 66 (2020) 1377-1398
- [2] D. Durville *Contact-friction modeling within elastic beam assemblies: an application to knot tightening*, Computational Mechanics, 49 (2012) 687-707
- [3] M. Bonneric, V. Aubin, D. Durville. *Finite element simulation of a steel cable-rubber composite under bending loading: influence of rubber penetration on the stress distribution in wires*, International Journal of Solids and Structures, 160 (2019) 158-167

A finite strain isogeometric solid-beam element with assumed natural strain method

Abdullah Shafqat ¹, Oliver Weeger ², Bai-Xiang Xu ¹

¹ Mechanics of Functional Materials Division , Department of Materials Science, Technical University of Darmstadt, abdullah.shafqat@tu-darmstadt.de, xu@mfm.tu-darmstadt.de

² Cyber-Physical Simulation, Department of Mechanical Engineering, Technical University of Darmstadt, weeger@cps.tu-darmstadt.de

Keywords: Solid-Beam Element, Assumed Natural Strain Method, Locking, Isogeometric Analysis

1. Introduction

Standard continuum finite element formulations are unable to capture the deformation behaviour of slender beams due to the presence of spurious strains or stresses, which will overestimate the stiffness. This leads to the underestimation of field variables, i.e., locking. On the other hand, beam theories have limitations due to the abstraction of kinematic and stress quantities from the three-dimensional geometric model to the beam axis. Thus, constitutive models have to use the reduced stress state, which yields complications for finite strains with hyperelastic or inelastic material models. Furthermore, the coupling with the continuum elements is not straightforward. To tackle these problems, in this work a solid-beam element is developed which inherits the advantageous property of solid elements of having only displacement degrees of freedom. To eliminate transverse shear and membrane locking, the assumed natural strain (ANS) method is used [1]. Furthermore, the concept of isogeometric analysis (IGA) is applied by NURBS basis functions for the description of the geometry and the discretization of unknown field variables [2]. This yields a highly accurate, locking-free solid-beam formulation that is applicable to also to slender beams.

2. Governing Equations

The governing equations correspond to the balance of linear momentum of the solid continuum:

$$\left. \begin{array}{l} \text{Div}(\mathbf{FS}) + \rho_0 \mathbf{b} = \mathbf{0} \quad \text{in } \Omega_0 \\ \mathbf{u} = \bar{\mathbf{u}} \quad \text{on } \Gamma_d \\ (\mathbf{FS}) \cdot \mathbf{n} = \mathbf{t} \quad \text{on } \Gamma_n \end{array} \right\} \Rightarrow \int_{\Omega_0} \delta \mathbf{E} : \mathbf{S} dV - \int_{\Gamma_n} \delta \mathbf{u} \cdot \mathbf{t} dA - \int_{\Omega_0} \delta \mathbf{u} \cdot \rho_0 \mathbf{b} dV = 0 \quad \forall \delta \mathbf{u}. \quad (1)$$

Here, the weak form is discretized by an isogeometric finite element discretization of the solid displacement field $\mathbf{u} : \Omega_0 \rightarrow \mathbb{R}^3$. The Green-Lagrange strains are computed from the deformation gradient $\mathbf{F} = \mathbf{I} + \nabla \mathbf{u}$ as $\mathbf{E} = \frac{1}{2}(\mathbf{F}^T \mathbf{F} - \mathbf{I})$ and the 2nd Piola-Kirchhoff stress from a hyperelastic strain energy potential W as $\mathbf{S} = dW/d\mathbf{E}$.

3. Assumed Natural Strain Method

To cure transversal shear and membrane locking effects for slender continua, the ANS method [1] is applied to the IGA discretization of eq. (1). The main idea behind the ANS method is to calculate the strains components of \mathbf{E} at tying points and then projecting them to the integration points with the help of interpolation functions. The tying points are defined with the help of a reduced integration method. Following Caseiro et al. [2] for the isogeometric analysis of solid-shell finite elements, the ANS method for the isogeometric solid-beam element is defined accordingly. The tying points for the membrane strain $E_{\xi\xi}$ and the transversal shear strains $E_{\xi\eta}$, $E_{\xi\zeta}$ are illustrated in Fig. 1. They can be expressed as:

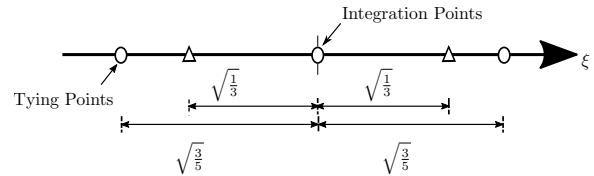


Figure 1: Tying points for the integration of $E_{\xi\xi}$, $E_{\xi\eta}$ and $E_{\xi\zeta}$

$$E_i^{ANS}(\xi, \eta, \zeta) = \sum_{j=1}^{n_t} N_j(\xi) \bar{E}_i(\hat{\xi}_j, \eta, \zeta) \quad \text{with } i \in \{\xi\xi, \xi\eta, \xi\zeta\}, \quad (2)$$

where n_t is the number of tying points and N_j are the univariate basis functions of the local NURBS space in the ξ -direction, calculated at the Gauss integration point k . $\bar{E}_i(\hat{\xi}_j, \eta, \zeta)$ is the compatible strain field calculated

in the local space with the help of the tying points with coordinates (ξ_j, η, ζ) . Thus, in the finite element implementation, the strain displacement operator that maps \mathbf{u} to \mathbf{E} is adjusted to account for the modified membrane strain and transverse shear strains.

4. Numerical Example

To verify the IGA solid beam formulation for large (finite) rotations, a cantilever beam with an applied bending moment is considered. The bending moment is applied by means of a non-conservative equivalent load. In Figure 2, the geometry and the material parameters of the cantilever beam are shown. The solid beam is meshed with 5 or 20 elements (knot spans) in the longitudinal direction. The horizontal and vertical displacements and the rotation angle are calculated at the centre of the free-end cross-section of the beam. The horizontal displacement of the solid-beam element (HnANSB) is compared with the analytical beam solution, an IGA solid element (Hn) and an isoparametric solid beam element [1] (Q1STb), see Fig. 3a, where n is the degree of the shape functions along the beam axis. Furthermore, in Fig. 3b, the results of the formulation are compared with an IGA solid element (H2) for different slenderness ratios.

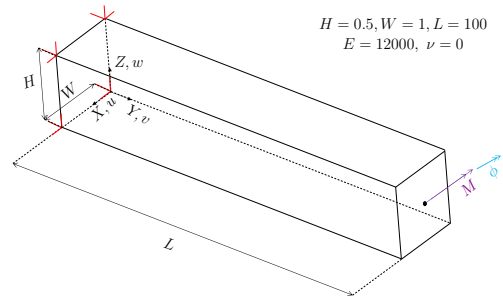
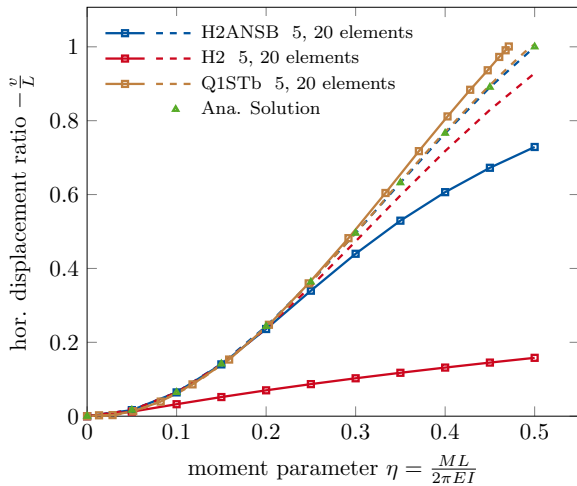
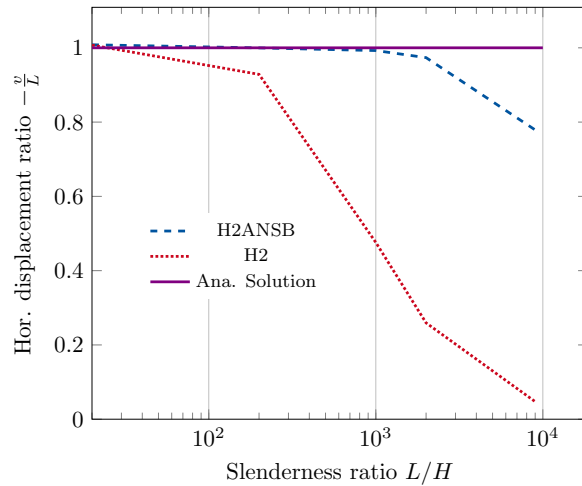


Figure 2: Geometry and material properties of cantilever beam under bending



(a) Horizontal displ. ratio vs. moment parameter



(b) Horizontal displ. ratio vs. slenderness ratio

Figure 3: Large rotation of cantilever beam under bending

5. Summary

The developed solid-beam formulation is able to elevate locking effects and yields results comparable to beam formulations even for highly slender beams. In further research, the IGA solid beam element will be used to analyse metamaterials and will be coupled with a diffusion equation to analyse the chemo-mechanical behaviour of battery microstructures.

Acknowledgments

The authors acknowledge financial support of the Deutsche Forschungsgemeinschaft (DFG, German Research Foundation) – grant no. 460684687.

References

- [1] J Frischkorn and S Reese. *A solid-beam finite element and non-linear constitutive modelling*, Comput. Methods Appl. Mech. Eng. **265** (2013) 195–212
- [2] JF Caseiro, RA Valente, A Reali, J Kiendl, F Auricchio, and RJ Alves De Sousa. *On the Assumed Natural Strain method to alleviate locking in solid-shell NURBS-based finite elements*, Comput. Mech. **53** (2014) 1341–1353

A mixed-dimensional beam-to-solid interaction framework: From embedded fibers to contact

Ivo Steinbrecher¹, Christoph Meier², Alexander Popp¹

¹ Institute for Mathematics and Computer-Based Simulation (IMCS),
Universität der Bundeswehr München Neubiberg, Germany

² Institute for Computational Mechanics, Technical University of Munich, Germany

Keywords: Mixed-dimensional interaction, Nonlinear beam theory, Mortar methods

1. Introduction

The interaction between slender fiber- or rod-like components, where one spatial dimension is much larger than the other two, with three-dimensional (2D) structures (solids) is an essential mechanism of mechanical systems in numerous fields of science, engineering and bio-mechanics. Various modeling techniques exist to create a numerical model of the described problems, almost all of them being based on the finite element method. Classical modeling techniques usually require a compromise between a detailed description of the slender structures and overall model complexity. Based on the example of fibers embedded in a material matrix, common approaches can be categorized into 2 categories: homogenization approaches where the stiffness contributions from the fibers and matrix are homogenized, thus resulting in an anisotropic material law for the combined volume. The fibers are not explicitly modeled which reduces the modeling and meshing effort, however, the results obtained with such methods only give limited insight on the detailed interaction between the fibers and the matrix. In the second commonly used approach the fibers as well as the material matrix are fully resolved using 3D continuum theory, thus resulting in a highly accurate description of the compound structure and the interactions between fibers and matrix. However, the resulting model comes with considerable modeling effort computational complexity. The main idea of the presented framework is to provide finite element formulations to combine the successful and rich history of nonlinear beam theories based on 1D-Cosserat continua with classical 3D continuum finite elements. This allows to explicitly model the fibers while still maintaining a moderate overall model complexity compared to the fully resolved model. The resulting problems are referred to as beam-to-solid (BTS) interaction problems.

2. Beam-to-solid modeling assumptions

Since the dimensions of the coupled differential equations are not equal in, the resulting combined interaction problem is a mixed-dimensional beam-to-solid interaction problem. Not only the governing equations of the beam but also the developed interaction schemes are exclusively formulated along the one-dimensional beam centerline. From a mechanical point of view, the resulting mixed-dimensional interaction of nonlinear geometrically exact beam finite elements with classical continuum finite elements introduces a singular solution, similar to the problem of a concentrated line load acting on a three-dimensional continuum. It can be shown that this singularity does not affect the usability of the BTS interaction framework as long as the solid element dimensions are larger than the beam cross-section, i.e., if the beam cross-section is smaller than a solid element, the exact distribution of the interaction forces does not effect the global system response. The second main modeling assumption for the case of embedded fibers is that the volume occupied by the fibers is not removed from the modeled matrix volume, thus resulting in overlapping volumes. For the typical stiffness relations between fiber and matrix material, this modeling inconsistency can be neglected. Since the matrix volume is not affected by the fibers, matrix and fibers can be discretized independently of each other. This drastically reduces the required meshing effort and allows for arbitrary configurations of the beams with respect to the solid, thus resulting in inevitably non-matching finite element grids.

3. Finite element formulation for beam-to-solid interaction

The presented beam-to-solid interaction framework can be applied to existing beam and solid formulations, i.e., it allows for the combination of modern finite element technologies developed for pure beam or pure solid

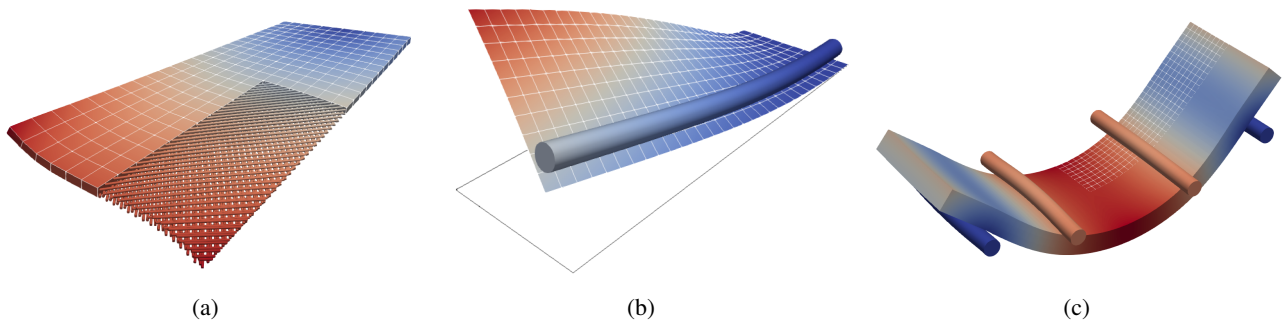


Figure 1: Illustration of various BTS application scenarios – fiber-reinforced composite plate (a), supported shell (b) and four-point bending test (c).

problems. The interaction constraints act along the beam centerline and they are discretized in a weighted sense using a mortar-type approach [1]. A penalty regularization is performed to eliminate the Lagrange multipliers from the global system of equations, which results in a robust coupling scheme. Special caution has to be taken when the rotations of the Cosserat continua are coupled to the solid. This requires the construction of a suitable rotation (i.e., triad) field inside the solid (Boltzmann) continuum [2]. Furthermore, the interaction between 1D beams and 2D surfaces of solid continua introduces the additional complexity of having to account for the surface normal vector in the coupling constraints. The presented framework is able to handle and combine all of the complexities mentioned above.

4. Numerical examples

Figure 1 showcases possible application scenarios for the presented beam-to-solid interaction framework. In Figure 1(a) a fiber-reinforced composite plate is shown where the fiber reinforcements are explicitly modeled using 1D beam elements. Due to the non-symmetric layer buildup of the plate, the plate twists even though the loading is entirely in-plane. Figure 1(b) illustrates a beam-reinforcement coupled to an isogeometric shell, based on NURBS basis functions. Finally, Figure 1(c) illustrates a four-point bending test modeled with unilateral beam-to-solid contact. The employed beam models are based on the geometrically exact beam theory [3].

5. Conclusions

Among the main topics addressed in this talk are a detailed outline of the beam-to-solid interaction framework, as well as a discussion of the characteristic traits of mixed-dimensional interaction in solid mechanics. Selected quantitative and qualitative examples are presented to highlight in order to underline the usability for real life science and engineering applications. Furthermore, the open-source beam finite element pre-processor MeshPy¹ is presented.

References

- [1] Steinbrecher, I., Mayr, M., Grill, M.J., Kremheller, J., Meier, C. and Popp, A. A mortar-type finite element approach for embedding 1D beams into 3D solid volumes. *Computational Mechanics*. 66, 6 (2020), 1377–1398, 2020
- [2] Steinbrecher, I., Popp, A. and Meier, C. Consistent coupling of positions and rotations for embedding 1D Cosserat beams into 3D solid volumes. *Computational Mechanics*. 69, 3 (2022), 701–732, 2022
- [3] Meier, C., Popp, A. and Wall, W.A. Geometrically exact finite element formulations for slender beams: Kirchhoff–Love theory versus Simo–Reissner theory. *Archives of Computational Methods in Engineering*. 26, 1 (2019), 163–243, 2019

¹<https://github.com/imcs-compsim/meshpy>

MS-6: Slender beam-like structures with scientific passion – mini-symposium in honour of prof. Miran Saje

A review of beam formulations with consistent equilibrium in a cross-section

Peter Češarek¹,

¹ University of Ljubljana, Faculty of Civil and Geodetic Engineering, peter.cesarek@fgg.uni-lj.si

Keywords: Consistency conditions, Mixed formulation, Beam, Review

1. Introduction

Formulations of the mixed type of finite elements are generally considered to solve special problems: analysis of nearly incompressible solids, locking in shells and beams. When additional unknown fields are constrained to the original (variational) problem by means of Lagrange multipliers, additional equations in the Euler-Lagrange system of equations result. In case where kinematic equations are constrained to original problem, the Lagrange multipliers are interpreted as ‘equilibrium’ stresses, and the expanded problem contains the so-called *consistency conditions* which ensure that the equilibrium stresses are equal to the ‘true’ or constitutive stresses resulting from the strain-dependent constitutive law. The equilibrium and constitutive stresses are theoretically identical, however this need not be the case in the numerical implementation of standard finite elements, therefore consistency conditions are proposed to solve this problem [1].

In the research group at Chair of Mechanics at the Faculty of Civil and Geodetic Engineering (University of Ljubljana), a large number of finite element formulations for beams have been developed over the last 25 years, in which consistency conditions play a central role.

2. Consistency of beams cross-sectional equilibrium and constitutive stress-resultants

Consistent equilibrium of the cross-section of a beam is defined as

$$\begin{aligned}\vec{f}^C(x) &= \vec{f}(x) \\ \vec{m}^C(x) &= \vec{m}(x)\end{aligned}\tag{1}$$

Here, x is the material coordinate of the beam’s reference line, \vec{f}^C and \vec{m}^C denote stress-resultant constitutive force and moment vectors, which depend only on strain measures of the beam $\vec{\gamma}$ and $\vec{\kappa}$: $\vec{f}^C = C_F(\vec{\gamma}, \vec{\kappa})$, $\vec{m}^C = C_M(\vec{\gamma}, \vec{\kappa})$ ¹. \vec{f} and \vec{m} are equilibrium force and moment vectors of the beam’s cross-section, that correspond to balance equations: $\frac{d}{dx}\vec{n} + \vec{n}_{ext} = \frac{d}{dt}(A_\rho \vec{v})$ and $\frac{d}{dx}\vec{m} + \frac{d}{dx}\vec{r} \times \vec{n} + \vec{m}_{ext} = \frac{d}{dt}(J_\rho \vec{\Omega})$ ².

2.1. Discrete form of consistency conditions

Continuous equations (1) can be converted to discrete equations when Galerkin-type finite element method is used. When standard interpolation points are used, consistency conditions are satisfied at some discrete points that lay between integration and interpolation points [2]. However, when integrating through interpolation points, the consistency is satisfied at integration/interpolation points and the discretization can be considered as a collocation method [6].

3. Beam formulations employing consistency conditions

The phenomenon of inequality of equilibrium and constitutive internal forces in a cross-section of an elastic-plastic planar beam is discussed in a paper by Vratinar and Saje [1] and a possible treatment – the use of consistency conditions – is presented. In the paper by Planinc et al. [2] a weak formulation of the Reissner theory for plane beams with finite strain, using the consistency condition, is presented. The pseudocurvature of the deformed axis is the only unknown function. A finite element formulation of a geometrically and materially nonlinear plane beam for the structural analysis of reinforced concrete frames is presented in the paper

¹Operators C_F and C_M must be invariant under superimposed rigid-body motions and at least once differentiable with respect to $\vec{\gamma}$, $\vec{\kappa}$.
² \vec{n}_{ext} and \vec{m}_{ext} are the external distributed force and moment, A_ρ and J_ρ are mass-area and mass-inertia matrix of the cross-section.

by Bratina et al. [3]. In the formulation, the strain measures are the only interpolated unknowns, and the constitutive and equilibrium internal forces are equal at the integration points. Čas et al. [4] presented finite element formulation for the non-linear analysis of two-layer composite planar beams with an interlayer slip. An extension of the planar geometrically exact beam, where strain measures are the interpolated unknowns, to dynamics was given by Gams et al. [5]. The pioneering strain-based formulation for geometrically exact spatial beams was presented by Zupan and Saje [6]. In their work, the consistency condition is enforced to be satisfied at selected points, and the solution is found by a collocation algorithm. Češarek et al. [7] presented a special derivation of the formulation presented in [6], assuming a constant strain field along the element. A strain-based finite-element formulation was presented where numerical integration in the governing equations and their variations is completely omitted and replaced by analytical integrals. A further extension of the original strain-based formulation [6] was presented by Pirmanšek et al. [8] in which the strain field is enhanced with embedded discontinuity. The newly developed beam finite element can account for the softening of the material. In the paper, it was shown that the consistency condition is naturally suited for the implementation of the discontinuous formulation. An extension of the static formulation [6] to dynamics was presented by Češarek et al. [9]. Another application of consistency constraints in the dynamic formulation of spatial beams was presented by Zupan et al. [10]. In their work, the configuration variables are interpolated and the rotations are described with quaternions. A special formulation of spatial beam dynamics was presented by Češarek and Zupan [11], in which the spatial derivatives of velocities and angular velocities are the primary interpolated unknowns and consistency conditions are used.

Acknowledgments

The authors acknowledge the financial support from the Slovenian Research Agency (research core funding No. P2-0260).

References

- [1] B. Vratinar, M. Saje. *A consistent equilibrium in a cross-section of an elastic-plastic beam*, International Journal of Solids and Structures, 36 (1999), 311–337.
- [2] I. Planinc, M. Saje, B. Čas. *On the local stability condition in the planar beam finite element*. Structural Engineering and Mechanics, 12 (2001), 507–526.
- [3] S. Bratina, M. Saje, I. Planinc. *On materially and geometrically non-linear analysis of reinforced concrete planar beams*. International Journal of Solids and Structures 41 (2004), 7181–7207.
- [4] B. Čas, M. Saje, I. Planinc. *Non-linear finite element analysis of composite planar frames with an interlayer slip*. Computers & Structures 82 (2004), 1901–1912.
- [5] M. Gams, M. Saje, S. Srpčič, I. Planinc. *Finite element dynamic analysis of geometrically exact planar beams*. Computers & Structures 85 (2007), 1409–1419.
- [6] D. Zupan, M. Saje. *Finite-element formulation of geometrically exact three-dimensional beam theories based on interpolation of strain measures*, Computer methods in applied mechanics and engineering, 192 (2003), 5209–5248.
- [7] P. Češarek, M. Saje, D. Zupan. *Kinematically exact curved and twisted strain-based beam*. International Journal of Solids and Structures 49 (2012), 1802–1817.
- [8] K. Pirmanšek, P. Češarek, D. Zupan, M. Saje. *Material softening and strain localization in spatial geometrically exact beam finite element method with embedded discontinuity*. Computers & Structures 182 (2017), 267–283.
- [9] P. Češarek, M. Saje, D. Zupan. *Dynamics of flexible beams: Finite-element formulation based on interpolation of strain measures*. Finite Elements in Analysis and Design 72 (2013), 47–63.
- [10] E. Zupan, M. Saje, D. Zupan. *Dynamics of spatial beams in quaternion description based on the Newmark integration scheme*. Computational Mechanics 51 (2013), 47–64.
- [11] P. Češarek, D. Zupan. *Velocity-based approach in non-linear dynamics of three-dimensional beams*. The 4th Canadian Conference on Nonlinear Solid Mechanics (CanCNSM 2013), E. M. Croitoro, E. Babilio, M. Amabili, F. Alijani, eds., Paper ID MS1-730, 2013.

Kinematically exact beam with embedded discontinuity

Peter Češarek¹, Miran Saje²

¹ University of Ljubljana, Faculty of Civil and Geodetic Engineering, peter.cesarek@fgg.uni-lj.si

² University of Ljubljana, Faculty of Civil and Geodetic Engineering, miran.saje@fgg.uni-lj.si

Keywords: Beam, Strain-based, Kinematically exact, Embedded discontinuity, Material softening

1. Introduction

One particular challenge in the numerical analysis of structures using the finite element method is the handling of strain localization caused by localized decreases in the bearing capacity of structural elements commonly referred to as ‘softening’. To address this issue, the finite element method with embedded discontinuities was introduced [1]. This approach involves superimposing discrete displacement increments onto the continuous strain or displacement field within the finite element. By doing so, the discontinuous nature of the localized strain at the element level is accounted for, while maintaining the chosen degree of interpolation for the continuous part of the strains or displacements.

2. Formulation of kinematically exact beam finite element with embedded strain discontinuity

Here, we focus on the formulation of geometrically exact beam finite element with embedded discontinuity. Formulation is an enhancement of kinematically exact beam finite element, presented by Češarek et al. [2], with discontinuous strain field.

2.1. Kinematics of a beam with discontinuous strain field

Kinematic equations³ of the beam read: $\frac{d}{dx}\mathbf{\Lambda}(x) = \mathbf{\Lambda}(x) \left(\widehat{\mathbf{K}}(x) - \widehat{\mathbf{K}}^0(x) \right)^4$ and $\frac{d}{dx}\mathbf{r}(x) = \mathbf{\Lambda}^T(x) \left(\bar{\mathbf{F}}(x) - \bar{\mathbf{F}}^0 \right)^5$, where the strain measures $\bar{\mathbf{F}}$ and $\bar{\mathbf{K}}$ denote the rate of change of the position vector \mathbf{r} and rotation matrix $\mathbf{\Lambda}$, with respect to x^6 . In the localization model with embedded discontinuity, the onset of localization is assumed in discrete (singular) cross-section, located at x_s . At this material point, the discontinuity of strains is assumed to take the form of an impulse function embedded in the continuous field of strains. This variation of strains along the beam axis can be represented by a generalized function that combines regular continuous functions $\bar{\mathbf{F}}(x)$ and $\bar{\mathbf{K}}(x)$ with peak-like strain jumps $\delta_{x_s}\Delta\mathbf{U}^7$ and $\delta_{x_s}\Delta\mathbf{\Theta}^7$, respectively.

We assume a uniform (regular) strain field along the axis of the element, i.e. $\bar{\mathbf{K}}(x) = \bar{\mathbf{K}}$ and $\bar{\mathbf{F}}(x) = \bar{\mathbf{F}}$. The enhanced strain field of the beam is defined as $\mathbf{K}(x) = \bar{\mathbf{K}} + \delta_{x_s}\Delta\mathbf{\Theta}$, $\mathbf{F}(x) = \bar{\mathbf{F}} + \delta_{x_s}\Delta\mathbf{U}$, however, it is important to note that vector addition applies only to vectors expressed in the same (moving) reference frame. The strain vectors $\bar{\mathbf{K}}$ and $\bar{\mathbf{F}}$ are defined in the reference frame of regular cross-sections. Therefore, it is necessary to rotate them accordingly starting from the discontinuity point $x > x_s$. Here we can only make an assumption about the rotation $\Delta\mathbf{\Lambda}$ caused by the discontinuity: $\Delta\mathbf{\Lambda} = \exp\left(H_{x_s}\Delta\widehat{\mathbf{\Theta}}\right)^7$. The kinematic equations of the beam with enhanced strain field then read

$$\frac{d}{dx}\mathbf{\Lambda}(x) = \mathbf{\Lambda}(x) \left(\exp\left(H_{x_s}\Delta\widehat{\mathbf{\Theta}}^T\right) \left(\widehat{\mathbf{K}} - \widehat{\mathbf{K}}^0 \right) \exp\left(H_{x_s}\Delta\widehat{\mathbf{\Theta}}\right) + \delta_{x_s}\Delta\widehat{\mathbf{\Theta}} \right), \quad (1)$$

$$\frac{d}{dx}\mathbf{r}(x) = \mathbf{\Lambda}(x) \left(\exp\left(H_{x_s}\Delta\widehat{\mathbf{\Theta}}\right) \left(\bar{\mathbf{F}} - \bar{\mathbf{F}}^0 \right) + \delta_{x_s}\Delta\mathbf{U} \right). \quad (2)$$

³Vectors in a fixed frame are written with emphasized lowercase letters, vectors in a moving frame are written with emphasized uppercase letters.

⁴ $\mathbf{\Lambda}(x)$ is rotation matrix representing rotation of the moving frame, which is attached to the beam’s cross-section, with respect to the fixed spatial frame. $\widehat{\mathbf{K}}$ denotes skew-symmetric matrix composed from vector $\bar{\mathbf{K}}$. $\bar{\mathbf{K}}^0(x)$ describes the initial curvature or twist of the beam centerline.

⁵ $\mathbf{r}(x)$ is the position vector of the beam’s reference line. $\bar{\mathbf{F}}^0$ coincides with the normal of the cross section.

⁶ x represents the arc length of the reference line in the reference configuration.

⁷ $\delta_{x_s} = \delta(x - x_s)$ is the Dirac delta function, $H_{x_s} = H(x - x_s)$ is the Heaviside step function.

For the assumed constant $\bar{\mathbf{K}}$, the solution of the kinematic equation (1) with the initial condition $\mathbf{\Lambda}(0) = \mathbf{\Lambda}_0$ is

$$\mathbf{\Lambda}(x) = \mathbf{\Lambda}_0 \exp\left(x \left(\widehat{\mathbf{K}} - \widehat{\mathbf{K}}^0\right)\right) \exp\left(H_{x_s} \Delta \widehat{\mathbf{\Theta}}\right) = \bar{\mathbf{\Lambda}}(x) \exp\left(H_{x_s} \Delta \widehat{\mathbf{\Theta}}\right). \quad (3)$$

The proof of solution (3) is straightforward if we differentiate the presumed solution with respect to x . Furthermore, if we consider the solution (3) in the kinematic equation (2), the equation simplifies to

$$\frac{d}{dx} \mathbf{r}(x) = \mathbf{\Lambda}_0 \exp\left(x \left(\widehat{\mathbf{K}} - \widehat{\mathbf{K}}^0\right)\right) \bar{\mathbf{F}} + \mathbf{\Lambda}(x) \delta_{x_s} \Delta \mathbf{U}. \quad (4)$$

Integration of equation (4), assuming initial condition $\mathbf{r}(0) = \mathbf{r}_0$, gives exact solution for the position vector:

$$\mathbf{r}(x) = \mathbf{r}_0 + \mathbf{\Lambda}_0 \mathbf{W}\left(x \left(\widehat{\mathbf{K}} - \widehat{\mathbf{K}}^0\right)\right) \bar{\mathbf{F}} + \mathbf{\Lambda}(x_s) H_{x_s} \Delta \mathbf{U} = \bar{\mathbf{r}}(x) + \mathbf{\Lambda}(x_s) H_{x_s} \Delta \mathbf{U}, \quad (5)$$

where $\mathbf{W}\left(x \left(\widehat{\mathbf{K}} - \widehat{\mathbf{K}}^0\right)\right) = \int_0^x \exp\left(\tilde{x} \left(\widehat{\mathbf{K}} - \widehat{\mathbf{K}}^0\right)\right) d\tilde{x}$.

Equations (3) and (5) reveal the nature of the jumps of strains \mathbf{K} and \mathbf{F} :

- $\Delta \mathbf{\Theta}$ is the rotation of the localized cross-section with respect to the adjacent regular cross-section, and $\exp\left(H_{x_s} \Delta \widehat{\mathbf{\Theta}}\right)$ rigidly rotates all cross-sections following the localized cross-section for the rotation vector $\Delta \mathbf{\Theta}$, which is exactly what we assumed in equations (1) and (2).
- $\Delta \mathbf{U}$ is the displacement of the localized cross-section written in the local frame of this cross-section.

2.2. Finite element formulation

The procedure for deriving the finite element formulation of the beam with strain vectors with embedded discontinuity is presented in reference [3], except that in the present work, instead of a general interpolation function for strains, we assume constant strain vectors and the solutions of the kinematic equations (3) and (5). The formulation is an enhancement of the kinematically exact beam presented in [2] with two independent vector unknowns – rotation and displacement jumps $\Delta \mathbf{\Theta}$ and $\Delta \mathbf{U}$, and two vector equations recognized as consistency conditions of the singular cross-section (see [2, 3] for details): $\mathbf{\Lambda}(x_s) \mathbf{N}^C(x_s) = \mathbf{n}(x_s)$ and $\mathbf{\Lambda}(x_s) \mathbf{M}^C(x_s) = \mathbf{m}(x_s)$ ⁸. The resulting spatial finite element with discontinuities inherits crucial features from its continuous counterpart [2], such as strain objectivity and locking-free behaviour. Additionally, the results for discontinuities are insensitive to mesh refinement.

Acknowledgments

The authors acknowledge the financial support from the Slovenian Research Agency (research core funding No. P2-0260).

References

- [1] J.C. Simo, J. Oliver, F. Armero, *An analysis of strong discontinuities induced by strain-softening in rate-dependent inelastic solids*, Computational Mechanics 12 (1993), 277–296.
- [2] P. Češarek, M. Saje, D. Zupan, *Kinematically exact curved and twisted strain-based beam*, Int. J. Solids Struct. 49 (2012), 1802–1817.
- [3] K. Pirmanšek, P. Češarek, D. Zupan, M. Saje. *Material softening and strain localization in spatial geometrically exact beam finite element method with embedded discontinuity*. Computers & Structures 182 (2017), 267–283.

⁸ $\mathbf{N}^C(x_s)$ and $\mathbf{M}^C(x_s)$ are constitutive force and moment vectors of the singular cross-section, which are obtained from constitutive equations $\mathbf{N}^C(x_s) = C_N(\bar{\mathbf{F}}, \bar{\mathbf{K}}, \Delta \mathbf{U}, \Delta \mathbf{\Theta})$ and $\mathbf{M}^C(x_s) = C_M(\bar{\mathbf{F}}, \bar{\mathbf{K}}, \Delta \mathbf{U}, \Delta \mathbf{\Theta})$. $\mathbf{n}(x_s)$ and $\mathbf{m}(x_s)$ are equilibrium force and moment vectors of the singular cross-section, obtained from equilibrium equations.

Nonlinear dynamics of highly flexible beam structures: frequency domain-based finite element computation of the nonlinear modes

Marielle Debeurre^{1,2}, Aurélien Grolet¹, Olivier Thomas^{1,2}

¹ Arts et Métiers Institute of Technology, HESAM Université, 8 boulevard Louis XIV, 59046 Lille, France

² THREAD European Training Network

Keywords: Flexible Structures, Geometrical Nonlinearity, Nonlinear Modes, Finite Element Analysis, Continuation Methods

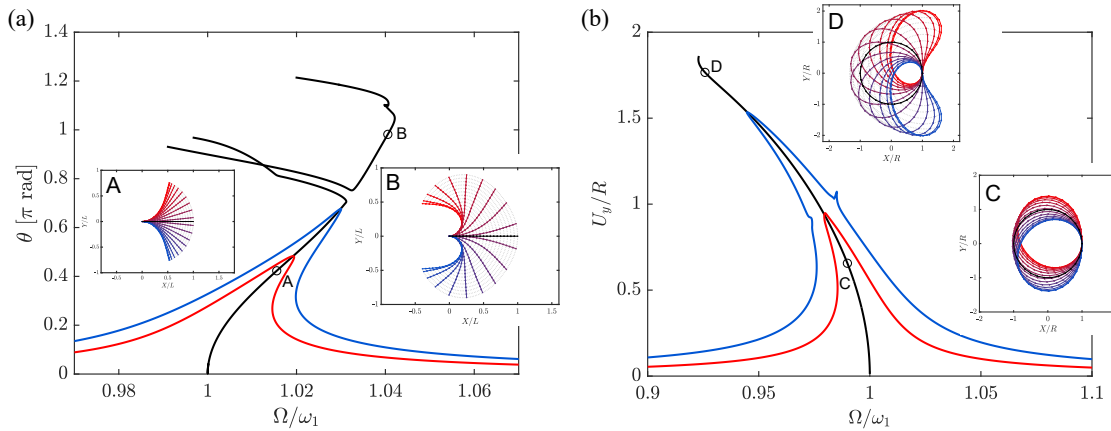


Figure 1: First nonlinear mode of (a) cantilever beam: forced responses ($\hat{F}_0 = 0.05$, $\hat{F}_0 = 0.08$ in [1]) and backbone curve of cross-section rotation θ at the free end of the beam plus snapshots of the nonlinear deformed shape; (b) the same as (a) but for a ring structure ($\hat{F}_0 = 0.5$, $\hat{F}_0 = 1$) and showing the dimensionless transverse displacement U_y/R of the node opposite the clamp.

1. Introduction

In this work, we propose a new method for simulating the nonlinear dynamics of highly flexible slender beam structures based on a finite element discretization of the geometrically exact beam model solved entirely in the frequency domain. The geometrically exact beam model is especially advantageous in modeling slender beam structures since the geometrical nonlinearities tied to large displacement amplitudes are kept exact in the equations, allowing the dynamical behavior to be captured even at extreme amplitudes of vibration (Fig. 1).

2. Geometrically exact beam model

A full derivation of the equations of motion of the geometrically exact beam model has been presented in previous works (such as [2] in general or [1, 3] in 2D). In our method, Timoshenko kinematics is combined with a total Lagrangian formulation in order to derive the governing equations. These are then discretized into finite elements.

2.1. Finite element model

The finite element (FE) model is derived through discretization of the weak form of the equations of motion ([1, 2, 3]). In our model, Timoshenko beam elements with linear (in 2D) or quadratic (in 3D) shape functions are used. The complexity of the geometrically exact beam model centers largely on treatment of the cross-section rotations described by the rotation operator (\mathbf{R} in [2]) which houses the geometrical nonlinearities. In 2D, the trigonometric functions characterizing the orientation of the cross-section are kept within the equations of motion [1], while in 3D, the more numerically efficient quaternion parametrization of rotations is used [4, 5]. The FE dynamic equations ultimately fall into the general form:

$$\mathbf{M}\ddot{\mathbf{u}} + \mathbf{D}\dot{\mathbf{u}} + \mathbf{f}_{\text{int}}(\mathbf{u}) = \mathbf{f}_{\text{ext}}, \quad (1)$$

where \mathbf{u} is the vector of nodal degrees of freedom, \mathbf{M} the mass matrix and \mathbf{D} the damping matrix, \mathbf{f}_{int} the internal force vector and \mathbf{f}_{ext} the vector of applied forces.

3. Numerical resolution in the frequency domain

Periodic solutions of Eq. (1) are then found in either forced or free oscillation conditions using a combination of the harmonic balance method (HBM) and the asymptotic numerical method (ANM) in a strategy which is automated by the MANLAB software [6]. The details of this procedure being complex, it is recommended to see Section 2.3 of [1] for a brief overview. However, two important points should be highlighted here, the quadratic recast formalism and the solutions available with this method.

3.1. Quadratic recast

A subtlety imposed by the use of the ANM for continuation of periodic solutions is the *quadratic recast*. In order to improve computational efficiency, Eq. (1) is rewritten as a differential-algebraic system of equations (DAE) with polynomial nonlinearities of (at most) quadratic order. For example, in 2D, the trigonometric geometrical nonlinearities are “recast” by introducing additional *auxiliary* variables and equations (see *e.g.* [1, 7, 8]). Our specific quadratic recast has been outlined in [5] for 3D motions and in [1] when restricted to 2D in the plane.

3.2. Continuation with MANLAB

It is noteworthy to mention that solving with MANLAB permits two kinds of solutions, computation of the periodic response under harmonic forcing (forced solution) or of the free and undamped solution (nonlinear modes). In the former case, Eq. (1) takes the form:

$$\mathbf{M}\ddot{\mathbf{u}} + \mathbf{D}\dot{\mathbf{u}} + \mathbf{f}_{\text{int}}(\mathbf{u}) = \mathbf{F} \sin \Omega t, \quad (2)$$

where \mathbf{F} is the vector of harmonic forcing amplitudes, Ω is the frequency of the forcing and t is time. In the latter case, however, Eq. (1) becomes:

$$\mathbf{M}\ddot{\mathbf{u}} + \mathbf{f}_{\text{int}}(\mathbf{u}) = \mathbf{0}, \quad (3)$$

which allows for computation of the nonlinear modes of the system (graphically represented as the so-called “backbone” curves, see [1] for numerical details). An example of both types of solution can be found in Fig. 1.

4. Conclusion

We have briefly introduced our method for solving highly flexible nonlinear dynamical systems based on a finite element discretization of the geometrically exact beam model solved in the frequency domain. There are many advantages to using this approach, notably that the computational capacity of this method extends to a multitude of structures so long as these can be discretized into beam elements.

Acknowledgments

This project has received funding from the European Union’s Horizon 2020 research and innovation programme under the Marie Skłodowska-Curie grant agreement No. 860124.



References

- [1] M. Debeurre, A. Grolet, B. Cochelin, O. Thomas. *Finite element computation of nonlinear modes and frequency response of geometrically exact beam structures*, Journal of Sound and Vibration, 548 (2023) 117534.
- [2] M. Géradin, A. Cardona. *Flexible Multibody Dynamics: A Finite Element Approach*, John Wiley & Sons Ltd, Chichester, 2001.
- [3] O. Thomas, A. Sénéchal, J.-F. Deü. *Hardening/softening behavior and reduced order modeling of nonlinear vibration of rotating cantilever beams*, Nonlinear Dynamics, 86 (2016) 1293-1318.
- [4] E. Zupan, M. Saje, D. Zupan. *The quaternion-based three-dimensional beam theory*, Computer Methods in Applied Mechanics and Engineering, 198 (2009) 3944-3956.
- [5] E. Cottanceau, O. Thomas, P. Véron, M. Alochét, R. Deligny. *A finite element/quaternion/asymptotic numerical method for the 3D simulation of flexible cables*, Finite Elements in Analysis and Design, 139 (2017) 14-34.
- [6] *Manlab: An interactive path-following and bifurcation analysis software*, available at: <http://manlab.lma.cnrs-mrs.fr>.
- [7] L. Guillot, B. Cochelin, C. Vergez. *A generic and efficient Taylor series-based continuation method using a quadratic recast of smooth nonlinear systems*, International Journal for Numerical Methods in Engineering, 119 (2019) 261-280.
- [8] S. Karkar, B. Cochelin, C. Vergez. *A high-order, purely frequency based harmonic balance formulation for continuation of periodic solutions: The case of non-polynomial nonlinearities*, Journal of Sound and Vibration, 332 (2013) 968-977.

On the convergence of nonconforming finite element solutions to the unique solution of Reissner's Elastica

Rado Flajs¹, Miran Saje²

¹ University of Ljubljana, Faculty for Civil and Geodetic Engineering, rflajs@fgg.uni-lj.si

² University of Ljubljana, Faculty for Civil and Geodetic Engineering, msaje@fgg.uni-lj.si

Keywords: Reissner's beam, cantilever, existence, uniqueness, Stummel's generalized Patch test, Irons Patch test, nonconforming finite element, convergence

1. Introduction

The sufficient conditions for the existence and uniqueness of the classical and generalized solutions of a highly flexible, planar, elastic, cantilever beam of the Reissner type when based solely on rotations and loaded by a conservative load are presented. The derived inequalities are sharp. Under similar conditions, the global convergence of Newton's method is also derived. The numerical solution is obtained using simple nonconforming finite element approximations that violate the requirements of the Iron's Patch test. Since the numerical solutions converge to the exact solution, the necessity of the Iron's Patch test is questioned.

2. Reissner's planar beam

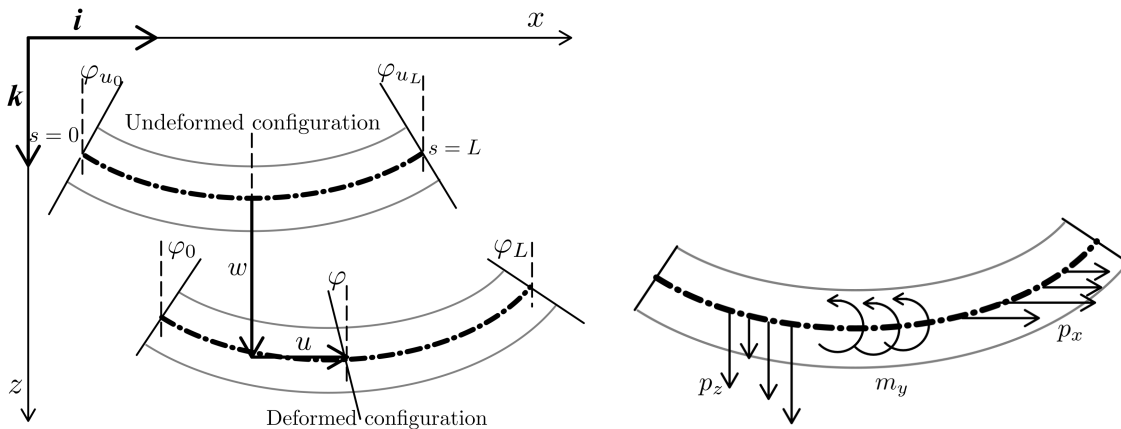


Figure 1: Reissner's beam (left), line loads (right).

The generalised solution of the Reissner's planar cantilever beam, $\phi \in H^1(0, L) = \{u \in W^{1,2}(0, L), u(L) = 0\}$, can be obtained from the minimization of the functional Φ

$$\begin{aligned} \Phi(\phi) = & \int_0^L \left(\frac{\phi'^2}{2} + \frac{R_1}{EJ} (\cos \phi_u - \cos \phi) + \frac{R_2}{EJ} (\sin \phi - \sin \phi_u) \right. \\ & \left. - \frac{c(R_1^2 - R_2^2)}{4EJ} (\cos(2\phi_u) - \cos(2\phi)) - \frac{cR_1R_2}{2EJ} (\sin(2\phi) - \sin(2\phi_u)) - \frac{m_y}{EJ} \phi \right) ds \end{aligned} \quad (1)$$

where the solution satisfies the prescribed boundary conditions $\phi'(0) = 0$ and $\phi(L) = 0$. We have used abbreviations $c = \frac{1}{GA_s} - \frac{1}{EA}$ and $\phi = \phi_u - \phi$ where ϕ , ϕ_u , L , m_y , EA , GA_s , EJ , R_1 and R_2 denote the rotations of the cross section of deformed and undeformed cantilever, the length of the cantilever, the prescribed line moment, the elastic axial, shear, and bending stiffnesses, and Lagrange multipliers, respectively

3. Existence and uniqueness of classical and generalized solution

Let be the distributed load functions, p_x , p_z , m_y , and the initial pseudocurvature of the beam axis ϕ_u' , satisfy the conditions

$$-R_1' = p_x \in L_1(0, L), \quad -R_2' = p_z \in L_1(0, L), \quad m_y \in C[0, L], \quad (\phi_u)' \in B[0, L]. \quad (2)$$

where $B[0, L]$ denotes a set of bounded functions on interval $[0, L]$. Under these conditions one can prove [1], that the boundary value problem corresponding to Equation (1) has a unique solution $\varphi \in C^2[0, L]$ if

$$\frac{1}{EJ} (\|R\|_\infty + c \|R\|_\infty^2) < \frac{\pi^2}{4L^2}, \quad \text{where } R(s) = \sqrt{R_1^2(s) + R_2^2(s)}. \quad (3)$$

4. Convergence of Newton's method

In the paper [2] the global convergence of Newton's method is proved under the following condition

$$\frac{1}{EJ} (\|R\|_\infty + c \|R\|_\infty^2) < \frac{1}{3} \frac{\pi^2}{4L^2}. \quad (4)$$

5. Convergence of nonconformig finite elements that violate the Iron's Patch test

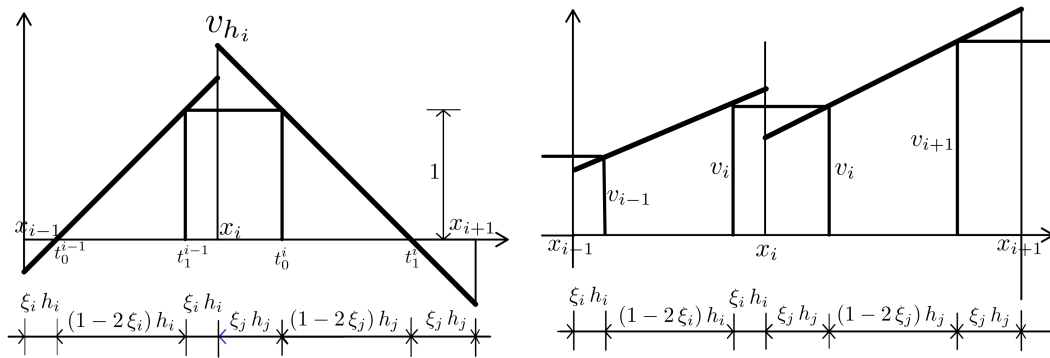


Figure 2: i -th base shape function v_{h_i} (left), interpolation section (right) .

Following Ciarlet, one can denote the finite element in R^1 with triple (I, P, Σ) where: (i) I is an open interval in R^1 of length h ; (ii) P is two-dimensional space of real valued functions over the interval I ; (iii) Σ is a set of two linear forms denoted by degrees of freedom, $\Sigma = \{v_h \mapsto v_h(t_0), v_h \mapsto v_h(t_1)\}$, with two points $t_0, t_1 \in I$ with distances $\zeta h = o(h)$ from the initial and final points of the interval I , respectively [3]. We have also used the well-known Landau symbol o . By applying the Shi F-E-M test, we can prove the convergence of presented finite elements solutions [3].

6. Conclusions

The paper presents a summary of some related published results [1, 2, 3] for the planar Reissner's cantilever beam concerning the existence and uniqueness of classical and generalized solutions as well as the convergence of numerical nonconforming finite element solutions using Newton's method. Special attention has also been given to the validity of Irons' Patch test, which has been replaced by Stummel's generalized Patch test.

Acknowledgments

The work was financially supported by the Slovenian Research Agency (ARRS) under contract P2-0260. The support is gratefully acknowledged.

References

- [1] R. Flajs, M. Saje, E. Zakrajšek, *On the Existence and Uniqueness of the Generalized Solution of Reissners Elastica*, Mathematics and Mechanics of Solids, 8(1), (2003), 3-19.
- [2] R. Flajs, M. Saje, E. Zakrajšek, *Global convergence of Newton's method to the solution of equations of Reissners Elastica*, ZAMM, 81, (2001), 719-720.
- [3] R. Flajs, M. Saje, *Note on the necessity of the Patch test*, WASET, (2012), 713-716.

Interdependence of helicoidal and fixed-pole interpolation in linear elasticity with linked interpolation, and application in FE modelling of Cosserats' continuum

Laura Grbac¹, Gordan Jelenić²,

Faculty of Civil Engineering, University of Rijeka, Rijeka, Croatia,

¹ laura.zikovic@uniri.hr, ² gordan.jelenic@uniri.hr

Keywords: Micropolar continuum, Fixed-pole approach, Linked interpolation, Helicoidal interpolation, FEM.

1. Introduction

In order to accurately describe the behaviour of heterogeneous materials and to capture the *size-effect* phenomena, several continuum theories have been developed as alternatives to the classical (Cauchy) model. One such theory is the *micropolar* or *Cosserats' theory* of elasticity, which in addition to the Cauchy stress tensor includes a couple-stress tensor. The presence of the couple-stress causes an additional independent kinematic field (microrotation) and now, to describe a linear-elastic isotropic micropolar material, it is necessary to know the values of six material parameters. The micropolar theory has been developed significantly so far, but it is still not widely considered in the numerical analysis of structures for practical purposes. Therefore, the further development of highly-quality micropolar finite elements is of great importance for the future progress of Cosserat theory and its application. With the aim of developing a new 3D micropolar FE for linear static and dynamic analysis, we start here with standard and some more innovative schemes used in non-linear mechanics involving large 3D rotations and investigate how they transform when the analysis becomes linear. Among these formulations, we specifically address helicoidal interpolation [1], fixed-pole approach [2] and linked interpolation [3], in addition to conventional Lagrangian interpolation, pin-point the similarities in these interpolations and numerically assess the particular interpolation which in this analysis has come up as optimal.

2. Relationship between the standard and innovative interpolations

In the process of the linearisation of Simo-Reissner beam theory, we derive Timoshenko beam, which is, in fact, a 1D linear micropolar continuum. Therefore, in the following we provide an overview and the analysis of the known standard and innovative interpolations in their linearised forms. All considered interpolation functions for interpolating displacement \mathbf{u} and rotation $\boldsymbol{\phi}$ fields may be unified in a simple manner as

$$\mathbf{u}(x_1) = \sum_{i=1}^m N_i(x_1) \left(\mathbf{u}_i + \frac{1}{n} \widehat{\boldsymbol{\phi} - \boldsymbol{\phi}_i} \mathbf{r}_{o,i} \right), \quad \boldsymbol{\phi}(x_1) = \sum_{i=1}^m N_i(x_1) \boldsymbol{\phi}_i, \quad (1)$$

where $N_i(x_i)$ are the Lagrangian polynomials of order $m - 1$ and $\mathbf{r}_o(x_1) = \sum_{i=1}^m N_i(x_1) \mathbf{r}_{o,i}$ is an initial position vector. Their main difference manifest itself in the coefficients m which stands for the number of nodes of an element, and n , whose values are shown in Table 1. A well-known shortcoming of standard Lagrangian interpolation is that we are facing a shear-locking problem when reduced numerical integration is not applied. This problem is eliminated using helicoidal interpolation [1], which arises from the requirement that the finite element solution of a beam problem should be independent of the choice of the reference axis and consistent with the configuration space. In linear analysis, the helicoidal interpolation is equivalent to the linked interpolation [3] (for a two-node beam) which provides exact solutions for arbitrary polynomial loading and a sufficient finite number of nodal points. Moreover, Bottasso and Borri introduced and applied the *fixed-pole* concept in the dynamic analysis of geometrically exact 3D beams [2] where their main idea is to replace the resultant of the stress-couple and the specific angular momentum, defined with respect to the beam reference axis, with new ones, now defined with respect to the unique point as the origin of the whole observed system (fixed-pole). The implementation of this concept demonstrates the ability of simultaneous conservation of both energy and momentum vectors and can be applied to finite element beams of arbitrary order. Besides that, the fixed-pole concept naturally introduces a new kinematic field $\boldsymbol{\rho}$ combining the displacement field and the rotational field, which results in non-standard degrees of freedom in place of displacements. The linearisation of the fixed-pole interpolation eventually leads to the same stiffness matrix as that obtained using Lagrange interpolation. Therefore, the coefficient $n = m$ is introduced instead of the original coefficient $n = 1$ to achieve an improvement

which emerges from the comparison with the linked interpolation. From this follows the so-called *enhanced fixed-pole interpolation (EFP)* [5].

Table 1: Coefficients m and n from the unified expression (1) of the considered interpolation functions.

Interpolation	m	n
Lagrangian	≥ 2	∞
Helicoidal [1], linearised form in [4]	2	2
Fixed-pole [2], linearised form in [5]	≥ 2	1
Linked [3]	≥ 2	m

3. Vibration analysis of 3D micropolar continuum

The presented *EFP* interpolation has been then used for the development of new 3D hexahedral micropolar FE with 8 nodes (Hex8EFP) which have been validated first through standard patch tests. The analysis of the first natural frequencies of cantilever (i) plate and (ii) plate with a circular hole discretised by Hex8EFP elements has been presented here, where all geometric and material characteristics are given in [5]. The results are compared with Lagrangian elements (Hex8L) and Figure 1 shows a much faster convergence of Hex8EFP elements.

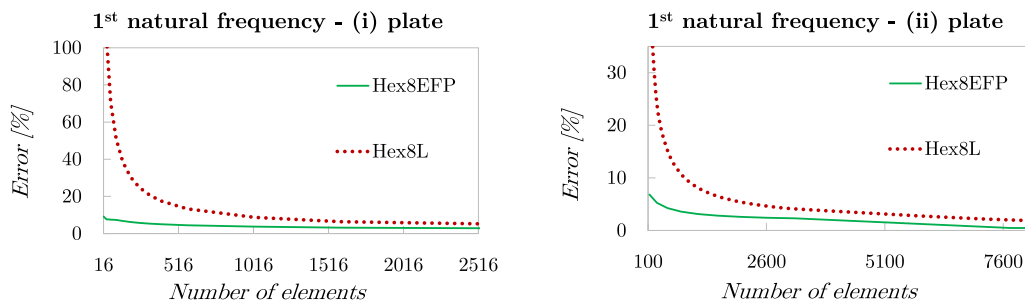


Figure 1: Convergence study of the 1st natural frequencies of the cantilever (i) plate and (ii) plate with a hole.

4. Conclusions

We have introduced and applied the *EFP* interpolation in vibration analysis of the 3D micropolar continuum and showed its better convergence towards the solution than the Lagrangian interpolation. More details on the *EFP* formulation and additional numerical examples can be found in [5].

Acknowledgments

The presented research has been financially supported by the CSF projects (HRZZ-IP-2018-1732) and (HRZZ-DOK-2018-09-8806) as well as the grant (uniri-tehnic-18-248 1415).

References

- [1] M. Borri and C. Bottasso. An intrinsic beam model based on a helicoidal approximation—Part I: Formulation. *International Journal for Numerical Methods in Engineering*, 37(13):2267–2289, 1994.
- [2] C. Bottasso and M. Borri. Integrating finite rotations. *Computer Methods in Applied Mechanics and Engineering*, 164(3-4):307–331, 1998.
- [3] G. Jelenić and E. Papa. Exact solution of 3D Timoshenko beam problem using linked interpolation of arbitrary order. *Archive of Applied Mechanics*, 81(2):171–183, 2011.
- [4] E. Papa Dukić. *Configuration-Dependent Interpolation in Non-linear Higher-order 2D Beam Finite Elements*. PhD thesis, University of Rijeka, 2013.
- [5] L Grbac, G. Jelenić, and D. Ribarić. Hexahedral finite elements with enhanced fixed-pole interpolation for linear static and vibration analysis of 3d micropolar continuum. *Submitted*, 2023.

Enhanced finite-element performance in high-curvature micropolar pure-bending

Sara Grbčić Erdelj¹, Gordan Jelenić¹, Adnan Ibrahimbegović²

¹ University of Rijeka, Faculty of Civil Engineering, Croatia, {sara.grbcic, gordan.jelenic}@uniri.hr

² Université de Technologie Compiègne, France, adnan.ibrahimbegovic@utc.fr

Keywords: Micropolar Continuum, Geometrical Nonlinearity, Enhanced Interpolation, Pure Bending, Micropolar Elasticity

1. Introduction

In the micropolar continuum theory additional fields are present, leading to additional material parameters needed to describe a micropolar material. Such a mathematical setup allows the description of new phenomena which cannot be captured by the classical continuum theory. In this work geometrical nonlinearity in the linear elastic region is considered. It is observed that the geometrically nonlinear finite elements presented in [1] are computationally expensive and fail to converge in certain highly deformed configurations. Due to that, a need for enhanced finite elements which would be able to describe such states in a reasonable computational time persists. Here we analyse the new geometrically nonlinear hexahedral finite element of first order derived in [3]. The performance of the finite element is tested against Lagrangian elements of first and second order derived in [1] (Hex8NL and Hex27NL).

2. Analytical and numerical geometrically non-linear micropolar continuum models

The analytical geometrically nonlinear micropolar continuum model analysed here is defined in terms of the Biot-like stress and couple-stress tensors, together with their energy conjugate Biot-like strain and curvature tensors. The constitutive equations are kept linear, which, for a micropolar continuum model, are expressed in terms of six independent material parameters. The strong form of equilibrium equations in the material description, together with the non-linear kinematic equations and the linear constitutive equations can be found in [1].

A 3D hexahedral finite element with enhanced displacement interpolation (Hex8NLIM) is derived in [3] by introducing the interpolation of the displacement and microrotation fields into the principle of virtual work. The Lagrange interpolation of the displacement field is enhanced with appropriate local (incompatible) interpolation functions. The virtual microrotation field is interpolated using only the standard Lagrange interpolation. After straightforward, but extensive linearisation of the element residual force vector, the obtained system of equations is solved using the standard Newton-Raphson solution procedure, as described in detail in [3].

3. Numerical analysis of pure bending

The enhanced finite element (Hex8NLIM) is tested on a pure-bending problem and compared against the Lagrangian finite elements of first and second order (Hex8NL and Hex27NL).

First, a thin cantilever beam with a length-to-height ratio $\frac{L}{h} = 100$ is loaded by a resultant bending moment at the free end. In order to capture the size-effect phenomenon the characteristic bending length is varied while keeping the remaining micropolar material parameters fixed. The numerical results are then compared against the analytical solution derived in [2]. It is observed that the Hex8NL element shows very poor results for a coarse mesh, especially so for small values of the characteristic bending length. However, by refining the finite element mesh, the analytical solution is approached in all fields. On the other hand, both Hex27NL and Hex8NLIM elements almost reproduce the analytical solution for a coarse mesh, with a slightly higher accuracy of the Hex8NLIM element. More importantly, the computational time needed to obtain the solution using Hex8NLIM is significantly lower than that needed by the Hex27NL element.

Next, in order to increase the strain energy of the problem analysed, the height of the cantilever, together with

the resultant bending moment applied, are both increased. The Lagrangian finite element Hex27NL fails to converge to a numerical solution, while the Hex8NLIM finite element converges to a numerical solution which is in a satisfying agreement with the analytical solution (Figure 1). Interestingly for certain values of material parameters a numerical convergence is not achieved, even though the value of those material parameters should not affect the deformed configuration as they are not present in the analytical solution [2].

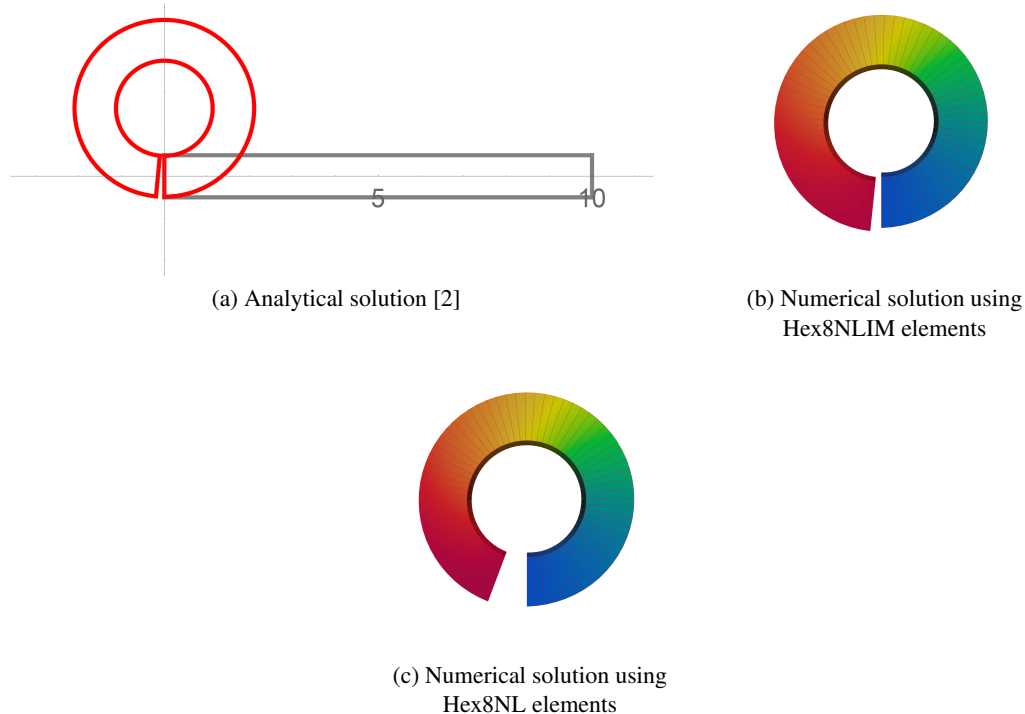


Figure 1: Cantilever beam subject to pure bending - high curvature deformation

4. Conclusions

Within this work an enhanced geometrically nonlinear finite element is tested against the Lagrangian finite elements of first and second order derived in [1] on a pure-bending problem. It can be concluded that the displacement enhancement is significant since the element derived in [3] is more efficient and robust than the elements derived in [1]. More details about the formulation, together with additional numerical examples, can be found in [3].

Acknowledgments

This work has been financially supported by the Croatian Science Foundation research project "Fixed-Pole Concept in Numerical Modelling of Cosserat Continuum" (HRZZ-IP-2018-01-1732) and the University of Rijeka Young Researchers grant "Analysis of the pure bending problem in the geometrically non-linear micropolar continuum theory" (uniri-mladi-tehnic-22-482835).

References

- [1] S. Grbčić Erdelj, G. Jelenić, A. Ibrahimbegović, *Geometrically non-linear 3D finite-element analysis of micropolar continuum*, International Journal of Solids and Structures, 202 (2020), 745-764.
- [2] G. Jelenić, *Pure bending in non-linear micropolar elasticity*, International Journal of Mechanics and Materials in Design, 18 (2022), 243-265.
- [3] S. Grbčić Erdelj, G. Jelenić, A. Ibrahimbegović, *Incompatible modes geometrically non-linear finite element for micropolar elasticity*, to be submitted

Rough and sharp estimates of extensional and transverse shear strains for equilibrium configurations of elastic Cosserat rods

Joachim Linn¹, Fabio Schneider-Jung¹, Michael Roller¹, Tomas Hermansson²

¹ Fraunhofer ITWM, (joachim.linn, fabio.schneider-jung, michael.roller)@itwm.fraunhofer.de

² Fraunhofer–Chalmers Centre FCC, tomas.hermansson@fcc.chalmers.se

Keywords: Cosserat rods, effective stiffness parameters, extensional and shear strains.

1. Introduction

In industrial applications where large spatial deformations of cables have to be simulated interactively [3], typical boundary conditions lead to deformed configurations showing a considerable amount of bending of the centerline, accompanied by a moderate amount of approximately uniform twisting of the cross sections along the configuration. Geometrically exact rod models [1] occur in three different variants w.r.t. the kinematical properties of their configuration variables [2]: (i) inextensible Kirchhoff rods, (ii) extensible Kirchhoff rods, and (iii) Cosserat rods. In the cases mentioned above, configurations computed by either of the three model variants turn out to be practically the same, as illustrated by Fig. 1:

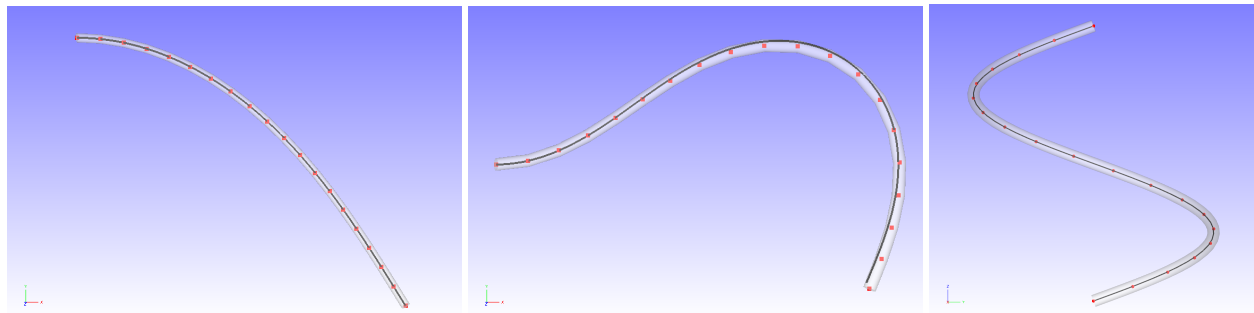


Figure 1: Analytical centerline curves of an inextensible Kirchhoff rod (solid lines) in plane bending (*left*: cantilever type, *middle*: both ends clamped) and helical (*right*) configurations. The red dots show the vertex positions computed with a discrete Cosserat rod model by minimization of the elastic energy (see [4] for details).

In our contribution, we investigate the influence of the effective stiffness parameters $[EA]$ and $[GA]$ of a Cosserat rod model that govern extension (or compression) of the centerline as well as transverse shearing of the cross sections on its equilibrium configurations in such cases. Our results open up the possibility to *set* the stiffness parameters $[EA]$ and $[GA]$ to proper values by *modeling* rather than measurements.

2. Modelling details and methodical approach

As explained in [2], the moving frames $\mathbf{R}(s) = \mathbf{a}^{(k)}(s) \otimes \mathbf{e}_k$ remain adapted to the centerline also in deformed configurations for model variants (i) and (ii), such that the unit tangent vector $\mathbf{t}(s) = \mathbf{r}'(s)/\|\mathbf{r}'(s)\|$ stays always orthogonal to the frame directors $\mathbf{a}^{(1,2)}(s)$ spanning the local cross section plane, and transverse shearing of the cross sections is kinematically inhibited. Variant (i) additionally postulates an inextensible centerline by requiring that $\|\mathbf{r}'(s)\| = 1$ holds for all deformed configurations. Differently, for variant (iii) neither adapted frames nor an inextensible centerline are assumed for deformed configurations.

Bending and twisting are affected by the related effective stiffness parameters $[EI]$ and $[GJ]$, respectively. For composite cables, one needs to treat these stiffness parameters as independent quantities. Often the mass per length ρ_L of a cable is sufficiently low, such that the influence of gravity can be considered as weak, and the shape of deformed configurations in static equilibrium mainly depends on the ratio $[GJ]/[EI]$. Therefore it is important to measure these stiffness parameters properly [3, 5].

While for homogeneous elastic specimens the measurement of extensional stiffness $[EA]$ is an elementary experimental task, obtaining reproducible results from measurements of composite cables turns out to be far more difficult [5], and a measurement of the shear stiffness $[GA]$ is practically impossible. Therefore it is important to understand the influence of the effective stiffness parameters $[EA]$ and $[GA]$ on the rod configurations in equilibrium both qualitatively and quantitatively. Apart from the overall shape, estimates of the extensional strain $\varepsilon_t(s) := \|\mathbf{r}'(s)\| - 1$ and shear angle $\vartheta_s(s) := \arccos(\langle \mathbf{a}^{(3)}(s), \mathbf{t}(s) \rangle)$ are of interest.

Assuming for simplicity zero gravity, equilibrium configurations of a straight inextensible Kirchhoff rod are local minima of its elastic bending and torsional energy, which in the case of transversally isotropic bending stiffness $[EI]$, torsional stiffness $[GJ]$ and cross sections with coinciding shear and area centers is given by $\mathcal{W}_{bt} = \frac{1}{2} \int_0^L ds [EI] \varkappa^2 + [GJ] \tau^2$, where $\varkappa(s)$ is the Frenet curvature of the centerline, and $\tau(s)$ is the twist of the adapted frame. For extensible Kirchhoff rods, the total elastic energy consists of the sum $\mathcal{W}_{el} = \mathcal{W}_{bt} + \mathcal{W}_{ext}$ with the extensional energy $\mathcal{W}_{ext} = \frac{1}{2} \int_0^L ds [EA] \varepsilon_t^2$. For Cosserat rods, the latter is replaced by the more complex energy term $\mathcal{W}_{es} = \frac{1}{2} \int_0^L ds [EA] (\Gamma^{(3)} - 1)^2 + [GA] (\Gamma^{(1)2} + \Gamma^{(2)2})$ measuring the elastic energy stored in extension and transverse shearing, where $\sqrt{\Gamma^{(1)2} + \Gamma^{(2)2}} = (1 + \varepsilon_t) \sin(|\vartheta_s|) \approx |\vartheta_s|$ and $\Gamma^{(3)} = (1 + \varepsilon_t) \cos(\vartheta_s) \approx 1 + \varepsilon_t$.

Introducing L as the characteristic unit to measure length induces $1/L$ as characteristic unit for curvature. The elastic energy terms can be scaled to dimensionless form as $\tilde{\mathcal{W}}_{bt} = \mathcal{W}_{bt}/W_{bt}^0$ and $\tilde{\mathcal{W}}_{es} = \mathcal{W}_{es}/W_{es}^0$, with characteristic energy values $W_{bt}^0 := [EI]/L$ and $W_{es}^0 := [EA]L$. For boundary value problems leading to deformed configurations dominated by bending and torsion, one needs to find local minima of the scaled elastic energy $\tilde{\mathcal{W}}_{el} = \mathcal{W}_{el}/W_{bt}^0 = \tilde{\mathcal{W}}_{bt} + \tilde{\mathcal{W}}_{es}/\lambda_0^2$, where $\lambda_0^2 := [EI]/([EA]L^2)$ is a small dimensionless parameter that can be estimated as $\lambda_0 \simeq \mathcal{O}(r_{IA}/L) \ll 1$ for the effective cross section radius $r_{IA} = 2\sqrt{I/A}$.

The energy minimization problem can be treated by Berdichevsky's approach of variational asymptotic analysis [7] to find approximate solutions for the Cosserat rod model, which to leading order coincide with those of the inextensible Kirchhoff model. For equilibrium values of both the extensional strains and shear angles one finds the rough order of magnitude estimates $\varepsilon_t, |\vartheta_s| \sim \mathcal{O}(\lambda_0^2)$. The same estimates can be obtained by applying similar arguments as brought forward by Audoly and Pomeau [6] (see section 3.7).

By considering the first integral $\mathbf{m} + \mathbf{r} \times \mathbf{f}$ of the equilibrium equations $\mathbf{f}' = \mathbf{0}$, $\mathbf{m}' + \mathbf{r}' \times \mathbf{f} = \mathbf{0}$, which hold for all rod model variants independent of the kinematical constraints, we derive sharp estimates of the extensional and transverse shear strains in equilibrium [8], and we illustrate our findings by numerical experiments.

References

- [1] S.S. Antman: *Nonlinear Problems of Elasticity*. Springer (2005).
- [2] J. Linn: *Discrete Cosserat Rod Kinematics Constructed on the Basis of the Difference Geometry of Framed Curves – Part I: Discrete Cosserat Curves on a Staggered Grid*. Journal of Elasticity **139**, 177–236 (2020).
- [3] J. Linn, F. Schneider, K. Dreßler, O. Hermanns: *Virtual Product Development and Digital Validation in Automotive Industry*. In Bock, H.G., Küfer, KH., Maass, P., Milde, A., Schulz, V. (eds): *German Success Stories in Industrial Mathematics*. Mathematics in Industry, Vol. **35**, 45-54, Springer (2021)
- [4] J. Linn, T. Hermansson, F. Andersson, F. Schneider. *Kinetic aspects of discrete Cosserat rods based on the difference geometry of framed curves*. In M. Valasek et al. (Eds.): *Proceedings of the ECCOMAS Thematic Conference on Multibody Dynamics 2017*, 163–176 (2017).
- [5] V. Dörlich, J. Linn, S. Diebels: *Flexible beam-like structures—experimental investigation and modeling of cables*. In: Altenbach, H., et al. (eds.): *Advances in Mechanics of Materials and Structural Analysis. Advanced Structured Materials*, Vol. **80**, 27–46, Springer (2018).
- [6] Audoly, B., Pomeau, Y.: *Elasticity and Geometry — From hair curls to the non-linear response of shells*. Oxford UP (2010).
- [7] Berdichevsky, V.L.: *On the energy of an elastic rod*. J. Appl. Math. Mech. **45**(4), 518–529 (1981).
- [8] J. Linn, F. Schneider-Jung, M. Roller, T. Hermansson: *Impact of shear and extensional stiffness on equilibrium configurations of elastic Cosserat rods*, submitted (2023).

Overview of numerical models for mechanical analysis of beam elements in fire developed by Chair of mechanics at UL FGG

Anita Ogrin¹, Robert Pečenko², Sebastjan Bratina³, Tomaž Hozjan⁴

¹ University of Ljubljana, Faculty of civil and geodetic engineering, anita.ogrin@fgg.uni-lj.si

² University of Ljubljana, Faculty of civil and geodetic engineering, robert.pecenko@fgg.uni-lj.si

³ University of Ljubljana, Faculty of civil and geodetic engineering, tomaz.hozjan@fgg.uni-lj.si

⁴ University of Ljubljana, Faculty of civil and geodetic engineering, sebastjan.bratina@fgg.uni-lj.si

Keywords: Beam finite elements, Numerical models, Fire analysis, Overview, UL FGG

1. Introduction

Influence of fire on mechanical behaviour of beam structural elements has been extensively addressed by researchers from Chair of mechanics at the University of Ljubljana, Faculty of civil and geodetic engineering (UL FGG) over the period of last 30 years. Our first software for calculation of nonlinear and non-stationary planar heat transfer over cross-section has been presented in 1987 [1] and the first numerical model for 2D mechanical analysis of steel frames in fire has been presented in 1991 [2]. The framework for development of numerical models for fire analysis of beam structural elements and frame structures have been various beam finite elements (FE) [3, 4, 5], which were also developed by members of Chair of mechanics at UL FGG. These are presented at HFSS 2023 conference in complementary contribution. Hereinafter, the two main steps in upgrading a numerical model for mechanical analysis of beam elements in normal temperature conditions into a numerical model for mechanical analysis of beam elements in fire are outlined, together with a brief overview of the developed numerical models.

2. Including influence of fire in numerical model for mechanical analysis of beam elements

2.1 Temperature dependent material properties

In general, material characteristics are included in a beam numerical model through constitutive equations, which connect equilibrium internal forces with constitutive internal forces and, consequently, with deformation quantities. The dependance of constitutive internal forces on deformation quantities follows the constitutive law, appropriately selected for the considered material, which is often presented in form of a stress-strain relationship. A shape of the stress-strain diagram is determined by a function, which describes the behaviour of material as linear, bi-linear, non-linear, elastic, elasto-plastic, visco-elastic, etc., and by values of mechanical properties of the material such as for example strengths, Young's modulus or limit strains. In fire, temperatures and therefore temperature dependent material properties change with time, they vary over cross-section and possibly also along the length of the structural element, depending on boundary conditions. At each time step and for each point, where stresses need to be evaluated, corresponding stress-strain relationship must be applied in the calculation. Temperature dependency of the material properties thus introduces non-linear behaviour even for the simplest linear-elastic material model.

2.2 Thermally induced strains

In the numerical models for mechanical analysis of beam elements, developed by Chair of mechanics at UL FGG, an additive decomposition of increment of geometrical strain has been assumed. An increment of geometrical strain, ΔD , at certain point of the beam is thus defined as the sum of different increments of strains:

- mechanical strain, ΔD_m , which is directly related to stresses through stress-strain relationship and can be further additively decomposed into elastic and plastic strain,
- thermal strain, ΔD_{th} , caused by expansion of material at elevated temperatures,
- creep strain, ΔD_{cr} , which also depends on temperature (besides time and stresses), and
- other strains inherent to certain materials, such as mechano-sorptive strain, ΔD_{ms} , related to the change of moisture content in timber, or transient strain in concrete, ΔD_{tr} , which occurs as a result of fast increase of temperatures in previously not loaded material.

Table 1. Numerical models for mechanical analysis of beam elements in fire, by Chair of mechanics at UL FGG.

Material	Numerical models and corresponding research focus	Components of ΔD
Steel	<ul style="list-style-type: none"> • Srpčič, 1991 [2], viscous creep, 2D, FE by [3] • Ogrin, 2017 [6], temperature gradient in transverse direction, 3D, FE by [5] 	$\Delta D_m, \Delta D_{th}, \Delta D_{cr}$
Reinforced concrete (RC)	<ul style="list-style-type: none"> • Bratina, 2003 [7], material softening, 2D, FE by [4] • Krauberger, 2008 [8], prestressed concrete, 2D, FE by [4] • Bajc, 2015 [9], buckling and spalling, 2D, FE by [4] • Ružič, 2015 [10], partially delaminated curved beams, 2D, FE by [4] 	Concrete : $\Delta D_m, \Delta D_{th}, \Delta D_{cr}, \Delta D_{tr}$ Reinforcing and prestressing steel : $\Delta D_m, \Delta D_{th}, \Delta D_{cr}$
Composite steel – RC	<ul style="list-style-type: none"> • Hozjan, 2009 [11], longitudinal slip, 2D, FE by [4] • Kolšek, 2013 [12], longitudinal and perpendicular slip, 2D, FE by [4] 	Concrete : $\Delta D_m, \Delta D_{th}, \Delta D_{cr}, \Delta D_{tr}$ Reinforcing and structural steel : $\Delta D_m, \Delta D_{th}, \Delta D_{cr}$
Timber	<ul style="list-style-type: none"> • Schnabl, 2007 [13], composite timber beams with longitudinal slip, 2D, FE by [4] • Pečenko, 2016 [14], variable beam height, 2D, FE by [4] 	[13]: ΔD_m (elastic part), ΔD_{th} [14]: $\Delta D_m, \Delta D_{th}, \Delta D_{cr}$

3. Conclusions

Each numerical model for mechanical analysis of beams in fire has been accompanied by extensive research on heat transfer through considered structural material. Among others, this research included thermal insulation of structural elements [6], spalling [9], charring [13, 14] and coupled moisture-heat transfer [8–14]. Development of an accurate and effective numerical model for coupled thermo-mechanical analysis of beams in fire remains one of our future goals.

Acknowledgements

The authors gratefully acknowledge the financial support from the Slovenian Research Agency (research core funding No. P2-0260 and Z2-3203).

References

- [1] G. Turk. *Programska oprema za račun nelinearnega in nestacionarnega prevajanja toplote z upoštevanjem raznih robnih pogojev in notranjega vira toplote zaradi hidratacije cementa*, Bachelor thesis, UL FGG, Ljubljana, 1987.
- [2] S. Srpčič. *Račun vpliva požara na jeklene konstrukcije*, PhD thesis, UL FGG, Ljubljana, 1991.
- [3] J. Banovec. *Geometrijska in materialna nelinearnost pri ravninskih okvirnih konstrukcijah*, PhD thesis, UL FGG, Ljubljana, 1986.
- [4] I. Planinc. *Račun kritičnih točk konstrukcij s kvadratično konvergentnimi metodami*, PhD thesis, UL FGG, Ljubljana, 1998.
- [5] P. Češarek. *Dinamika prostorskih linijskih elementov z interpolacijo deformacijskih količin*, PhD thesis, UL FGG, Ljubljana, 2013.
- [6] A. Ogrin. *Dinamična analiza prostorskih jeklenih okvirjev v požaru*, PhD thesis, UL FGG, Ljubljana, 2017.
- [7] S. Bratina. *Odziv armiranobetonskih linijskih konstrukcij na požarno obtežbo*, PhD thesis, UL FGG, Ljubljana, 2003.
- [8] N. Krauberger. *Vpliv požara na obnašanje ojačanih betonskih linijskih konstrukcij*, PhD thesis, UL FGG, Ljubljana, 2008.
- [9] U. Bajc. *Uklonska nosilnost armiranobetonskih okvirjev med požarom*, PhD thesis, UL FGG, Ljubljana, 2015.
- [10] D. Ružič. *Požarna analiza delno razslojenih ukrivljenih armiranobetonskih linijskih konstrukcij*, PhD thesis, UL FGG, Ljubljana, 2015.
- [11] T. Hozjan. *Nelinearna analiza vpliva požara na sovprežne linijske konstrukcije*, PhD thesis, UL FGG, Ljubljana, 2009.
- [12] J. Kolšek. *Požarna analiza dvoslojnih kompozitnih linijskih konstrukcij*, PhD thesis, UL FGG, Ljubljana, 2013.
- [13] S. Schnabl. *Mehanska in požarna analiza kompozitnih nosilcev*, PhD thesis, UL FGG, Ljubljana, 2007.
- [14] R. Pečenko. *Mehanski odziv ukrivljenih lesenih nosilcev s spremenljivo višino pri požarni obtežbi*, PhD thesis, UL FGG, Ljubljana, 2016.

Buckling of slender layered composite columns with incomplete interaction between the layers

M. Saje¹, I. Planinc², G. Turk³, G. Jelenić⁴, S. Schnabl⁵

¹ Faculty of Civil and Geodetic Engineering, University of Ljubljana, miran.saje@fgg.uni-lj.si

² Faculty of Civil and Geodetic Engineering, University of Ljubljana, igor.planinc@fgg.uni-lj.si

³ Faculty of Civil and Geodetic Engineering, University of Ljubljana, goran.turk@fgg.uni-lj.si

⁴ Faculty of Civil Engineering, University of Rijeka, gordan.jelenic@gradri.uniri.hr

⁵ Faculty of Chemistry and Chemical Technology, University of Ljubljana, simon.schnabl@fktk.uni-lj.si

Keywords: Buckling, Composite, Column, Slender, Slip

1. Introduction

Layered columns made of different or similar materials are often used in a variety of applications. Due to their high strength to weight ratio and stiffness to weight ratio, slender composite columns are commonly used in aerospace, building construction, shipbuilding and other industries. Typical examples of the above layered structures in construction are steel-concrete and wood-concrete composite columns, layered wood columns, sandwich columns, concrete columns reinforced externally with laminates and many more. The behaviour of these structures depends largely on the type of connection between the layers and the quality of the materials used. Since an absolutely rigid connection between the layers cannot be achieved in practise, slip and also uplift may occur between the layers, which can significantly affect the mechanical behaviour of the layered structure. Accordingly, slip and sometimes uplift between layers must be taken into account in the so-called partial interaction analysis of composite structures. Therefore, there are many publications in the literature that consider sliding and uplift between layers analytically or numerically. The strength of columns with straight layers depends to a large extent on their stability and the cohesion between the layers. It is therefore of practical importance to derive exact solutions to such problems. So far, few exact slip and buckling models for composite columns have been developed in the literature and no attempt is made to discuss them here. In this paper, we briefly review our various approaches to modelling layered composite columns with incomplete interaction between layers. In all these attempts the critical buckling loads of geometrically perfect, materially linear and nonlinear two-layer composite columns with linear and nonlinear compliant interfaces are analysed using the linearised stability theory. Therefore, the exact critical buckling forces are determined from the solution of a linear eigenvalue problem, i.e. $\det \mathbf{K}=0$.

2. Review

In the following, a brief overview of some papers dealing with the buckling behaviour of layered composite columns with partial interaction between layers is given. First, the inelastic buckling of a two-layer composite column with nonlinear interfacial compliance is analysed and illustrated in Figure 1, see [1].

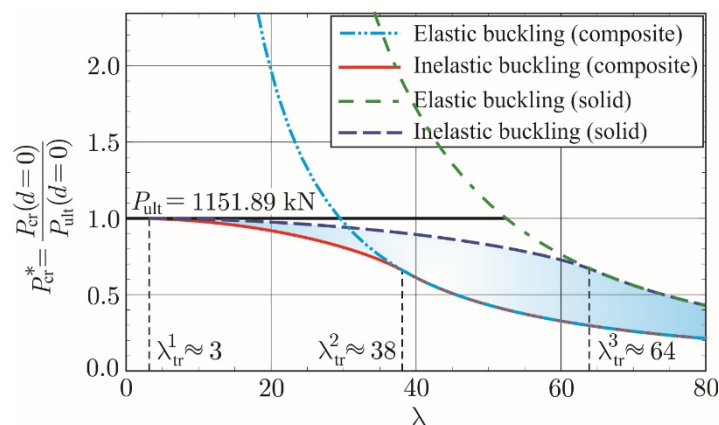


Figure 1. Non-dimensional column elastic and inelastic buckling curves for solid and two-layer composite column.

P_{cr} in Figure 1 is the critical buckling load, and λ is the slenderness. Furthermore, the work of Schnabl and Planinc [2] deals with the exact buckling loads of two-layer Reissner composite columns with interlayer slip and uplift. Figure 2 shows the buckling forces and modes for different uplift contact stiffnesses C .

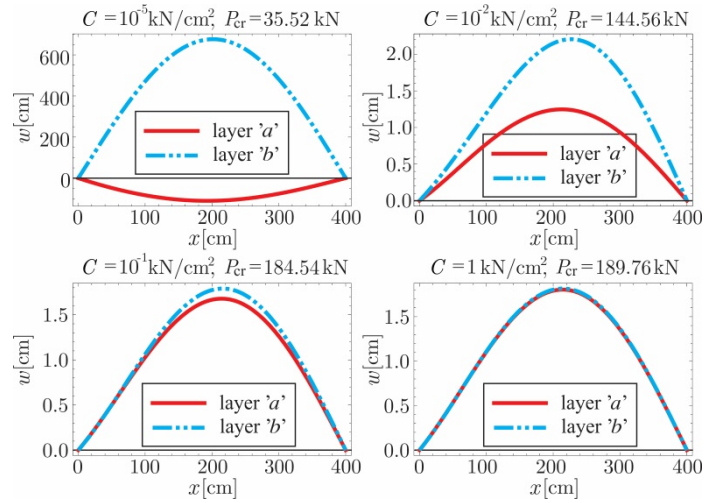


Figure 2. First buckling modes of layers a and b , and critical buckling loads P_{cr} of pinned-pinned composite column for $K=1$ kN/cm² and various values of C .

Similarly, Schnabl et al. [3] was analyzing analytically the buckling of slender circular concrete-filled steel

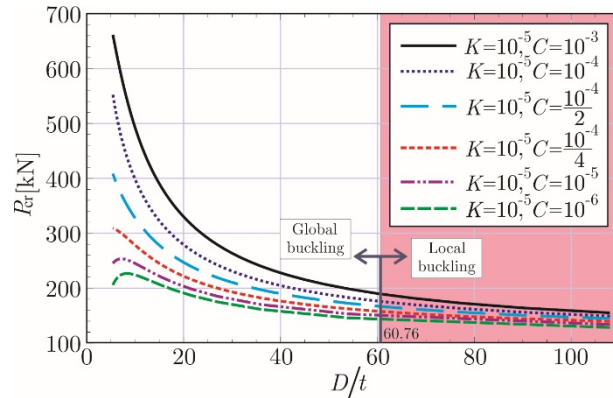


Figure 3. Effect of diameter-to-thickness ratio on critical buckling loads of circular pinned-pinned CFST composite columns for various interfacial stiffnesses K and C .

tubular columns (CFST) with compliant interfaces. Figure 3 shows a critical buckling load P_{cr} versus diameter-to-thickness ratio of the CFST column for various interfacial stiffnesses K and C .

3. Conclusions

It is shown that incomplete interaction between layers can have a significant effect on the buckling behaviour of layered composite columns.

References

- [1] S. Schnabl, I. Planinc. *Inelastic buckling of two-layer composite columns with non-linear interface compliance*, International Journal of Mechanical Sciences, 53 (2011) 1077-1083.
- [2] S. Schnabl, I. Planinc. *Exact buckling loads of two-layer composite Reissner's columns with interlayer slip and uplift*, International Journal of Solids and Structures, 50 (2013) 30-37.
- [3] S. Schnabl, G. Jelenić, I. Planinc. *Analytical buckling of slender circular concrete-filled steel tubular columns with compliant interfaces*, Journal of Constructional Steel Research, 115 (2015) 252-262.

Low-order analytical solution for vibration of tensioned cables

Alexandre de M. Wahrhaftig¹, Eduardo M. de O. Lopes², Gabriel R. do Amaral³, José M. Balthazar⁴,
 Kevin M. M. Ribeiro⁵

¹ Federal University of Bahia (UFBA), alixa@ufba.br, iagogo@ufba.br

^{2,3} Federal University of Paraná (UFPR), eduardo_lopes@ufpr.br, eng.kevin.mmr@gmail.com

⁴ São Paulo State University (UNESP), manael.balthazar@unesp.br

⁵ Institute of Technology for Development (ITD), gabriel.amaral@lactec.org.br

Keywords: Low-order Analytical Solution, Rayleigh Method, Highly Flexible Slender Structures, Cables, Finite Element Method

1. Introduction

Cables are extraordinarily slender and eminently flexible structures on their own nature. Often, these elements need to be tensioned to enable the construction of systems formed by them. The use of a tensile force modifies the frequencies of lateral vibrations because it alters the portion of geometric stiffness [1]. In determining these frequencies, low-order analytical models are particularly desired due to the ease they provide for analysis. In this work, a low-order analytical solution is compared with results that come from the finite element method (FEM) obtained by computational modelling.

2. Low-order analytical solution

The adopted low-order analytical solution was based on Rayleigh's method assuming a sinusoidal function $\phi(x) = \sin(n\pi x/L)$ [2] as a shape function to describe the lateral vibration modes, n , from 1 up to 3. The method reduces the system into another one with just a single degree-of-freedom. The solution is obtained directly in the continuum, and the adopted shape function is admitted valid in the entire domain of the problem. Thus, it is possible to obtain a closed-form equation for the present problem, Eq. (1).

$$f = \frac{1}{2} \left[\frac{n^2 \cos(n\pi) \sin(n\pi) ((-n^2)\pi^2 EI + PL^2) + n^3 \pi^3 EI + PL^2 n\pi}{L^4 \bar{m} [(-\cos(n\pi)) \sin(n\pi) + n\pi]} \right]^{1/2} \text{ Hz} . \quad (1)$$

3. FEM solution

The analytical results were assessed through a modal analysis of non-linear geometric characteristics using FEM [3]. The individual elements in modelling were beam elements with 6 degrees of freedom [4]. The FEM solution was obtained by solving the secular Eq. (2) where ω are the eigenvalues and ϕ the eigenvectors. In FEM, the shape functions are polynomial equations valid for the given subdomain, i. e., the individual elements. In Eq. (2), $[M]$ is the mass matrix, and $[K]$ is the total stiffness matrix, which includes the flexural and geometric parcels [5]. The frequencies, in Hz, are found by doing $f = \omega/2\pi$.

$$\{[K] - \omega^2 [M]\} \phi = 0 . \quad (2)$$

4. Cable description

A system AB consisting of a steel cable with Young's modulus $E = 2010.82 \text{ N/mm}^2$, diameter $d = 18.30 \text{ mm}$ (area $A = \pi d^2/4$, inertia $I = \pi d^4/64$), span length $L = 13385 \text{ mm}$, and density $\rho = 30301.13 \text{ kg/m}^3$, was used in the simulations. The cable was tensioned by a force $P = 15.86 \text{ kN}$ as shown in Figure 1, where f indicates frequencies and $\bar{m} = A\rho$ is mass per unity length.

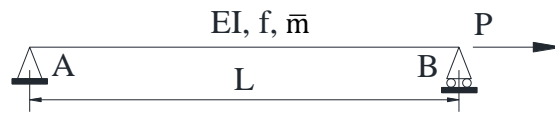


Figure 1. Cable description and static model.

5. Results and discussions

The natural frequencies and mode shapes can be found in Table 1 and Figure 2. In FEM, the domain of the problem was divided into 50 beam elements.

Table 1. Natural frequency values (in Hz).

Vibration mode – n	Analytical – Eq. (1)	FEM – Eq. (2)	Difference (%)
1	5.218509	5.218502	0.000134
2	10.437620	10.437546	0.000709
3	15.657935	15.657782	0.000977

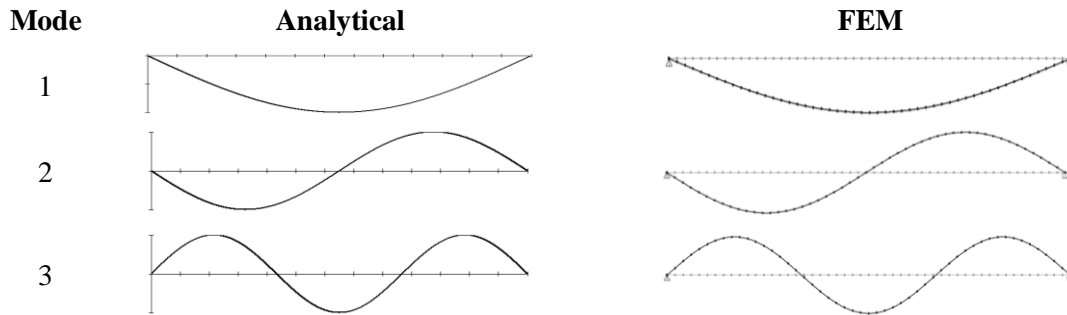


Figure 2. Mode shapes of lateral vibration.

6. Conclusions

It is verified that the results obtained by the adopted low-order solution match well with those produced by computational modelling via FEM of geometric non-linear characteristics, for both frequencies and vibration modes from 1 up to 3.

References

- [1] M. Khalkhaliha, P. Zarfam, R. Zarfam. *Nonlinear Structural Behavior and Vibration Control of a Double Curved Cable net under the Dynamic Excitations*. Lat. Am. J. Solids Struct, 17 (2020). <https://doi.org/10.1590/1679-78255884>
- [2] A. Wahrhaftig, R. Rodrigues, R. Carvalho, A. Fortes. *Strengthening Reinforced Concrete Beams with Carbon Fiber Laminate Mounted in a U-Shape for Static and Vibration Purposes*. Int J Civ Eng 20 (2022) 27–40. <https://doi.org/10.1007/s40999-021-00654-4>.
- [3] A. Wahrhaftig, J. Dantas, R. Brasil, L. Kloda. *Control of the Vibration of Simply Supported Beams Using Springs with Proportional Stiffness to the Axially Applied Force*. J. Vib. Eng. Technol. 10 (2022) 2163–2177. <https://doi.org/10.1007/s42417-022-00502-2>
- [4] A. Wahrhaftig, K. Magalhães, R. Brasil, K. Murawski. *Evaluation of Mathematical Solutions for the Determination of Buckling of Columns Under Self-weight*. J. Vib. Eng. Technol. 9 (2021) 733–749. <https://doi.org/10.1007/s42417-020-00258-7>
- [5] A. Wahrhaftig, K. Magalhães, M. Silva, R. Brasil, J. Banerjee. *Buckling and free vibration analysis of non-prismatic columns using optimized shape functions and Rayleigh method*, Eur. J. Mech - A/Solids, 94 (2022) 104543. <https://doi.org/10.1016/j.euromechsol.2022.104543>

On solving the kinematical equations of Cosserat beams

E. Zupan¹, A. Ogrin², D. Zupan³

¹ University of Ljubljana, Faculty of Civil and Geodetic Engineering, eva.zupan.lj@gmail.com

² University of Ljubljana, Faculty of Civil and Geodetic Engineering, anita.ogrin@fgg.uni-lj.si

³ University of Ljubljana, Faculty of Civil and Geodetic Engineering, dejan.zupan@fgg.uni-lj.si

Keywords: Kinematic equations, strains, rotations, kinematic compatibility

1. Introduction

Geometry of a three-dimensional beam is described by the line of centroids of cross-sections and by the family of the cross-sections not necessarily normal to the line of centroids at the deformed state; therefore, the configuration space of the beam consists of (i) the linear space of position vector of the line of centroids, and (ii) the non-linear space of rotations of cross-sections. Thus, the configuration space of a beam is a non-linear manifold, which makes their treatment so challenging. Although the configurational quantities are important for the description of the current state of the structure, their derivatives with respect to axis coordinate and their derivatives with respect to time are the natural quantities for the description of the total mechanical energy of the system. This suggests alternative, in many perspectives more natural, choices for the primary interpolated variables in finite-element formulations.

We will here focus on formulations where the strains and/or the velocities and angular velocities are the primary interpolated quantities of the beam-like structure. The fundamental problem of such approaches is the integration of configurational quantities, i.e. displacements and rotations, from the given or assumed field at the level of derivatives. In general, the exact solution of the kinematic equations of a three-dimensional beam is not known which was a motivation for several numerical and approximative solution strategies discussed here.

2. Kinematic equations

In Cosserat beam model, the resultant strains of the cross section are directly introduced. They will be presented here with respect to the local frame. The translational strain vector, $\mathbf{\Gamma}$, consists of an extensional strain and two shear strain components. It is defined by the following equation

$$\mathbf{\Gamma} = \mathbf{R}^T \mathbf{r}' + \mathbf{\Gamma}_0, \quad (1)$$

where \mathbf{r} is the position vector, \mathbf{R} denotes the rotation matrix, and $\mathbf{\Gamma}_0$ a constant that is determined from known initial configuration of the beam. The prime ($'$) denotes the derivative with respect to x – the arc-length parameter of the axis of the beam. The rotational strain, \mathbf{K} , consists of a torsional and two bending strain components. It is determined by

$$\mathbf{S}(\mathbf{K}) = \mathbf{R}^T \mathbf{R}', \quad (2)$$

where the skew-symmetric matrix $\mathbf{S}(\mathbf{K})$ composed from the components of vector \mathbf{K} describes the rate of change of the local basis with respect to the local basis.

In dynamics, the measures for the rate of change of configuration variables with respect to time are also needed. For the reference curve, we simply have

$$\mathbf{v} = \dot{\mathbf{r}}, \quad (3)$$

describing its velocity with respect to the fixed basis, while the angular velocity of cross sections is defined as

$$\mathbf{S}(\mathbf{\Omega}) = \mathbf{R}^T \dot{\mathbf{R}}. \quad (4)$$

The dot above a symbol ($\dot{\cdot}$) denotes the time derivative.

3. Solution procedures

To preserve the properties of configuration space, equations (2) and (4) need to be solved in such way that the orthogonality of rotational matrices is conserved, which in matrix notation introduces six scalar constraints. To

reduce the complexity of the problem we propose two approaches: i) the rotational vector-based approach and ii) the quaternion-based approach.

When rotations are parametrised with rotational vector, $\boldsymbol{\vartheta}$, the rotational strain can be expressed as:

$$\mathbf{K} = \mathbf{T}^T \boldsymbol{\vartheta}', \quad \boldsymbol{\Omega} = \mathbf{T}^T \dot{\boldsymbol{\vartheta}}, \quad (5)$$

where \mathbf{T} denotes a transformation matrix dependent solely on $\boldsymbol{\vartheta}$. For solving (5) standard numerical methods for ordinary differential equations can be efficiently used as reported by Zupan and Saje [1]. However, with the introduction of rotational vector we cannot avoid the need to evaluate rotational matrices since the rotational vectors cannot be treated as elements of Euclidean space – they are not additive.

A promising alternative are the four-parameter rotational quaternions. In quaternion notation equations (2) and (4) read

$$\mathbf{K} = 2\hat{\mathbf{q}}^* \circ \hat{\mathbf{q}}' \quad \boldsymbol{\Omega} = 2\hat{\mathbf{q}}^* \circ \dot{\hat{\mathbf{q}}} \quad (6)$$

where $\hat{\mathbf{q}}$ is a four-dimensional vector that has a unit norm, $|\hat{\mathbf{q}}| = 1$, called rotational quaternion, while " \circ " denotes the quaternion multiplication. The introduction of rotational quaternions elegantly avoids the need to use both rotational matrices and rotational vectors in numerical procedures while introducing only one algebraic constraint. The numerical integration of rotational quaternions from angular velocities was studied by Saje and Zupan [2] which resulted in successful implementation of quaternion approach to beam formulations. Latter, Zupan and Zupan [3] proposed the exact and approximate closed-form results for the integration of angular velocities.

We need to stress that these approaches study the problem in only one dimension, i.e. only in space or only in time, and do not treat the problem as coupled.

4. Coupled systems

Despite complete analogy between the kinematic equations in space and time the coupled treatment of both equations brings additional complexity. Let us focus on the coupling between the strains and the velocities. By comparing mixed partial derivatives of (1)–(4), we get

$$\dot{\boldsymbol{\Gamma}} = \hat{\mathbf{q}}^* \circ \mathbf{v}' \circ \hat{\mathbf{q}} + (\boldsymbol{\Gamma} - \boldsymbol{\Gamma}_0) \times \boldsymbol{\Omega}, \quad \dot{\mathbf{K}} = \boldsymbol{\Omega}' + \mathbf{K} \times \boldsymbol{\Omega}. \quad (7)$$

The significance of equation (7) was pointed out by Ogrin and Saje [4] and used for proposing approximate solution for the angular velocity in case of known rotational strain, while Zupan and Zupan [5] employed the mid-time discretization of these equations to propose a novel energy-preserving numerical formulation for velocity-based geometrically exact three-dimensional beams.

Acknowledgement

This work was supported by the Slovenian Research Agency through the research programme P2-0260. The support is gratefully acknowledged.

References

- [1] D. Zupan and M. Saje. Finite-element formulation of geometrically exact three-dimensional beam theories based on interpolation of strain measures. *Comput. Meth. Appl. Mech. Eng.*, 192(49-50):5209–5248, 2003.
- [2] E. Zupan, M. Saje, and D. Zupan. The quaternion-based three-dimensional beam theory. *Comput. Meth. Appl. Mech. Eng.*, 198(49-52):3944–3956, 2009.
- [3] E. Zupan and D. Zupan. On higher order integration of angular velocities using quaternions. *Mech. Res. Commun.*, 55:77–85, 2014.
- [4] A. Ogrin and M. Saje. Integrating rotation and angular velocity from curvature. *Adv. Eng. Softw.*, 85:26–42, 2015.
- [5] Zupan, E., Zupan, D. On conservation of energy and kinematic compatibility in dynamics of nonlinear velocity-based three-dimensional beams. *Nonlinear Dynamics*, 95:1379–1394, 2019.

Challenges in dynamics of non-linear beams

P. Češarek¹, E. Zupan², M. Gams³, D. Zupan⁴

¹ Faculty of Civil and Geodetic Engineering, University of Ljubljana, peter.cesarek@fgg.uni-lj.si

² Faculty of Civil and Geodetic Engineering, University of Ljubljana, eva.zupan.lj@gmail.com

³ Faculty of Civil and Geodetic Engineering, University of Ljubljana, matija.gams@fgg.uni-lj.si

⁴ Faculty of Civil and Geodetic Engineering, University of Ljubljana, dejan.zupan@fgg.uni-lj.si

Keywords: beams, dynamics, strain-based formulations, velocity-based formulations, energy conservation

1. Introduction

Since the pioneering works by Simo and his coworkers [1] many innovative numerical formulations for the dynamic analysis of geometrically non-linear beams have been proposed, where displacements and rotations are taken as primary variables for the spatial and time discretization. However, from the implementation perspective, other aspects like accuracy, stability and robustness count more. We focus here on two interesting aspects of dynamic formulations: i) the use of strain measures for spatial discretization and ii) the long-term stability achieved by algorithmic preservation of total mechanical energy for conservative systems.

2. Governing equations

The balance equations of a three-dimensional beam read

$$\mathbf{n}' + \tilde{\mathbf{n}} - \frac{d}{dt}(\rho A \mathbf{v}) = \mathbf{0}, \quad \mathbf{m}' + \mathbf{r}' \times \mathbf{n} + \tilde{\mathbf{m}} - \frac{d}{dt}(\mathbf{R} \mathbf{J}_\rho \boldsymbol{\Omega}) = \mathbf{0}. \quad (1)$$

Here, \mathbf{n} and \mathbf{m} represent the stress-resultant force and moment vectors of the cross-section, while $\tilde{\mathbf{n}}$ and $\tilde{\mathbf{m}}$ are the external distributed force and moment vectors, all expressed with respect to the fixed basis; ρ is mass per unit of the initial volume; A is the area of the cross-section; \mathbf{J}_ρ is the mass-inertia matrix of the cross-section. The prime ($'$) denotes the derivative with respect to the parameter of the axis of the beam and the dot above a symbol ($\dot{\cdot}$) denotes the time derivative.

The velocity and angular velocity, \mathbf{v} and $\boldsymbol{\Omega}$, are directly related to configurational variables – the position vector, \mathbf{r} , and the rotation matrix, \mathbf{R} , through kinematic equations

$$\mathbf{v} = \dot{\mathbf{r}}, \quad \mathbf{S}(\boldsymbol{\Omega}) = \mathbf{R}^T \dot{\mathbf{R}}. \quad (2)$$

where the skew-symmetric matrix $\mathbf{S}(\boldsymbol{\Omega})$ composed from the components of vector $\boldsymbol{\Omega}$ describes the rate of change of the local basis with respect to the local basis. In spatial dimension the same configurational variables define the resultant strain measures through analogous differential equations:

$$\boldsymbol{\Gamma} = \mathbf{R}^T \mathbf{r}' + \boldsymbol{\Gamma}_0, \quad \mathbf{S}(\mathbf{K}) = \mathbf{R}^T \mathbf{R}'. \quad (3)$$

Thus, translational strain vector, $\boldsymbol{\Gamma}$, describes the rate of change of the position vector along the length of the beam, while the rotational strain, \mathbf{K} , describes the rate of change of the local basis along the length. They are both expressed with respect to the local basis.

The stress-resultants are here assumed to be depended directly on strain vectors through the constitutive relations

$$\mathbf{n} = \mathbf{R} \mathcal{C}_N(\boldsymbol{\Gamma}, \mathbf{K}), \quad \mathbf{m} = \mathbf{R} \mathcal{C}_M(\boldsymbol{\Gamma}, \mathbf{K}), \quad (4)$$

with operators \mathcal{C}_N and \mathcal{C}_M being invariant under superimposed rigid-body motions and at least once differentiable, but otherwise arbitrary.

3. Strain-based approach

In static analysis of frame-like structures the strain-based beam formulations represent an interesting alternative with several advantages and proven computational efficiency, see, e.g., the paper by Zupan and Saje [2]. To

extend the strain-based formulations for dynamics several numerical models were proposed. Gams, Planinc and Saje [3] proposed a strain-based formulation for the dynamic analysis of planar frames, which was later extended by Češarek, Saje and Zupan [4] for spatial-frame dynamics. The crucial idea of these formulations is to replace the strain vectors with discrete values at the given points x_p , $p = 1, \dots, N$ and interpolate them by a set of N interpolation functions $I_p(x)$:

$$\mathbf{\Gamma}(x, t) = \sum_{p=1}^N I_p(x) \mathbf{\Gamma}^p(t), \quad \mathbf{K}(x, t) = \sum_{p=1}^N I_p(x) \mathbf{K}^p(t). \quad (5)$$

The proposed formulations are strain-objective, path independent, locking-free and convenient in describing materially non-linear problems. Combining strain based approach with time integration scheme does not automatically assure energy preservation, which was the motivation for further enhancements.

4. Energy conservation

Despite complete analogy between the kinematic equations in space and time the coupled treatment of both equations brings additional complexity. Let us focus on the coupling between the strains and the velocities. By comparing mixed partial derivatives of (2)–(3), we get

$$\dot{\mathbf{\Gamma}} = \widehat{\mathbf{q}}^* \circ \mathbf{v}' \circ \widehat{\mathbf{q}} + (\mathbf{\Gamma} - \mathbf{\Gamma}_0) \times \mathbf{\Omega}, \quad \dot{\mathbf{K}} = \mathbf{\Omega}' + \mathbf{K} \times \mathbf{\Omega}. \quad (6)$$

A finite-size incremental strain update based on the time discrete compatibility relations (6) is a distinctive property of the unconventional energy preserving scheme by Gams, Planinc and Saje [5]. The kinematic compatibility (6) was also a motivation for the formulation based on the spatial derivatives of velocities and angular velocities of Češarek and Zupan [6] and the formulation where velocities and angular velocities are interpolated proposed by Zupan and Zupan [7]. The velocity-based approach shows improved robustness and stability but does not automatically guarantee energy preservation. This was the motivation for energy-conserving method by Zupan and Zupan [8] that is preserving the advantages of the velocity-based approach presented .

Acknowledgement

This work was supported by the Slovenian Research Agency through the research programme P2-0260. The support is gratefully acknowledged.

References

- [1] J. C. Simo and L. Vu-Quoc. On the dynamics in space of rods undergoing large motions - a geometrically exact approach. *Comput. Meth. Appl. Mech. Eng.*, 66(2):125–161, 1988.
- [2] Dejan Zupan and Miran Saje. Finite-element formulation of geometrically exact three-dimensional beam theories based on interpolation of strain measures. *Comput. Meth. Appl. Mech. Eng.*, 192(49-50):5209–5248, 2003.
- [3] M. Gams, I. Planinc, and M. Saje. The strain-based beam finite elements in multibody dynamics. *J. Sound Vibr.*, 305(1-2):194–210, 2007.
- [4] P. Češarek, M. Saje, and D. Zupan. Dynamics of flexible beams: Finite-element formulation based on interpolation of strain measures. *Finite Elem. Anal. Des.*, 72:47–63, 2013.
- [5] M. Gams, I. Planinc, and M. Saje. Energy conserving time integration scheme for geometrically exact beam. *Comput. Meth. Appl. Mech. Eng.*, 196(17-20):2117–2129, 2007.
- [6] P. Češarek and D. Zupan. On the stability of Lie group time integration in multibody dynamics. In H. M. Götzt and P. Ziegler, editors, *The 2nd Joint Conference on Multibody System Dynamics, May 29–June 1, 2012, Stuttgart, Germany. Book of Abstracts*, pages 42–43, 2012.
- [7] E. Zupan and D. Zupan. Velocity-based approach in non-linear dynamics of three-dimensional beams with enforced kinematic compatibility. *Comput. Meth. Appl. Mech. Eng.*, 310:406–428, 2016.
- [8] Zupan, E., Zupan, D. On conservation of energy and kinematic compatibility in dynamics of nonlinear velocity-based three-dimensional beams. *Nonlinear Dynamics*, 95:1379–1394, 2019.

MS-7: Modelling and simulation of textile and fibrous materials

Finite element analysis of textile cords in rubber-cord composites under compressive loadings: a filament scale approach

G. Auteri¹, M. Chassagne², D. Durville¹, J. Neggers¹

¹ Université Paris-Saclay, CentraleSupélec, ENS Paris-Saclay, CNRS, LMPS - Laboratoire de Mécanique Paris-Saclay, 3 rue Joliot-Curie, Gif-sur-Yvette 91190, France,
{gianluca.auteri, damien.durville, jan.neggers}@centralesupelec.fr

² Conception Tests et Modèles Matériaux Textiles, Centre de Technologie Michelin Europe, Site de Ladoux, 63040 Clermont Ferrand Cedex 9

Keywords: cords-rubber composites, finite element analysis, kink band, textile reinforcements

1. Introduction

Textile cords reinforced rubber composites constitute the structural core of many industrial components such as tyres, hoses and conveyor belts [1]. A textile cord can be described as a hierarchical structure, composed by two twisted yarns, in turn, made up of many twisted polymer filaments (PET, Nylon, etc.). When the whole assembly undergoes macroscopic loading, capturing its response at the scale of the filaments is crucial for understanding the textile reinforcement damage mechanism. Compressive solicitation in the filament may lead to the creation of kink bands: defects generated by localized buckling in the oriented fibre structure [2]. This defect severely weakens the fibre, making it more prone to fracture under tensile loads, eventually reducing the lifespan of the composite.

2. Methodology

In this work, the cord mechanics is simulated with Multifil, a finite element code dedicated to entangled structures. The initial configuration of the cord is obtained by simulating first the twisting of a bundle of filaments to form a single ply, and then by simulating the twisting of two plies. The cord is then embedded within a matrix. The solid element mesh for the matrix and the beam element mesh for the twisted yarn are overlapping, and special connection elements are introduced at the periphery of the yarn to ensure the coupling between both structures. Each filament is represented with a kinematically enriched beam model and the general problem addressed is the mechanical equilibrium of beam assemblies undergoing large deformations and developing contact-friction interactions [3]. The kinematic of the beam allows to express the position vector of a general particle in the beam as a first Taylor expansion with respect to its transverse coordinates. This allows to compute the axial Green-Lagrange strain over a beam cross-section as:

$$E_{33}(\xi_1, \xi_2) = E_{33}^0(\xi_3) + \xi_1 E_{33}^1(\xi_3) + \xi_2 E_{33}^2(\xi_3), \quad (1)$$

where ξ_1 and ξ_2 are the transverse coordinates, ξ_3 is the curvilinear abscissa, E_{33}^0 is the longitudinal strain at the centre of the cross-section while E_{33}^1 and E_{33}^2 are the values at two points on the periphery of the section. Therefore, it is possible to identify the filament local curvature with:

$$k = \sqrt{E_{33}^1(\xi_3) + E_{33}^2(\xi_3)}. \quad (2)$$

3. Findings

As global bending and compression are applied to the elastomer-cord specimen, the cord tends to open, meaning that a gap is created between the two yarns. The filaments have the freedom to curve locally and some of them are subjected to severe bending, leading to high compressive strains in specific filament sections. This mechanism is highlighted in Figure 1, which also shows the axial strain along the cord filaments. Since a textile cord is made up of a considerable number of components, the most effective way to look at the filaments state is to plot the distribution of a quantity of interest along discretized cross-sections, rather than the absolute minimum or maximum quantities. The local curvature provides direct evidence of the freedom that single filaments have to curve locally while the minima cross-sectional strain directly allows to detect the amount of filament zones that could potentially be affected by the creation of a defect. The methodology proposed

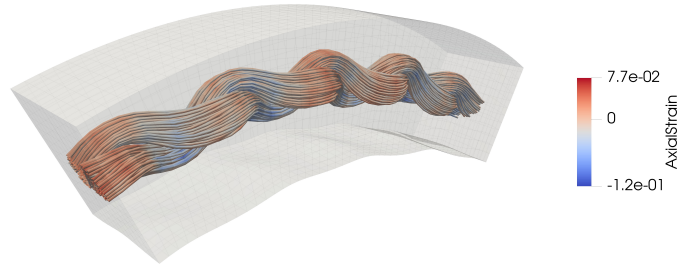


Figure 1: Filament scale finite element simulation of a textile cord undergoing bending-compression deformations: axial strains.

allows to reveal the difference between different cord loading states. As an example, the difference between free bending and bending with a transverse pressure (over a rigid body) is proposed. Figure 2 provides the distributions of local curvatures and minima longitudinal strains under both conditions. In the case of free bending, the local curvature distribution is significantly shifted towards higher values. Thus, indicating that, under this condition, more freedom is given to the local movements of the single filaments. As a consequence of the acute local bending, in the free bending case, the filaments can also reach significant values of longitudinal compressive strain (up to -10%), which could be critical for kink band initiation. The outcome is that the application of a transverse pressure is beneficial for the damage mechanism of filaments, as it reduces their freedom to create sharp local bends, hence critical compressive strains.

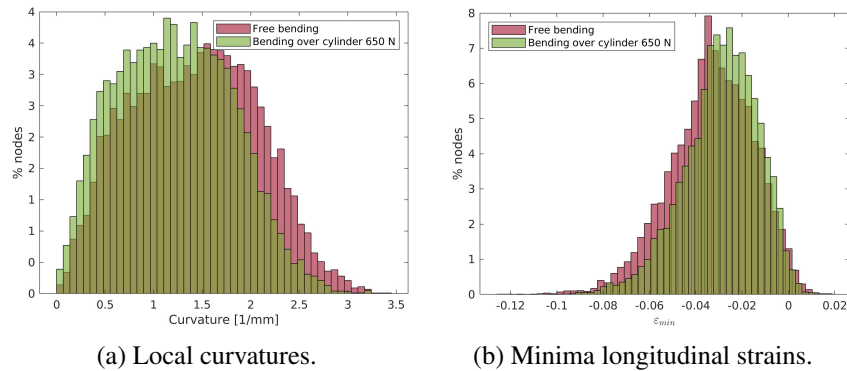


Figure 2: Cord after free bending (red) and bending over cylinder (green). Distribution of (a) local curvatures and (b) minima longitudinal strains along the nodes of cords filaments.

4. Conclusions

The study of cord-elastomer composites at the scale of the filaments allows to better understand the complex deformation behavior of entangled structures. The methodology proposed allows to quantify and compare the filament state under different conditions. In the case of bending/compression macroscopic loadings, the opening mechanism of the cord leaves freedom for the filaments to locally bend, achieving high compressive strains. Finally, it is shown that a transverse pressure has the effect of limiting the movement of the filaments, reducing the compressive strains, therefore slowing down the damage mechanism.

References

- [1] Maikson LP Tonatto, Maria MC Forte, and Sandro C Amico. Compressive-tensile fatigue behavior of cords/rubber composites. *Polymer Testing*, 61:185–190, 2017.
- [2] MG Dobb, DJ Johnson, and BP Saville. Compressional behaviour of kevlar fibres. *Polymer*, 22(7):960–965, 1981.
- [3] Damien Durville. Contact-friction modeling within elastic beam assemblies: an application to knot tightening. *Computational Mechanics*, 49(6):687–707, 2012.

Modeling the friction between yarns within a laid-strand synthetic ropes by hyperelasto-plasticity in finite deformation

L. Civier^{1,2,3}, G. Bles¹, N. Hamila⁴, P. Davies^{2,3}, Y. Marco¹

¹ IRDL-UMR CNRS 6027, ENSTA Bretagne, 2 Rue François Verny, 29200, Brest, France,
laure.civier@ensta-bretagne.org, guilhem.bles@ensta-bretagne.fr

² IFREMER Centre Bretagne, Marine Structures Laboratory, 29280, Plouzané, France

³ France Energies Marines, 525 Av. Alexis de Rochon, 29280, Plouzané, France

⁴ IRDL-UMR CNRS 6027, ENI Brest, 29200, Brest, France

Keywords: synthetic rope, large deformation, multi-scale, numerical simulation, FEA

1. Motivation

Polyamide-fiber parallel-laid-strand ropes are candidate for the shallow-water mooring lines of the future floating offshore wind turbines [1]. Their mesoscopic scale follows a hierarchical architecture: subrope, strands, rope-yarns, yarns, filaments. Their mechanical behavior is the result of friction between components and the visco-elasto-plastic behavior of the filament material. Today, some varying hysteretic phenomena with cyclic loadings are observed but we are not able to distinguish the material and fibres re-arrangement contributions. Moreover, a pretension procedure called bedding-in is usually performed at installation stage to stabilize the rope elongation. This stabilization is partly related to fibres re-arrangement driven by internal friction but also due to material properties. A better understanding of these both contributions may ease the bedding-in procedure specification. Also, under cyclic loading, a fatigue damage based on the component frictions occurs and is a matter of concern for a 20-year service life. To distinguish the dissipated energy due to the friction from viscoelasticity will help us to improve the fatigue life prediction by self-heating measurements, based on the dissipated energy during cycling. Because friction phenomena and fibre re-arrangement at the different scales are difficult to obtain experimentally, we adopted a modeling approach.

2. Method

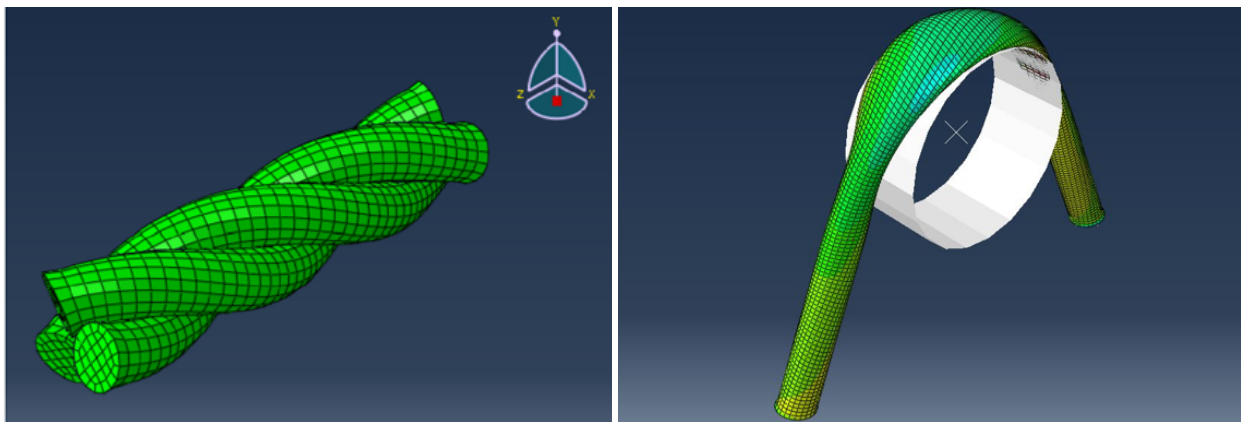


Figure 1: LEFT – Finite element simulation of a tensioned synthetic subrope composed of three laid strands. RIGHT – Finite element simulation of the contact between one strand and a rigid rod.

The studied subrope is composed of three laid or twisted strands (fig. 1-left). Each strand is composed of 10 twisted rope-yarns. We model the 3 strands by volumic finite elements. At each integration point of these elements, a behavior law has then to be implemented. This law has to model the mechanical behavior of a rope-yarn bundle, that is assumed to be the material of the strands. The challenge of this law is to model the viscoelasticity of the rope-yarn in tension and also the friction sliding between the rope-yarns in a bundle. Figure 2-a presents a rope-yarn bundle (blue, green and yellow rods) in the reference configuration, before any loading. Two friction deformation modes are described at figure 2-b and -c.

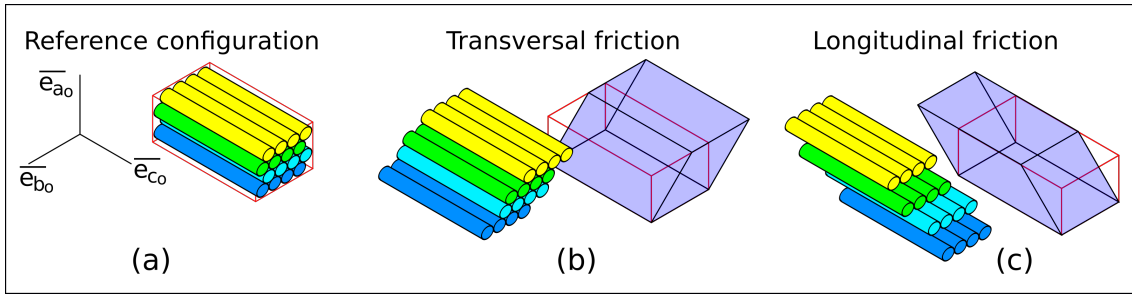


Figure 2: Two deformation modes (b,c) describing the transversal and longitudinal frictions within a rope-yarn bundle. The strand is assumed to be composed of rope-yarn bundle.

We adopted Charmetant's model [2] for describing the deformations of the rope-yarn bundle. Charmetant et al. decomposed the deformation gradient of a fiber bundle into four modes : the elongation of the bundle along the fiber direction, the compaction and the distortion (fig. 2-b) of the bundle transverse section and finally the longitudinal shear of the bundle (fig. 2-c). For each of these strain modes, a dedicated and relevant behavior law is proposed.

While Charmetant et al. considered one invariant scalar state variable as parameter of this longitudinal shear mode, we proposed two scalar state variables because actually two shears in two orthogonal planes occurs in this mode. Again, for the transversal friction mode (distortion of transverse section), Charmetant proposed one scalar state variable as parameter of this mode, but this 2D strain has one independent eigenvalue and two orthogonal eigenvectors within the transverse plane. So, we proposed two parameters as actually needed. These improvements of the Charmetant's model will allow us to include plasticity dedicated to the friction behaviors.

3. Results

The proposed method allowed us to model the contact between one strand and a rigid rod (fig.1-right). The section, initially axi-symmetric, is highly compacted due to the contact. The identification of the model parameters at the strand and rope-yarn scales will be presented shortly. This will be applied to model the tension of a subrope, predicting the cross-section shape of the strands, the friction sliding within the strands and the dissipated energy due to friction.

4. Conclusions

A modeling approach, for the tension of a synthetic rope, at the two smaller scales is proposed. The expected result is an understanding of the friction modes in the rope strands, the dissipated energy due to friction and due to the viscoelasticity of rope-yarns. But this model should also offer a tool for predicting the impact of rope construction parameters (lay-lengths) on the rope tensile behavior. The impacts of the rope-yarn behavior and the frictions on the tensile behavior can be also analyzed with this model.

Acknowledgments

This work was performed within the FEM/ANR MONAMOOR project of the French National Research Agency project (ANR-10-IEED-06-34, Investissements d'Avenir). This is led by France Energies Marines with partners Saipem, Bureau Veritas, BEXCO Ropes, ENSTA Bretagne, IFREMER, Total Energies, University of Nantes, University Gustave Eiffel, NCD, IFSTTAR, GeM, CNRS, WEAMEC and RWE.

References

- [1] Y. Chevillotte. *Characterization of the long-term mechanical behavior and the durability of polyamide mooring ropes for floating wind turbines*, ENSTA Bretagne, *Ph.D. Thesis*, 2020.
- [2] A. Charmetant, E. Vidal and P. Boisse. *Hyperelastic modelling for mesoscopic analyses of composite reinforcements*, *Composites Science and Technology*, 71 (2011) 1623-1631.

Characterizing a yarn's mechanical behaviour on microscale level using a high-fidelity geometrical fiber model

Axel Bral¹, Lode Daelemans², Joris Degroote^{1,3}

¹ Department of Electromechanical, Systems and Metal Engineering, Ghent University; Axel.Bral@UGent.be

² Department of Materials, Textiles and Chemical Engineering (MaTCh), Ghent University

³ Flanders Make, Belgium

Keywords: Fiber model, Finite Element Analysis (FEA), Microcomputed Tomography (μ CT), Multi-scale analysis, Yarn

1. Introduction

Air-jet weaving is nowadays one of the most popular weaving methods thanks to the high production rates combined with low maintenance costs when compared to e.g. projectile or rapier weaving looms. However, the use of compressed air to propel the yarn leads to a high energy demand. Attempts to reduce the energy use of these air-jet weaving machines are often limited by the weaving stability. As a consequence, it is necessary to understand the interaction between the weft yarns and the air jets since it is precisely this interaction that determines whether or not the yarn insertion is successful. Unfortunately, numerical studies considering these interactions are scarce. If Fluid-Structure Interaction (FSI) is considered at all, it mostly focuses on monofilament yarns where the yarn is represented by a smooth cylinder, such as in Delcour et al. [1]. However, monofilament yarns are generally not suited for air-jet weaving due to their smooth surface. In reality, multifilament yarns having an irregular surface appearance are encountered more often.

Since the difference in scales between the weaving machine (order of meters) and the fibers (order of μm) is large, it currently seems unfeasible to simulate the complete yarn insertion using a yarn geometry on the level of the fibers. Therefore, the multi-physics nature of the FSI framework as in Delcour et al. [1] is extended with a multi-scale approach. This work focuses on the mechanical yarn behaviour on microscale level, that is, on the level of the fibers.

2. Methodology

In this research, a wool fiber yarn of fineness 28.8 tex is considered. A sample of 4.491 mm was subjected to a microcomputed tomography (μ CT) scan to obtain the geometrical details of the yarn. This μ CT data is subsequently used to trace the fiber centerlines from which a geometrical fiber model of the yarn is constructed.

The resulting geometrical model serves as input for the structural model, where the fibers are represented in the Finite Element Analysis (FEA) software package Abaqus 2021 (Dassault Systèmes) as linear Timoshenko beam (B31) elements with an element length of 20 μm which is similar to the fiber diameter. Contact between the fibers is modelled using the penalty method and friction using Coulomb's law with a fixed friction coefficient of 0.25. The stress-strain behaviour of the fibers is extracted from tensile tests according to the EN ISO 5079 (2020) norm and is represented in the model by a bilinear approximation of the resulting curves. The mechanical behaviour of the yarn is assessed by simulating a linear tensile test and the Peirce cantilever test [2].

Finally, the yarn's mechanical behaviour is assessed in an experimental manner as well in order to validate the simulations. The tensile tests are performed according to the EN ISO 2062 (2010) norm using the Textechno Statimat M, while the Peirce cantilever test complies with the ASTM D1388-18 standard.

For a more detailed description of the methodology, the reader is referred to Bral et al. [3].

3. Results

The validity of the proposed microstructural yarn model is assessed by comparing the results of the tensile test simulations to those of the experiments. Despite the simplifications in the model regarding to mechanical fiber behaviour, both in terms of tensile and frictional models, the agreement is excellent, see Figure 1a. The major advantage of the simulation strategy is illustrated in Figure 1b, where the axial stress distribution S_{11} of

the fibers inside the yarn is shown. It is clear from this figure that for low strains, the fibers in the yarn core take up the majority of the axial reaction force while the outer fibers still have the freedom to straighten before contributing to the reaction force of the yarn.

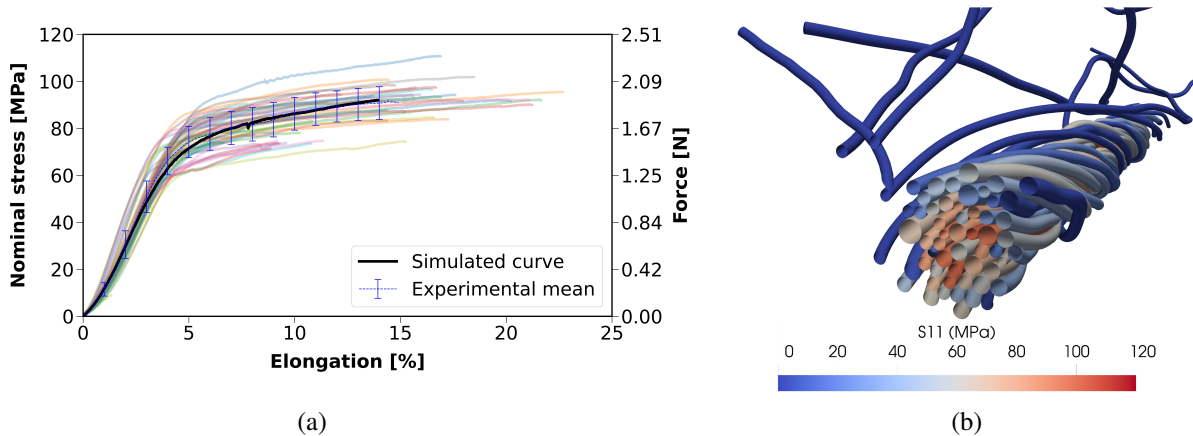


Figure 1: Results of the tensile simulations: (a) comparison of stress-strain behaviour of yarn model compared with experiments; (b) cross-section halfway the yarn during the tensile test at 2.5 % elongation. (Coloured figures in [3].)

The bending rigidity EI of the yarn model is estimated by fitting the deformations according to the Euler-Bernoulli beam theory to the displacement of the yarn, similar to Cornelissen and Akkerman [4]. As a result, a bending rigidity of $1.908 \cdot 10^{-9} \text{ Nm}^2$ is observed, which is 14.4 % lower than the experimental mean, albeit within one standard deviation from this average value. The underestimation of the bending rigidity is mainly believed to be caused by the relative absence of inter-fiber contact in the yarn model when subjected to low loadings. At the end of the bending simulation, only 10 nodes (0.075 % of the total number of nodes in the model) were in slipping contact. In contrast, for the tensile test, 28 % of the nodes are in contact when the yarn reaction force equals 0.5 cN/tex.

4. Conclusion

A simulation strategy is proposed in this work to characterize the mechanical behaviour of a multifilament yarn using a high-fidelity geometrical fiber model originating from μCT scan data. The simulation results of a yarn tensile and Peirce cantilever test are compared to their experimental counterparts and show excellent agreement. An inherent advantage of the numerical nature of this strategy is that it allows to gain insight in the stress distributions inside real yarns without relying on geometrical simplifications.

5. Acknowledgments

This project has received funding from the Research Foundation Flanders (FWO) with grant number 1S30822N.

References

- [1] L. Delcour, J. Peeters, J. Degroote. *Three-dimensional fluid-structure interaction simulations of a yarn subjected to the main nozzle flow of an air-jet weaving loom using a Chimera technique*, Textile Research Journal, 90 (2020) 194-212.
- [2] F.T. Peirce. *The "handle" of cloth as a measurable quantity*, Journal of the Textile Institute Transactions, 21 (1930) T377-T416.
- [3] A. Bral, L. Daelemans, J. Degroote. *A novel technique to simulate and characterize yarn mechanical behavior based on a geometrical fiber model extracted from microcomputed tomography imaging*, Textile Research Journal, 0 (2022) 1-21.
- [4] B. Cornelissen, R. Akkerman. *Analysis of yarn bending behaviour*, 17th International Conference on Composite Materials (ICCM), 1-10, 2009.

Technological and modelling aspects of the fiber level modelling of textile yarns

Yordan Kyosev^{1,2}, Ann-Malin Schmidt²

¹ TU Dresden, ITM, Chair of Development and Assembly of Textile Structures, Dresden, Germany
yordan.kyosev@tu-dresden.de , ann-malin.schmidt@tu-dresden.de

² TexMind UG, Heidenau, Germany, info@texmind.com

Keywords: modelling, textile yarns, ropes, fiber level, contact, distribution

1. Introduction

Textile yarns are the building structural element of the woven and knitted textile structures, used for clothing, home textiles, technical and many other applications. Each yarn in the real product consists of at least 60 short or continuous fibers in each cross section, which determine its properties. In analogous way as the multifilament fibers, the yarns are building the twisted and braided ropes. The modelling of the textile yarns as fiber level and the ropes at yarn level is connected with several challenges which are demonstrated in this work, based on original developed algorithms and software.

2. Modelling and technological aspects

The mathematical fundamentals theory about the orientation of single element of fibers in yarns are described in several works, as for instance the teams of Ron Postle [1] and Bohuslav Neckar [2]. These models remain mainly analytical considerations, based on geometrical, statistical or mechanical relations for specific types of yarn structures. Intensive development of methods for computational simulations at the yarn level is performed by D. Durville, in which works the fibers are modelled as beams and the contact between these is considered [3]. Technologically, there are different **types** of textile yarns and ropes, with (completely) different structure. The stable fiber yarns consists of fibers with length between 30 and 120 mm (again subdivided in “short” and “long” stable for cotton and wool fiber production), where the proper modelling have to consider the fiber length distribution and the spinning method. The most simple for modelling are the DREF yarns, which are similar to twisted ropes (Fig. 1a and Fig 2b and c), but these have very limited practical use. The ring and rotor spinning yarns have different, but already similar distribution of the fibers in the cross section, while air-jet yarns are again completely different with more parallel yarns in the middle and highly twisted layer outside. For all these types of yarns there is no known method or software for proper parametric modelling the structure at fiber level until know.

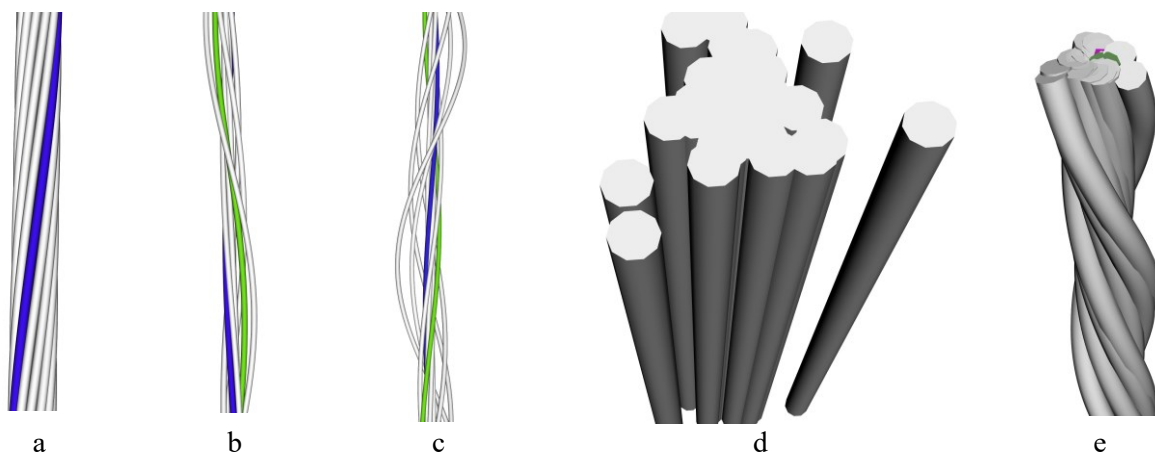


Figure 1. Modelled yarns with multiple filaments a) one layer twisted, b) and c) with randomized filament position at $\sigma = 2d$ and at $\sigma = 4d$, respectively, d) and e) intersection problems by random position generation for parallel and twisted yarns respectively

Some initial trials for representation of such structures are reported in [4]. For twisted ropes, the situation remains similar to the yarns, and for braided ropes, from other side the structure is well defined and reported in [5] and [6] and implemented in commercial software of company TexMind.

3. Modelling problems

Creating list of coordinates for the axis of multiple fibers or filaments with well defined regular orientation is not a problem. Fig. 1a and Fig.2a represents generated such yarns with C++ implementation within the software TexMind Braider, as described in [5]. Randomization of the fiber axis following any statistical distribution is as well connected with three lines of code and results are visualized in Fig. 1b and 1c. Figure 1d and 1e represents one of the main problem in such method – the generated coordinates for one point of the fiber axis based on some statistic distribution can be in a position, where already another fiber piece is located. The interlacement problem occurs additionally for the case of twisting of the yarns. During the twisting, the fibers change their orientation, this is a process, which can be simulated with active contact detection, but can not be included as common analytical or parametric solution for any type of multilayer yarn structure and simple rotation of the yarn cross section leads to interlacement between the fibers too, as visualized in Fig. 2b and Fig. 2c.

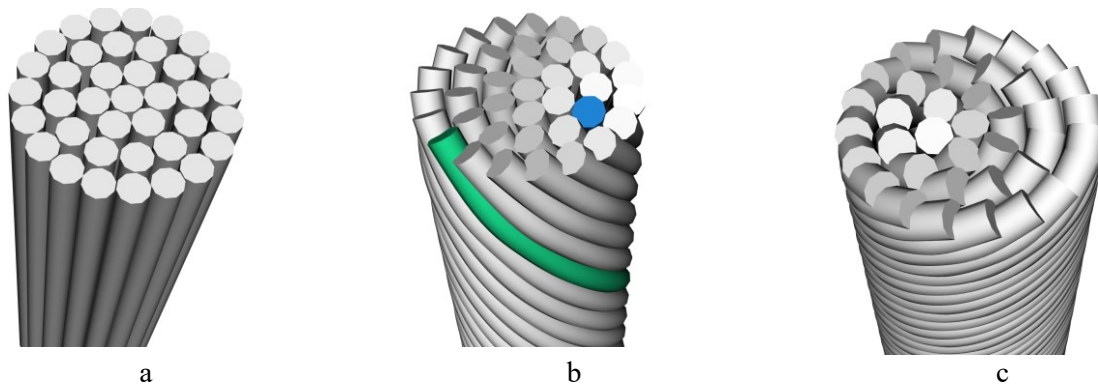


Figure 2 Four layer rope structure a) without twist b) with S Twist and slight intersection c) with Z twist and high intersection

4. Conclusions

The generation of textile yarns at fiber level requires separated algorithms for different type of structures. Applying randomization of the coordinated of the single fibers in parametric models allows creating models, which are closer to the reality, but without additional contact detection steps leads to interlacement between the fibers. One future effective textile yarn generator should contain at least contact solver and should include different types of yarn or braiding types, in order to be able to create geometries, usable as starting point for FEM or other simulations.

References

- [1] R. H. Driscoll, R. Postle, *Modelling the Distribution of Fibres in a Yarn*, Journal of the Textile Institute, 79:1, DOI: 10.1080/00405008808659158 (1988), 140-143
- [2] B. Neckar, D. Das, *Theory of Structure and Mechanics of Yarns*, Woodhead Publishing, India, 2018.
- [3] D. Durville, Numerical simulation of entangled materials mechanical properties, *Journal Material Science*, 40, (2005) 5941–5948, <https://doi.org/10.1007/s10853-005-5061-2>
- [4] D.B: Aychilie, Y. Kyosev, *Automatic Modeller of Textile Yarns at Fibre Level*, Materials. (2022); 15(24):8887. <https://doi.org/10.3390/ma15248887>
- [5] Y. Kyosev, *Topology based modelling of textile structures and their assemblies*, Springer, Cham,(2019).
- [6] Kyosev Y. Generalized geometric modeling of tubular and flat braided structures with arbitrary floating length and multiple filaments. *Textile Research Journal*;86(12), (2016),1270-1279.

Study Of Frictional Contact Interactions Within Jacquard Harness In Weaving Process For 3d Interlock Fabrics

Salah Eddine Mermouli^{1,2}, Damien Durville¹, Pietro del-Sorbo², Bastien Tranquart², Dominique Coupé²,

¹ Université Paris-Saclay, CentraleSupélec, ENS Paris-Saclay, CNRS, Laboratoire de Mécanique Paris-Saclay,
{ salah-eddine.mermouli , damien.durville } @centralesupelec.fr

² Safran Tech, Safran Composites.
{ pietro.del-sorbo , bastien.tranquart , dominique.coupe } @safrangroup.com

Keywords: Frictional contact interactions, Finite element simulation, Jacquard harness, 3D Weaving

1. Abstract

3D interlock fabrics made from carbon tows, which contain a large number of interweaving layers, are used as preforms for manufacturing composite parts. They are produced on Jacquard looms which incorporate a large number of components (heddles and yarns) within the small space of the harness. During 3D weaving, the movement of warp yarns and heddles within a Jacquard harness generates frictional contact interactions that may lead to congestion mechanisms. This may result in damage to yarns, blockage of heddle movement, and ultimately leading to errors in the weaving process. Previous numerical simulations of the weaving process, among others [1] [2] [3] [4], have not focused the congestion phenomena within the harness. This study proposes a simulation model, based on an implicit resolution scheme [5], to account for contact-friction interactions that occur in Jacquard harnesses of looms. The model uses finite strain beam elements to represent all components of the harness [6]. Frictional contact elements are automatically created between the different components, see Figure 1. The heddles are modeled by associating ten beam sections representing their different parts (the rope, the rods, the eyelet and the spring) while the reed is modeled using beam elements with steel properties. The warp yarns are modeled as beam elements with adjusted bending and torsional stiffness coefficients. The simulation model's accuracy is verified by comparing the heddles' force simulation results with experimental data from a real loom using an appropriate deformation sensors.

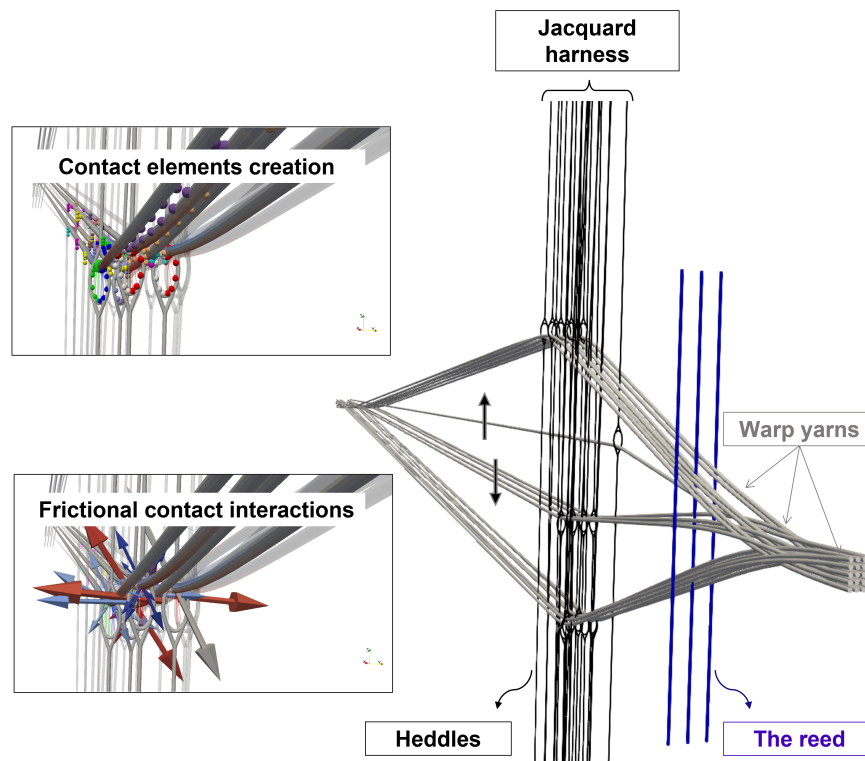


Figure 1: Simulation model demonstrating frictional contact interactions during shed opening

The aim of the study is to investigate how contact-friction interactions within the harness affect heddles movement (heddles forces are shown in Figure 2). The results analysis revealed the presence of multiple friction zones in the harness, especially at the beginning and at the end of the shed opening cycle, and also during the crossing of yarns in the middle of the cycle. The force curves provide a way to identify possible blocking events caused by high friction interactions, when a heddle remains stuck while moving. Simulating the movements of a 5-layer interlock fabric with 20 warp yarns over 20 shed openings, including the reed beating phase and tack-up phase, can be carried out within 24 hours.

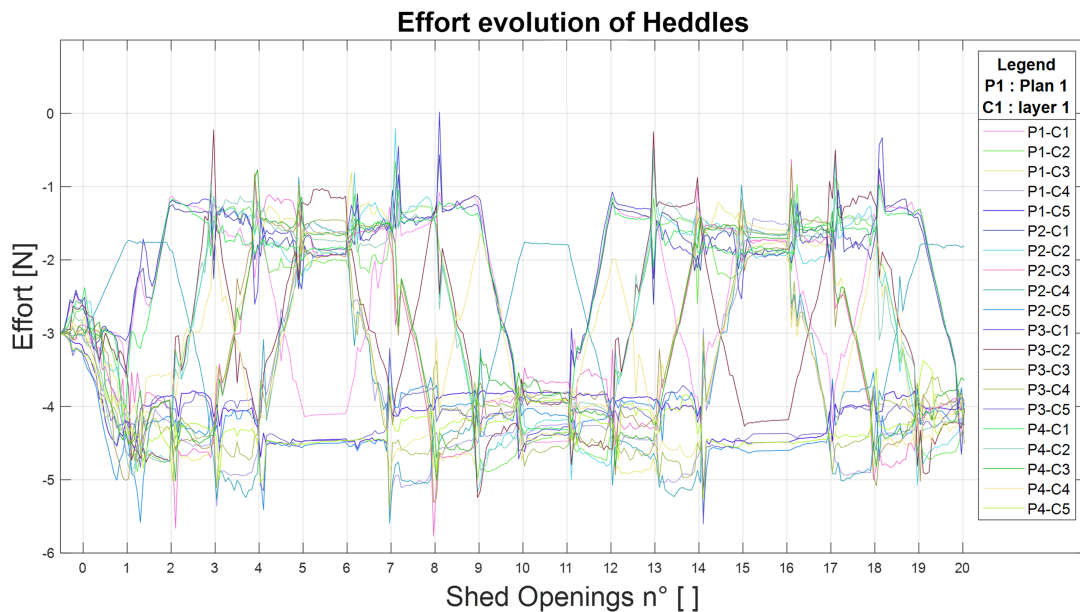


Figure 2: Heddles effort variation during successive shedding openings

References

- [1] H. Finckh. Numerische simulation der mechanischen eigenschaften textiler flächengebilde - gewebeherstellung. *LS-DYNA Anwenderforum*, pages 1–15, 2004.
- [2] L. Russcher, E. Lamers, C. Dufour, F. Boussu, P. Wang, and D. Soulat. Modelling the micro-structure of multilayer woven fabrics. In *Proceedings of the 13th Autex World Textile Conference, Dresden, Germany, 22–24 May 2013*.
- [3] J. Vilfayeau. *Modélisation numérique du procédé de tissage des renforts fibreux pour matériaux composites*. PhD dissertation, L'institut national des sciences appliquées de Lyon, 2014.
- [4] X. Yang. *Dynamic simulation of 3D weaving process*. PhD dissertation, Kansas state university, Manhattan, Kansas, 2015.
- [5] Damien Durville. Contact-friction modeling within elastic beam assemblies: an application to knot tightening. *Computational Mechanics*, 49(6):687–707, 2012.
- [6] Salah Eddine Mermouli, Pietro Del Sorbo, Damien Durville, Bastien Tranquart, and Dominique Coupé. Simulation of frictional contact interactions between warp yarns and heddles within jacquard harness for 3d weaving. In *14th WCCM-ECCOMAS Congress 2020*, volume 1000, 2021.

Modelling a braiding process as a constrained multibody system with frictional contacts

Indrajeet Patil, Alejandro Cosimo, Olivier Bruls

Department of Aerospace and Mechanical Engineering, University of Liège, Allée de la Découverte 9, 4000 Liège, Belgium, (ikpatil, acosimo, o.bruls)@uliege.be

Keywords: Nonsmooth dynamics, Textiles, Lie group, Switching constraints, Gauß-Seidel

1. Introduction

Automated braiding machines are used to fabricate near-net-shaped preforms for composite manufacturing. Typically, slender textile yarns are driven by bobbin carriers with synchronized horn gear motions and deposited on the surface of a rigid body (the mandrel). The combined framework of nonlinear finite elements with multibody dynamics is used for the transient modelling of such mechanical systems with rigid and flexible bodies undergoing contact-friction interactions. For representing systems with finite transformations, a differential geometric framework is helpful. Therefore, the equations of motion are defined on a Lie group together with bilateral and unilateral constraints. In nonsmooth mechanics, the non-penetration condition is expressed as a unilateral constraint in the form of a Signorini condition with a Coulomb friction law. The bilateral and unilateral constraints can be simultaneously imposed at position and velocity levels to avoid constraint drift, and to capture instantaneous jumps at velocity level. Standard time integration schemes fail to model the nonsmooth contributions, which demands the need of a specialized time integrator capable of handling discontinuities. In this work, the carrier kinematics is formulated as switching bilateral constraints, which represent nonsmooth boundary conditions for the yarns. The yarn-to-mandrel frictional interactions are further introduced.

2. Method

The yarns are modelled as geometrically exact beams [5] on the Lie group $SE(3)$ and driven by the imposed carrier motion. The yarn-to-mandrel frictional interactions are introduced as contacts between beams and rigid bodies and solved using a collocation approach by representing the neutral axis of the beam with proxy collision geometries [6]. The time discrete equations are solved using the decoupled version of the nonsmooth generalized- α time integration scheme [3] with the Gauß-Seidel solver So-bogus [4]. Three decoupled sub-problems are solved using the splitting strategy as $\Delta \mathbf{q}_{n+1} = \Delta \tilde{\mathbf{q}}_{n+1} + \mathbf{U}_{n+1}$ and $\mathbf{v}_{n+1} = \tilde{\mathbf{v}}_{n+1} + \mathbf{W}_{n+1}$, where, $\Delta \tilde{\mathbf{q}}_{n+1}$ and $\tilde{\mathbf{v}}_{n+1}$ are smooth displacements and velocities, and \mathbf{U}_{n+1} and \mathbf{W}_{n+1} are position corrections and velocity jumps. For instance, the velocity jump \mathbf{W}_{n+1} is computed at time step t_{n+1} as in [2]:

$$\mathbf{M}(q_{n+1})\mathbf{W}_{n+1} - h\mathbf{f}_{n+1}^* - \mathbf{g}_{q,n+1}^T \boldsymbol{\Lambda}_{n+1} = 0 \quad (1a)$$

$$-\mathbf{g}_{q,n+1}^{\bar{u}} \mathbf{v}_{n+1} = 0 \quad (1b)$$

$$-(\mathbf{g}_{Nq,n+1}^j \mathbf{v}_{n+1}^j + e_N^j \mathbf{g}_{Nq,n+1}^j \mathbf{v}_n^j) \in \partial \psi_{\mathbb{R}^+}(\Lambda_{N,n+1}^j) \quad \text{if } g_N^j(q) \leq 0, \quad (1c)$$

$$-(\mathbf{g}_{Tq,n+1}^j \mathbf{v}_{n+1}^j + e_T^j \mathbf{g}_{Tq,n}^j \mathbf{v}_n^j) \in \partial \psi_C(\Lambda_{N,n+1}^j) \quad \text{if } g_N^j(q) \leq 0, \quad (1d)$$

where, $\mathbf{f}_{n+1}^* = \mathbf{f}(q_{n+1}, \mathbf{v}_{n+1}, t_{n+1}) - \mathbf{f}(\tilde{q}_{n+1}, \tilde{\mathbf{v}}_{n+1}, t_{n+1}) + (\mathbf{g}_{q,n+1}^T - \mathbf{g}_{\tilde{q},n+1}^T) \tilde{\boldsymbol{\lambda}}_{n+1} - (\mathbf{M}(q_{n+1}) - \mathbf{M}(\tilde{q}_{n+1})) \tilde{\mathbf{v}}_{n+1}$. q is the configuration variable, \mathbf{v} is the velocity, \mathbf{M} is the mass matrix, h is the time step size, $\boldsymbol{\Lambda}$ is the Lagrange multiplier representing the impulse with Λ_N^j and Λ_T^j as the normal and tangential components respectively, \bar{u} is the set of indices for bilateral constraints and j is the contact point with the gap (relative position) split into normal component g_N^j and tangential component g_T^j . A Newton impact law is defined with e_N^j and e_T^j as the normal and tangential restitution coefficients ($e_T^j = 0$ for contact involving flexible bodies). $\psi_{\mathbb{R}^+}$ is the indicator function of the real half line \mathbb{R}^+ and ψ_C for the section of the Coulomb's friction cone.

3. Preliminary results

The simulation of biaxial braiding process involving 30 yarns subjected to carrier motion and deposited on the surface of a cylindrical shaped mandrel has been performed using Odin [1]. The radius of beam is $r = 0.001$ m with $l = 3$ m and the material properties are $E = 89$ GPa, $\nu = 0.21$ and $\rho = 2750$ kg/m³. Each yarn is discretized using 50 beam finite elements with spherical collision elements (radius = r) attached to the nodes. The simulation time is 30 seconds with time step size $h = 0.001$ seconds. The coefficient of friction $\mu = 0.1$.

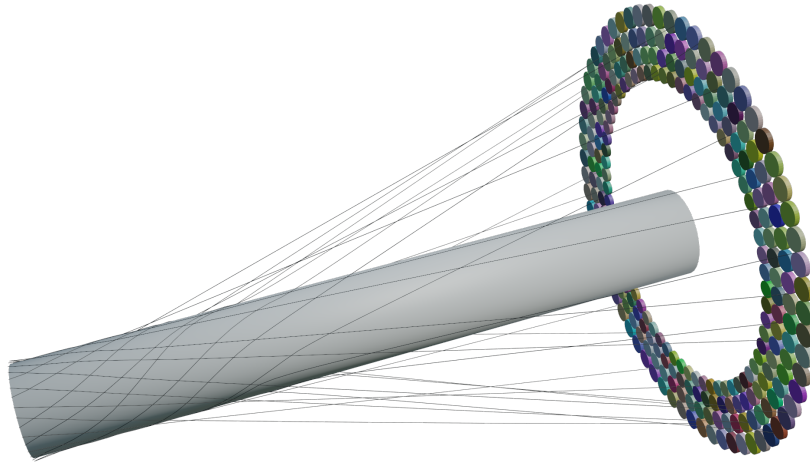


Figure 1: Transient simulation of 30 beams driven by the carrier motions and interacting by frictional contact with a cylindrical mandrel

4. Conclusions

The carrier kinematics is formulated as switching constraints and applied as nonsmooth boundary conditions to beams. The yarn-mandrel frictional interactions are further modelled based on a collocation approach. In the future, a beam-to-beam contact formulation shall be further introduced for the modelling of yarn-yarn contact.

Acknowledgments

This project has received funding from the European Union’s Horizon 2020 research and innovation programme under the Marie Skłodowska-Curie grant agreement No 860124. The present paper only reflects the author’s view. The European Commission and its Research Executive Agency (REA) are not responsible for any use that may be made of the information it contains.

References

- [1] A. Cosimo and O. Brüls. Odin. DOI: <https://doi.org/10.5281/zenodo.7468114>, 2022.
- [2] A. Cosimo, F. J. Cavalieri, J. Galvez, A. Cardona, and O. Brüls. A general purpose formulation for nonsmooth dynamics with finite rotations: Application to the woodpecker toy. *Journal of Computational and Nonlinear Dynamics*, 16(3), 2021.
- [3] A. Cosimo, J. Galvez, F. Cavalieri, A. Cardona, and O. Brüls. A robust nonsmooth generalized- α scheme for flexible systems with impacts. *Multibody System Dynamics*, 48(2):127–149, 2020.
- [4] G. Daviet, F. Bertails-Descoubes, and L. Boissieux. A hybrid iterative solver for robustly capturing Coulomb friction in hair dynamics. In *Proceedings of the 2011 SIGGRAPH Asia Conference*, pages 1–12, 2011.
- [5] V. Sonneville, A. Cardona, and O. Brüls. Geometrically exact beam finite element formulated on the special Euclidean group SE(3). *Computer Methods in Applied Mechanics and Engineering*, 268:451–474, 2014.
- [6] A. Tasora, S. Benatti, D. Mangoni, and R. Garziera. A geometrically exact isogeometric beam for large displacements and contacts. *Computer Methods in Applied Mechanics and Engineering*, 358:112635, 2020.

MS-8: Modelling beam-like layered structures with compliant interfaces

An inverse approach treating large rotations to simulate composite single-layer peeling-based disassembly

M. Becker¹, M. Imbert¹, M. May¹

¹ Fraunhofer Institute for High Speed Dynamics, moritz.becker@emi.fraunhofer.de

Keywords: beam theory, inverse modeling, large rotations, peeling

1. Introduction

Multi-layer and wound fiber reinforced composite materials feature an outstanding potential for energy savings in the transport sector. However, the classical shredding-based recycling methods for composites lead systematically to a strong downcycling. In this context, the peeling-based disassembly of composite structures is a very promising strategy [1]. Peeling-based disassembly enables to recover unitary layers of the original material with preserved continuous and aligned fibers and therefore preserved mechanical properties. Nevertheless, the peeled layer is susceptible to be damaged by an excessive curvature resulting in fiber kinking, or by excessive tensile peeling force resulting in fiber breaking. Thus, being able to model properly and efficiently the peeling of composite single-layers is of interest to provide information on the quality of the recovered material. However, the current analytical and numerical strategies to model peeling, rely on analytical models [2] or the use of Finite Element methods [3] with a cohesive zone model and consist of assuming material properties and imposing force or displacement boundary conditions to determine the position of the crack tip and the deformation of the peeled layer (direct approach). In so far as the mechanical and geometrical properties of the layer to be recovered are not exactly known a priori, using the available direct methods to determine the local material properties requires time consuming optimization approaches. In this context an innovative numerical model is proposed, which can be used in both a direct way (computation of displacements from known material properties and peeling force) as well as inverse way (computation of material properties from prescribed displacement field and peeling force).

2. Mathematical model

The peeled single-layer is considered as a 1D beam which might be subjected to various types of loads. In peeling conditions, cohesive forces given by an analytical cohesive zone model compensate the peeling forces at the end of the layer. The numerical model is inspired from [4]. It is not a finite element model in the classical sense, but obtained by W cuts through the cantilever beam in the deformed configuration (Figure 1).

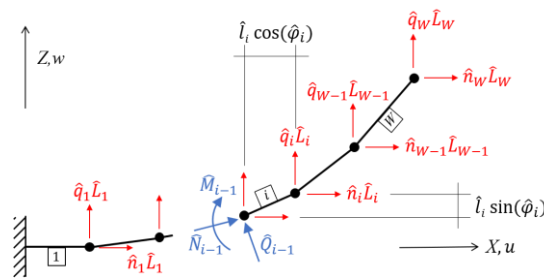


Figure 1. Discretization and a cut through the system for the example of a cantilever beam.

To each element are associated eight unknowns (length of the element, angle of the element to the horizontal axis, local bending stiffness, internal forces in the longitudinal and transverse directions, the local bending moment in the element and the external forces in the X and Z-directions). In order to determine these unknowns, the principle of the model consists in defining eight corresponding equations (local force and moment equilibriums, elastic longitudinal deformation of the element, definition of the external forces applied on the beam, definition of the local bending stiffness and relationship between the local curvature and the bending moment) for each element. The set of equations is then solved using the SymPy-library in Python and the Newton Raphson method [1]. Depending on the used equations, the values of certain unknowns can be prescribed to be fixed values or defined indirectly by using equations giving the conditions to be satisfied. Regarding the material bending stiffness, in the direct configuration, the value of the bending stiffness is

prescribed. In the inverse configuration, the local element angle is prescribed. In so far as the bending stiffness of the elements are defined as unknowns and are appearing in the equation relating the local curvature to the bending moment, the values of the local bending stiffness (Eq. (1)), which are required to satisfy the local element angles, will be determined automatically through the resolution of the set of equations. Therefore, it enables to extract directly the local bending properties along the layer using the local angles recorded during the peeling process. This inverse strategy enables to treat bending stiffness distributions, which might only be obtained by complex and difficult to characterize material models. Furthermore, it avoids the use of optimization tools and is seen as advantageous towards a future in-line determination of the residual material properties. The mathematical model, which defines the overall tape bending behavior, must be able to consider large rotations of the beam. It is given in Eq. (1) by the relationship between internal bending moment \hat{M}_i at cut i and the curvature κ_i for an exact expression of the curvature using Euler-Bernoulli beam theory.

$$\hat{M}_i = \hat{E}_i I_y \kappa_i = \hat{E}_i I_y \frac{\hat{w}_i''}{(1+(\hat{w}_i')^2)^{\frac{3}{2}}} \quad (1)$$

The longitudinal force \hat{N}_i in node i is determined using Green – Lagrange strain and the deformed- and undeformed length of element (Eq. (2)):

$$\hat{N}_i = \hat{E}_i A \frac{1}{2} \frac{(\hat{l}_i)^2 - (\hat{L}_i)^2}{(\hat{L}_i)^2} \quad (2)$$

The second derivative of the vertical displacement \hat{w}_i is obtained using the difference quotient (Eq. (3))

$$\hat{w}_i'' = \frac{\hat{\varphi}_i - \hat{\varphi}_{i-1}}{\hat{l}_i} \quad , \quad \hat{w}_i' = \hat{\varphi}_i \quad (3)$$

and the angle of rotation $\hat{\varphi}_i$ is related to the unknown displacement fields \hat{u}_i and \hat{w}_i by Eq. (4):

$$\tan \hat{\varphi}_i = \frac{\hat{w}_i}{\hat{L}_i + \hat{u}_i} \quad (4)$$

Variables \hat{q}_i and \hat{n}_i denote external vertical and horizontal forces in node i , which can be prescribed, or given by a cohesive zone model. \hat{L}_i and \hat{l}_i denote the undeformed and deformed length of the element i . \hat{Q}_i denotes the internal shear force. \hat{E}_i and I_y denote the Youngs Modulus and the area moment of inertia.

3. Validation and Results

The model has been validated using a commercial finite element software and the results were compared to three-point-bending experiments on steel and on unidirectional fiber reinforced PA6-Carbon specimens loaded up to large deflections. Additional nonlinear material behavior due to bending-induced damage was introduced to the model by assuming a reduction of the local bending stiffness.

Acknowledgements

This research work has received funding from the Sustainability Center of Freiburg in the frame of the projects Digitain and WEiter.

References

- [1] Imbert, M., Hahn, P., Jung, M., Balle, F., May, M. (2022). *Mechanical laminae separation at room temperature as a high-quality recycling process for laminated composites*. Materials Letters, Bd. 306, 130964.
- [2] Yuan, H., Chen, J. F., Teng, J. G., & Lu, X. Z. (2007). *Interfacial stress analysis of a thin plate bonded to a rigid substrate and subjected to inclined loading*. International journal of solids and structures, Bd. 44, Nr. 16, pp. 5247-5271.
- [3] Cañas, J., Távara, L., Blázquez, A., Estefani, A., & Santacruz, G. (2018). *A new in situ peeling test for the characterisation of composite bonded joints*. Composites Part A: Applied Science and Manufacturing, Bd. 113, pp. 298-310.
- [4] M. Imbert, H. Finckh, G. T. Gresser, *Mechanical analytical modelling of non-axisymmetric overbraiding*, Journal of Composite Materials, Bd. 55, Nr. 10, 2021, pp. 1385 – 1404.

Finite Element Model for Simulation of Complex Delamination in Three-Dimensional Composite Beams

Damjan Lolić¹, Miha Brojan², Dejan Zupan³

¹ Faculty of Mechanical Engineering, University of Ljubljana, damjan.lolic@fs.uni-lj.si

² Faculty of Mechanical Engineering, University of Ljubljana, miha.brojan@fs.uni-lj.si

³ Faculty of Civil and Geodetic Engineering, University of Ljubljana, dejan.zupan@fgg.uni-lj.si

Keywords: three-dimensional beam, quaternion rotations, interface modeling, delamination

1. Introduction

The article presents an efficient computational model for the study of delaminations in three-dimensional composite beams. The model is based on the Reissner beam theory and includes virtual springs between two layers. The stiffness of the springs is defined by a general function of the relative displacement vector in middle frame. The model is validated using experimental data from the literature and is shown to be superior in efficiency compared to solid finite element models.

2. Theoretical formulation

For a comprehensive theoretical formulation of beams, we refer the reader to the articles [1, 2, 3]. In this contribution, we extend the three-dimensional beam model to simulate all three modes of delaminations in composite beams. For brevity, we give only a brief overview of the basic concepts.

The position vector $\hat{r}_g(s)$ represents the beam axis in the global frame, while the local frame G defines the orientation of a cross section, as shown in Fig. 1. Spatial rotations are parameterized using quaternion algebra. Hence, $\hat{G}_i(s) = \hat{q}(s) \circ \hat{g}_i \circ \hat{q}^*(s) = Q(\hat{q}(s))\hat{g}_i$, where $\hat{q}(s)$ is a rotational quaternion at location s along the beam axis and $Q(\hat{q}(s))$ is a four-dimensional rotational matrix constructed from the quaternion $\hat{q}(s)$.

In composite beams, each layer is interpreted separately and satisfies the equilibrium, kinematic, and constitutive equations. These equations form a system of nonlinear equations that is later solved iteratively using the Newton-Raphson algorithm.

Layered beams are modeled by connecting individual beams with nonlinear springs that can have arbitrary stiffness laws to simulate contact, friction, or cohesive forces between layers. The adjacent layers are referred to as the primary element and secondary element, which are connected at a node by springs. To avoid unwanted forces, a middle triad, denoted G^P , is introduced between the local frames G^I and G^{II} to define relative displacements and forces between the layers in normal and tangential directions. A quaternion \hat{x} is used to describe the transformation from the primary or secondary frame to G^P , where the transformation between the two frames is expressed as $\hat{w} = \hat{x} \circ \hat{x} = \hat{q}^{II} \circ \hat{q}^{I*}$.

The effective opening displacement vector considers normal and shear delamination components as $\Delta\hat{r}_{G^P} = \hat{r}_{G^P}^I - \hat{r}_{G^P}^{II} = [\Delta r_t \quad \Delta r_n]^T$, where $\Delta r_t = \sqrt{\Delta r_{t1}^2 + \Delta r_{t2}^2}$ is resultant of tangential relative displacements, since shear delamination modes have same properties in both tangential directions.

Finally, we can write exponential cohesive zone stress functions for opening and sliding fracture modes using relative displacement vector in middle frame. For more information on cohesive zones, see [3].

$$F_{G_n^P}(\Delta r_n) = \sigma_{Cn} \frac{\Delta r_n}{\delta_n} e^{(1 - \frac{\Delta r_n}{\delta_n})} \quad \text{and} \quad F_{G_t^P}(\Delta r_t) = \sigma_{Ct} \frac{\Delta r_t}{\delta_t} e^{(1/2 - \frac{\Delta r_t}{2\delta_t^2})}. \quad (1)$$

3. Results and discussion

We demonstrate the performance of our computational model with an L-shaped DCB test. This modification requires the use of 3D finite elements, which makes it a suitable test for our model. The L-shaped cantilever beams are connected by an adhesive layer modeled with nonlinear springs according to an exponential cohesive zone model. By varying the parameters of the model, their influence on the response of the structure is analyzed.

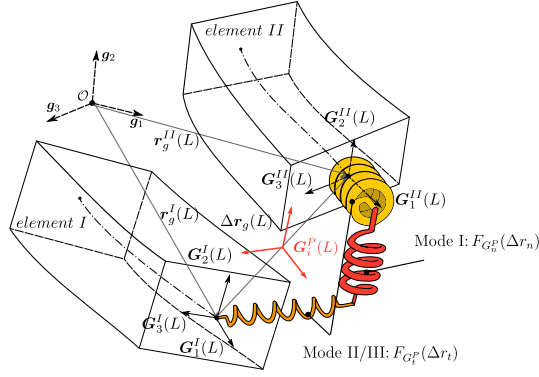


Figure 1: Schematic representation of the elements sharing a node via springs with specific properties. The middle triad G_i^P is represented with red color.

Increasing the critical normal stress σ_C leads to a higher force required to break the bond and a more severe response, while increasing the cohesive energy release rate G_{IC} shifts the force-displacement curve upward, as shown in Fig. 2.

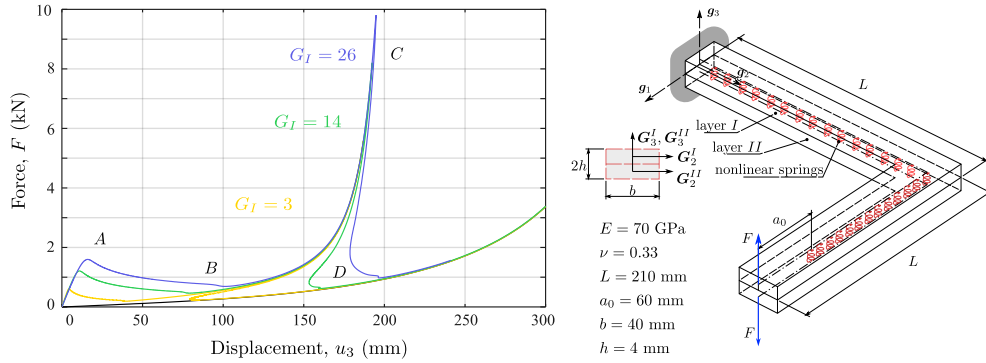


Figure 2: The force-displacement curves of the free end of the upper beam for different values of the strain energy release rate. The black line shows the result of unconnected beams. In all cases, $\sigma_C = 13$ MPa.

4. Conclusions

The beam model used in this study is designed to be both simple and effective, making it an excellent starting point for the study of delamination when interlayer relationships are included. Through validation with examples from the literature, we have demonstrated the ability of the model to effectively investigate three-dimensional delamination. As such, this model offers a valuable tool for delamination analysis.

Acknowledgments

This work was supported by the Slovenian Research Agency through Grants P2-0263 and J2-8170. The support is gratefully acknowledged.

References

- [1] D. Lolić, D. Zupan, M. Brojan. *A consistent strain-based beam element with quaternion representation of rotations*, *Comput. Mech.*, 65 (2020) 1–16
- [2] E. Zupan, D. Zupan. *On higher order integration of angular velocities using quaternions*, *Mech. Res. Commun.*, 55 (2014) 77–85
- [3] L. Škec, G. Jelenić. *Geometrically non-linear multi-layer beam with interconnection allowing for mixed-mode delamination*, *Eng. Fract. Mech.*, 169 (2017) 1–17

Experimental validation of a novel numerical model for rate-dependent mode-I failure of adhesive joints

Leo Škec¹, Giulio Alfano²

¹ Faculty of Civil Engineering, University of Rijeka, Radmile Matejčić 3, 51000 Rijeka, Croatia,
leo.skec@uniri.hr

² Department of Mechanical and Aerospace Engineering, Brunel University London, Kingston Lane,
Uxbridge UB8 3PH, UK, giulio.alfano@brunel.ac.uk

Keywords: Adhesive joints, DCB experiment, Debonding, Rate-dependent behaviour, Cohesive-zone models

1. Introduction

Adhesive joints are nowadays used in a very wide ranging variety of structural engineering applications, because of the associated reduction of stress concentrations and their suitability for joining lightweight components. Although a number of procedures are available to characterise the interface fracture resistance in such structures for quasi-static problems, the increasing use of adhesive bonding in the automotive and aerospace sectors makes it particularly important to evaluate the rate dependence of the fracture resistance, because of the importance of modelling these structures under dynamic loading, and in particular during impact loading. In this work, we present a numerical and experimental study of the rate dependence of the mode-I failure of adhesive joints based on DCB tests.

2. Experimental part

For the experimental part, we tested 24 aluminium joints with a prescribed cross-head displacement rate ranging between 0.1 to 5000 mm/min. It has been shown that the fracture resistance of the adhesive (and therefore the overall bearing capacity of the adhesive joint) increases with the load-line displacement speed (see Figure 1). Because results for the two lowest speeds (namely 0.1 and 1 mm/min) essentially overlap, we concluded that the slow limit (i.e. the limit below which the rate dependence of the adhesive is negligible) has been reached. On the other hand, because of the limitations of the equipment (maximum speed was 5000 mm/min), the high-speed plateau or peak (maximum) could not be determined (for additional details see [1]).

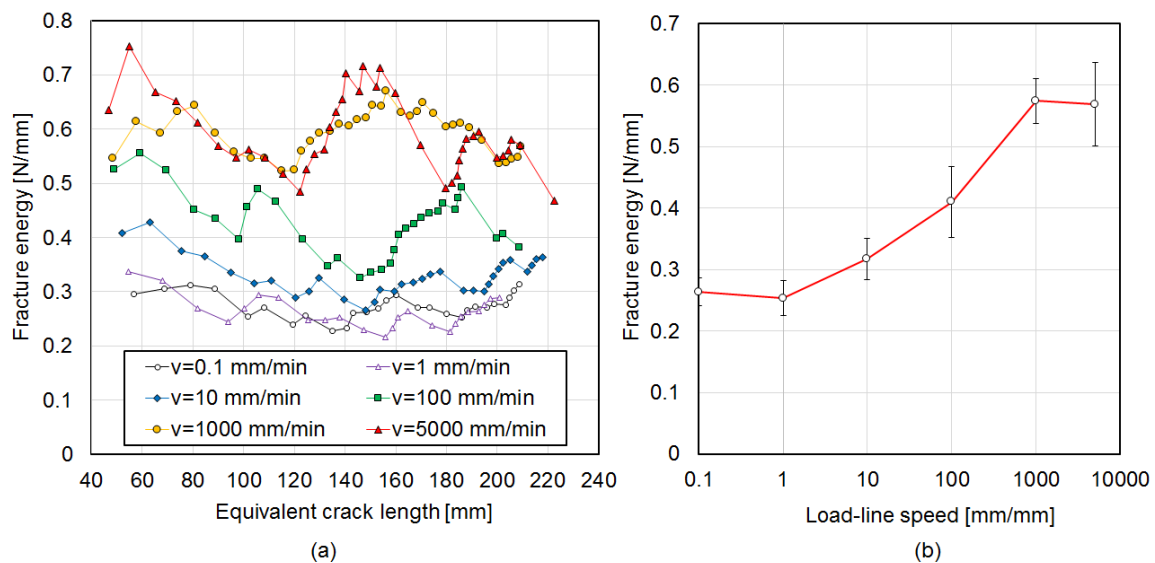


Figure 1: Fracture energy of the adhesive at different load-line displacement speeds: (a) the average R-curves (average is computed from four tests at each speed), (b) the mean value of the fracture energy for each speed (each point represents the mean value of the average R-curves).

3. Numerical part

The numerical simulations use a previously proposed cohesive-zone model (CZM) based on fractional viscoelasticity [2] and a novel computationally efficient finite element (FE) combining a Timoshenko beam and an interface element. A simple procedure for identification of 7 material parameters of the model is proposed based on the previously proposed algorithm [3] implemented in software DCB PAR.

The comparison between experimental and numerical results shown in Figure 2 confirms the capability of the CZM of capturing the experimental response over a wide range of speeds with the same set of 7 parameters, only two of which are related to the model rate dependence. This is unlike models based on experimental kernels, which require a much larger number of parameters. In [1] we also present an effective procedure to determine the ‘fracture resistance–crack growth’ curve without the need for measuring the crack length and the crack speed, but only by post-processing of the measurements of the load and the cross-head displacement, immediately available at the end of the tests.

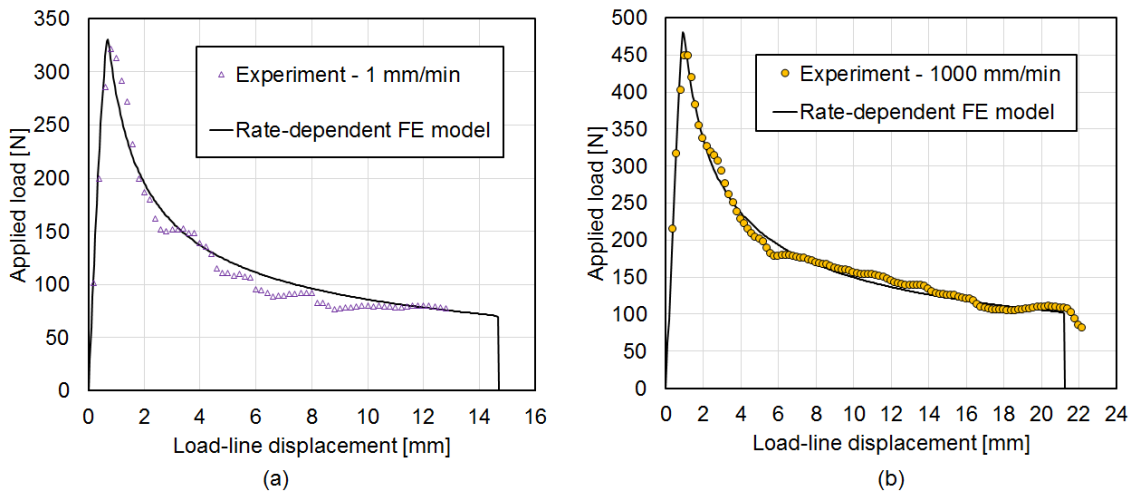


Figure 2: Fit between the experimental load-displacement data and the model prediction with the identified CZM parameters for load-line displacement speed of: (a) 1 mm/min, (b) 1000 mm/min.

4. Conclusions and future work

We presented an experimental–numerical study to characterise the rate dependence of fracture energy of adhesive joints under mode-I crack propagation and to validate a previously formulated rate-dependent cohesive-zone model based on fractional viscoelasticity [2]. The model is currently being extended to take into account the presence of defects at the interface (voids and interfacial failure) in order to determine the ‘true’ fracture resistance of the adhesive.

Acknowledgments

This project has received funding from the European Union’s Horizon 2020 research and innovation programme under the Marie Skłodowska-Curie grant agreement No. 701032.

References

- [1] L. Škec, G. Alfano. *Experimental and numerical study of rate-dependent mode-I failure of a structural adhesive*, The Journal of Adhesion, 99(8) (2022) 1323–1355
- [2] M. Musto, G. Alfano. *A fractional rate-dependent cohesive-zone model*, International Journal for Numerical Methods in Engineering, 103 (2015) 313–341
- [3] L. Škec. *Identification of parameters of a bi-linear cohesive-zone model using analytical solutions for mode-I delamination*, Engineering Fracture Mechanics, 214 (2019) 558–577

Author index

- Adam C., 57
Alfano G., 197
Alzate Cobo J.C., 29
Amaral G.R. do, 171
Arnold M., 51, 111, 113, 125
Auteri G., 129
Bali S., 73
Balthazar J.M., 171
Bauchau O., 3
Becker M., 193
Benacchio S., 65
Bertails-Descoubes F., 5, 37, 89, 93, 103
Betsch P., 9
Bijalwan A., 97
Bleffert C., 43
Bles G., 181
Borković A., 137
Bosten A., 31, 75, 91
Bral A., 183
Bratina S., 167
Brojan M., 195
Brüls O., 31, 75, 77, 91, 189
Čanadija M., 33
Cardiff P., 73
Castello D., 85
Celledoni E., 113, 119, 129
Češarek P., 153, 155, 175
Chassagne M., 179
Choi M-J., 139
Civier L., 181
Çokaj E., 113
Cosimo A., 189
Coupé D., 187
Crespel O., 89
Cuomo M., 85
Daelemans L., 183
Davies P., 181
De Almagro R.T.S., 63, 121
De O. Lopes E.M., 171
Debeurre M., 65, 115, 157
Degroote J., 183
Del Sorbo P., 187
Devigne O., 77
Dickinson R., 141
Diebels S., 47, 67
Döhrer E., 101
Dörlich V., 11, 45, 51, 63, 67, 91, 133
Dreyer L., 43
Durville D., 59, 145, 179, 187
Düster A., 47
Escalona J.L., 79, 95, 131
Eugster S.R., 81, 87
Ferri G., 35
Flajs R., 159
Furtmüller T., 57
Gams M., 175
Gandiolle C., 145
Geradin M., 15
Gerstmayr J., 83, 99
Gfrerer M.H., 137
Giraud-Audine C., 65
Gramegna V., 103
Grbac L., 161
Greco L., 85
Grolet A., 65, 115, 157
Hamila N., 181
Hariz-Belgacem K., 117
Harsch J., 81, 87
Hawwash M., 31, 45
Hermansson T., 165
Hildebrandt-Raj A., 47
Hohnadel E., 89, 93
Hozjan T., 167
Humer A., 107
Ignesti D., 35
Imbert M., 193
Ivanković A., 73
Jelenić G., 105, 123, 161, 169
Jiménez F., 117
Kawata T., 93
Klarmann S., 143
Klinkel S., 139, 143
Korkealaakso P., 95
Košmerl V., 33
Kouhia R., 55
Kulkarni A., 91
Kusuma Chandrashekhara S., 49
Kyosev Y., 185
Leok M., 17
Leone A., 113, 119
Leyendecker S., 63, 121, 129
Linn J., 31, 45, 51, 67, 69, 91, 133, 165

Lolić D., 195
 Manfredo D., 51
 Marco Y., 181
 Marino E., 35
 Marjoribanks T.I., 141
 Marussig B., 137
 Matikainen M., 55
 May M., 193
 Meier C., 23, 149
 Mermouli S.E., 187
 Métivet T., 93, 103
 Michel S.J., 53
 Mohammadi N., 95
 Müller R., 69
 Munoz J., 97
 Murari D., 119
 Neggers J., 179
 Neukirch S., 37
 Ntarladima K., 83, 99
 Ober-Blöbaum S., 117
 Obrezkov L., 55
 Ogrin A., 167, 173
 Owren B., 113, 119, 129
 Pakrashi V., 73
 Palmeri A., 141
 Patil I., 189
 Patreider M., 57
 Pečenko R., 167
 Planinc I., 169
 Popp A., 149
 Poussard V., 145
 Reiter P., 101
 Ribeiro K.M.M., 171
 Röhrig-Zöllner M., 43
 Roller M., 31, 165
 Rouvinen A., 95
 Saadat M.A., 59
 Sailer S., 81
 Saje M., 155, 159, 169
 Sano T.G., 93
 Sauer A. Roger, 137, 139
 Schmidt A-M., 185
 Schnabl S., 169
 Schneider-Jung F., 69, 165
 Schumacher H., 101
 Shafqat A., 147
 Sharma P., 47, 67
 Sipos A.A., 39, 53, 61
 Škec L., 197
 Skouras M., 103
 Sonnevile V., 25
 Stavole M., 63, 121
 Steinbrecher I., 149
 Teixeira da Silva A., 103
 Thomas O., 65, 115, 157
 Tomec J., 105, 123
 Tranquart B., 187
 Tsegouog C., 67
 Turković Ž., 73
 Tumiotto D., 113, 125
 Turk G., 169
 Varkonyi P.L., 39
 Vetyukov Y., 107
 Vizzaccaro A., 115
 Wackerfuß J., 143
 Wahrhaftig A. de M., 171
 Weeger O., 29, 147
 Wenin M., 57
 Xu B-X., 147
 Zhao T., 69
 Zlatic M., 33
 Zupan D., 49, 173, 175, 195
 Zupan E., 173, 175

ISBN 978-953-6953-61-5